SUBSEQUENT BEHAVIOUR OF THE OSCILLATIONS OF THE DOUBLE PENDULUM UNDER VARIOUS INITIAL CONDITIONS

by
Ömer Eren

Submitted to Graduate School of Natural and Applied Sciences
in Partial Fulfillment of the Requirements
for the Degree of Doctor of Philosophy in
Physics

Yeditepe University
2023

SUBSEQUENT BEHAVIOUR OF THE OSCILLATIONS OF THE DOUBLE PENDULUM UNDER VARIOUS INITIAL CONDITIONS

APPROVED BY:

Assist. Prof. Dr. Ercüment Akat ……
(Thesis Supervisor)
(Yeditepe University)

Prof. Dr. Avadis S. Hacınlıyan ……
(Yeditepe University)

Prof. Dr. Mehmet Özer ……
(Istanbul Kültür University)

Prof. Dr. İpek Karaaslan ……
(Yeditepe University)

Prof. Dr. Merih Serin ……
(Yıldız Technical University)

DATE OF APPROVAL: ..../..../20..

I hereby declare that this thesis is my own work and that all information in this thesis has been obtained and presented in accordance with academic rules and ethical conduct. I have fully cited and referenced all material and results as required by these rules and conduct, and this thesis study does not contain any plagiarism. If any material used in the thesis requires copyright, the necessary permissions have been obtained. No material from this thesis has been used for the award of another degree.

I accept all kinds of legal liability that may arise in case contrary to these situations.

Name, Last name Ömer Eren

Signature ……..

ACKNOWLEDGEMENTS

I would like to thank my supervisor Assist. Prof. Dr. Ercüment Akat for his invaluable supervision, support and tutelage during the course of my PhD degree.

I would like to thank Prof. Dr. Avadis Hacınlıyan, Prof. Dr. Mehmet Özer for their kindness to attend my thesis progress committees, for their time, for their guidance they provided.

I would also like to thank all the professors of Yeditepe University Physics Department and all the research assistants of Physics Departments for all their supports.

I would like to extend my heartfelt thanks to Altınay Robot Technologies Inc. for generously providing me with the necessary resources and facilities to complete my thesis.

Finally, many thanks to my family and children for their endless love and support, which makes everything more beautiful.

ABSTRACT

SUBSEQUENT BEHAVIOUR OF THE OSCILLATIONS OF THE DOUBLE PENDULUM UNDER VARIOUS INITIAL CONDITIONS

In this study, we analyzed the pendulum case which is a good model for several oscillating phenomena. Also we investigated nonlinearities and sensitivity to initial conditions in pendulum systems. It is known that a simple pendulum that consists of a bob of mass m attached to the free end of a massless rod of length b, performing simple harmonic motion is widely used in physics. There are various kinds of pendula such as double, triple, inverted, conical or mathematical pendulum. Although it exhibits a nonlinear behaviour its motion can be approximated to be linear for relatively small angles. The pendulum systems are one of the primary topics in mechanical structures for nonlinear dynamics and chaos researches.

In this thesis, we have examined double and triple pendula. Our aim is to examine and find the motional structure of the pendulum according to different initial values. There are two basic parameters on the pendulum, m being the mass at the end of the rope and b being the length of the massless rod. m_1, m_2, b_1, b_2 are for the double pendulum, m_1, m_2, m_3, b_1, b_2, b_3 are for the triple pendulum. In our study, pendulum motion was examined for different values of mass and massless rod lengths and a behaviour model was derived. In addition, after solving the equations on the fixed pendulum, horizontal and vertical oscillations were superimposed to the fixed pendulum application and the equations of motion of the pendulum were derived again and its motion was examined. All of our equation solutions, variation of model parameters and motion structures at the initial values in the specified intervals in each different model setup were examined by the help of Lagrange formalism and solved by computer programs. We examined the motion behaviours of double and triple pendula under various physical conditions and critical motion regions on the different initial conditions. By subjecting system variables to analyses using phase portraits, bifurcation diagrams and Lyapunov Exponents, we examined the motion behaviour models.

ÖZET

DIŞ KUVVET VE FARKLI BAŞLANGIÇ KOŞULLARI ALTINDA İKİLİ SARKAÇIN SALINIM DAVRANIŞLARI

Bu çalışmada, salınımla ilgili araştırmalarda iyi bir model olan sarkaç durumunu analiz ettik. Ayrıca sarkaç sistemlerindeki doğrusal olmayan sistemleri, başlangıç koşullarına olan duyarlılıkları araştırdık. b uzunluğunda kütlesiz bir çubuğun serbest ucuna bağlı, basit harmonik hareket gerçekleştiren m kütleli bir toptan oluşan basit bir sarkacın fizikte yaygın olarak kullanıldığı bilinmektedir. İkili, üçlü, ters, konik ya da matematiksel sarkaç gibi çeşitli sarkaç türleri vardır. Sarkaç sistemleri, mekanik yapılar için nonlinear dinamik ve kaos araştırmalarının öncelikli konularından biridir. Doğrusal olmayan bir davranış sergilemesine karşın, hareketi görece küçük açılar için doğrusal olduğu varsayılabilir.

Bu çalışmada, ikili ve üçlü sarkaçları inceledik. Amacımız sarkacın hareket yapısını farklı başlangıç değerlerine göre incelemek ve bulmaktır. Sarkaç üzerinde iki temel parametre vardır, m ipin ucundaki kütle ve b kütlesiz çubuğun uzunluğudur. . m_1, m_2, b_1, b_2 ikili sarkaç, , m_1, m_2, m_3, b_1, b_2, b_3 ise üçlü sarkaç için seçim parametreleridir. Çalışmamızda kütle ve kütlesiz çubuk uzunluklarının farklı değerleri için sarkaç hareketi incelenmiş ve bir davranış modeli türetilmiştir. Ayrıca sabit sarkaç üzerindeki denklemler çözüldükten sonra sabit sarkaç uygulamasına yatay ve düşey salınımlar eklenmiş ve sarkacın hareket denklemleri yeniden çıkarılarak hareketi incelenmiştir. Tüm denklem çözümlerimiz, model parametrelerinin değişimi ve hareket yapılarının her farklı model kurulumunda belirlenen aralıklarda başlangıç değerlerindeki değişimi, Lagrange yaklaşımlarından ve bilgisayar programlarından yararlanılarak incelenmiştir. İkili ve üçlü sarkacın hareket davranışları, çeşitli fiziksel koşullar altında ve farklı başlangıç koşullarında incelenerek kritik hareket bölgeleri belirlenmiştir. Sistem değişkenleri, faz diagramaları, çatallanma diagramları ve Lyapunov üstelleri kullanılarak analiz edilerek hareket modelleri incelenmiştir.

TABLE OF CONTENTS

ACKNOWLEDGEMENTS iv

ABSTRACT v

ÖZET vi

LIST OF FIGURES ix

LIST OF TABLES xix

LIST OF SYMBOLS/ABBREVIATIONS xx

1. INTRODUCTION 1

2. THEORETICAL PART 6

2.1. EULER-LAGRANGE FORMALISM 9

2.2. DOUBLE PENDULUM SOLUTIONS 11

2.3. TRIPLE PENDULUM SOLUTIONS 17

2.4. ROTATIONAL INERTIA 22

2.5. ANGULAR MOMENTUM 23

2.6. FORCE ON JOINTS 24

2.7. OSCILLATIONS AND CHAOS 25

2.7.1. Poincare Sections 27

2.7.2. Bifurcation Diagram 27

2.7.3. Lyapunov Exponents 28

3. MATERIALS AND METHODS 31

4. STATIONARY STATES OF DOUBLE PENDULUM 36

4.1. REPRESENTATIONS OF STATIONARY OF DOUBLE PENDULUM 37

4.2. REPRESENTATIONS OF STATIONARY STATES FOR DIFFERENT MASS RATIOS 51

4.3. REPRESENTATIONS OF STATIONARY STATES FOR DIFFERENT LENGTH RATIOS 63

5. VIBRATING STATES OF DOUBLE PENDULUM 75

5.1. HORIZONTAL VIBRATIONS 75

5.2. HORIZONTAL VIBRATING STATES 77
5.3. VERTICAL VIBRATIONS 88
5.4. VERTICAL VIBRATING STATES 89
6. STATIONARY STATES OF THE TRIPLE PENDULUM 99
7. RESULTS AND DISCUSSIONS 104
8. CONCLUSIONS 112
REFERENCES 113
APPENDIX A 120
APPENDIX B 122
APPENDIX C 124

LIST OF FIGURES

Figure 2.1. The schematic representation of a double pendulum consisting of two bobs of different masses and two light rods of different lengths, joining the bobs. It is also the coordinate system used for the double pendulum. 7

Figure 2.2. A typical representation of a macro state among various variables. 14

Figure 2.3. The least energy case among the macrostates chosen, where $\theta_1 = 0°$ and $\theta_2 = 5°$. 15

Figure 2.4. The energetically degenerate states for which upper angles are identical and lower angles are symmetrical. 16

Figure 2.5. The schematic representation of a triple pendulum consisting of three bobs of different masses and three light rods of different lengths, joining the bobs. It is also the coordinate system used for the triple pendulum. 17

Figure 2.6. General representation of rotational inertia of the double pendulum. 23

Figure 2.7. The angular momentum vectors (L) for counterclockwise (left) and clockwise (right) rotations of a simple pendulum. 24

Figure 2.8. The forces, i.e. tensions and weights, acting on the system when it is oscillating. 25

Figure 2.9. The neighbour trajectories with difference , ε 28

Figure 2.10. The perturbations from uniform to chaotic. 30

Figure 3.1. The design view of experimental triple pendulum set 31

Figure 3.2. The representation of solution graphics, angles values, positions of bobs and phase spaces versus initial angle values. 33

Figure 3.3. The examination path of double and triple pendulum. 34

Figure 4.1. The example graphics of small, medium and large angle regions. 38

Figure 4.2. The graphical solutions of $\theta_2 = 15, 30, 45,60,75, 90$ for small, medium, and large values corresponding to the small angle value of $\theta_1 = 15$. The other parameters are $b_1 = 1, b_2 = 1, m_1 = 1, m_2 = 1, a = 0, \omega = 0$. 39

Figure 4.3. The graphical solutions of $\theta_2 = -15, -30, -45, -60, -75, -90$ for small, medium, and large values corresponding to the small angle value of $\theta_1 = 15$. The other parameters are $b_1 = 1, b_2 = 1, m_1 = 1, m_2 = 1, a = 0, \omega = 0$. 40

Figure 4.4. The graphical solutions of $\theta_2 = 15, 30, 45, 60, 75, 90$ for small, medium, and large values corresponding to the medium angle value of $\theta_1 = 45$. The other parameters are $b_1 = 1, b_2 = 1, m_1 = 1, m_2 = 1, a = 0, \omega = 0$. 42

Figure 4.5. The graphical solutions of $\theta_2 = -15, -30, -45, -60, -75, -90$ for small, medium, and large values corresponding to the medium angle value of $\theta_1 = 45$. The other parameters are $b_1 = 1, b_2 = 1, m_1 = 1, m_2 = 1, a = 0, \omega = 0$. 43

Figure 4.6. The graphical solutions of $\theta_2 = 15, 30, 45, 60, 75, 90$ for small, medium, and large values corresponding to the large angle value of $\theta_1 = 75$. The other parameters are $b_1 = 1, b_2 = 1, m_1 = 1, m_2 = 1, a = 0, \omega = 0$. 44

Figure 4.7. The graphical solutions of $\theta_2 = -15, -30, -45, -60, -75, -90$ for small, medium, and large values corresponding to the large angle value of $\theta_1 = 75$. The other parameters are $b_1 = 1, b_2 = 1, m_1 = 1, m_2 = 1, a = 0, \omega = 0$. 45

Figure 4.8. The graphical solutions of $\theta_2 = 15, 30, 45, 60, 75, 90$ for small, medium, and large values corresponding to the small angle value of $\theta_1 = 90$. The other parameters are $b_1 = 1, b_2 = 1, m_1 = 1, m_2 = 1, a = 0, \omega = 0$. 47

Figure 4.9. The graphical solutions of $\theta_2 = -15, -30, -45, -60, -75, -90$ for small, medium, and large values corresponding to the small angle value of $\theta_1 = 90$. The other parameters are $b_1 = 1, b_2 = 1, m_1 = 1, m_2 = 1, a = 0, \omega = 0$. 48

Figure 4.10. The representation of phase portraits and Poincaré sections for system of double pendulum, $\theta_1 = \theta_2 = 15, 45, 90$ 49

Figure 4.11. The graphic of the lyapunov exponents of double pendulum, $\theta_1 = 45$ and $\theta_2 = 45$, $b_1 = 1, b_2 = 1, m_1 = 1, m_2 = 1, a = 0, \omega = 0$. 50

Figure 4.12. The graphical solutions of $\theta_2 = 15, 30, 45, 75, 90$ for small, medium, and large values corresponding to the large angle value of $\theta_1 = 75$. The other parameters are $b_1 = 1, b_2 = 1, m_1 = 1, m_2 = 0.5, a = 0, \omega = 0$. 53

Figure 4.13. The graphical solutions of $\theta_2 = -15, -30, -45, -75, -90$ for small, medium, and large values corresponding to the large angle value of $\theta_1 = 75$. The other parameters are $b_1 = 1, b_2 = 1, m_1 = 1, m_2 = 0.5, a = 0, \omega = 0$. 54

Figure 4.14. The graphical solutions of $\theta_2 = 15, 30, 45, 75, 90$ for small, medium, and large values corresponding to the large angle value of $\theta_1 = 90$. The other parameters are $b_1 = 1, b_2 = 1, m_1 = 1, m_2 = 0.5, a = 0, \omega = 0$. 55

Figure 4.15. The graphical solutions of $\theta_2 = -15, -30, -45, -75, -90$ for small, medium, and large values corresponding to the large angle value of $\theta_1 = 90$. The other parameters are $b_1 = 1, b_2 = 1, m_1 = 1, m_2 = 0.5, a = 0, \omega = 0$. 56

Figure 4.16. The graphical solutions of $\theta_2 = 15, 30, 45, 75, 90$ for small, medium, and large values corresponding to the large angle value of $\theta_1 = 75$. The other parameters are $b_1 = 1, b_2 = 1, m_1 = 1, m_2 = 2, a = 0, \omega = 0$. 58

Figure 4.17. The graphical solutions of $\theta_2 = -15, -30, -45, -75, -90$ for small, medium, and large values corresponding to the large angle value of $\theta_1 = 75$. The other parameters are $b_1 = 1, b_2 = 1, m_1 = 1, m_2 = 2, a = 0, \omega = 0$. 59

Figure 4.18. The graphical solutions of $\theta_2 = 15, 30, 45, 75, 90$ for small, medium, and large values corresponding to the large angle value of $\theta_1 = 90$. The other parameters are $b_1 = 1, b_2 = 1, m_1 = 1, m_2 = 2, a = 0, \omega = 0$. 60

Figure 4.19. The graphical solutions of $\theta_2 = -15, -30, -45, -75, -90$ for small, medium, and large values corresponding to the large angle value of $\theta_1 = 90$. The other parameters are $b_1 = 1, b_2 = 1, m_1 = 1, m_2 = 2, a = 0, \omega = 0$. 61

Figure 4.20. The graphic of the lyapunov exponents of double pendulum, (a) $\theta_1 = 45$ and $\theta_2 = 45$, $b_1 = 1, b_2 = 1, m_1 = 1, m_2 = 0.5, a = 0, \omega = 0$. (b) $\theta_1 = 45$ and $\theta_2 = 45$, $b_1 = 1, b_2 = 1, m_1 = 1, m_2 = 2, a = 0, \omega = 0$. 62

Figure 4.21. The graphical solutions of $\theta_2 = 15, 30, 45, 75, 90$ for small, medium, and large values corresponding to the large angle value of $\theta_1 = 75$. The other parameters are $b_1 = 1, b_2 = 0.5, m_1 = 1, m_2 = 1, a = 0, \omega = 0$. 64

Figure 4.22. The graphical solutions of $\theta_2 = -15, -30, -45, -75, -90$ for small, medium, and large values corresponding to the large angle value of $\theta_1 = 75$. The other parameters are $b_1 = 1, b_2 = 0.5, m_1 = 1, m_2 = 1, a = 0, \omega = 0$. 65

Figure 4.23. The graphical solutions of $\theta_2 = 15, 30, 45, 75, 90$ for small, medium, and large values corresponding to the large angle value of $\theta_1 = 90$. The other parameters are $b_1 = 1, b_2 = 0.5, m_1 = 1, m_2 = 1, a = 0, \omega = 0$. 66

Figure 4.24. The graphical solutions of $\theta_2 = -15, -30, -45, -75, -90$ for small, medium, and large values corresponding to the large angle value of $\theta_1 = 90$. The other parameters are $b_1 = 1, b_2 = 0.5, m_1 = 1, m_2 = 1, a = 0, \omega = 0$. 67

Figure 4.25. The graphical solutions of $\theta_2 = 15, 30, 45, 75, 90$ for small, medium, and large values corresponding to the large angle value of $\theta_1 = 75$. The other parameters are $b_1 = 1, b_2 = 2, m_1 = 1, m_2 = 1, a = 0, \omega = 0$. 69

Figure 4.26. The graphical solutions of $\theta_2 = -15, -30, -45, -75, -90$ for small, medium, and large values corresponding to the large angle value of $\theta_1 = 75$. The other parameters are $b_1 = 1, b_2 = 2, m_1 = 1, m_2 = 1, a = 0, \omega = 0$. 70

Figure 4.27. The graphical solutions of $\theta_2 = 15, 30, 45, 75, 90$ for small, medium, and large values corresponding to the large angle value of $\theta_1 = 90$. The other parameters are $b_1 = 1, b_2 = 2, m_1 = 1, m_2 = 1, a = 0, \omega = 0$. 71

Figure 4.28. The graphical solutions of $\theta_2 = -15, -30, -45, -75, -90$ for small, medium, and large values corresponding to the large angle value of $\theta_1 = 90$. The other parameters are $b_1 = 1, b_2 = 2, m_1 = 1, m_2 = 1, a = 0, \omega = 0$. 72

Figure 4.29. The representation of phase portraits and Poincaré sections for system of double pendulum, ($\theta 1; \theta 2$) = (15,15),(45,45),(90,90), The other parameters are $b_1 = 1, b_2 = 0.5, m_1 = 1, m_2 = 1, a = 0, \omega = 0$. 73

Figure 4.30. The graphic of the lyapunov exponents of double pendulum, (a) $\theta_1 = 45$ and $\theta_2 = 45$, $b_1 = 1, b_2 = 0.5, m_1 = 1, m_2 = 1, a = 0, \omega = 0$. (b) θ_1=45 and θ_2=45, $b_1 = 1, b_2 = 2, m_1 = 1, m_2 = 1, a = 0, \omega = 0$. 74

Figure 5.1. External horizontal vibrations of the joint according to a sinusoidal function. 75

Figure 5.2. The graphical solutions of $\theta_2 = 15, 30, 45, 60, 75, 90$ for small, medium, and large values corresponding to the large angle value of $\theta_1 = 75$. The other parameters are $b_1 = 1, b_2 = 1, m_1 = 1, m_2 = 1, a = 0.5, \omega = 1$, horizontal vibrating.....79

Figure 5.3. The graphical solutions of $\theta_2 = -15, -30, -45, -60, -75, -90$ for small, medium, and large values corresponding to the large angle value of $\theta_1 = 75$. The other parameters are $b_1 = 1, b_2 = 1, m_1 = 1, m_2 = 1, a = 0.5, \omega = 1$, horizontal vibrating. 80

Figure 5.4. The graphical solutions of $\theta_2 = 15, 30, 45, 60, 75, 90$ for small, medium, and large values corresponding to the large angle value of $\theta_1 = 90$. The other parameters are $b_1 = 1, b_2 = 1, m_1 = 1, m_2 = 1, a = 0.5, \omega = 1$, horizontal vibrating.....81

Figure 5.5. The graphical solutions of $\theta_2 = -15, -30, -45, -60, -75, -90$ for small, medium, and large values corresponding to the large angle value of $\theta_1 = 90$. The other parameters are $b_1 = 1, b_2 = 1, m_1 = 1, m_2 = 1, a = 0.5, \omega = 1$, horizontal vibrating. 82

Figure 5.6. The graphical solutions of $\theta_2 = 15, 30, 45, 60, 75, 90$ for small, medium, and large values corresponding to the large angle value of $\theta_1 = 75$. The other parameters are $b_1 = 1, b_2 = 1, m_1 = 1, m_2 = 1, a = 0.5, \omega = 3$, horizontal vibrating.....83

Figure 5.7. The graphical solutions of $\theta_2 = -15, -30, -45, -60, -75, -90$ for small, medium, and large values corresponding to the large angle value of $\theta_1 = 75$. The other parameters are $b_1 = 1, b_2 = 1, m_1 = 1, m_2 = 1, a = 0.5, \omega = 3$, horizontal vibrating. 84

Figure 5.8. The graphical solutions of $\theta_2 = 15, 30, 45, 60, 75, 90$ for small, medium, and large values corresponding to the large angle value of $\theta_1 = 90$. The other parameters are $b_1 = 1, b_2 = 1, m_1 = 1, m_2 = 1, a = 0.5, \omega = 3$, horizontal vibrating.....85

Figure 5.9. The graphical solutions of $\theta_2 = -15, -30, -45, -60, -75, -90$ for small, medium, and large values corresponding to the large angle value of $\theta_1 = 90$. The other parameters are $b_1 = 1, b_2 = 1, m_1 = 1, m_2 = 1, a = 0.5, \omega = 3$, horizontal vibrating. 86

Figure 5.10. The graphic of the lyapunov exponents of double pendulum, (a) $\theta_1 = 90$ and $\theta_2 = 90$, $b_1 = 1, b_2 = 1, m_1 = 1, m_2 = 1, a = 0.5, \omega = 1$. (b) $\theta_1 = 90$ and $\theta_2 = 90$, $b_1 = 1, b_2 = 1, m_1 = 1, m_2 = 1, a = 0.5, \omega = 3$. 87

Figure 5.11. External vertical vibrations of the joint according to a sinusoidal function....88

Figure 5.12. The graphical solutions of θ_2 =15, 30, 45, 75, 90 for small, medium, and large values corresponding to the large angle value of $\theta_1 = 75$. The other parameters are $b_1 = 1, b_2 = 1, m_1 = 1, m_2 = 1, a = 0.5, \omega = 1$, vertical vibrating.....90

Figure 5.13. The graphical solutions of $\theta_2 = -15, -30, -45, -75, -90$ for small, medium, and large values corresponding to the large angle value of $\theta_1 = 75$. The other parameters are $b_1 = 1, b_2 = 1, m_1 = 1, m_2 = 1, a = 0.5, \omega = 1$, vertical vibrating. 91

Figure 5.14. The graphical solutions of $\theta_2 = 15, 30, 45, 75, 90$ for small, medium, and large values corresponding to the large angle value of $\theta_1 = 90$. The other parameters are $b_1 = 1, b_2 = 1, m_1 = 1, m_2 = 1, a = 0.5, \omega = 1$, vertical vibrating.....92

Figure 5.15. The graphical solutions of $\theta_2 = -15, -30, -45, -75, -90$ for small, medium, and large values corresponding to the large angle value of $\theta_1 = 90$. The other parameters are $b_1 = 1, b_2 = 1, m_1 = 1, m_2 = 1, a = 0.5, \omega = 1$, vertical vibrating. 93

Figure 5.16. The graphical solutions of $\theta_2 = 15, 30, 45, 75, 90$ for small, medium, and large values corresponding to the large angle value of $\theta_1 = 75$. The other parameters are $b_1 = 1, b_2 = 1, m_1 = 1, m_2 = 1, a = 0.5, \omega = 3$, vertical vibrating.....94

Figure 5.17. The graphical solutions of $\theta_2 = -15, -30, -45, -75, -90$ for small, medium, and large values corresponding to the large angle value of $\theta_1 = 75$. The other parameters are $b_1 = 1, b_2 = 1, m_1 = 1, m_2 = 1, a = 0.5, \omega = 3$, vertical vibrating. 95

Figure 5.18. The graphical solutions of $\theta_2 = 15, 30, 45, 75, 90$ for small, medium, and large values corresponding to the large angle value of $\theta_1 = 90$. The other parameters are $b_1 = 1, b_2 = 1, m_1 = 1, m_2 = 1, a = 0.5, \omega = 3$, vertical vibrating. 96

Figure 5.19. The graphical solutions of $\theta_2 = -15, -30, -45, -75, -90$ for small, medium, and large values corresponding to the large angle value of $\theta_1 = 90$. The other parameters are $b_1 = 1, b_2 = 1, m_1 = 1, m_2 = 1, a = 0.5, \omega = 3$, vertical vibrating. 97

Figure 5.20. The graphic of the lyapunov exponents of double pendulum, (a) $\theta_1 = 90$ and $\theta_2 = 90$, $b_1 = 1, b_2 = 1, m_1 = 1, m_2 = 1, a = 0.5, \omega = 1$.(b) $\theta_1 = 90$ and $\theta_2 = 90$, $b_1 = 1, b_2 = 1, m_1 = 1, m_2 = 1, a = 0.5, \omega = 3$. 98

Figure 6.1. The graphical solutions of $\theta_3 = 15, 30, 45, 75, 90$ for small, medium, and large values corresponding to the large and small angle values of $\theta_1 = 75$, $\theta_2 = 15$. The other parameters are $b_1 = 1, b_2 = 1, b_3 = 1, m_1 = 1, m_2 = 1, m_3 = 1, a = 0, \omega = 0$. 100

Figure 6.2. The graphical solutions of $\theta_3 = -15, -30, -45, -75, -90$ for small, medium, and large values corresponding to the large and small angle values of $\theta_1 = 75$, $\theta_2 = 15$. The other parameters are $b_1 = 1, b_2 = 1, b_3 = 1, m_1 = 1, m_2 = 1, m_3 = 1, a = 0, \omega = 0$. 101

Figure 6.3. The graphical solutions of $\theta_3 = 15, 30, 45, 75, 90$ for small, medium, and large values corresponding to the large and small angle values of $\theta_1 = 90$, $\theta_2 = 15$. The other parameters are $b_1 = 1, b_2 = 1, b_3 = 1, m_1 = 1, m_2 = 1, m_3 = 1, m3 = 1, a = 0, \omega = 0$. 102

Figure 6.4. The graphical solutions of $\theta_3 = -15, -30, -45, -75, -90$ for small, medium, and large values corresponding to the large and small angle values of $\theta_1 = 90$, $\theta_2 = 15$. The other parameters are $b_1 = 1, b_2 = 1, b_3 = 1, m_1 = 1, m_2 = 1, m_3 = 1, a = 0, \omega = 0$. 103

Figure 7.1. Maximum θ_2 angle values occurring versus θ_1, θ_2 values for all initial conditions. (Angle values are in degrees) 104

Figure 7.2. Maximum θ_1 angle values occurring versus θ_1, θ_2 values for all initial conditions. (Angle values are in degrees) 105

Figure 7.3. The representation of θ_1, θ_2 generating the maximum angle values for all initial conditions under different parameters. (Angle values are in degrees) 108

Figure 7.4. a) maximum θ_1, b) maximum θ_2 angle values occurring versus initial energy levels under different parameters. 109

Figure 7.5. The representation of the values of lyapunov expoents for the system of double pendulum (a) $\theta_1 = 0$ to 90, $\theta_2 = -90$ to 90, $b_1 = 1, b_2 = 0.5, m_1 = 1, m_2 = 0.5, a = 0, \omega = 0$. (b) $\theta_1 = 0$ to 90, $\theta_2 = -90$ to 90, $b_1 = 1, b_2 = 0.5, m_1 = 1, m_2 = 2, a = 0, \omega = 0$. 110

Figure 7.6. The representation of the maximum values of lyapunov exponents for the system of double pendulum (a) $\theta_1 = 0$ to 90, $\theta_2 = -90$ to 90, $b_1 = 1, b_2 = 2, m_1 = 1, m_2 = 0.5, a = 0, \omega = 0$. (b) $\theta_1 = 0$ to 90, $\theta_2 = -90$ to 90, $b_1 = 1, b_2 = 2, m_1 = 1, m_2 = 2, a = 0, \omega = 0$. 110

Figure 7.7. The representation of the spectrum of lyapunov exponents for system of double pendulum. $\theta_1 = 0$ to 90, $\theta_2 = -90$ to 90, $b_1 = 1, b_2 = 1, m_1 = 1, m_2 = 1, a = 0, \omega = 0$. 111

Figure A.1. The model of experimental pendulum 120

Figure A.2. The encoder and electric structure of experimental pendulum. (hardware, software application.) 121

Figure A.3. The user interface of encoder data on PC of experimental pendulum. 121

Figure C.1. The graphical solutions of $\theta_2 = 15, 30, 45, 60, 75, 90$ for small, medium, and large values corresponding to the small angle value of $\theta_1 = 15$. The other parameters are $b_1 = 1, b_2 = 1, m_1 = 1, m_2 = 0.5, a = 0, \omega = 0$. 125

Figure C.2. The graphical solutions of $\theta_2 = -15, -30, -45, -60, -75, -90$ for small, medium, and large values corresponding to the small angle value of $\theta_1 = 15$. The other parameters are $b_1 = 1, b_2 = 1, m_1 = 1, m_2 = 0.5, a = 0, \omega = 0$. 126

Figure C.3. The graphical solutions of $\theta_2 = 15, 30, 45, 60, 75, 90$ for small, medium, and large values corresponding to the small angle value of $\theta_1 = 45$. The other parameters are $b_1 = 1, b_2 = 1, m_1 = 1, m_2 = 0.5, a = 0, \omega = 0$. 127

Figure C.4. The graphical solutions of $\theta_2 = -15, -30, -45, -60, -75, -90$ for small, medium, and large values corresponding to the small angle value of $\theta_1 = 45$. The other parameters are $b_1 = 1, b_2 = 1, m_1 = 1, m_2 = 0.5, a = 0, \omega = 0$. 128

Figure C.5. The graphical solutions of $\theta_2 = 15, 30, 45, 60, 75, 90$ for small, medium, and large values corresponding to the large angle value of $\theta_1 = 15$. The other parameters are $b_1 = 1, b_2 = 1, m_1 = 1, m_2 = 1, a = 0.5, \omega = 1$, vertical vibrating. 129

Figure C.6. The graphical solutions of $\theta_2 = -15, -30, -45, -60, -75, -90$ for small, medium, and large values corresponding to the large angle value of $\theta_1 = 15$. The other parameters are $b_1 = 1, b_2 = 1, m_1 = 1, m_2 = 1, a = 0.5, \omega = 1$, vertical vibrating. 130

Figure C.7. The graphical solutions of $\theta_2 = 15, 30, 45, 60, 75, 90$ for small, medium, and large values corresponding to the large angle value of $\theta_1 = 15$. The other parameters are $b_1 = 1, b_2 = 1, m_1 = 1, m_2 = 1, a = 0.5, \omega = 3$, vertical vibrating. 131

Figure C.8. The graphical solutions of $\theta_2 = -15, -30, -45, -60, -75, -90$ for small, medium, and large values corresponding to the large angle value of $\theta_1 = 15$. The other parameters are $b_1 = 1, b_2 = 1, m_1 = 1, m_2 = 1, a = 0.5, \omega = 3$, vertical vibrating. 132

Figure C.9. The graphical solutions of $\theta_2 = 15, 30, 45, 60, 75, 90$ for small, medium, and large values corresponding to the large angle value of $\theta_1 = 45$. The other parameters are $b_1 = 1, b_2 = 1, m_1 = 1, m_2 = 1, a = 0.5, \omega = 1$, vertical vibrating. 133

Figure C.10. The graphical solutions of $\theta_2 = -15, -30, -45, -60, -75, -90$ for small, medium, and large values corresponding to the large angle value of $\theta_1 = 45$. The other parameters are $b_1 = 1, b_2 = 1, m_1 = 1, m_2 = 1, a = 0.5, \omega = 1$, vertical vibrating. 134

Figure C.11. The graphical solutions of $\theta_2 = 15, 30, 45, 60, 75, 90$ for small, medium, and large values corresponding to the large angle value of $\theta_1 = 45$. The other parameters are $b_1 = 1, b_2 = 1, m_1 = 1, m_2 = 1, a = 0.5, \omega = 3$, vertical vibrating. 135

Figure C.12. The graphical solutions of $\theta_2 = -15, -30, -45, -60, -75, -90$ for small, medium, and large values corresponding to the large angle value of $\theta_1 = 45$. The other parameters are $b_1 = 1, b_2 = 1, m_1 = 1, m_2 = 1, a = 0.5, \omega = 3$, vertical vibrating. 136

LIST OF TABLES

Table 1.1. The examples of research areas of pendulum. 2

Table 2.1. Equations of motion of triple pendulum. 22

Table 2.2. The Lyapunov exponents, λ values and results. 30

Table 3.1. The three angular regions under investigation for the pendulum at initial conditions. 35

Table 7.1. Number of full turns of upper bob for all solutions. 106

Table 7.2. Number of full furns of lower bob for all solutions 106

LIST OF SYMBOLS/ABBREVIATIONS

m	Mass
b	Length
θ	Angle
ω	Frequency
x	Horizontal axis
y	Vertical axis
x_1	Horizontal coordinates of bob1
x_2	Horizontal coordinates of bob2
x_3	Horizontal coordinates of bob3
y_1	Vertical coordinates of bob1
y_2	Vertical coordinates of bob2
y_3	Vertical coordinates of bob3
m_1	Mass of bob1
m_2	Mass of bob2
m_3	Mass of bob3
θ_1	Angle of the rod1
θ_2	Angle of the rod2
θ_3	Angle of the rod3
ω_1	Frequency of the bob1
ω_2	Frequency of the bob2
ω_3	Frequency of the bob3
L	Lagrangian
T	Kinetic Energy
V	Potential Energy
g	Gravity of Earth
I	Inertia
r	Radius
I_1	Inertia of bob1

I_2	Inertia of bob2
I_3	Inertia of bob3
$\vec{L}$	Angular momentum
L_{max}	Maximum value of angular momentum
T_1	Tension on the rod1
T_2	Tension on the rod2

1. INTRODUCTION

The pendulum and its various forms have been widely used in research across multiple fields, including physics, mathematics, engineering, and biology. The simple harmonic motion of the pendulum has served as a model for other physical phenomena [1], such as waves and oscillations. [2,3] The oscillatory motion is an extensively investigated topic in physics. There are several types of oscillations /vibrations in nature, including the macroscopic planar oscillations of simple pendula and microscopic vibrations of atoms in a solid around the equilibrium positions at two extremes. These are the simplest, yet quite widespread classes of oscillations in physics. The motion of a simple pendulum is quite well studied. For instance the local value of the gravitational acceleration g can be found at a certain point on Earth by just measuring the length of the rope and the average period of the simple pendulum, [4] provided that the amplitude of the oscillations is sufficiently small such that $sin\theta \cong \theta$ according to Taylor's approximation. [4,5] Also thanks to Foucault's pendulum the spin of the Earth is proven. The Foucault pendulum has been used to demonstrate the rotation of the Earth and torsional pendula have been used to measure the torsional properties of materials. Overall, the pendulum and its different types have played a significant role in advancing scientific understanding and have contributed to the development of various mathematical and physical concepts. Also, the "mass-spring" system is a good model for the examination of the motion of the atoms in a solid material around fixed, equilibrium positions. In general, the proportionalities in linear and angular motion can be converted to equalities as follows:

Force is proportional to linear displacement:

$$F \propto x \quad \rightarrow \quad F \cong k\,x \qquad \text{(linear)}$$

Torque is proportional to angular displacement:

$$\tau \propto \theta \quad \rightarrow \quad \tau \cong \kappa\,\theta \qquad \text{(angular)}$$

where k and κ are the force and torque constants of the simple and torsional pendulum respectively. In both cases the second order and higher terms are neglected for small displacements.

Pendulum is an important tool in both physics and mathematics. In Table 1.1, some important research and uses based on pendulum are tabulated.

Table 1.1. The examples of research areas of pendulum.

Foucault pendulum	Invented by the French physicist Léon Foucault in the 19^{th} century, this pendulum demonstrates the rotation of the Earth and is used to measure the Earth's rotation rate.
Simple pendulum	This is a simple pendulum created using a single bob and string. It is used to learn about topics such as pendulum motion, harmonic motion, and periodic motion.
Compound pendulum	This is the case where a fixed object such as a rod or cylinder swings around an axis. This type of pendulum can be used to determine the mass of an object or analyse mechanical systems such as a robotic arm.
Double pendulum	This is a pendulum created using two masses and two strings. This type of pendulum can be used for chaotic motion, mathematical solutions, and interesting applications in different fields such as art and music.
Torsion pendulum	This is created by attaching a weight to one end of a rod while the other end is fixed. This pendulum can be used to measure the torsion coefficient and analyze the effects of external forces.

The double pendulum has been studied extensively due to its complex motion and chaotic behaviour and various methods have been employed to analyze their behaviour, including Lagrangian formulations, Hamiltonian formulations or numerical simulations.

Double and triple pendulum research is based on fundamental principles in mathematics, physics, and engineering. These include kinematics, dynamics and control theories. Kinematics is the branch of science that defines the variables of motion such as position, velocity and acceleration. The kinematics of double and triple pendula can be modelled using equations that determine the angular position and velocity of each joint. Dynamics is the branch of science that studies the causes and effects of motion. The dynamics of double and triple pendula can be explained using mathematical models based on principles such as Newton's laws and Lagrange's equations. Control theory deals with the design of control

systems that are designed to achieve specific goals for a given system. The control of double and triple pendula is typically achieved using feedback control or nonlinear control methods. These fundamental principles provide the mathematical tools necessary to understand and control the dynamics of double and triple pendulum.

Double pendulum, unlike a simple pendulum, is a mechanical system consisting of two connection points and exhibits a more complex motion. The dynamic behaviour of the double pendulum is highly rich and chaotic. Therefore, the double pendulum has become the subject of many studies in the fields of physics, mathematics and engineering.

The double pendulum is used in the investigation of topics such as chaos theory and nonlinear dynamics. Additionally, this system can also be used in applied fields such as robotics and control systems. The double pendulum can also be used as a model for understanding the behaviour of larger systems. In particular, studying the double pendulum can be beneficial when other mechanical systems exhibit similar behaviours, such as systems with mass springs, flexible connections, or various connection elements.

The double pendulum is an important research topic in many fields, including the examination of the dynamic behaviour of complex systems, mathematical modelling, applied engineering and robotics.

Double pendulum has various applications in robotics. In particular, it can be used in the control of industrial robots. Industrial robots are programmable machines capable of performing precise and repeatable tasks automatically. In the control of these robots, traditional methods can sometimes be insufficient and robotic control algorithms can become more complex. The double pendulum can be used as a tool for controlling and learning robotic systems. [6] Therefore, researchers working in fields such as robotics engineering, control systems, artificial intelligence, and machine learning can conduct research on double pendula and design advanced robotic systems.

Double pendulum can also be used in the development of robotic control algorithms. In particular, double pendulum examples can be used in cases where factors such as angular velocity and acceleration need to be taken into account to control the motion of the robot more effectively. [7] During the learning process of robots, the behaviour can be improved by using feedback and control algorithms. [8] Furthermore, the double pendulum has become a popular tool for designing and testing robotic learning algorithms. [9] Robotics

research has contributed to the development of technologies that make people's lives easier in many fields. Specifically, the benefits provided by robotics research are as follows; industrial automation, medicine, automotive, military, defense etc.

Double pendula are a simple model used in multibody dynamics research. [10,11] Because this model includes multiple connection points and connection elements, it can be applied to the analysis of more complex systems in the field of multibody dynamics. [12] The benefits provided by double pendula to multibody dynamics research are as follows:

- Understanding more complex systems: Double pendula can be used to analyze more complex multibody dynamic systems, allowing for a better understanding of their behaviour. This can lead to the development of more effective methods for designing and controlling more complex systems.
- Simulations and testing: Double pendula can be used to conduct simulations and tests in multibody dynamics. This enables the simulation and testing of real-world scenarios.
- Motion control and management: Double pendula can be used for motion control and management of multibody dynamics systems, especially in robotic systems or vehicles.
- Structural analysis: Double pendula can be used for structural analysis of multibody dynamics systems, especially in structural strength analysis.

Direct modelling using double-pendulum-like models [13] with proper input of parameters is employed in the calculation and application domains of overhead [14,15] or rotary cranes. [16,17] The most crucial aspect of crane modelling is the precise calculation of the expected motion of the hook groups where the load is suspended. [18,19] Here, double-pendulum solutions are applied with solution equations for relevant friction [20] and variable load values. [21,22]

There are also cases where a pendulum consists of more than a single massless rod and a massive bob, but rather, two massless rods and two bobs attached to them, called the “double pendulum” or three rods and three bobs, called the “triple pendulum”. As stated above, one may encounter such double pendula in some sophisticated automotive systems and even as simple toys. Once such a double pendulum is set into motion, the subsequent behaviour is determined by the initial conditions, namely the initial values of the two angles, the initial

potential energy of the system, the ratio of the masses of the bobs, the ratio of the lengths of the rods etc. for the cases where the joint that connects the upper end of the upper rod to the ceiling stays stationary. However, the system may be more complicated as will be studied in the latter part of the thesis. If the joint does not stay at rest, but instead, is also vibrated externally and either horizontally or vertically by a sinusoidal function as will be seen in the thesis, the outcomes may be quite interesting. The relationship between the amplitude and frequency of the external vibrations and the resulting motion will be studied for at least some limited number of cases. To investigate those motions a well-known principle, the least action principle, Lagrange formalism and some simple physical laws are used. But a computer programme is developed and run yielding various graphs that are drawn by the help of the computer. After obtaining the motion equations through calculations, possible chaotic behaviours can be studied in various ways. For instance, methods such as polynomial optimization, as shown in the study "A study of the double pendulum using polynomial optimization" [23], or by calculating changes over time based on initial conditions to track chaotic motions. Additionally, machine learning approaches can be applied to solve Hamiltonian systems, as demonstrated in the study "Learning Hamiltonian dynamics with reservoir computing" [24,25]. In their solution, a different architecture enables accurate long-term prediction of system dynamics based on short-period data. Furthermore, external factors such as friction can affect pendulum systems, and research frequently considers not only massless rods but also those with mass or even flexible arms. Particularly, friction can be a distinguishing factor in revealing faster chaos and nonlinear effects. Taking friction into account can lead to the formation of damping forces and the exploration of vibration modes or chaos regions by obtaining motion equations accordingly.

Although we utilized various physical conditions in this thesis, our aim is to derive and produce results without a dampened system. By changing only the basic parameter values that make up the pendulum and examining the resulting motion structures and chaos parameters, we aimed to identify the sensitivities of initial conditions for all pendulum types derived. We discovered that some systems are more sensitive than others. Using methods such as motion equation analysis, phase portraits, bifurcation diagrams, and Lyapunov exponents, we highlighted these sensitivities in different pendulum structures.

2. THEORETICAL PART

It is known that a simple pendulum that consists of a bob of mass *m* attached to the free end of a massless rod of length *b*, performing simple harmonic motion is widely used in physics. It is a good model for several oscillating phenomena and there are various kinds of pendula such as double, triple, inverted, conical or mathematical pendulum. [26] Although it exhibits a nonlinear behaviour its motion can be approximated to be linear for relatively small angles (applying Taylor's approximation $\sin\theta \cong \tan\theta \cong \theta$ provided that the angle is expressed in radians). Then the equation of motion simply becomes a second order ordinary differential equation whose solutions are sine, cosine or complex exponential functions. Also the mass of the pendulum which does not appear in the equation, is assumed to concentrate at the bob whose radius is much less than the length of the rod and the mass of the light rod is neglected.

On the other hand, a planar double or triple pendulum consisting of bobs of mass m_n and again massless rods of length b_n ($n = 1$, 2 for the double pendulum), denoted in Fig. 1, may show nonlinear behaviour after it is set in motion at $t = 0$ under various initial conditions for the angles $\theta_n(0)$ ($n = 1$ and 2) where θ_1 and θ_2 are the angles for the rods connecting the bobs of masses m_1, m_2, both angles being measured from the vertical *y* axis, having positive values in the counter clockwise sense as shown. The horizontal coordinates of the bobs are denoted by x_1 and x_2 and the vertical coordinates by y_1 and y_2 respectively (positively up).

However, in this analysis, unlike the cases where Taylor's approximation is used, the angles are not limited to only small initial values, they may start from and pass through very large values, for some cases. The rods may even turn several times (clockwise or counter clockwise). The pieces can move independently, the light rods are tight, not flexible and the system is always at rest initially (at $t = 0$). In the first part of the study, the joint (the upper end of the upper rod that is connected to the fixed base) is stationary during the oscillations of the bobs. But in the second part, also the joint is made to vibrate horizontally (in *x*-dir.) and vertically (in *y*-dir.) in turn, in a sinusoidal way at an amplitude equal to the length of the rods (*b*) and at two frequencies (ω). All kinds of dissipative forces such as friction are always neglected, so there is no loss of energy in the analyses during the oscillations. [27]

At $t = 0$ there is no kinetic energy in the system but only some potential energy depending on the initial positions of the bobs, hence only on the initial values of the two angles. The level of the joint is taken as $y = 0$ and the positive *y*-axis is upward as seen in the Figure 1. In the calculations of the analyses $m_1 \neq m_2$ and $b_1 \neq b_2$ in general, but it is assumed first that $m_1 = m_2 = m$ and $b_1 = b_2 = b$. In the last part there is an analysis assuming different ratios for m_1 / m_2 and b_1 / b_2. Our main target is to examine the subsequent motion of the double pendulum for various initial values of angles $\theta_n(0)$ at $t = 0$. Several phenomena in the motion of the double pendulum can be investigated for different initial conditions, such as the possibility of the lower part (m_2 and b_2) to complete a full turn (θ_2 may pass through $\theta_2 = \pi$ while turning counter clockwise or through $\theta_2 = -\pi$ while turning clockwise). Also the subsequent motion of the centre of mass (c. m.) of the system and the number of times the velocity of the c. m. changes direction horizontally or vertically can be seen from the figures for different initial cases.

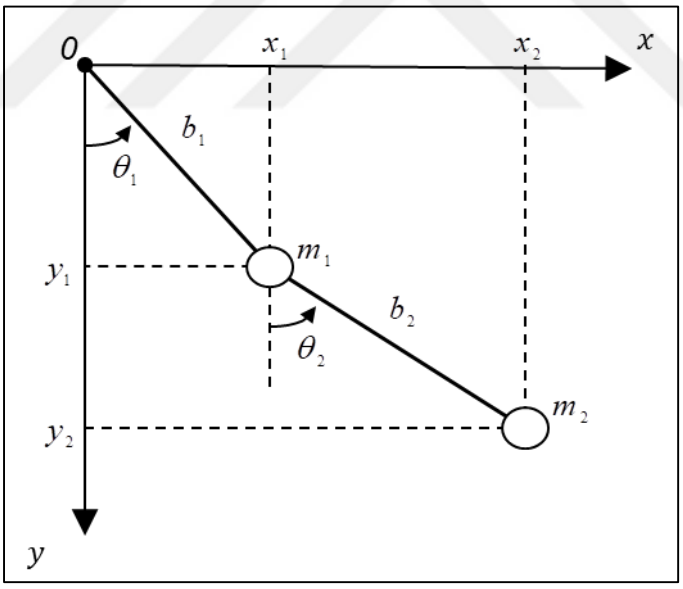


Figure 2.1. The schematic representation of a double pendulum consisting of two bobs of different masses and two light rods of different lengths, joining the bobs. It is also the coordinate system used for the double pendulum.

In the first part of this analysis, the subsequent motion of the system, that is, the positions of the bobs as functions of time are calculated for each case, according to the initial values of the two angles (θ_1 and θ_2) and using a computer programme working on the equations of

motion written by Euler-Lagrange formalism which will be summarized below. Several graphs are drawn for each case, such as the time variations of the angles and angular velocities, the relative variations of the angular velocities and the angles etc.

In the second part the effect of the external vibrations on the double pendulum is also studied. For this purpose the joint is externally oscillated in a sinusoidal way, first horizontally (in *x*-direction) for instance according to a function like $x = a\cos\omega t$, then vertically (in *y*-direction) like $y = a\cos\omega t$, at a certain value of the amplitude (*a*) and at two values of the frequency (ω). As for the amplitude *a* different values have been tried but the effect of the amplitude turned out to be less significant than that of the frequency ω. So we decided to set the amplitude to only one value, such as $a = b$ where *b* is the length of the rod and instead, set the values of the frequency to $\omega_1 = 2\pi$ rad/s and $\omega_2 = 4\pi$ rad/s.

The complicated motion of the double pendulum can also be interpreted as a combination of

i- the motion of the centre of mass (c. m.) and

ii- the motion around the c. m. Since the rods are taken to be massless, the overall c. m. of the double pendulum is somewhere between the two bobs, along the lower rod. For the first part of the analysis we take $m_1 = m_2 = m$, therefore the c.m. is at exactly half way between the bobs because of

$r_{cm} = \dfrac{0 + m_1 b}{m_1 + m_1} = b/2$ (from either end of the lower rod).

Otherwise, if for instance $(m_1 / m_2) = 1/5,$ then the c.m. is at the position $r_{cm} = \dfrac{0 + 5m_1 b}{m_1 + 5m_1} = (5/6)b$ from m_1 etc. Now let us see the method and the equations used in the analyses.

2.1. EULER-LAGRANGE FORMALISM

In physics a problem can sometimes be solved by more than one way. Especially in cases where it is difficult to write the momentary forces acting on the system as a function of the time or position for the whole time interval, conservations of linear and angular momentum and/or energy can be applied.

We may also apply Euler-Lagrange formalism dealing only with the kinetic and potential energies of the system. In some situations the system prefers a particular way to follow, out of a great number of choices. For instance a ball (or some amount of water) at the top of an irregularly shaped hill reaches the bottom of the hill by following a *particular* path rather than choosing a great number of other possibilities. There are infinetely many paths that join a point A and another point B which is at a lower level than A. If the two ends of a frictionless rope are held fixed at A and B and a bead is allowed to slide from A to B, it takes different amounts of time for different paths. Only one of these paths corresponds to the least amount of time and the problem of finding the shape of this special path is called "brachistochrone" meaning *shortest time.* In such cases we can find out the preferred one by applying the Euler-Lagrange formalism. [28] This method makes the systems much easier to solve. Before dealing with the details of the double pendulum let us briefly see the derivation of the formula used:

We want to have the extremum value of a functional *K* (function of a function) defined as

$$K = \int_{t_1}^{t_2} f\,[\,x(t), \dot{x}(t); t\,]dt \tag{2.1}$$

where t is the independent variable and y is the dependent variable.

$$x_\mu(t) = x_0(t) + \mu\,\sigma(t) \tag{2.2}$$

Now by varying the small quantity μ we seek to find the correct function. μ is multiplied by a function $\sigma\,(t)$ which vanishes at the limits $t = t_1$ and $t = t_2$ and $x_0(t)$ is the term without any μ.

$$\frac{\partial}{\partial \mu} A\left[x_\mu(t)\right] = \frac{\partial}{\partial \mu} \int_{t_1}^{t_2} L\, dt = \int_{t_1}^{t_2} \left(\frac{\partial L}{\partial \mu}\right) dt \tag{2.3}$$

$$= \int_{t_1}^{t_2} \left[\frac{\partial L}{\partial x_\mu} \frac{\partial x_\mu}{\partial \mu} + \frac{\partial L}{\partial \dot{x}_\mu} \frac{\partial \dot{x}_\mu}{\partial \mu}\right] dt \tag{2.4}$$

where L is the Lagrangian.

$\frac{\partial x_\mu}{\partial \mu} = \sigma$ and $\frac{\partial \dot{x}_\mu}{\partial \mu} = \dot{\sigma}$ (ignoring the t - dependence for simplicity)

Substituting in Eq. (2.2)

$$\frac{\partial}{\partial \mu} A\left[x_\mu(t)\right] = \int_{t_1}^{t_2} \left[\left(\frac{\partial L}{\partial x_\mu}\right)\sigma + \left(\frac{\partial L}{\partial \dot{x}_\mu}\right)\dot{\sigma}\right] dt \tag{2.5}$$

We can apply integration by parts to the second part of the above integral.

Let $u = \frac{\partial L}{\partial \dot{x}_\mu}$ and $dv = \dot{\sigma}$ then

$du = \frac{d}{dt}\left(\frac{\partial L}{\partial \dot{x}_\mu}\right)$ and $v = \sigma$.

From $\int (u)dv = uv - \int (v)du$

$$\int \left(\frac{\partial L}{\partial \dot{x}_\mu}\right)\dot{\sigma}\, dt = \left(\frac{\partial L}{\partial \dot{x}_\mu}\right)\sigma\Big|_{t_1}^{t_2} - \sigma \int \left(\frac{d}{dt}\frac{\partial L}{\partial \dot{x}_\mu}\right) dt \tag{2.6}$$

Then Eq. (2.4) becomes

$$\frac{\partial}{\partial \mu} A\left[x_\mu(t)\right] = \int_{t_1}^{t_2} \left(\frac{\partial L}{\partial x_\mu}\right)\sigma dt + \left(\frac{\partial L}{\partial \dot{x}_\nu}\right)\sigma\Big|_{t_1}^{t_2} - \int_{t_1}^{t_2} \sigma\left(\frac{d}{dt}\frac{\partial L}{\partial \dot{x}_\mu}\right) dt \tag{2.7}$$

But since the function $\sigma(t)$ should vanish at the limits,

$\sigma(t_1) = \sigma(t_2) = 0$

Then the second term on the right-hand side becomes zero.

$$\frac{\partial}{\partial \mu} A\left[x_\mu(t)\right] = \int_{t_1}^{t_2} \left(\frac{\partial L}{\partial x_\mu} \right) \sigma dt - \int_{t_1}^{t_2} \sigma \left(\frac{d}{dt} \frac{\partial L}{\partial \dot{x}_\mu} \right) dt \tag{2.8}$$

$$\frac{\partial}{\partial \mu} A\left[x_\mu(t)\right] = \int_{t_1}^{t_2} \sigma \left(\frac{\partial L}{\partial x_\mu} - \frac{d}{dt} \frac{\partial L}{\partial \dot{x}_\mu} \right) dt = 0 \tag{2.9}$$

In order for the right-hand side to be zero, only the quantities inside the parentheses should be zero, so that

$$\frac{\partial L}{\partial x_\mu} - \frac{d}{dt} \left(\frac{\partial L}{\partial \dot{x}_\mu} \right) = 0 \tag{2.10}$$

$L = T - V$ and $\frac{d}{dt} \frac{\partial L}{\partial \dot{\theta}_1} - \frac{\partial L}{\partial \theta_1} = 0$ where L is the Lagrangian, T is the kinetic energy and V is the potential energy.

Since in this double pendulum system there are two variables that are the angles θ_1 and θ_2, we can also write the same expression with respect to θ_2, both angles being measured relative to the vertical y axis.

2.2. DOUBLE PENDULUM SOLUTIONS

As is shown in Figure 2.1, for the double pendulum system consisting of two bobs and two massless rods, the positions of the two bobs with respect to the origin in the given reference frame,

$$x_1 = b_1 \sin \theta_1 \tag{2.11}$$

$$y_1 = -b_1 \cos \theta_1 \tag{2.12}$$

$$x_2 = b_1 \sin \theta_1 + b_2 \sin \theta_2 \tag{2.13}$$

$$y_2 = -b_1 \cos \theta_1 - b_2 \cos \theta_2 \tag{2.14}$$

Then the kinetic and potential energies during the motion can be written as

$$T = \frac{m_1}{2}\left(\dot{x}_1^2 + \dot{y}_1^2\right) + \frac{m_2}{2}\left(\dot{x}_2^2 + \dot{y}_2^2\right) \tag{2.15}$$

where $\dot{x}_1$, $\dot{x}_2$, $\dot{y}_1$ and $\dot{y}_2$ are the time derivatives of the related variables.

$$V = m_1 g y_1 + m_2 g y_2 \tag{2.16}$$

$$V = -m_1 g b_1 \cos\theta_1 - m_2 g\left(b_1 \cos\theta_1 + b_2 \cos\theta_2\right) \tag{2.17}$$

The time derivatives of the coordinates are

$$\dot{x}_1 = b_1 \dot{\theta}_1 \cos\theta_1 \tag{2.18}$$

$$\dot{y}_1 = b_1 \dot{\theta}_1 \sin\theta_1 \tag{2.19}$$

$$\dot{x}_2 = b_1 \dot{\theta}_1 \cos\theta_1 + b_2 \dot{\theta}_2 \cos\theta_2 \tag{2.20}$$

$$\dot{y}_2 = b_1 \dot{\theta}_1 \sin\theta_1 + b_2 \dot{\theta}_2 \sin\theta_2 \tag{2.21}$$

So the kinetic and potential energy of the system are respectively,

$$\begin{aligned} T = {} & \frac{m_1}{2}\left[b_1^2 \dot{\theta}_1^2 \cos^2\theta_1 + b_1^2 \dot{\theta}_1^2 \sin^2\theta_1\right] \\ & + \frac{m_2}{2}\left[\begin{aligned} & b_1^2 \dot{\theta}_1^2 \cos^2\theta_1 + b_2^2 \dot{\theta}_2^2 \cos^2\theta_2 \\ & + 2 b_1 b_2 \dot{\theta}_1 \dot{\theta}_2 \cos\theta_1 \cos\theta_2 + b_1^2 \dot{\theta}_1^2 \sin^2\theta_1 + b_2^2 \dot{\theta}_2^2 \sin^2\theta_2 + 2 b_1 b_2 \dot{\theta}_1 \dot{\theta}_2 \sin\theta_1 \sin\theta_2 \end{aligned}\right] \end{aligned} \tag{2.22}$$

$$V = -m_1 g b_1 \cos\theta_1 - m_2 g\left(b_1 \cos\theta_1 + b_2 \cos\theta_2\right) \tag{2.23}$$

As was explained in the upper part, the Lagrangian can be written as

$$\begin{aligned} L = {} & \frac{m_1}{2}\left[b_1^2 \dot{\theta}_1^2\right] \\ & + \frac{m_2}{2}\left[+ b_1^2 \dot{\theta}_1^2 + b_2^2 \dot{\theta}_2^2 + 2 b_1 b_2 \dot{\theta}_1 \dot{\theta}_2 \cos\theta_1 \cos\theta_2 + 2 b_1 b_2 \dot{\theta}_1 \dot{\theta}_2 \sin\theta_1 \sin\theta_2\right] \\ & + m_1 g b_1 \cos\theta_1 + m_2 g\left(b_1 \cos\theta_1 + b_2 \cos\theta_2\right) \end{aligned} \tag{2.24}$$

Therefore the derivatives are

$$\frac{\partial L}{\partial \theta_1} = -m_2\left[b_1 b_2 \dot{\theta}_1 \dot{\theta}_2 \sin\theta_1 \sin\theta_2\right] - \left(m_1 + m_2\right) g b_1 \sin\theta_1 \tag{2.25}$$

$$\frac{\partial L}{\partial \dot{\theta}_1} = \frac{m_1}{2}\left[2b_1^2\dot{\theta}_1\right] + \frac{m_2}{2}\left[2b_1^2\dot{\theta}_1 + 2\left(b_1b_2\dot{\theta}_2\cos\theta_1\cos\theta_2\right) + 2b_1b_2\dot{\theta}_2\sin\theta_1\sin\theta_2\right] \quad (2.26)$$

$$\frac{\partial L}{\partial \dot{\theta}_1} = m_1b_1\left[b_1\dot{\theta}_1\right] + m_2b_1\left[b_1\dot{\theta}_1 + b_2\dot{\theta}_2\cos(\theta_1-\theta_2)\right] \quad (2.27)$$

$$\begin{aligned}&\frac{d}{dt}\frac{\partial L}{\partial \dot{\theta}_1} - \frac{\partial L}{\partial \theta_1} = m_1b_1\left[b_1\ddot{\theta}_1\right] \\ &+ m_2b_1\left[b_1\ddot{\theta}_1 - b_2\left[\ddot{\theta}_2\cos(\theta_1-\theta_2) - \dot{\theta}_2\sin(\theta_1-\theta_2)(\dot{\theta}_1-\dot{\theta}_2)\right]\right] + m_2b_1\left[b_2\dot{\theta}_1\dot{\theta}_2\cos\theta_1\sin\theta_2\right] = 0\end{aligned} \quad (2.28)$$

We apply the same procedure to θ_2 and get,

$$\frac{\partial L}{\partial \theta_2} = \frac{m_2}{2}\left[2\left(-b_1b_2\dot{\theta}_1\dot{\theta}_2\cos\theta_1\sin\theta_2\right) - 2b_1b_2\dot{\theta}_1\dot{\theta}_2\sin\theta_1\cos\theta_2\right] - m_2gb_2\sin\theta_2 \quad (2.29)$$

$$\frac{\partial L}{\partial \theta_2} = m_2b_2\left[-b_1\dot{\theta}_1\dot{\theta}_2\cos\theta_1\sin\theta_2 - b_1\dot{\theta}_1\dot{\theta}_2\sin\theta_1\cos\theta_2 - g\sin\theta_2\right] \quad (2.30)$$

$$\frac{\partial L}{\partial \dot{\theta}_2} = m_2\left[b_2^2\dot{\theta}_2 + b_1b_2\dot{\theta}_1\cos\theta_1\cos\theta_2 + b_1b_2\dot{\theta}_1\sin\theta_1\sin\theta_2\right] \quad (2.31)$$

$$\frac{\partial L}{\partial \dot{\theta}_2} = m_2b_2\left[b_2\dot{\theta}_2 + b_1\dot{\theta}_1\cos\theta_1\cos\theta_2 + b_1\dot{\theta}_1\sin\theta_1\sin\theta_2\right] \quad (2.32)$$

$$\frac{d}{dt}\frac{\partial L}{\partial \dot{\theta}_2} = m_2b_2\left[b_2\ddot{\theta}_2 + b_1\left(\begin{array}{l}\ddot{\theta}_1\cos\theta_1\cos\theta_2 - \dot{\theta}_1^2\sin\theta_1\cos\theta_2 - \dot{\theta}_1\dot{\theta}_2\cos\theta_1\sin\theta_2 + \\ \ddot{\theta}_1\sin\theta_1\sin\theta_2 + \dot{\theta}_1^2\cos\theta_1\sin\theta_2 - \dot{\theta}_1\dot{\theta}_2\sin\theta_1\sin\theta_2\end{array}\right)\right] \quad (2.33)$$

The plots in this study are obtained by a computer programme written according to the calculations based on Lagrange formalism given above. The codes are given in the Appendix. The motion of the double pendulum is investigated in the following criteria:

Since the initial conditions can be arranged in a continuous way, such as in steps of even 1 degree for both angles, a very large number of combinations can be obtained. But since some of them are quite similar, it is better to investigate in groups.

Each of the states is represented by a figure having four parts, *a*, *b*, *c* and *d*, each one giving a different aspect for the same particular set of initial conditions. In each of the cases, part *a* shows the variations of the two angles in terms of radians as a function of time *t*. The red curve gives the angle θ_1 swept by the upper and the black curve gives the angle θ_2 swept by the lower rod, both angles being measured with respect to the vertical axis. The time

interval is chosen to be the first 20 seconds after the system is set free from rest at the specified initial conditions.

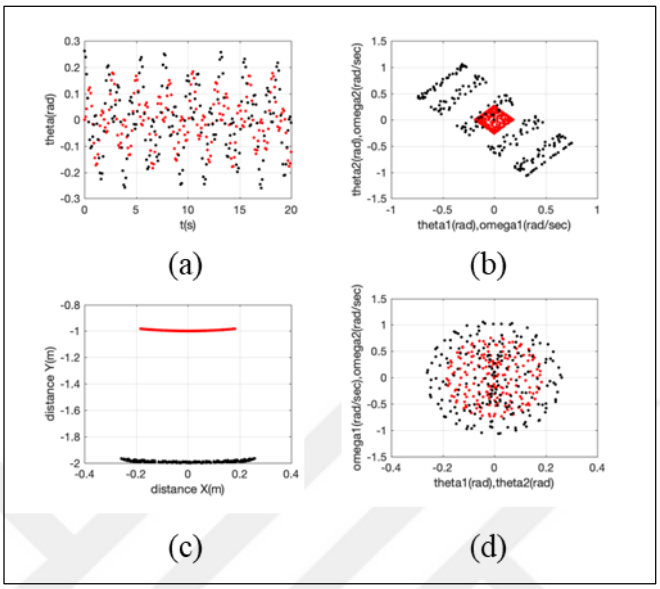


Figure 2.2. A typical representation of a macro state among various variables.

Part *b* in each figure is sort of a *phase space* giving the angular velocity $\dot{\theta}_1$ as a function of θ_1 (red curve) and $\dot{\theta}_2$ as a function of θ_2 (black curve). The angular velocities in units of radians / seconds are plotted in the vertical axis and the angles in units of radians along the horizontal. Each angle is bounded with an upper and a lower limit and those limits increase as the initial value of θ_2 and therefore the potential energy of the system get larger.

Part *c* in each figure which is like the collection of dots in a photograph printed by the photons coming from the objects, gives the tracks followed by the bobs, in terms of the lengths, the red (upper) curve corresponding to the upper bob, the lower one corresponding to the lower. Part *d* gives the relative variations of the angles, that is, θ_2 / θ_1 (red) and again the relative variations of the angular velocities, that is, $\dot{\theta}_2 / \dot{\theta}_1$ (black) for the same period of 20 seconds. (Previous b)

Before dealing with the cases studied, it is good to get familiar with the graphs. Let us examine the cases shown in Figure 1 and Fig 2. The system in Figure 2 has the least energy among the macro states chosen, where $\theta_1 = 0$ and $\theta_2 = 5^0$ only are chosen as the initial conditions. Because in this case the initial position of the centre of mass is lowest. As is

easily expected, after the system is set free under these conditions the two rods oscillate in opposite senses, with very small amplitudes, the lower one sweeping a slightly larger interval of angle. It is also obvious that at any time the two angles have opposite signs, that is, as the upper rod turns counter clockwise ($\theta_1 > 0$, *positive*), the lower one turns clockwise ($\theta_2 < 0$, *negative*). This can be seen from the negative slopes in figure *d*.

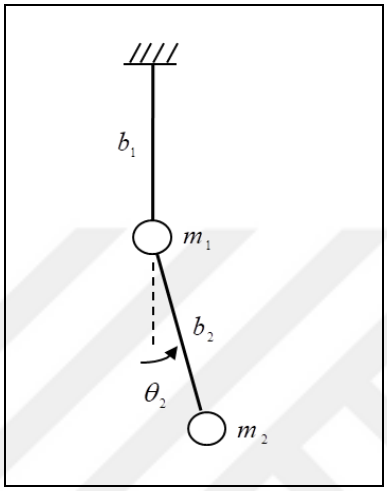


Figure 2.3. The least energy case among the macrostates chosen, where $\theta_1 = 0°$ and $\theta_2 = 5°$.

Initial conditions (in phase):

But as we will see in this work the subsequent motions of two symmetric cases like $|\theta_1, \theta_2\rangle$ and $|\theta_1, -\theta_2\rangle$ are somewhat different, for any set of angles, although they initially have exactly the same potential energy because the initial position of the centre of mass (the midpoint of the lower rod) is at the same vertical distance from the joint ($y = 0$). For those sets of angles where the initial values of the two angles are near each other, the following motions are almost in phase, they reach their maxima and minima simultaneously as can be seen from part *a* of the figures. Again we give some typical cases from this family.

As far as the angles θ_1 and θ_2 are concerned each initial state has two micro states with equal initial energy which is totally potential, because they start from rest (no initial kinetic energy). For instance the initial state "$\theta_1 = 30^0$ and $\theta_2 = 45^0$" has the same potential energy *V* as the initial state "$\theta_1 = 30^0$ and $\theta_2 = -45^0$" as long as the lengths of the two pieces are equal, that is, $b_1 = b_2 = b$. But although they are energetically degenerate states, the

subsequent motion of the double pendulum for the period taken ($0 \le t \le 20\,\text{s}$) is generally quite different.

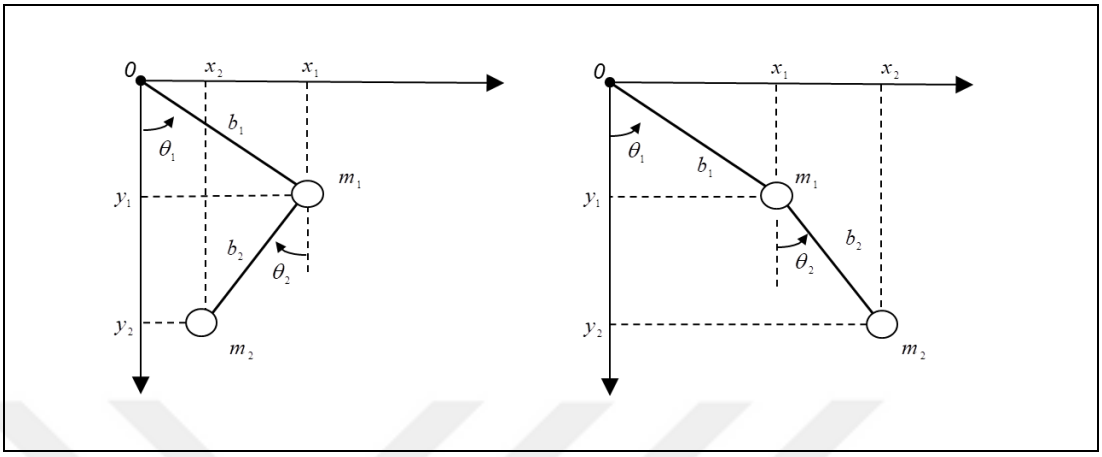


Figure 2.4. The energetically degenerate states for which upper angles are identical and lower angles are symmetrical.

We can also examine the changes in the angular velocities ω_1 $(=\dot{\theta}_1)$ and ω_2 $(=\dot{\theta}_2)$ together with the total angular momentum of the system (L_S). During the motion the two rods both start to rotate in the same sense or in opposite senses. Therefore during the course of the motion the two angular momenta are found by adding or subtracting, depending on whether the rods rotate in the same or in opposite senses respectively. [29] Also at some moments the net angular momentum vector turns out to be zero, because the two vectors may cancel exactly.

Initial conditions (out of phase):

In the following group of macrostates three of which are given below, both angles and both angular velocities are out of phase at each moment during the 20 seconds. So that in part *b* of the figures we observe a perfectly linear dependence. The pairs of initial angles that give almost the same linear behaviour in part *b* of the figures are tabulated below. But as can be seen from the table below, starting from $\theta_1 = 55^0$ and $\theta_2 = -65^0$ the linear behaviour deteriorates. In the linear cases both the angles and the angular velocities are almost opposite. That's why the graphs of "θ_2 vs. θ_1" and "$\dot{\theta}_2$ vs. $\dot{\theta}_1$" in part *b* have a slope of nearly – 1. For these cases we see from part *a* of the figures that the maxima of angle θ_1 correspond to

the minima of the other angle θ_2 and since the two rods become vertical almost simultaneously, the zeros of both angles occur at the same time.

2.3. TRIPLE PENDULUM SOLUTIONS

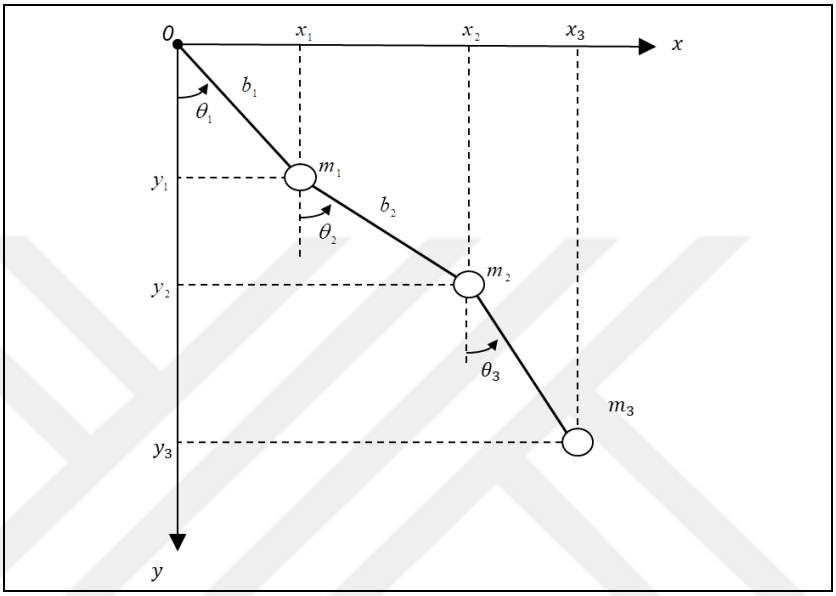


Figure 2.5. The schematic representation of a triple pendulum consisting of three bobs of different masses and three light rods of different lengths, joining the bobs. It is also the coordinate system used for the triple pendulum.

The coordinates of the three bobs of masses m_1, m_2 and m_3 that constitute a "triple pendulum". [30,31]

$$x_1 = b_1 \sin\theta_1 \tag{2.34}$$

$$y_1 = -b_1 \cos\theta_1 \tag{2.35}$$

$$x_2 = b_1 \sin\theta_1 + b_2 \sin\theta_2 \tag{2.36}$$

$$y_2 = -b_1 \cos\theta_1 - b_2 \cos\theta_2 \tag{2.37}$$

$$x_3 = b_1 \sin\theta_1 + b_2 \sin\theta_2 + b_3 \sin\theta_3 \tag{2.38}$$

$$y_3 = -b_1 \cos\theta_1 - b_2 \cos\theta_2 - b_3 \cos\theta_3 \tag{2.39}$$

The velocities of the masses:

$$\dot{x}_1 = b_1\dot{\theta}_1 \cos\theta_1 \tag{2.40}$$

$$\dot{y}_1 = -b_1\dot{\theta}_1 \sin\theta_1 \tag{2.41}$$

$$\dot{x}_2 = b_1\dot{\theta}_1 \cos\theta_1 + b_2\dot{\theta}_2 \cos\theta_2 \tag{2.42}$$

$$\dot{y}_2 = -b_1\dot{\theta}_1 \sin\theta_1 - b_2\dot{\theta}_2 \sin\theta_2 \tag{2.43}$$

$$\dot{x}_3 = b_1\dot{\theta}_1 \cos\theta_1 + b_2\dot{\theta}_2 \cos\theta_2 + b_3\dot{\theta}_3 \cos\theta_3 \tag{2.44}$$

$$\dot{y}_3 = -b_1\dot{\theta}_1 \sin\theta_1 - b_2\dot{\theta}_2 \sin\theta_2 - b_3\dot{\theta}_3 \sin\theta_3 \tag{2.45}$$

The kinetic and potential energies:

$$T = \frac{1}{2}m_1\left(\dot{x}_1^2 + \dot{y}_1^2\right) + \frac{1}{2}m_2\left(\dot{x}_2^2 + \dot{y}_2^2\right) + \frac{1}{2}m_3\left(\dot{x}_3^2 + \dot{y}_3^2\right) \tag{2.46}$$

Since

$$\begin{aligned} T = {} & \frac{m_1}{2}\left[b_1^2\dot{\theta}_1^2 \cos^2\theta_1 + b_1^2\dot{\theta}_1^2 \sin^2\theta_1\right] + \\ & \frac{m_2}{2}\left[b_1^2\dot{\theta}_1^2 \cos^2\theta_1 + b_2^2\dot{\theta}_2^2 \cos^2\theta_2 + 2b_1b_2\dot{\theta}_1\dot{\theta}_2 \cos\theta_1 \cos\theta_2 + \right. \\ & + \frac{m_3}{2}\left\{\left[b_1^2\dot{\theta}_1^2 \cos^2\theta_1 + b_2^2\dot{\theta}_2^2 \cos^2\theta_2 + b_3^2\dot{\theta}_3^2 \cos^2\theta_3\right] + \right. \\ & b_1^2\dot{\theta}_1^2 \sin^2\theta_1 + b_2^2\dot{\theta}_2^2 \sin^2\theta_2 + 2b_1b_2\dot{\theta}_1\dot{\theta}_2 \sin\theta_1 \sin\theta_2\Big] + \\ & \left[b_1^2\dot{\theta}_1^2 \sin^2\theta_1 + b_2^2\dot{\theta}_2^2 \sin^2\theta_2 + b_3^2\dot{\theta}_3^2 \sin^2\theta_3\right] + \\ & 2\left[b_1b_2\dot{\theta}_1\dot{\theta}_2 \cos\theta_1 \cos\theta_2 + b_1b_3\dot{\theta}_1\dot{\theta}_3 \cos\theta_1 \cos\theta_3 + b_2b_3\dot{\theta}_2\dot{\theta}_3 \cos\theta_2 \cos\theta_3\right] + \\ & \left. 2\left[b_1b_2\dot{\theta}_1\dot{\theta}_2 \sin\theta_1 \sin\theta_2 + b_1b_3\dot{\theta}_1\dot{\theta}_3 \sin\theta_1 \sin\theta_3 + b_2b_3\dot{\theta}_2\dot{\theta}_3 \sin\theta_2 \sin\theta_3\right]\right\} \end{aligned} \tag{2.47}$$

Now to simplify the situation we set the masses and lengths to be equal: $m_1 = m_2 = m_3 = m$ and $b_1 = b_2 = b_3 = b$.

So that

$$T = \frac{mb^2}{2}\left[\dot{\theta}_1^2 \cos^2\theta_1 + \dot{\theta}_1^2 \sin^2\theta_1\right] +$$

$$\frac{mb^2}{2}\left[\dot{\theta}_1^2 \cos^2\theta_1 + \dot{\theta}_2^2 \cos^2\theta_2 + 2\dot{\theta}_1\dot{\theta}_2 \cos\theta_1 \cos\theta_2 +\right.$$

$$\left.\dot{\theta}_1^2 \sin^2\theta_1 + \dot{\theta}_2^2 \sin^2\theta_2 + 2\dot{\theta}_1\dot{\theta}_2 \sin\theta_1 \sin\theta_2\right] +$$

$$+ \frac{mb^2}{2}\left\{\left[\dot{\theta}_1^2 \cos^2\theta_1 + \dot{\theta}_2^2 \cos^2\theta_2 + \dot{\theta}_3^2 \cos^2\theta_3\right] +\right.$$

$$2\left[\dot{\theta}_1\dot{\theta}_2 \cos\theta_1 \cos\theta_2 + \dot{\theta}_1\dot{\theta}_3 \cos\theta_1 \cos\theta_3 + \dot{\theta}_2\dot{\theta}_3 \cos\theta_2 \cos\theta_3\right] +$$

$$\left[\dot{\theta}_1^2 \sin^2\theta_1 + \dot{\theta}_2^2 \sin^2\theta_2 + \dot{\theta}_3^2 \sin^2\theta_3\right] +$$

$$\left.2\left[\dot{\theta}_1\dot{\theta}_2 \sin\theta_1 \sin\theta_2 + \dot{\theta}_1\dot{\theta}_3 \sin\theta_1 \sin\theta_3 + \dot{\theta}_2\dot{\theta}_3 \sin\theta_2 \sin\theta_3\right]\right\} \quad (2.48)$$

Choosing the lowest possible position (all the rods are vertical) as $y = 0$, the potential energy:

$$V = m_1 g\left[b_1 + b_2 + b_3 - \left(b_1 \cos\theta_1\right)\right] + m_2 g\left[b_1 + b_2 + b_3 - \left(b_1 \cos\theta_1 + b_2 \cos\theta_2\right)\right] +$$

$$m_3 g\left[b_1 + b_2 + b_3 - \left(b_1 \cos\theta_1 + b_2 \cos\theta_2 + b_3 \cos\theta_3\right)\right] \quad (2.49)$$

$$V = mg\left[3b - \left(b\cos\theta_1\right) + 3b - \left(b\cos\theta_1 + b\cos\theta_2\right) + 3b - \left(b\cos\theta_1 + b\cos\theta_2 + b\cos\theta_3\right)\right] \quad (2.50)$$

After the simplifications,

$$T = \frac{mb^2}{2}\left[3\dot{\theta}_1^2 + 2\dot{\theta}_2^2 + \dot{\theta}_3^2 + 4\dot{\theta}_1\dot{\theta}_2 \cos\left(\theta_1 - \theta_2\right) + 2\dot{\theta}_1\dot{\theta}_3 \cos\left(\theta_1 - \theta_3\right) + 2\dot{\theta}_2\dot{\theta}_3 \cos\left(\theta_2 - \theta_3\right)\right] \quad (2.51)$$

$$V = mgb\left[9 - 3\cos\theta_1 - 2\cos\theta_2 - \cos\theta_3\right] \quad (2.52)$$

Lagrangian is

$$L = T - V \quad (2.53)$$

$$L = \frac{mb^2}{2}\left[3\dot{\theta}_1^2 + 2\dot{\theta}_2^2 + \dot{\theta}_3^2 + 4\dot{\theta}_1\dot{\theta}_2\cos(\theta_1-\theta_2) + 2\dot{\theta}_1\dot{\theta}_3\cos(\theta_1-\theta_3) + 2\dot{\theta}_2\dot{\theta}_3\cos(\theta_2-\theta_3)\right] - mgb\left[9 - 3\cos\theta_1 - 2\cos\theta_2 - \cos\theta_3\right] \tag{2.54}$$

On the other hand Lagrange equations are

$$\frac{d}{dt}\left(\frac{\partial L}{\partial \dot{\theta}_1}\right) - \frac{\partial L}{\partial \theta_1} = 0 \tag{2.55}$$

$$\frac{d}{dt}\left(\frac{\partial L}{\partial \dot{\theta}_2}\right) - \frac{\partial L}{\partial \theta_2} = 0 \tag{2.56}$$

$$\frac{d}{dt}\left(\frac{\partial L}{\partial \dot{\theta}_3}\right) - \frac{\partial L}{\partial \theta_3} = 0 \tag{2.57}$$

$$\frac{\partial L}{\partial \theta_1} = \frac{mb^2}{2}\left[-4\dot{\theta}_1\dot{\theta}_2\sin(\theta_1-\theta_2) - 2\dot{\theta}_1\dot{\theta}_3\sin(\theta_1-\theta_3)\right] - 3mgb\sin\theta_1 \tag{2.58}$$

$$\frac{\partial L}{\partial \theta_2} = \frac{mb^2}{2}\left[4\dot{\theta}_1\dot{\theta}_2\sin(\theta_1-\theta_2) - 2\dot{\theta}_2\dot{\theta}_3\sin(\theta_2-\theta_3)\right] - 2mgb\sin\theta_2 \tag{2.59}$$

$$\frac{\partial L}{\partial \theta_3} = \frac{mb^2}{2}\left[2\dot{\theta}_1\dot{\theta}_3\sin(\theta_1-\theta_3) + 2\dot{\theta}_2\dot{\theta}_3\sin(\theta_2-\theta_3)\right] - mgb\sin\theta_3 \tag{2.60}$$

$$\frac{\partial L}{\partial \dot{\theta}_1} = \frac{mb^2}{2}\left[6\dot{\theta}_1 + 4\dot{\theta}_2\cos(\theta_1-\theta_2) + 2\dot{\theta}_3\cos(\theta_1-\theta_3)\right] \tag{2.61}$$

$$\frac{\partial L}{\partial \dot{\theta}_2} = \frac{mb^2}{2}\left[4\dot{\theta}_2 + 4\dot{\theta}_1\cos(\theta_1-\theta_2) + 2\dot{\theta}_3\cos(\theta_2-\theta_3)\right] \tag{2.62}$$

$$\frac{\partial L}{\partial \dot{\theta}_3} = \frac{mb^2}{2}\left[2\dot{\theta}_3 + 2\dot{\theta}_1\cos(\theta_1-\theta_3) + 2\dot{\theta}_2\cos(\theta_2-\theta_3)\right] \tag{2.63}$$

$$\frac{d}{dt}\left(\frac{\partial L}{\partial \dot{\theta}_1}\right) = \frac{mb^2}{2}\left[6\ddot{\theta}_1 + 4\ddot{\theta}_2\cos(\theta_1-\theta_2) - 4\dot{\theta}_2(\dot{\theta}_1-\dot{\theta}_2)\sin(\theta_1-\theta_2) + 2\ddot{\theta}_3\cos(\theta_1-\theta_3) - 2\dot{\theta}_3(\dot{\theta}_1-\dot{\theta}_3)\sin(\theta_1-\theta_3)\right] \tag{2.64}$$

$$\frac{d}{dt}\left(\frac{\partial L}{\partial \dot{\theta}_2}\right) = \frac{mb^2}{2}\left[4\ddot{\theta}_2 + 4\ddot{\theta}_1\cos(\theta_1-\theta_2) - 4\dot{\theta}_1(\dot{\theta}_1-\dot{\theta}_2)\sin(\theta_1-\theta_2) + 2\ddot{\theta}_3\cos(\theta_2-\theta_3) - 2\dot{\theta}_3(\dot{\theta}_2-\dot{\theta}_3)\sin(\theta_2-\theta_3)\right] \tag{2.65}$$

$$\frac{d}{dt}\left(\frac{\partial L}{\partial \dot{\theta}_3}\right)=\frac{mb^2}{2}\left[2\ddot{\theta}_3+2\ddot{\theta}_1\cos(\theta_1-\theta_3)-2\dot{\theta}_1(\dot{\theta}_1-\dot{\theta}_3)\sin(\theta_1-\theta_3)\right.$$
$$\left.+2\ddot{\theta}_2\cos(\theta_2-\theta_3)-2\dot{\theta}_2(\dot{\theta}_2-\dot{\theta}_3)\sin(\theta_2-\theta_3)\right] \tag{2.66}$$

$$\frac{d}{dt}\left(\frac{\partial L}{\partial \dot{\theta}_1}\right)-\frac{\partial L}{\partial \theta_1}=0 \tag{2.67}$$

$$\frac{mb^2}{2}\left[6\ddot{\theta}_1+4\ddot{\theta}_2\cos(\theta_1-\theta_2)-4\dot{\theta}_2(\dot{\theta}_1-\dot{\theta}_2)\sin(\theta_1-\theta_2)\right.$$
$$\left.+2\ddot{\theta}_3\cos(\theta_1-\theta_3)-2\dot{\theta}_3(\dot{\theta}_1-\dot{\theta}_3)\sin(\theta_1-\theta_3)\right] \tag{2.68}$$

$$-\frac{mb^2}{2}\left[-4\dot{\theta}_1\dot{\theta}_2\sin(\theta_1-\theta_2)-2\dot{\theta}_1\dot{\theta}_3\sin(\theta_1-\theta_3)\right]+3mgb\sin\theta_1=0 \tag{2.69}$$

$$\frac{mb^2}{2}\left[6\ddot{\theta}_1+4\ddot{\theta}_2+2\ddot{\theta}_3\right]+3mgb\theta_1=0 \tag{2.70}$$

$$3\ddot{\theta}_1+2\ddot{\theta}_2+\ddot{\theta}_3=-3\frac{g}{b}\theta_1 \tag{2.71}$$

$$\frac{d}{dt}\left(\frac{\partial L}{\partial \dot{\theta}_2}\right)-\frac{\partial L}{\partial \theta_2}=0 \tag{2.72}$$

$$\frac{mb^2}{2}\left[4\ddot{\theta}_2+4\ddot{\theta}_1\cos(\theta_1-\theta_2)-4\dot{\theta}_1(\dot{\theta}_1-\dot{\theta}_2)\sin(\theta_1-\theta_2)\right.$$
$$\left.+2\ddot{\theta}_3\cos(\theta_2-\theta_3)-2\dot{\theta}_3(\dot{\theta}_2-\dot{\theta}_3)\sin(\theta_2-\theta_3)\right]$$
$$-\frac{mb^2}{2}\left[4\dot{\theta}_1\dot{\theta}_2\sin(\theta_1-\theta_2)-2\dot{\theta}_2\dot{\theta}_3\sin(\theta_2-\theta_3)\right]+2mgb\sin\theta_2=0 \tag{2.73}$$

$$\frac{mb^2}{2}\left[4\ddot{\theta}_1+4\ddot{\theta}_2+2\ddot{\theta}_3\right]+2mgb\theta_2=0 \tag{2.74}$$

$$2\ddot{\theta}_1+2\ddot{\theta}_2+\ddot{\theta}_3=-2\frac{g}{b}\theta_2 \tag{2.75}$$

$$\frac{d}{dt}\left(\frac{\partial L}{\partial \dot{\theta}_3}\right)-\frac{\partial L}{\partial \theta_3}=0 \tag{2.76}$$

$$\frac{mb^2}{2}\left[2\ddot{\theta}_3+2\ddot{\theta}_1\cos(\theta_1-\theta_3)-2\dot{\theta}_1(\dot{\theta}_1-\dot{\theta}_3)\sin(\theta_1-\theta_3)\right.$$
$$\left.+2\ddot{\theta}_2\cos(\theta_2-\theta_3)-2\dot{\theta}_2(\dot{\theta}_2-\dot{\theta}_3)\sin(\theta_2-\theta_3)\right]$$
$$-\frac{mb^2}{2}\left[2\dot{\theta}_1\dot{\theta}_3\sin(\theta_1-\theta_3)+2\dot{\theta}_2\dot{\theta}_3\sin(\theta_2-\theta_3)\right]+mgb\sin\theta_3=0 \tag{2.77}$$

$$\frac{mb^2}{2}\left[2\ddot{\theta}_1 + 2\ddot{\theta}_2 + 2\ddot{\theta}_3\right] + mgb\theta_3 = 0 \tag{2.78}$$

$$\ddot{\theta}_1 + \ddot{\theta}_2 + \ddot{\theta}_3 = -\frac{g}{b}\theta_3 \tag{2.79}$$

After solving the above Lagrange equations for the triple pendulum system, and making appropriate mathematical simplifications for small angles, the resulting equations of motion are shown in Table 2.1.

Table 2.1. Equations of motion of triple pendulum.

Eom I	$3\ddot{\theta}_1 + 2\ddot{\theta}_2 + \ddot{\theta}_3 = -3\frac{g}{b}\theta_1$
Eom II	$2\ddot{\theta}_1 + 2\ddot{\theta}_2 + \ddot{\theta}_3 = -2\frac{g}{b}\theta_2$
Eom III	$\ddot{\theta}_1 + \ddot{\theta}_2 + \ddot{\theta}_3 = -\frac{g}{b}\theta_3$

2.4. ROTATIONAL INERTIA

It is known that if a point particle of mass *m* is to turn around an axis at a radius of *r*, then its moment of inertia is $I = mr^2$. But in our system there are two bobs, one with mass m_1 (rotating always at the same radius $r_1 = b_1$) and the other with mass m_2 (rotating at the variable radius $r_2^2 = x_2^2 + y_2^2$ relative to zero).

The total rotational inertia has a lower limit of $I_{\min} = m_1 b_1^2$ at times where the second bob passes by the origin and assuming that $b_1 = b_2 = b$. The total inertia has an upper limit of $I_{\max} = m_1 b_1^2 + m_2 (b_1 + b_2)^2$:

$$\left[m_1 b_1^2\right] \le I \le \left[m_1 b_1^2 + m_2 (b_1 + b_2)^2\right]$$

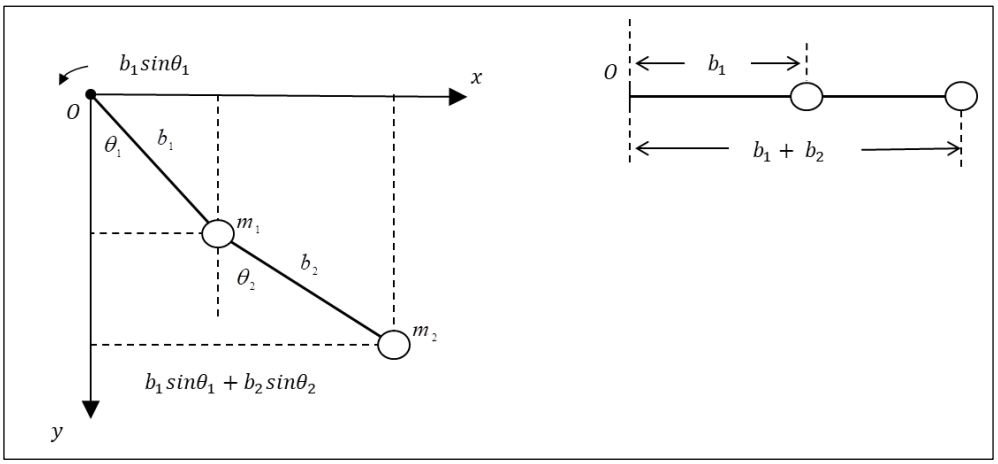


Figure 2.6. General representation of rotational inertia of the double pendulum.

If $b_1 = b_2 = b$ and $m_1 = m_2 = m$, then $\left[mb^2\right] \leq I \leq \left[5mb^2\right]$

A plot for inertia (*I*) vs. time (*t*) can be given for each of the above cases.

2.5. ANGULAR MOMENTUM

The double pendulum system has an angular momentum vector $\vec{L}$ during the motion given as

$$\vec{L} = I_1 \vec{\omega}_1 + I_2 \vec{\omega}_2 \tag{2.80}$$

For those parts of the motion where one segment is rotating clockwise while the other turns counterclockwise, the overall angular momentum vector may point in $+z$ or $-z$ direction. Also in passing from one sense to the other angular momentum becomes zero instantaneously. There are several combinations of masses, lengths and angular velocities for which $L = 0$.

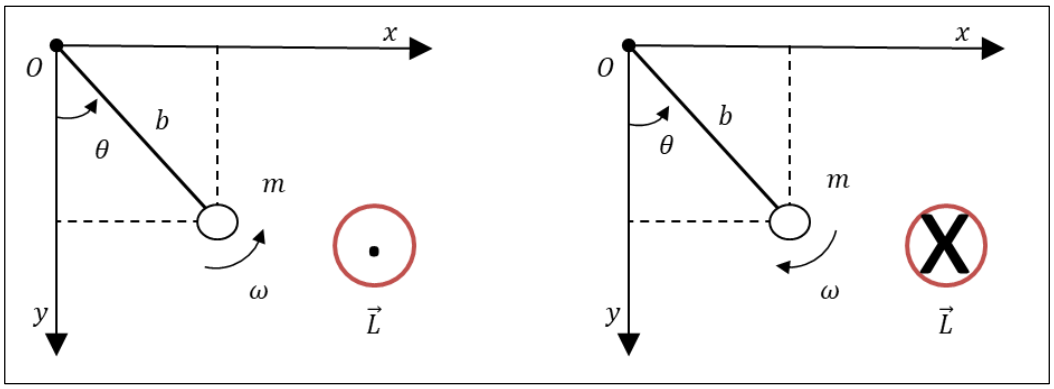


Figure 2.7. The angular momentum vectors ($\vec{L}$) for counterclockwise (left) and clockwise (right) rotations of a simple pendulum.

The maximum values for L are obtained where the two bobs move in the same sense and at relatively high angular velocities.

The overall maximum value for L is obtained for

$$L_{max} = mb^2\omega_1 + 4mb^2\omega_2 \tag{2.81}$$

where ω_1 and ω_2 are the angular velocities of the two bobs respectively.

2.6. FORCE ON JOINTS

In this analysis we will also examine the force exerted on the joint that attaches it to the frame under different initial conditions. At any time t ($t > 0$) during the motion there are tensions T_1 and T_2 in the upper and lower rods respectively. The tension T_1 will also act on the joint and will change around an average value. We will find this average $\langle T_1 \rangle$ and the fluctuations around it from the plots drawn by the help of a computer programme under various initial conditions of the angles θ_1 and θ_2. This analysis may give us for which initial values of the angles the maximum value of the tension will exceed the safety limit that was set beforehand. Also the time average of the tension will give an idea about the long term load on the joint. The equations of motion can be written as,

$$T_1 - (m_1 g)\cos\theta_1 - T_2\cos(\theta_2 - \theta_1) = m_1\omega_1^2 b_1 \tag{2.82}$$

$$T_2 - (m_2 g)\cos\theta_2 = m_2\omega_2^2 b_2 \tag{2.83}$$

$$\vec{v}_1 = (v_1\cos\theta_1)\hat{e}_1 + (v_1\sin\theta_1)\hat{e}_2 \tag{2.84}$$

$$\vec{v}_2 = (v_2\cos\theta_2)\hat{e}_1 + (v_2\sin\theta_2)\hat{e}_2 \tag{2.85}$$

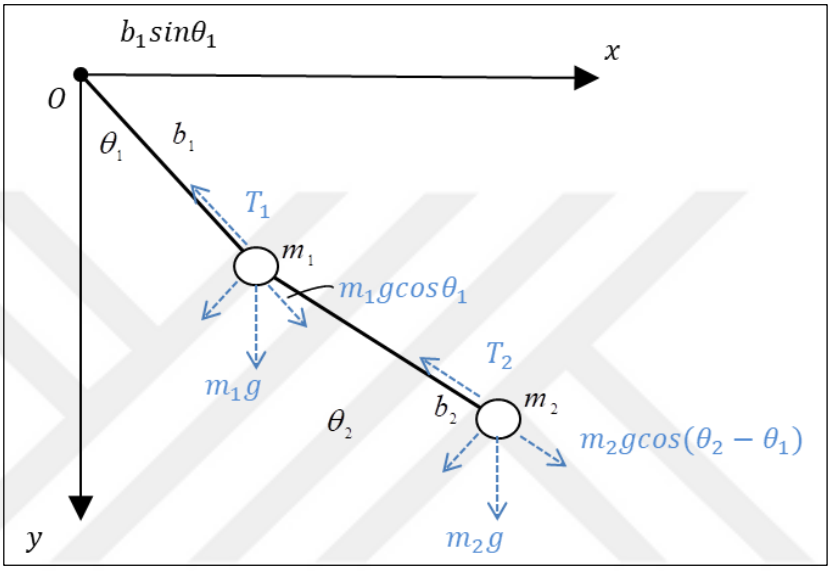


Figure 2.8. The forces, i.e. tensions and weights, acting on the system when it is oscillating.

In this analysis in order to calculate the values of the linear velocities v_1 and v_2, together with the angular velocities ω_1 and ω_2 we use Lagrangian dynamics. The system has two degrees of freedom, namely, *x* and *y*. It may only move in a vertical plane. In all cases the bobs are initially at rest so they do not have any *initial* kinetic energy *T*, but some (negative) potential energy *V*.

2.7. OSCILLATIONS AND CHAOS

Oscillations are systems that exhibit repetitive periodic movements. For example, in a pendulum, these systems can be mathematically described by oscillation equations and their movements can be expressed by periodic functions. The starting point is the observation of ordered and disordered motions like those occurring in the double pendulum. The

oscillations of double pendulum are an example of nonlinear phenomena which is a characteristic arising in a mathematical system or model when the outputs do not depend linearly on the inputs. This may cause the behaviour of the system in question to be sensitive to changes in input and may therefore increase the uncertainty. Nonlinear systems often exhibit chaotic behaviour and can give rise to deterministic chaos.

Toward the end of the nineteenth century, Henri Poincaré (1854 – 1912) who was a French mathematician and physicist, also the "father of nonlinear dynamics" pointed out for the first time that an irregular behaviour in mechanics is not at all an unusual feature if the system being studied involves a nonlinear interaction. A simple deterministic differential equation involving nonlinearities may have solutions the behaviour of which over longer time periods evolves quite irregularly and practically cannot be predicted. This is one of the characteristic features of chaotic systems. The meaning of this concept, which may be precisely defined in the frame of nonlinear dynamics, extends far beyond mechanics, since the phenomenon of chaos can be observed in various fields.

Chaos is the phenomenon where a system exhibits unpredictable and seemingly random movements despite behaving deterministically according to specific laws, due to the significant effects of small initial conditions. [32] These types of systems are called chaotic systems. Chaotic systems sometimes transition from periodic movements to chaotic movements when they exceed a certain threshold value (threshold). This transition is called a chaos transition and a small change in the system can trigger this transition.In this case, we are referring to deterministic chaos, which is defined as the motion of a system that is sensitive to initial conditions, rather than randomness. Deterministic chaos is always associated with nonlinear systems, as linearity is not a sufficient condition for chaos, although it is necessary. [33] Chaos arises when a system is sensitive to its previous state. Even a small effect can change the conditions so much that the future may be entirely different.

Chaos is an aperiodic long-time behaviour arising in a deterministic dynamical system that exhibits a sensitive dependence on initial conditions.

We use phase portraits to visually represent all possible movements in a dynamic system. A phase diagram takes all the variables of the system as coordinates and shows the current state of the system as a point on these coordinates. The phase portraits show how these points are

related to each other and what movements are possible. [34] For example, a phase portrait for a pendulum system takes the angular position and angular velocity of the pendulum as coordinates and shows the current state of the system as a point on these coordinates. These points show how the pendulum's movement evolves and provide a visual representation of the possible movements of the pendulum. The phase portrait is an important tool in the analysis of dynamic systems and is particularly useful in understanding the behaviour of chaotic systems. By plotting the trajectories of many different initial conditions in phase space, one can gain insight into the overall behaviour of the system, including the presence of fixed points, periodic orbits, and chaotic behaviour.

2.7.1. Poincare Sections

Poincaré section is a graphical representation of all possible motions in a dynamic system, on a specific surface. This representation was developed by Henri Poincaré and is an analysis method used to understand the complex nature of system movements. Poincaré section is used to capture the recurring behaviours of a system and to visualize its characteristics. When plotting the solutions to some nonlinear problems, the phase space can become overcrowded and the underlying structure may become obscured. To reduce these difficulties, a basic tool was proposed by Henri Poincaré. They also allow researchers to identify certain features of the system's dynamics, such as periodic orbits and bifurcations that might be difficult to see in the full phase space. By analysing Poincaré sections, researchers can gain insights into the structure of chaotic systems, predict the behaviour of these systems over time and even check chaotic behaviour through feedback control. To create a Poincaré section, it is necessary to calculate the moments when the system movements intersect with the surface and record the corresponding states at those moments. These data can then be graphically displayed and used to identify the repeated patterns in the movements of the system.

2.7.2. Bifurcation Diagram

A bifurcation is very simply a splitting into two (bi – two). It is so called due to the shape of the curves resembling a two-pin fork. At a certain point the subsequent development of the system may split into two different scenarios. A bifurcation diagram is a graph that visually

represents how the behaviour in a mathematical model changes depending on the variation of parameters. [35] In this diagram, for each parameter value, the system's behaviour is shown to be a point, a curve or chaos. In chaos, the bifurcation diagram can be used as a visual representation of the complex structure of the system's behaviour. In chaotic systems, a small change in a parameter can cause significant and unpredictable changes in the system's behavior. A bifurcation diagram, which represents these changes visually, is an important tool for understanding and predicting the behaviour of chaotic systems.

2.7.3. Lyapunov Exponents

One method to quantify the sensitive dependence on initial conditions for chaotic behaviour uses the Lyapunov (1857 – 1918) characteristic exponent, λ. It is the average rate of divergence (or convergence) of two neighbouring trajectories in the phase space. [36] Actually there is a whole spectrum of Lyapunov exponents. Their number is equal to the dimension of the phase space. [37] If only a single exponent is cited, it is the largest one.

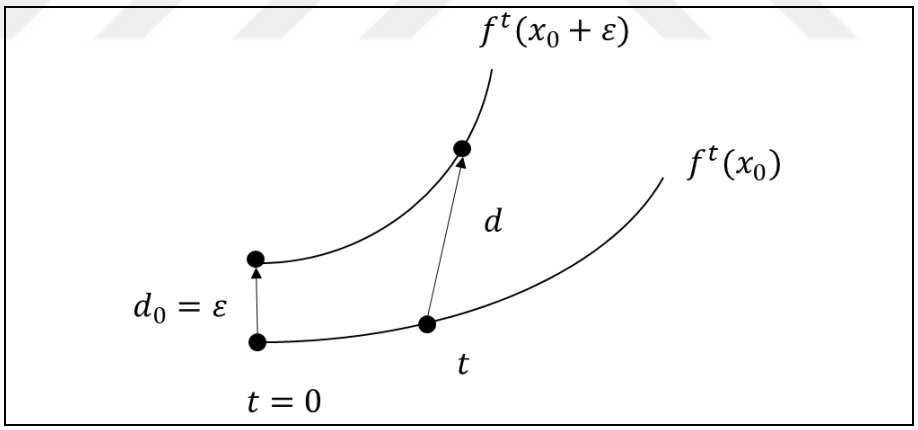


Figure 2.9. The neighbour trajectories with difference , ε

$$d_i = \varepsilon\, e^{\lambda i} \tag{2.86}$$

Let two initial states differ by a small amount, x_0, $x_0 + \varepsilon$ where epsilon $\ll x_0$. We reach the value of x_i after i iterations starting from two neighbouring initial values. After i iterations, the difference d_i between the two x_i values is approximately,

$$\Delta(\varepsilon, t) \approx |f^t(x_0+\varepsilon) - f^t(x_0)| \tag{2.87}$$

$$\varepsilon e^{t\lambda(x_0)} \approx |f^t(x_0+\varepsilon) - f^t(x_0)| \tag{2.88}$$

where ε is small, t is large. $\varepsilon \to 0$

$$\varepsilon e^{t\lambda(x_0)} \approx \lim_{\varepsilon\to 0}\left|\frac{f^t(x_0+\varepsilon) - f^t(x_0)}{\varepsilon}\right| \tag{2.89}$$

$$\varepsilon e^{t\lambda(x_0)} \approx \lim_{\varepsilon\to 0}\left|\frac{d}{d_x}f^t(x_0)\right| \tag{2.90}$$

$$\lambda(x_0) = \frac{1}{t}\ln\left|\frac{d}{d_x}f^t(x_0)\right| \tag{2.91}$$

$$\lambda(x_0) = \frac{1}{t}\ln\left|\frac{d}{d_x}f^t(x_0), \frac{d}{d_x}f^t(x_1) \dots \frac{d}{d_x}f^t(x_{t-1})\right| \tag{2.92}$$

$$\lambda(x_0) = \frac{1}{t}\sum_{k=0}^{t-1}\ln\left|\frac{d}{d_x}f^t(x_k)\right| \tag{2.93}$$

$$\lambda(x_0) = \lim_{t\to\infty}\frac{1}{t}\sum_{k=0}^{t-1}\ln\left|\frac{d}{d_x}f^t(x_k)\right| \tag{2.94}$$

If λ is negative, the two orbits finally converge, but if λ is positive, the nearby trajectories diverge and chaos results.

Given a continuous dynamical system in an *i* -dimensional phase space, we monitor the long-term evolution of an infinitesimal n-sphere of initial conditions. The sphere will become an n-ellipsoid due to the locally deforming nature of the flow. The $i-th$ one dimensional Lyapunov exponent be defined as follows:

$$\lambda_i = \lim_{t\to\infty}\frac{1}{t}\ ln\frac{\lambda_{i+1}}{\lambda_i} \tag{2.95}$$

The Figure 2.10 depicts the schematic representation of the transition from ordered motion to chaotic regime in a periodic motion. As shown in the equations above, the Lyapunov exponents are calculated using appropriate algorithms and can take positive, zero, or negative values. Based on these values, we can determine the predicted behaviors of the motion corresponding to these states in Table 2.2.

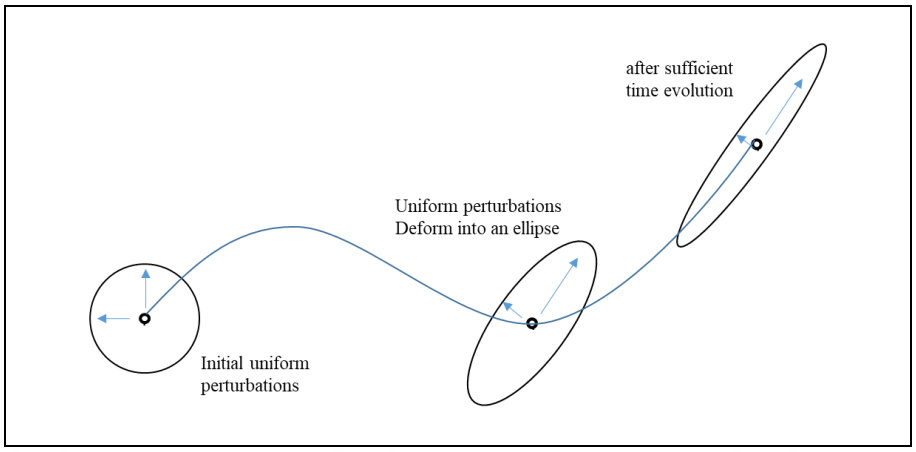
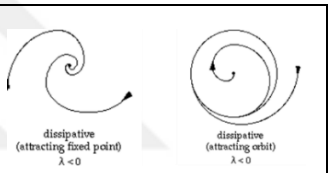
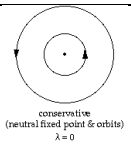


Figure 2.10. The perturbations from uniform to chaotic.

Table 2.2. The Lyapunov exponents, λ values and results.

$\lambda < 0$	the system is attracted to a fixed point or stable periodic orbit. These systems are nonconservative (dissipative) and exhibit asymptotic stability.	
$\lambda = 0$	the system is neutrally stable. Such systems are conservative and in a steady state mode. They exhibit Lyapunov stability.	
$\lambda > 0$	the system is chaotic and unstable. Nearby points will diverge irrespective of how close they are.	

3. MATERIALS AND METHODS

At the beginning of our study, we started with constructing a double pendulum in the lab and examining the motion experimentally. We compared the results obtained from the setup and from the solutions to the mathematical equations. The mechanical set was created as shown in the figure below. You can find the details of the experimental set in Appendix A.

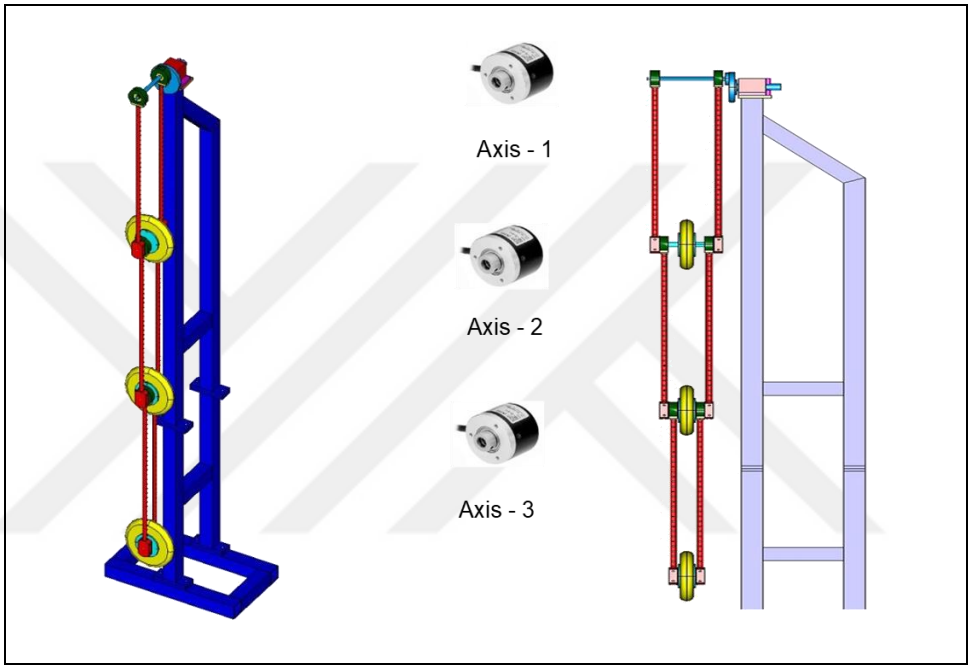


Figure 3.1. The design view of experimental triple pendulum set

The experimental setup was designed and produced with a steel pendulum mass and lightweight aluminium bars in order to approximate the system to a theoretical double pendulum. The intended model was a pendulum consisting of a massless bar and a weight positioned at its end. The designed mass and bar connections in the experimental setup had a structure that could be changed to fit the binary and ternary pendulum structures. To collect data on the pendulum design, encoders and communication cables were added to the pendulum structure. An optical and incremental encoder was selected to convert the data. An encoder is a device or process that converts data from one format to another. In position sensing, an encoder is a device that can detect and convert mechanical motion to an analog or digital coded output signal. Specifically, it measures position, while velocity, acceleration, and direction can be derived from the position in either linear or angular motion. We

connected the encoder to the computer using a converter and recorded the data based on motion and certain time intervals with the code we wrote in the C language on the computer. Thus, all the movements of the pendulum with different motions according to the initial conditions were recorded. However, as the initial values of the experimental setup increased, the created model began to fail against forces arising from physical motion and affect the pendulum's movement. Due to the mechanical constraints of the experimental setup, the operating range was limited to approximately 25-degree initial value inputs. To be able to work with a wider range of angles, we selected the simulation method due to the physical difficulties and uncertainty problems. Using the simulation programme, we could obtain all possible angle values with different initial conditions and observe critical angle values where certain phenomena occur and some parameters switch to a different regime.

The solutions for double pendulum problems involve mathematical techniques such as differential equations, numerical methods and chaos theory. [38] One approach to solving the double pendulum problem is to use Lagrangian mechanics and to derive a set of second-order differential equations that describe the motion of the system. Another method is to use numerical techniques to simulate the motion of the double pendulum system. This involves discretizing the equations of motion and using numerical integration techniques to solve them. This method is useful for studying the long-term behaviour of the system and for visualizing the complex and chaotic motion of the double pendulum. As for materials, a double pendulum can be constructed using simple materials such as two masses (e.g. small weights or balls), two massless strings and a support structure (such as a rod or stand). The masses can be attached to the strings and suspended from the support structure to create the double pendulum. The lengths of the strings and the masses of the weights can be varied to study the effects of these parameters on the motion of the system. [39]

In addition to these methods, chaos theory provides a useful framework for understanding the complex behaviour of the double pendulum system. The double pendulum is a classic example of a chaotic system, meaning that small differences in initial conditions can lead to vastly different outcomes over time. As such, chaos theory can be used to study the sensitivity of the system on initial conditions and to identify the regions of phase space where the system exhibits chaotic behaviour.

By the established mathematical model, a lot of data were obtained and some critical ranges were determined due to the estimated values. Accordingly using different mathematical tools

for the existing equation we planned to advance the work for defining and elaborating more of these regions.

For the tool for simulating and analysing the behaviour of complex physical systems, double and triple pendulum we use a computer programme which is written in Matlab. With the right initial conditions, equations and visualization tools, we can gain a deep understanding of the dynamics of this fascinating system. By the mathematical model we define the initial conditions: You need to define the initial values of the angles and angular velocities of the double pendulum. This will determine the starting position and motion of the pendulum. Set up the equations of motion: The equations of motion for the double pendulum need to be set up in Matlab. We obtained the equations of motion for pendulums by solving them both manually and symbolically in Matlab program. Solve the equations of motion: Matlab has built-in solvers such as ODE45 that can be used to solve the differential equations that describe the motion of the double pendulum. Visualize the results: Once you have solved the equations, you can plot the motion of the double pendulum using the visualization tools of Matlab. This can help you to better understand the behaviour of the system and to identify any interesting phenomena.

In the algorithm, each pendulum solution was run for 20 seconds, each second segment is divided into 100 intervals. Since it was understood that there were not enough data with shorter intervals, 20-second periods were chosen as the optimum time. In other words, all values such as position and speed are calculated 2001 times in a time period of 20 seconds.

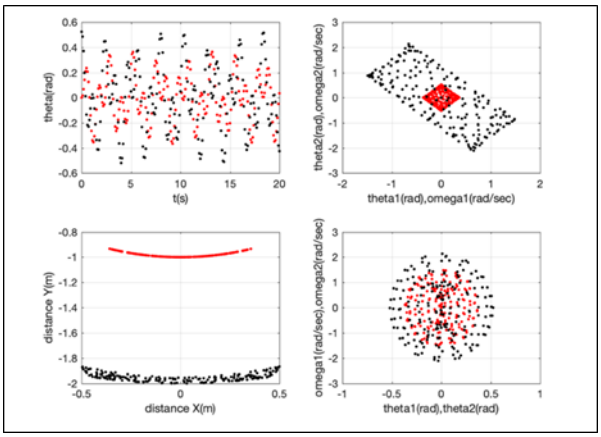


Figure 3.2. The representation of solution graphics, angles values, positions of bobs and phase spaces versus initial angle values.

In the Figure 3.2, there is a typical representation of the solutions obtained by the computer programme. Figure (a) represents the changing values of the two angles versus time. Red dots are θ_1 values of upper bob, black dots are θ_2 values of lower bob versus time, t(s). Figure (b) represents the angle and velocity values relative to each other. Red dots are the values of upper bob, θ_2 versus θ_1, black dots are the values of lower bob, ω_2 versus ω_1. Figure (c) represents the positions of the lower and upper masses of the pendula in x-y coordinates. Red dots represent the upper bob, black dots denote the lower bob. Figure (d) exhibits the relationship between the angles and angular velocities, horizontal axis for the angle, vertical axis for the velocity respectively. Red dots show the lower bob, black dots show the upper bob.

After establishing the pendulum model, we examined all the states of both the double and triple pendulum according to the diagram in the Figure 3.3. By generating the models for the motion, we were able to deduce the differences and behaviours between them.

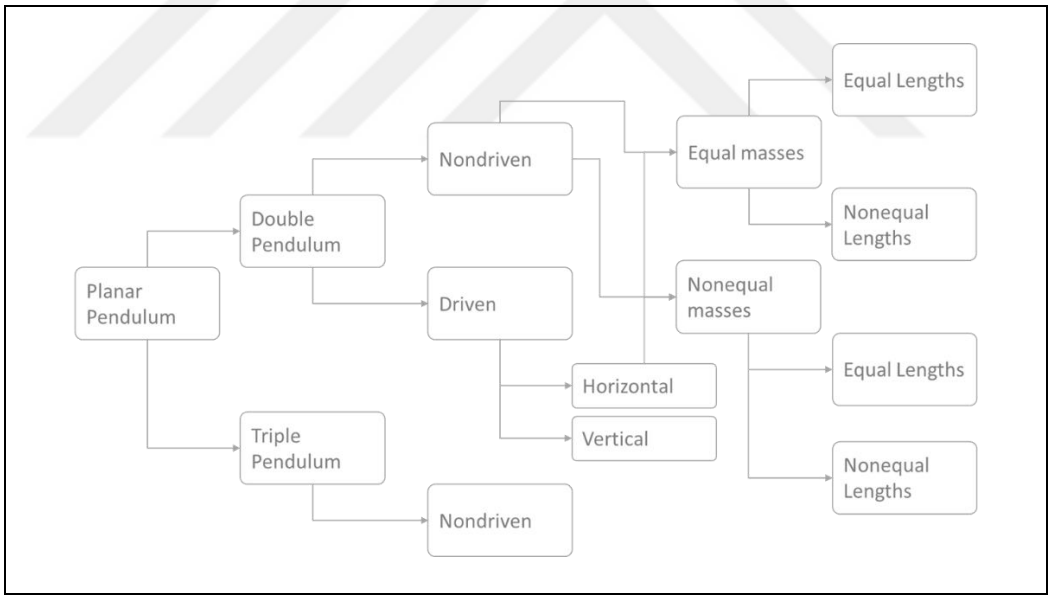


Figure 3.3. The examination path of double and triple pendulum.

Our work is summarized in the above schema. The calculations for all the boxes are carried out and some graphs for each are plotted in the thesis. For all states which are stationary states and vibrating states, the different combinations of the two angles are compared. The set of two angles that we group for simplicity are incremented in steps of 15 degrees. There are three zones as small, medium and large ranges.(as seen in Table 3.1)

Table 3.1. The three angular regions under investigation for the pendulum at initial conditions.

Small angles region	0 to 30 degrees
Medium angles region	30 to 60 degrees
Large angles region	60 to 90 degrees

The examined regions were changed from 0 to 90 degrees for θ_1, from -90 to 90 degrees for θ_2. In detailed calculations, we examined all angles by the one-degree intervals. As one set of work, we have obtained a total of 16.647 graphical results.

The total data set we reached amount to 15 sets. Solution set with equal parameters, Solution set for different lengths as b_2=0.5 and 1, Solution set for different masses as m_2=0.5 and 1, Solution set for external horizontal vibrations with different amplitudes and different frequencies such as a=0.25 and 0.5, ω=1 and 3, Solution set for external vertical vibrations with different amplitudes and different frequencies such as a=0.25 and 0.5, ω=1 and 3, Solution set for triple pendula with equal parameters. A total of 247.065 graphics were obtained in the calculations.

4. STATIONARY STATES OF DOUBLE PENDULUM

In this study the initial states are represented in a way similar to the quantum mechanical states by kets (vectors). For example a ket like $|\theta_1 = 15, \theta_2 = 45; S\rangle$ represents that at time $t = 0$ the upper angle is $\theta_1 = 15$ degrees, the lower angle is $\theta_2 = 45$ degrees and the *S* means that the joint where the double pendulum is attached to the wall is stationary.

In the following analysis the stationary (*S*) states using different combinations of the two angles are compared. In the study both of the two angles are incremented in steps of 1 degree but in this thesis we group them for simplicity, into three:

a- low (0^0 / 15^0)

b- medium (30^0 / 45^0 / 60^0)

c- high (75^0 / 90^0)

In each of the figures the red dots represent the position or velocity of the upper bob (ball) and the black dots do the same for the lower bob. Since we limit each of the angles θ_1 and θ_2 to three groups there are basically $3 \times 3 = 9$ combinations. Let us at first examine these combinations and then introduce the negative angles (all stationary) and finally examine the effects of the external vibrations of the joint on the subsequent motion of the double pendulum.

Each figure consists of four parts: Part **a** shows the time variations of the two angles within the first 20 seconds in terms of radians. For instance if the upper angle represented by the red dots or curve remains within the limits $-0.2 < \theta_1 < 0.2$ it means the upper rod oscillates between up to $0.2rad \cong 12^0$ (counter clockwise) and up to $-0.2rad \cong -12^0$ (clockwise). If the black dots representing the lower bob vary between $-10 < \theta_2 < 25$ in a certain figure, then this means that the lower rod oscillates up to 10 radians clockwise which corresponds to three clockwise rotations and up to 25 radians, a four-fold rotation in the counter clockwise sense.

4.1. REPRESENTATIONS OF STATIONARY OF DOUBLE PENDULUM

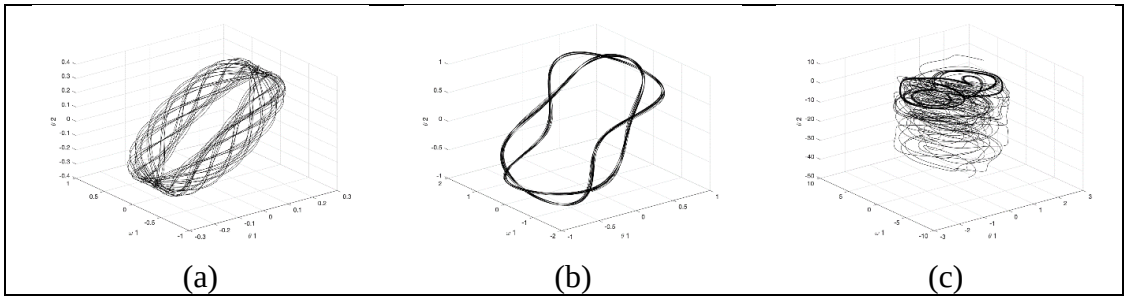
We have obtained solutions at a basic type for a double pendulum consisting of equal masses, $m_1 = m_2 = m$ and equal massless rods, $b_1 = b_2 = b$. Figure 4.2 illustrates the motion of θ_2 within the small, medium, and large angle ranges from 15 to 90 degrees, corresponding to the example of a 15-degree angle in the small angle range of θ_1. At the outset of the small range of θ_1 and θ_2 demonstrate close proximity in their motion and perform oscillatory movement in tandem. Figure 4.3 presents the resulting graphs of θ_2 with symmetric angles in Figure 4.2 for the same small angle value of θ_1. Due to the inverse angles of θ_1 and θ_2 at the outset, θ_2 synchronously oscillates in a narrower range. Similarly, Figures 4.4 and 4.5 depict the graphs corresponding to the medium angle range of θ_1, while Figures 4.6 and 4.7 portray those corresponding to the large angle range of θ_1. Finally, Figures 4.8 and 4.9 demonstrate the angle, position, and angular-velocity results over time for the θ_2 values corresponding to the largest θ_1 angle utilized in this study.

The entire set was solved for both positive and symmetric values, as well as negative angles. In order to examine the relationship between θ_1, θ_2, and their velocities, internal dimension graphs were obtained with θ_1, θ_2, and ω_1. Poincaré sections were also obtained to enable more convenient examination of these graphs for small, medium, and large angles. Different regions correspond to different energy levels depending on the initial angles. Initial angles with small angles correspond to low energy levels. The low energy levels are considered as regions where the upper and lower masses oscillate together and uniform motion occurs.

In Figure 4.2 it is seen that as θ_2 increases from 15 to 90 degrees in steps of 15 degrees, while θ_1 is set to 15 degrees for all the six microstates the two angles get a phase difference. Similarly, as seen from parts b also the angular velocities ω_1 and ω_2 follow such a pattern. It is also seen from the roughly circular shape in parts d that θ_2 has a larger range than θ_1. On the other hand as each of the angles gets the left or right limit, angular velocities drop to zero and start to increase in the opposite sense as in the elliptical graphs of $\dot{x}$ versus x in the undamped mass-spring system.

In Figure 4.3 the symmetric cases of Figure 4.2 are shown. Here we cannot talk about an in phase situation. For example if we compare the cases $\theta_1 = 15,\ \theta_2 = 15$ and $\theta_1 = 15,\ \theta_2 =$

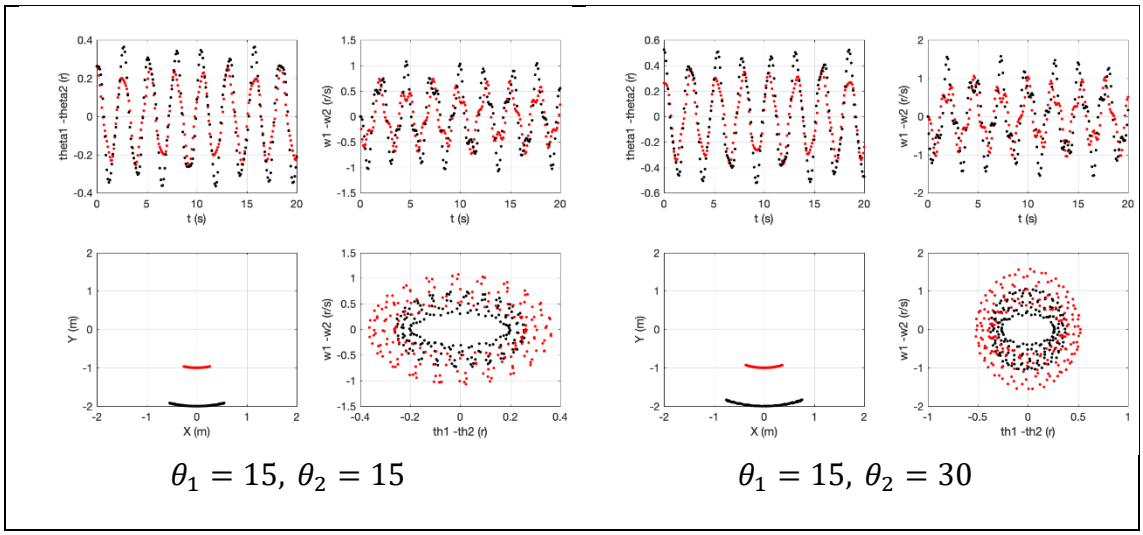
-15 , then angles and angular velocities do not follow a similar sinusoidal behaviour. Both angles have a shorter range.



(a) (b) (c)

Figure 4.1. The example graphics of small, medium and large angle regions.

A representation example was given in Figure 4.1, which represents 3D motion graphs consisting of $\theta_1, \omega_1 \; and \; \theta_2$. The phase portraits created by θ_1 and ω_1 were added with a third axis, which is θ_2. It allows us to track how the phase portraits change with respect to θ_2 position. We can follow the graph in different regions and interpreting the motion regime is facilitated by extracting special regions. In the following pages, we examined the phase diagrams and the Poincare sections that can be obtained from them. Here, the change in the sections according to the motion behavior helps us to determine how the mass will be directed towards a motion regime.



$\theta_1 = 15, \; \theta_2 = 15$ $\theta_1 = 15, \; \theta_2 = 30$

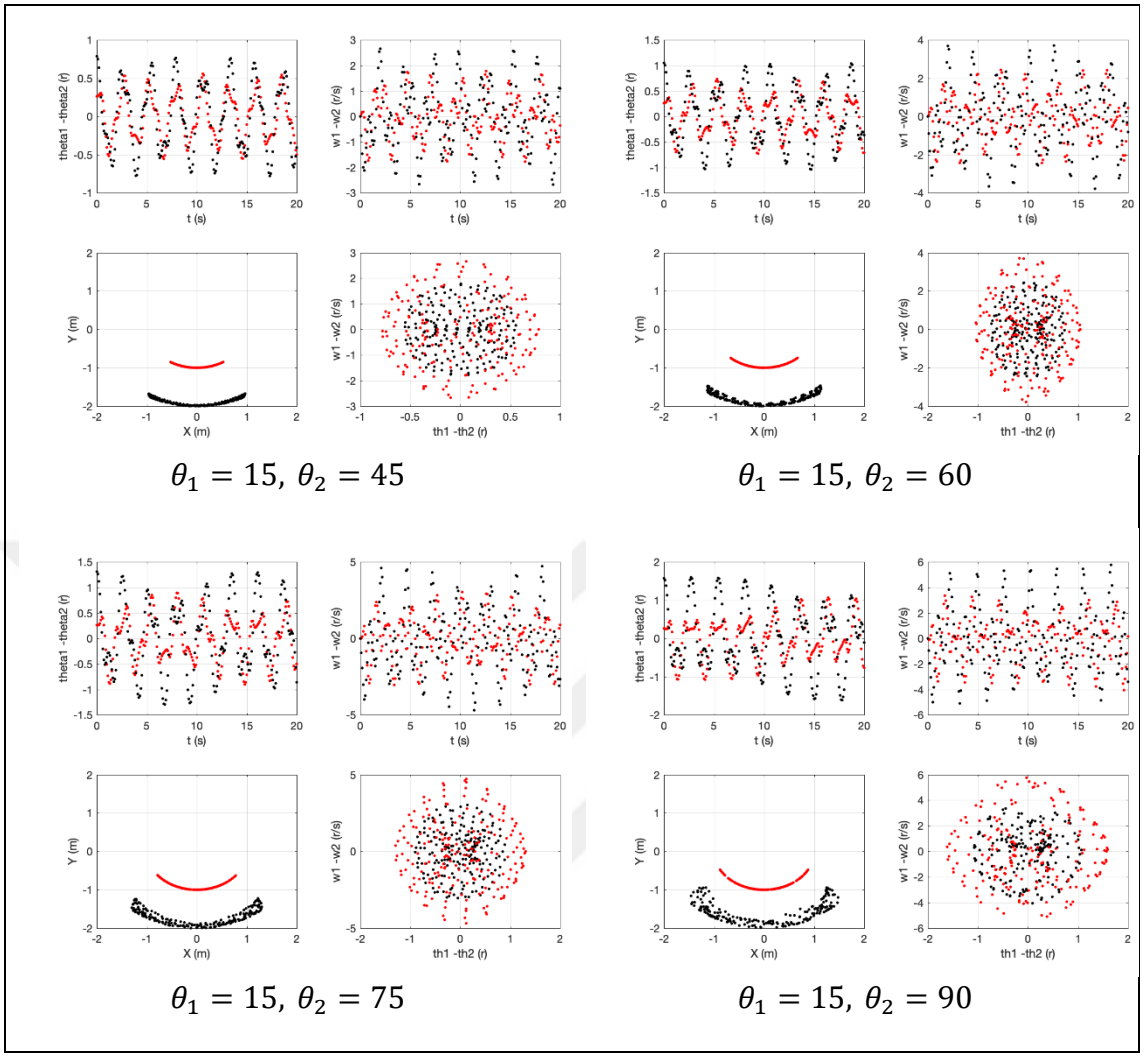


Figure 4.2. The graphical solutions of $\theta_2 = 15, 30, 45, 60, 75, 90$ for small, medium, and large values corresponding to the small angle value of $\theta_1 = 15$. The other parameters are $b_1 = 1, b_2 = 1, m_1 = 1, m_2 = 1, a = 0, \omega = 0$.

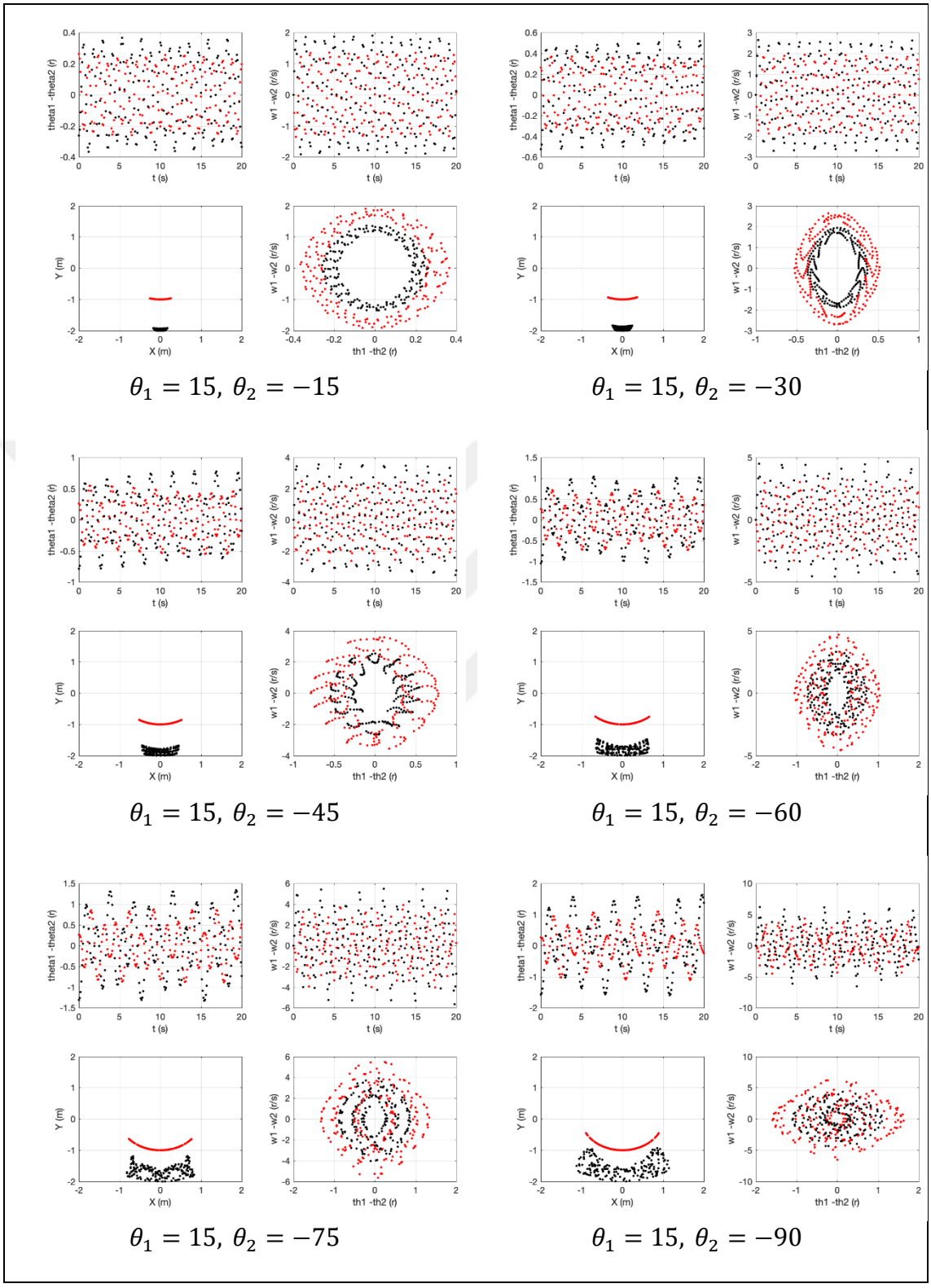


Figure 4.3. The graphical solutions of $\theta_2 = -15, -30, -45, -60, -75, -90$ for small, medium, and large values corresponding to the small angle value of $\theta_1 = 15$. The other parameters are $b_1 = 1, b_2 = 1, m_1 = 1, m_2 = 1, a = 0, \omega = 0$.

The difference between Figures 4.2 and 4.4 is the change in θ_1 , it is now set at $\theta_1 = 45$, while θ_2 increases again from 15 to 90 degrees in steps of 15 degrees. Due to the increase in the initial value of the upper angle the initial position of the centre of mass is higher, thus the initial value of the energy is larger. Hence the ranges of the angles and angular velocities get larger than the first set. Part d of the graphs where $\theta_2 = 15$ and $\theta_2 = 30$ show a circular pattern for both of the rods and the circular regions are full of data points. If we draw some vertical lines on the figure in part d there are lots of points on these vertical lines and the number of data points on the lines gets less as the line approaches the left or right limits, meaning that the rods pass through a certain angle (where the vertical line is drawn) with several different angular velocities during the 20-second interval. However, for the identical values of $\theta_1 = \theta_2 = 45$ (and partly at $\theta_2 = 60$) the same part d shows just a few elliptic curves indicating that on a hypothetical vertical line there can be only one or a few data points, hence just a few angular velocity values.

In Figure 4.5 the symmetric cases of Figure 4.4 are shown. For example if we compare the cases $\theta_1 = 45,\ \theta_2 = 45$ and $\theta_1 = 45,\ \theta_2 = -45$ although the angles and angular velocities exhibit a similar behaviour, the number of data points at the same angular values are a bit more.

In Figures 4.6 and 4.7 θ_1 is raised to $\theta_1 = 75$, while θ_2 increases from 15 to 90 degrees in steps of 15 degrees. Again due to the increase in the initial value of the upper angle the initial position of the centre of mass and thereby the initial value of the energy are larger. Obviously the ranges of the angles and angular velocities become even larger than the previous sets. In the middle range of θ_2, such as $\theta_2 = 60$ and $\theta_2 = 75$ the elliptic curves seem to split into two loops. The more interesting observation is the divergence of θ_2 at large angles such as around $\theta_2 = 90$. This divergence is also seen in part a of the figure where the red and black curves separate at around $t \cong 13$ s. The black curve drops abruptly and reaches a value like 14 radians, corresponding to more than two full revolutions (4π rad). This can also be understood from part d where the elliptical part is concentrated around $-1 \leq \theta_2 \leq 1$ rad. but it also reaches -14 rad, passing through the larger angles once. However, in the symmetrical cases where θ_2 start from negative initial values such divergence is not observed.

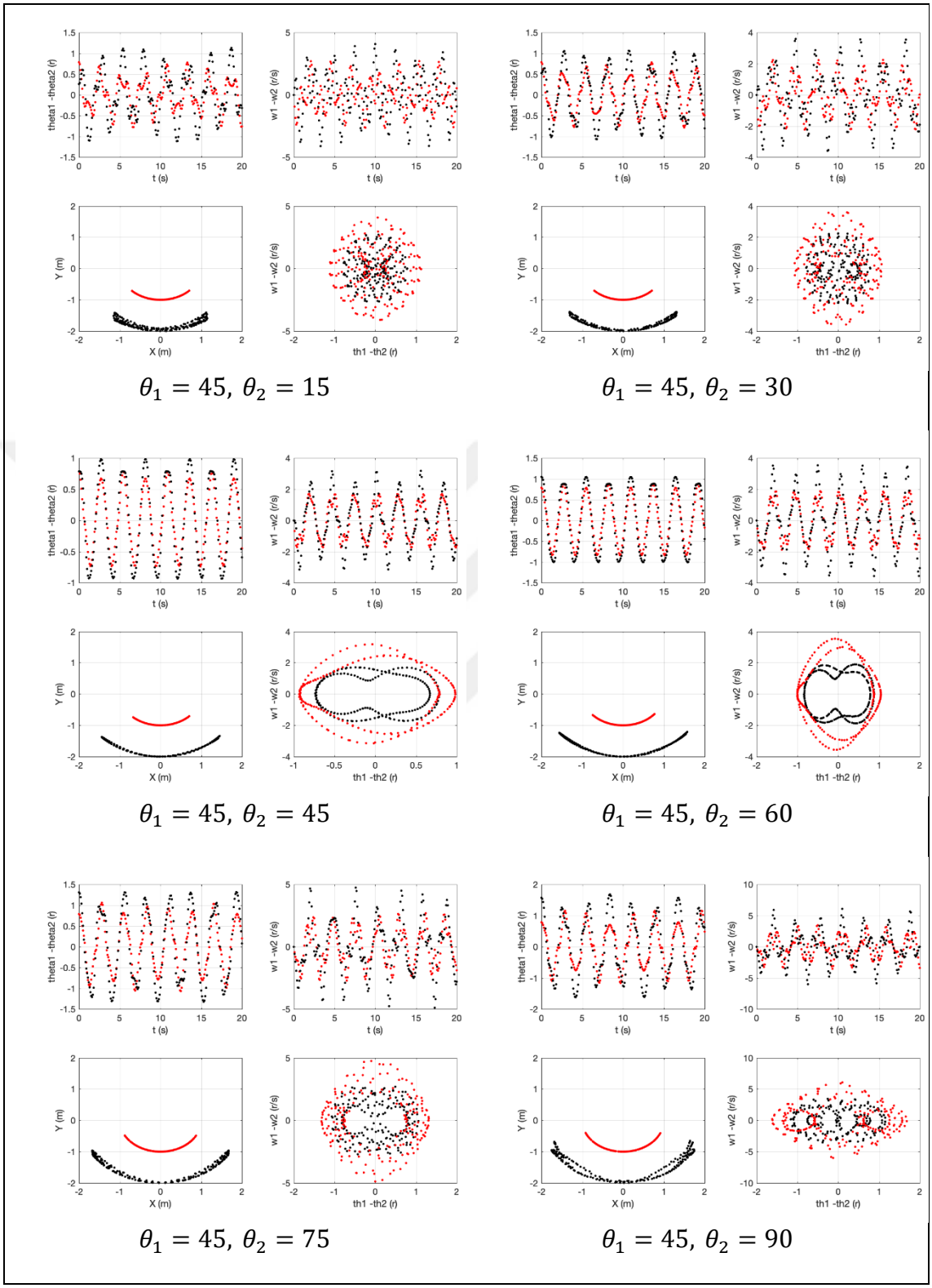


Figure 4.4. The graphical solutions of $\theta_2 = 15, 30, 45, 60, 75, 90$ for small, medium, and large values corresponding to the medium angle value of $\theta_1 = 45$. The other parameters are $b_1 = 1, b_2 = 1, m_1 = 1, m_2 = 1, a = 0, \omega = 0$.

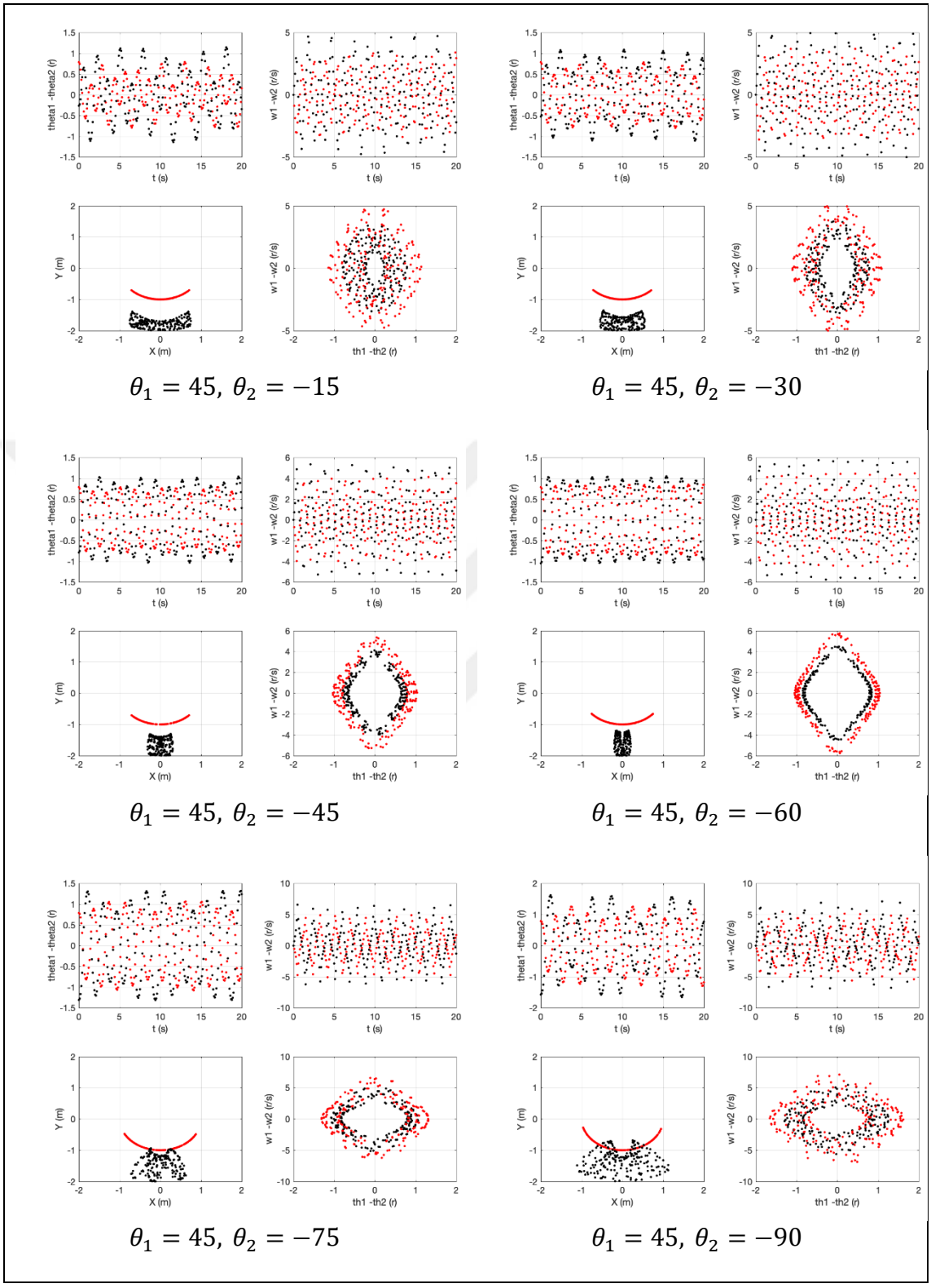


Figure 4.5. The graphical solutions of $\theta_2 = -15, -30, -45, -60, -75, -90$ for small, medium, and large values corresponding to the medium angle value of $\theta_1 = 45$. The other parameters are $b_1 = 1, b_2 = 1, m_1 = 1, m_2 = 1, a = 0, \omega = 0$.

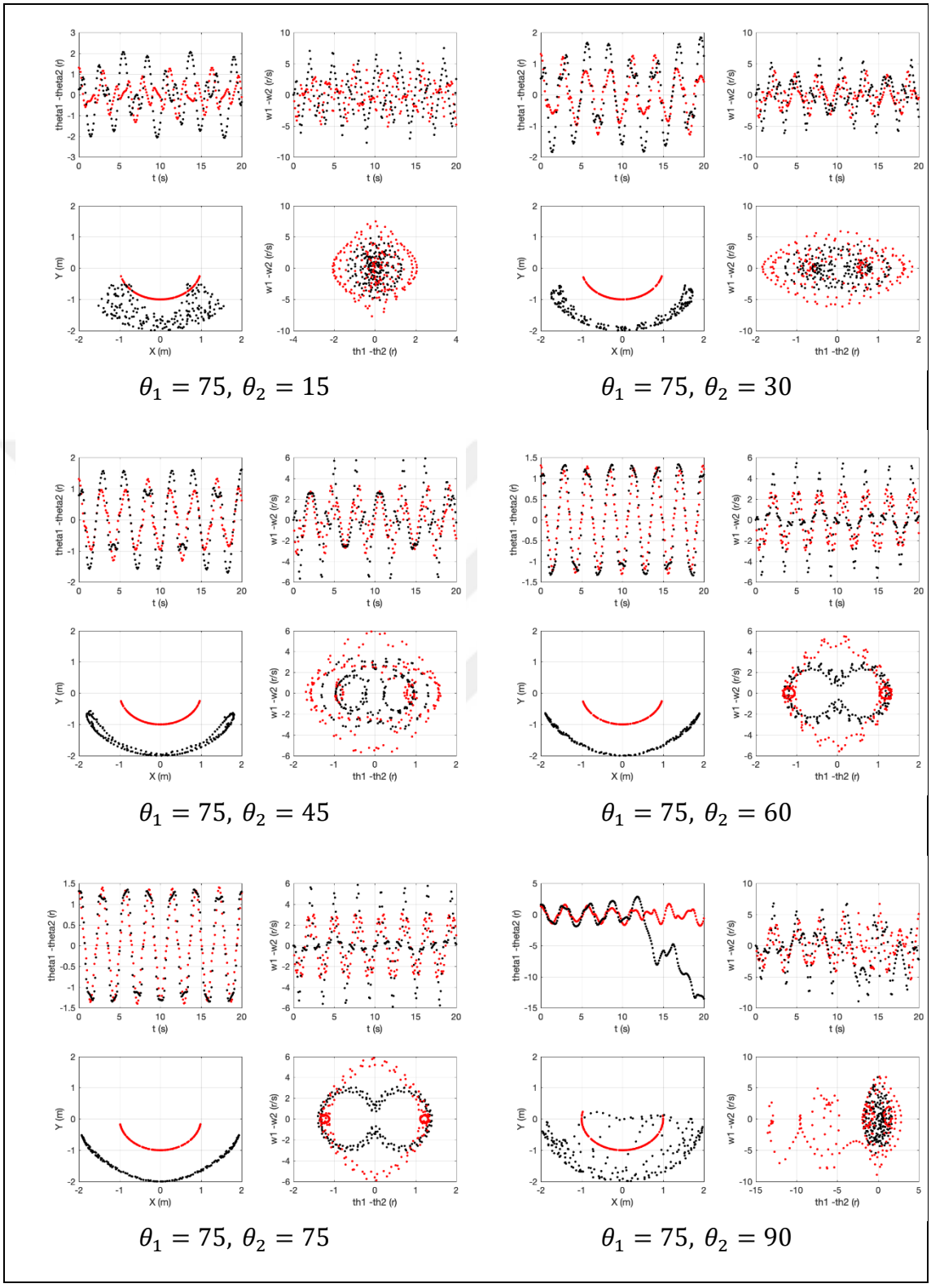


Figure 4.6. The graphical solutions of $\theta_2 = 15, 30, 45, 60, 75, 90$ for small, medium, and large values corresponding to the large angle value of $\theta_1 = 75$. The other parameters are $b_1 = 1, b_2 = 1, m_1 = 1, m_2 = 1, a = 0, \omega = 0$.

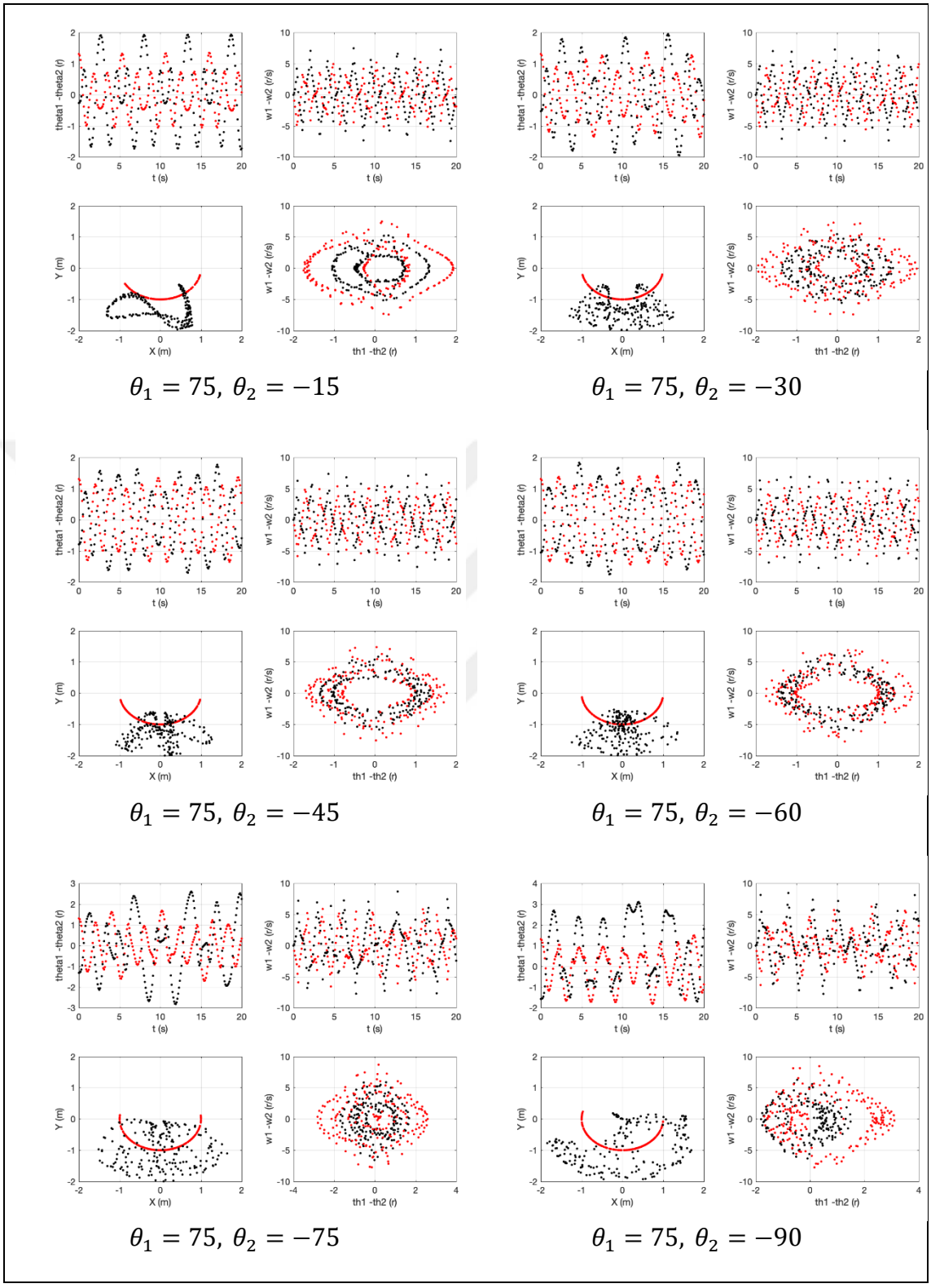


Figure 4.7. The graphical solutions of $\theta_2 = -15, -30, -45, -60, -75, -90$ for small, medium, and large values corresponding to the large angle value of $\theta_1 = 75$. The other parameters are $b_1 = 1, b_2 = 1, m_1 = 1, m_2 = 1, a = 0, \omega = 0$.

In Figure 4.8 where θ_1 is raised to $\theta_1 = 90$, while θ_2 increases from 15 to 90 degrees in steps of 15 degrees as before, the divergence of the angles is observed at intermediate values such as $\theta_2 = 30$ and $\theta_2 = 45$, but not at higher initial values. They are almost in phase at $\theta_2 = 75$, but at the highest possible initial values, namely at $\theta_1 = 90$ and $\theta_2 = 90$ the lower rod completes around 4 full turns ($\cong 24$ rad). The two symmetric microstates, especially $\theta_1 = 90,$ $\theta_2 = 75$ and $\theta_1 = 90$ and $\theta_1 = -75$ exhibit quite different behaviours, in the latter lower rod completing more than two full turns, while in the former they were oscillating almost in phase in Figure 4.11. If we compare the two highest values, namely $\theta_1 = 90,$ $\theta_2 = 90$ and $\theta_1 = 90,$ $\theta_2 = -90,$ we observe that although in both of these microstates the lower rod completes full turns, in the former it does so only in clockwise sense ($\theta_2 < 0$), while in the latter both clockwise and counterclockwise senses ($\theta_2 < 0$ and $\theta_2 > 0$) respectively. In Figure 4.9, we can observe the graphs of $\theta_2 = -60, -75, -90$ values, which indicate that the rotation of the lower mass, has completed a full turn in a somersault manner. Examining both positive and negative θ_2 values, we see the graphs representing the largest θ_1 angle family in the dataset. If it is in comparison to the smaller angle families we have analyzed so far, the motion where the lower mass performs the most somersaults and completes a full turn has been observed. Looking at the phase portraits for θ_2 corresponding to 30, 45, and 90 degrees for $\theta_1 = 90$ in Figure 4.10, for θ_2 corresponding to -60, -75, and -90 in Figure 4.9, it can be observed that the motion of the lower mass deviates significantly from periodic oscillations and enters into chaotic regime, exhibiting the bifurcation occurring during the full rotation of the lower mass.

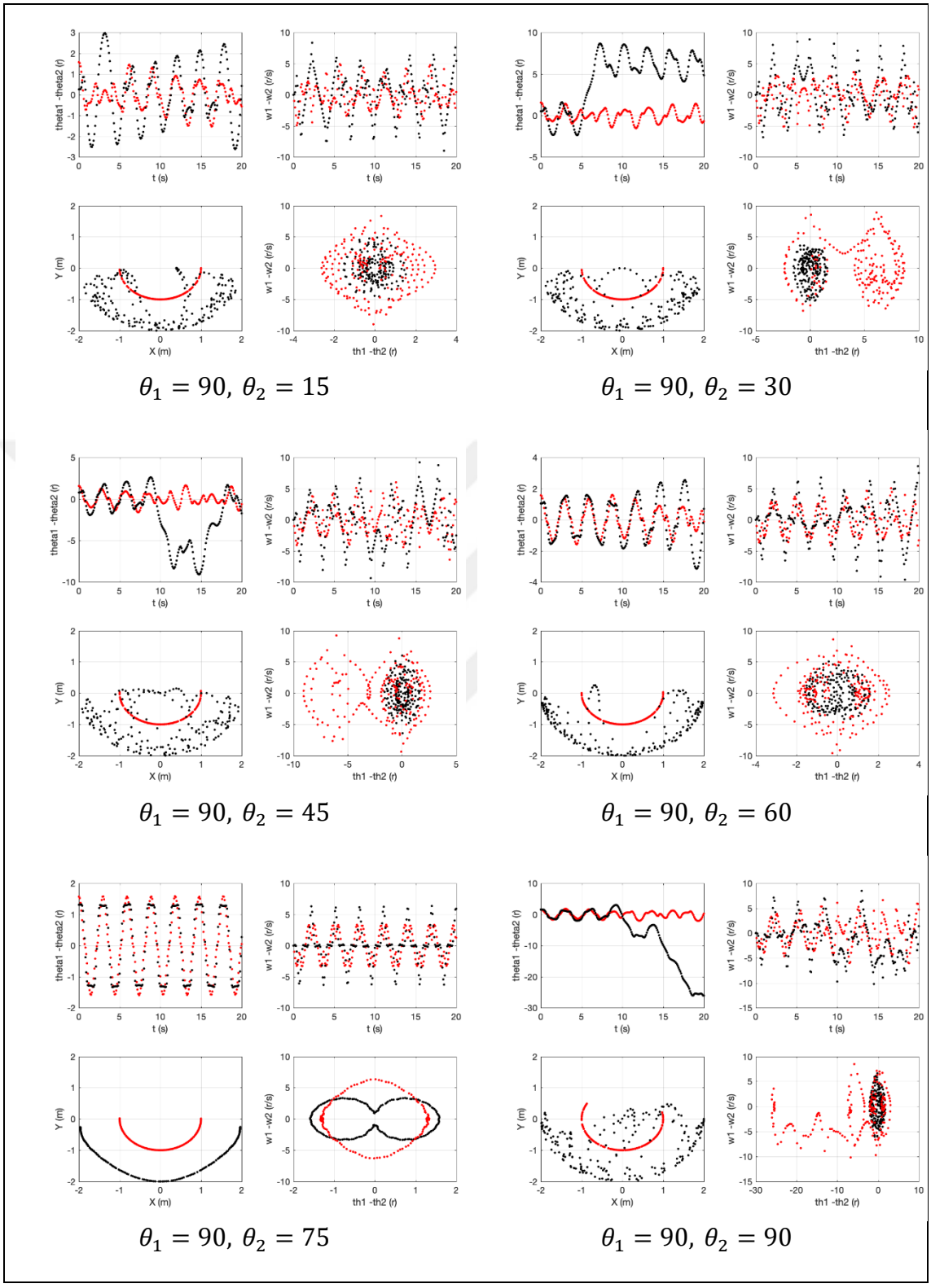


Figure 4.8. The graphical solutions of $\theta_2 = 15, 30, 45, 60, 75, 90$ for small, medium, and large values corresponding to the small angle value of $\theta_1 = 90$. The other parameters are $b_1 = 1, b_2 = 1, m_1 = 1, m_2 = 1, a = 0, \omega = 0$.

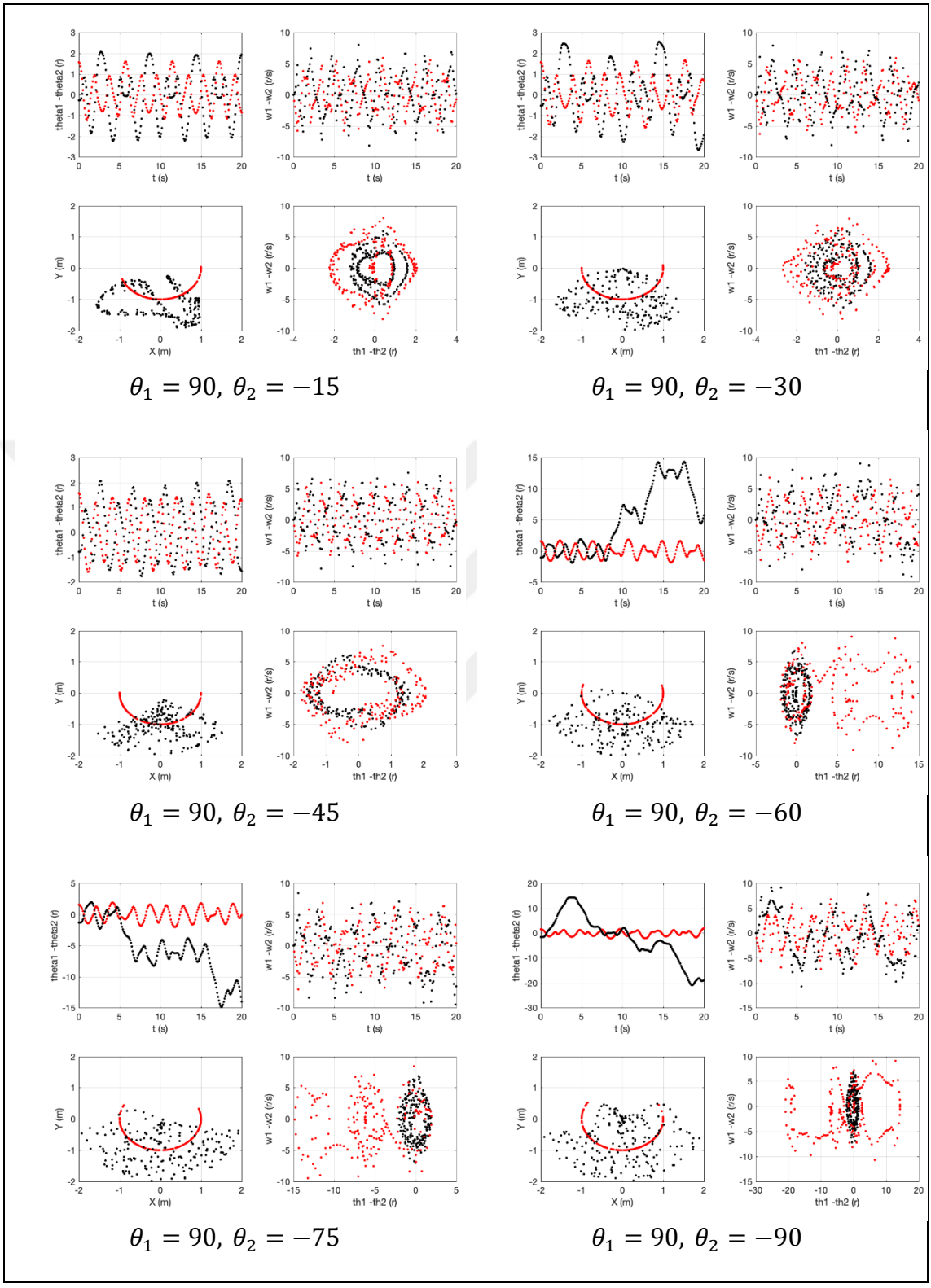


Figure 4.9. The graphical solutions of $\theta_2 = -15, -30, -45, -60, -75, -90$ for small, medium, and large values corresponding to the small angle value of $\theta_1 = 90$. The other parameters are $b_1 = 1, b_2 = 1, m_1 = 1, m_2 = 1, a = 0, \omega = 0$.

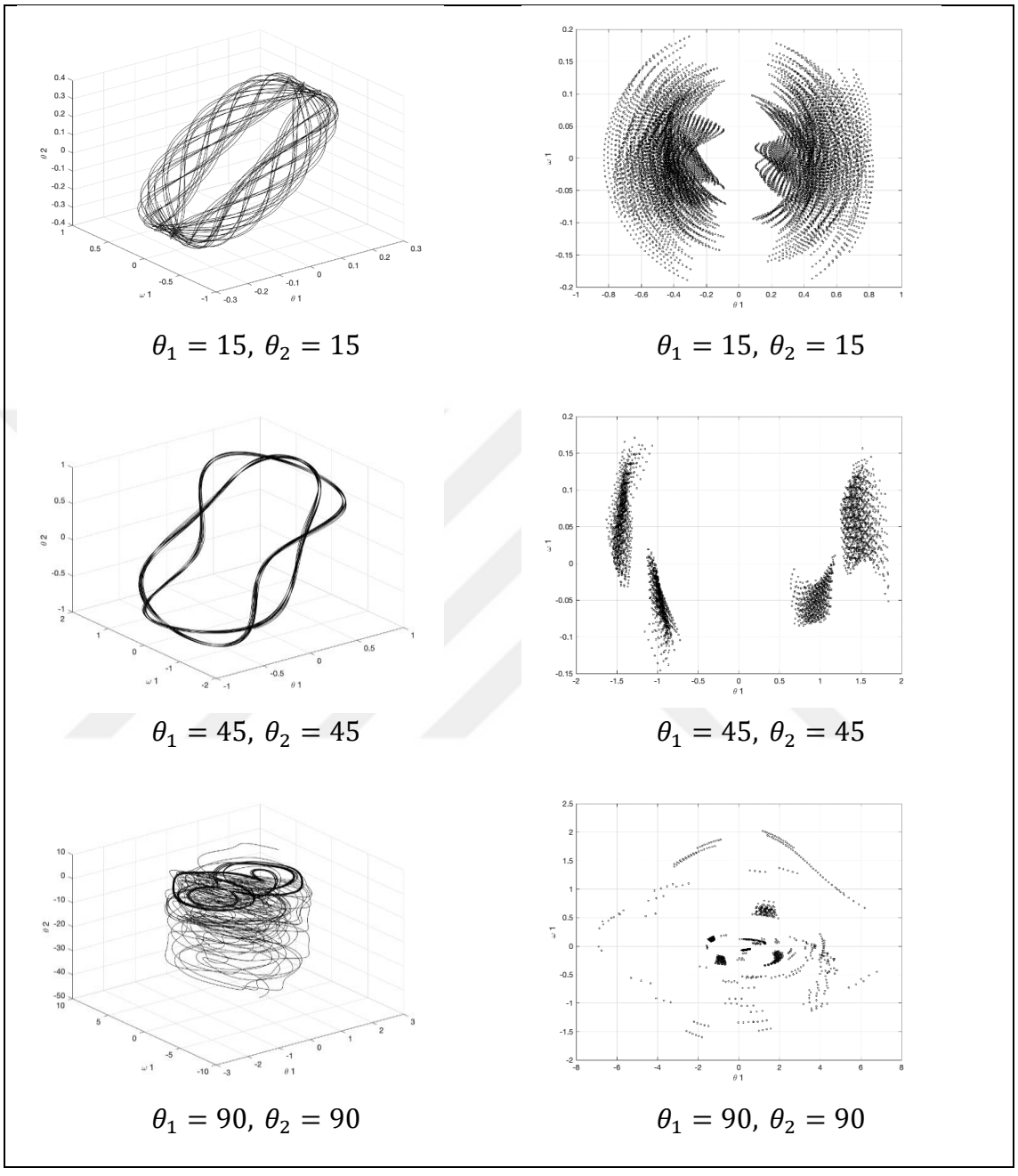


Figure 4.10. The representation of phase portraits and Poincaré sections for system of double pendulum, $\theta_1 = \theta_2 = 15, 45, 90$

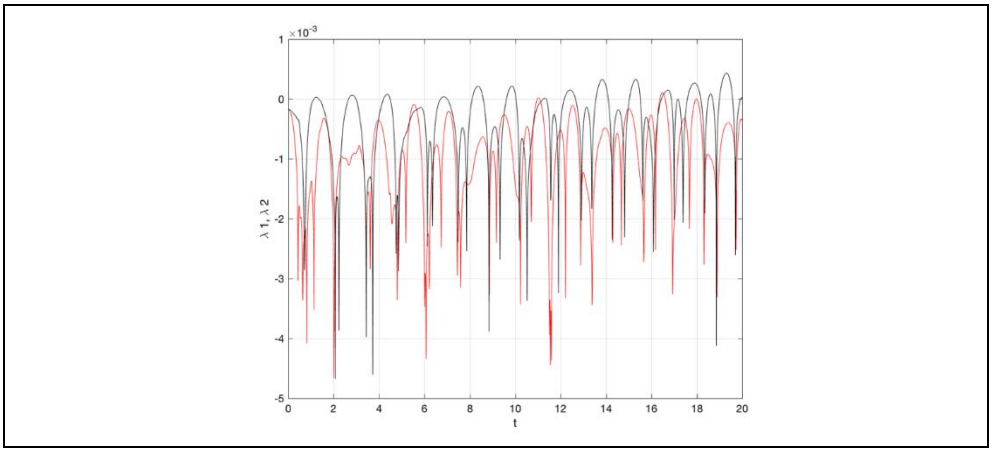


Figure 4.11. The graphic of the lyapunov exponents of double pendulum, $\theta_1 = 45$ and $\theta_2 = 45, b_1 = 1, b_2 = 1, m_1 = 1, m_2 = 1, a = 0, \omega = 0.$

If we look at the 3D graph consisting of $\theta_1, \omega_1, \theta_2$, for small, medium, and large angle values of $\theta_1 \; and \; \theta_2$ in Figure 4.10, we can see that oscillations starting with the same initial values for $\theta_1 \; and \; \theta_2$ exhibit oscillations in phase for small and medium angles, but for large angles, where the system actually has high energy, we see that the periodic values of the motion are exceeded in unpredictable ways. When the Poincare sections are also examined, we observe that the sections are periodic and in order for small and medium angles, but for large angles, they become irregular, completely deviating from order and transitioning to chaos. At very small angle values, we observe fixed points in the Poincare sections. As the initial angles of the system increase, periodic and quasiperiodic motion profiles exhibit regular behavior in a certain pattern.

In the double pendulum system we have modelled, Lyapunov exponents were obtained for the motion equations depending on the angle values for the case where the masses and lengths are equal. Figure 4.11 shows the graph displaying the λ_1 and λ_2 values for θ_1 and θ_2. As previously explained, Lyapunov exponents provide an advanced answer to whether there is chaotic behavior in a system based on initial conditions. As a reminder, Lyapunov exponents are mathematical results that measure the instability of a dynamic system.

4.2. REPRESENTATIONS OF STATIONARY STATES FOR DIFFERENT MASS RATIOS

In this part of the thesis the lengths of the rods are still the same but the masses of the bobs are not equal, $m_2 = \frac{m_1}{2}$ in the following analysis. This causes a change both in the position of the centre of mass and the moment of inertia of the system. So far the masses were taken to be equal, $m_1 = m_2$ and therefore the centre of mass of the system was at the midpoint of the lower rod because the rods were massless and the rotational inertia was

$$I_0 = 2\left[m\left(\frac{b}{2}\right)^2\right] = \frac{m\,b^2}{2} \rightarrow I_0 = \frac{m\,b^2}{2}$$

But now the distance between the new position of the centre of mass (cm') and m_1 is

$$r_{cm'} = \frac{\frac{m}{2}}{m+\frac{m}{2}}b \rightarrow r_{cm'} = \frac{b}{3}$$

Therefore the rotational inertia becomes

$$I_1 = m\left(\frac{b}{3}\right)^2 + \frac{m}{2}\left(\frac{2b}{3}\right)^2 \rightarrow I_1 = \frac{m\,b^2}{3}$$

As is easily seen the new rotational inertia is less than the previous one. This may cause an increase in the angular velocities because the angular momentum is the product of inertia and angular velocity:

$$L = I\,\omega$$

As I decreases ω increases. So we expect more full turns now compared with the previous part under the same initial conditions. When we compare the two sets

i- $m_1 = m_2$ and ii- $m_2 = \frac{m_1}{2}$

considering the microstates where the lower rod completes some full turns, we observe totally 7 cases in the first, while a total number of 17 cases in the latter.

As in the previous section, the mathematical model was constructed with equal masses and lengths in Figure 4.12. However, in this case, instead of the system modeled with equal mass and length, the modeling was changed by replacing the weight of the lower mass with half

of the weight of the upper mass. Here, it was observed that the movement profile underwent significant changes due to the expected lower mass being lighter. It is seen that as θ_2 increases from 15 to 90 degrees in steps of 15 degrees, while θ_1 is set to 75 degrees for all the six microstates the two angles get a phase difference. Similarly, as seen from parts b also the angular velocities ω_1 and ω_2 follow such a pattern. It is also seen from the roughly circular shape in parts d that θ_2 has a equal range with θ_1. In Figure 4.13. the symmetric cases of Figure 4.12. are shown. Here we cannot talk about an in phase situation. For example if we compare the cases $\theta_1 = 15,\ \theta_2 = 15$ and $\theta_1 = 15,\ \theta_2 = -15$, then angles and angular velocities do not follow a similar sinusoidal behaviour. Both angles have a shorter range. The difference between Figures 4.14. and 4.15. is the change in θ_1 , it is now set at $\theta_1 = 90$, while θ_2 increases again from 15 to 90 degrees in steps of 15 degrees. Additionally, we have placed the complete solution sets here. The representations for small and medium angle values can be followed in Appendix C.

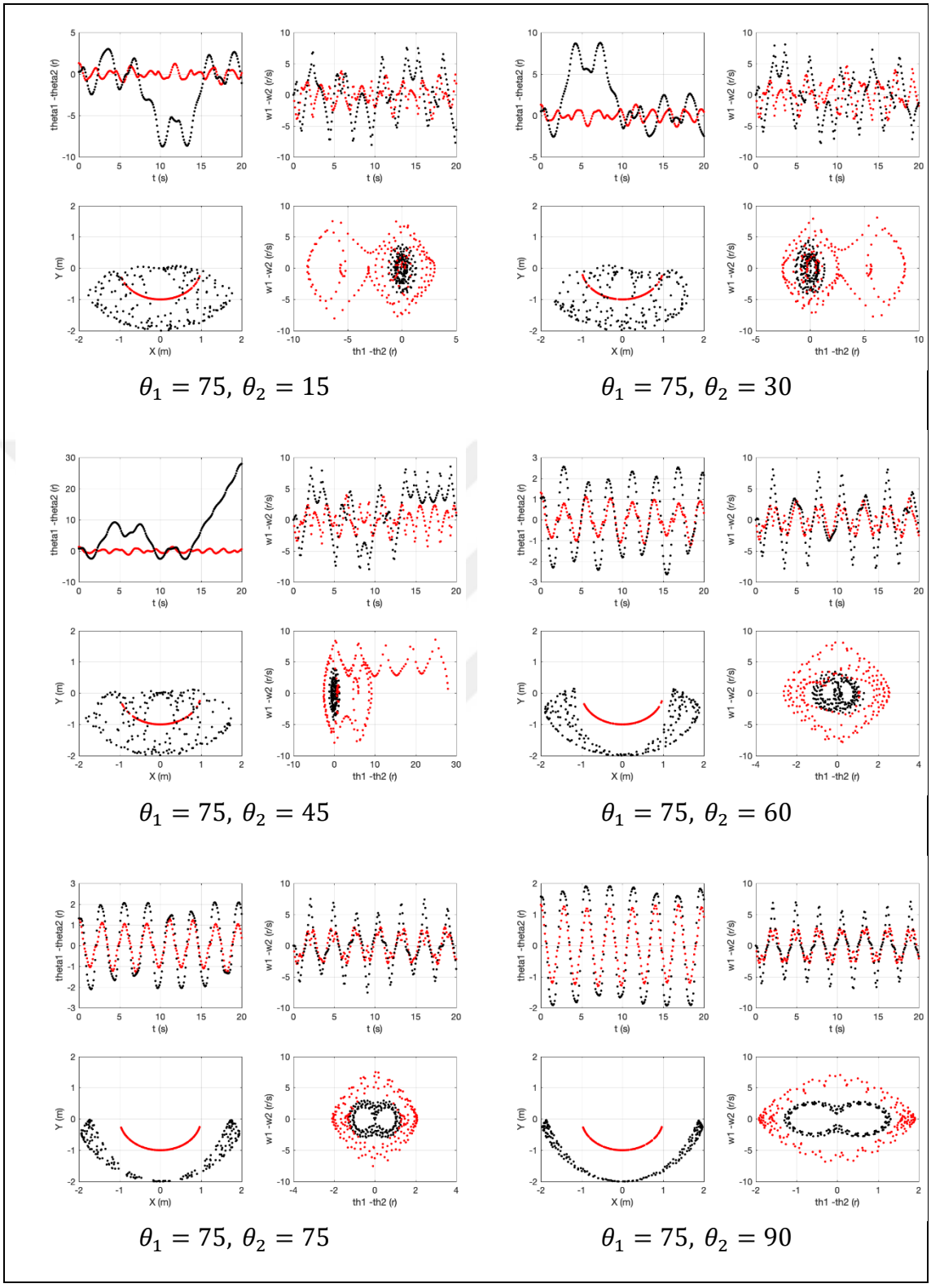


Figure 4.12. The graphical solutions of $\theta_2 = 15, 30, 45, 75, 90$ for small, medium, and large values corresponding to the large angle value of $\theta_1 = 75$. The other parameters are $b_1 = 1, b_2 = 1, m_1 = 1, m_2 = 0.5, a = 0, \omega = 0$.

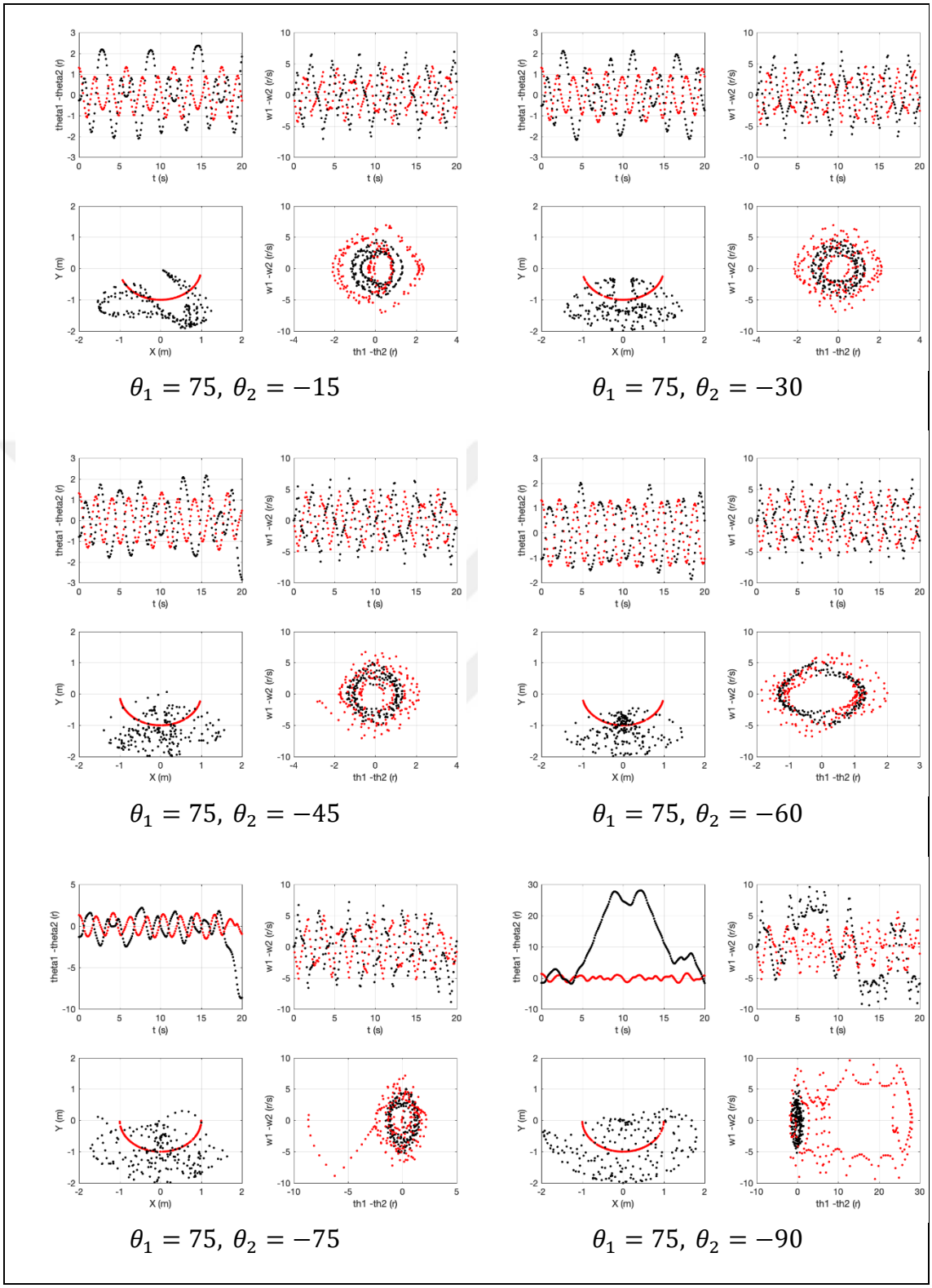


Figure 4.13. The graphical solutions of $\theta_2 = -15, -30, -45, -75, -90$ for small, medium, and large values corresponding to the large angle value of $\theta_1 = 75$. The other parameters are $b_1 = 1, b_2 = 1, m_1 = 1, m_2 = 0.5, a = 0, \omega = 0$.

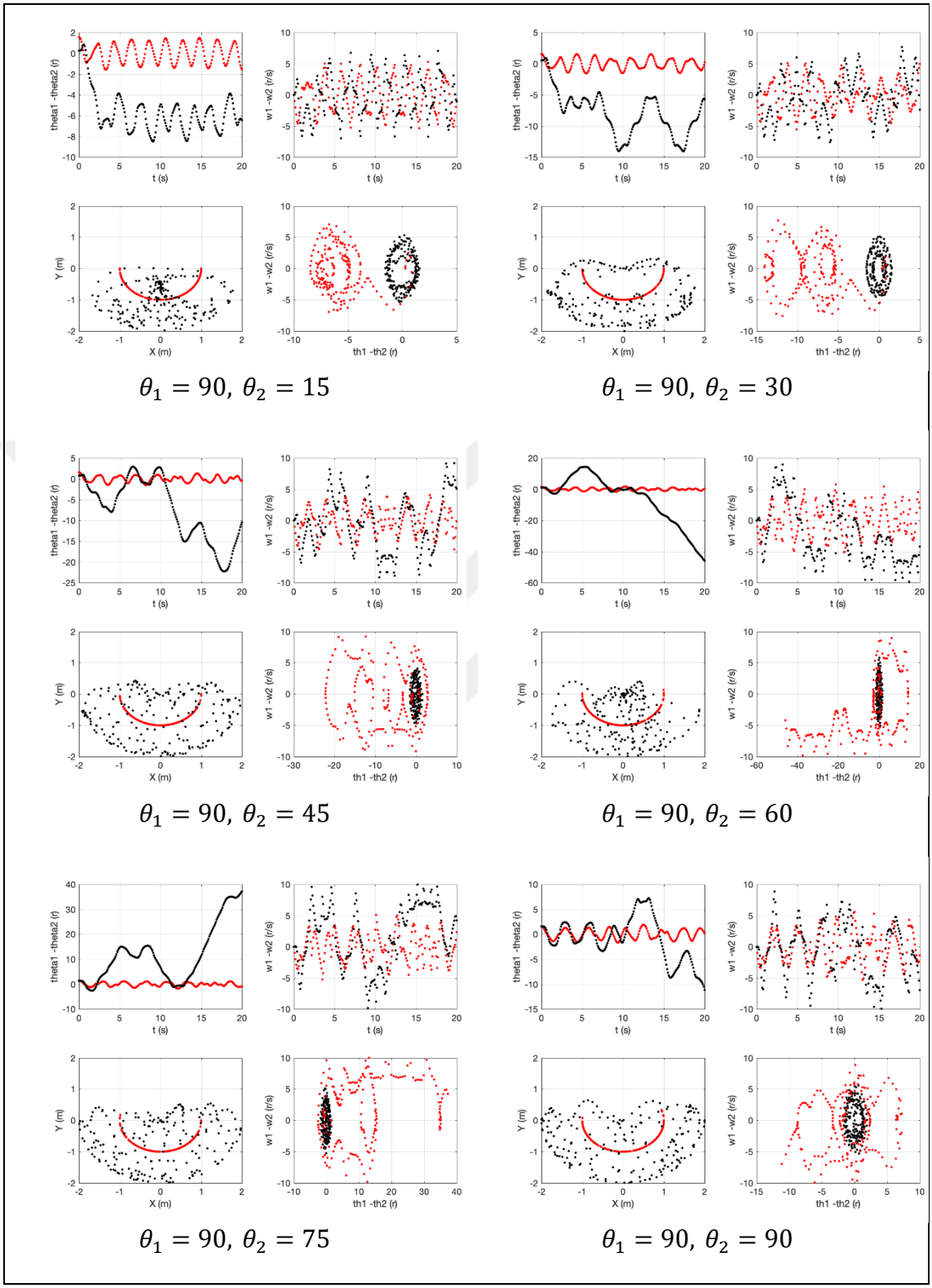


Figure 4.14. The graphical solutions of $\theta_2 = 15, 30, 45, 75, 90$ for small, medium, and large values corresponding to the large angle value of $\theta_1 = 90$. The other parameters are $b_1 = 1, b_2 = 1, m_1 = 1, m_2 = 0.5, a = 0, \omega = 0$.

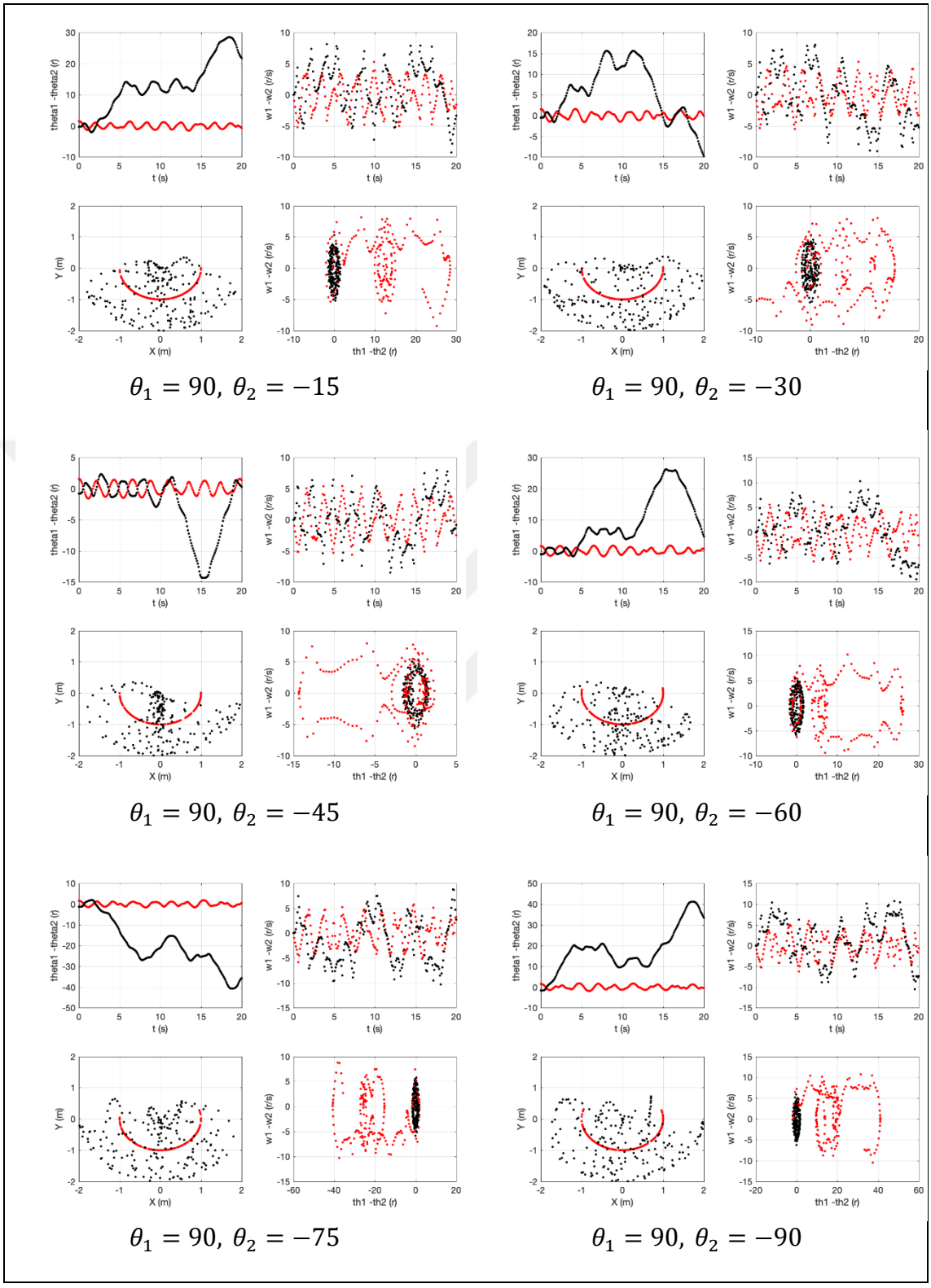


Figure 4.15. The graphical solutions of $\theta_2 = -15, -30, -45, -75, -90$ for small, medium, and large values corresponding to the large angle value of $\theta_1 = 90$. The other parameters are $b_1 = 1, b_2 = 1, m_1 = 1, m_2 = 0.5, a = 0, \omega = 0$.

In our system modeled with different mass ratios, the results of the model in which the lower mass was increased are presented below. Here, we applied the weight of the lower mass in the previous model as 2 times of the upper mass, instead of half of the upper mass. Again, assuming equal lengths, system parameters were established. Thus, a lower mass suspended with twice the weight of the upper mass was created. It is expected that the motion profile will have highly regular oscillations due to the heavier lower mass. In Figure 4.16. it is seen that as θ_2 increases from 15 to 90 degrees in steps of 15 degrees, while θ_1 is set to 75 degrees for all the six microstates the two angles get a phase difference. In Figure 4.13. the symmetric cases of Figure 4.17. are shown. Here we cannot talk about an in phase situation. For example if we compare the cases $\theta_1 = 15,\ \theta_2 = 15$ and $\theta_1 = 15,\ \theta_2 = -15$, then angles and angular velocities do not follow a similar sinusoidal behaviour. Both angles have a shorter range. The difference between Figures 4.18. and 4.19. is the change in θ_1 , it is now set at $\theta_1 = 90$, while θ_2 increases again from 15 to 90 degrees in steps of 15 degrees. Additionally, we have placed the complete solution sets here. The representations for small and medium angle values can be followed in Appendix C.

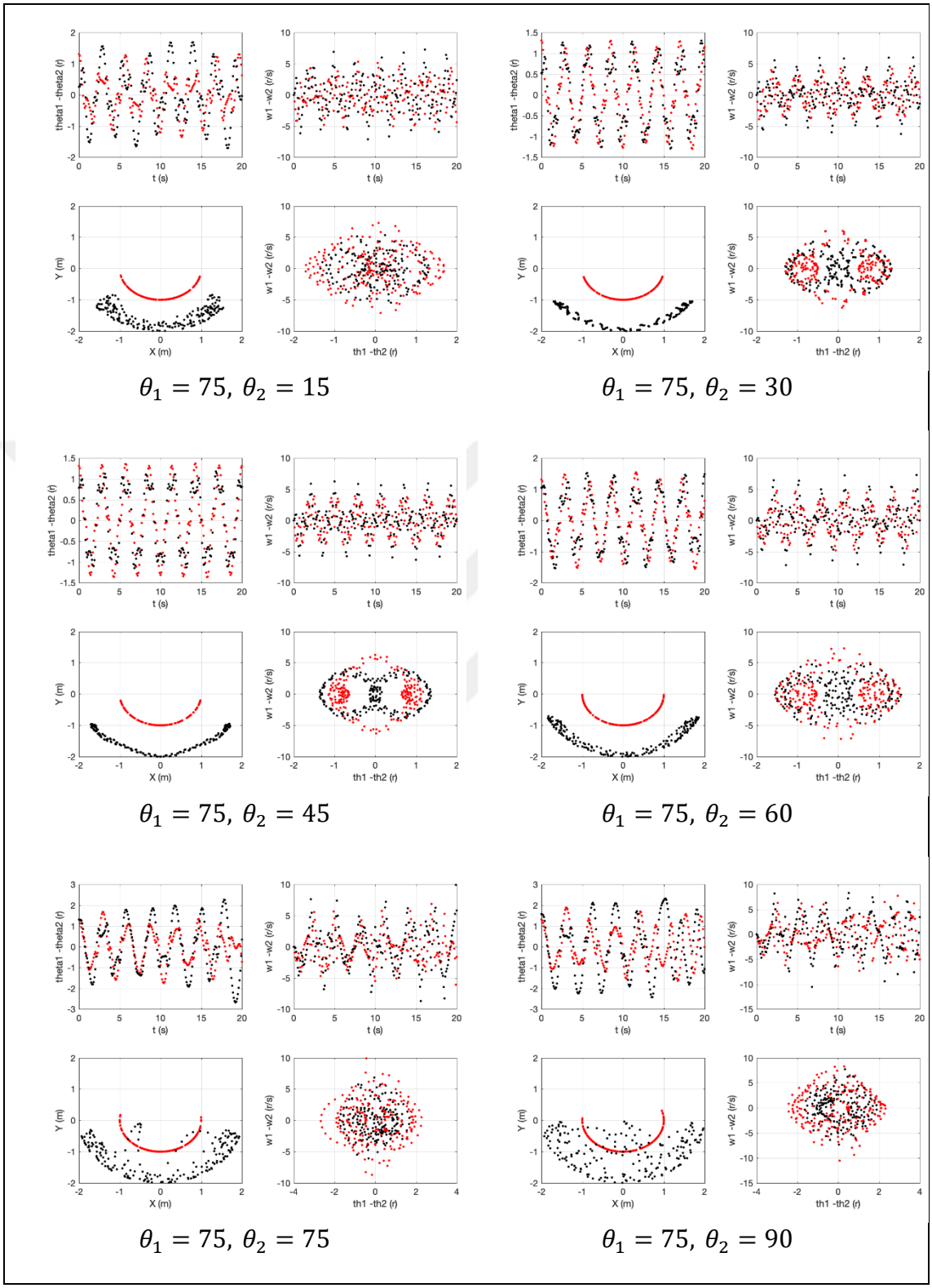


Figure 4.16. The graphical solutions of $\theta_2 = 15, 30, 45, 75, 90$ for small, medium, and large values corresponding to the large angle value of $\theta_1 = 75$. The other parameters are $b_1 = 1, b_2 = 1, m_1 = 1, m_2 = 2, a = 0, \omega = 0$.

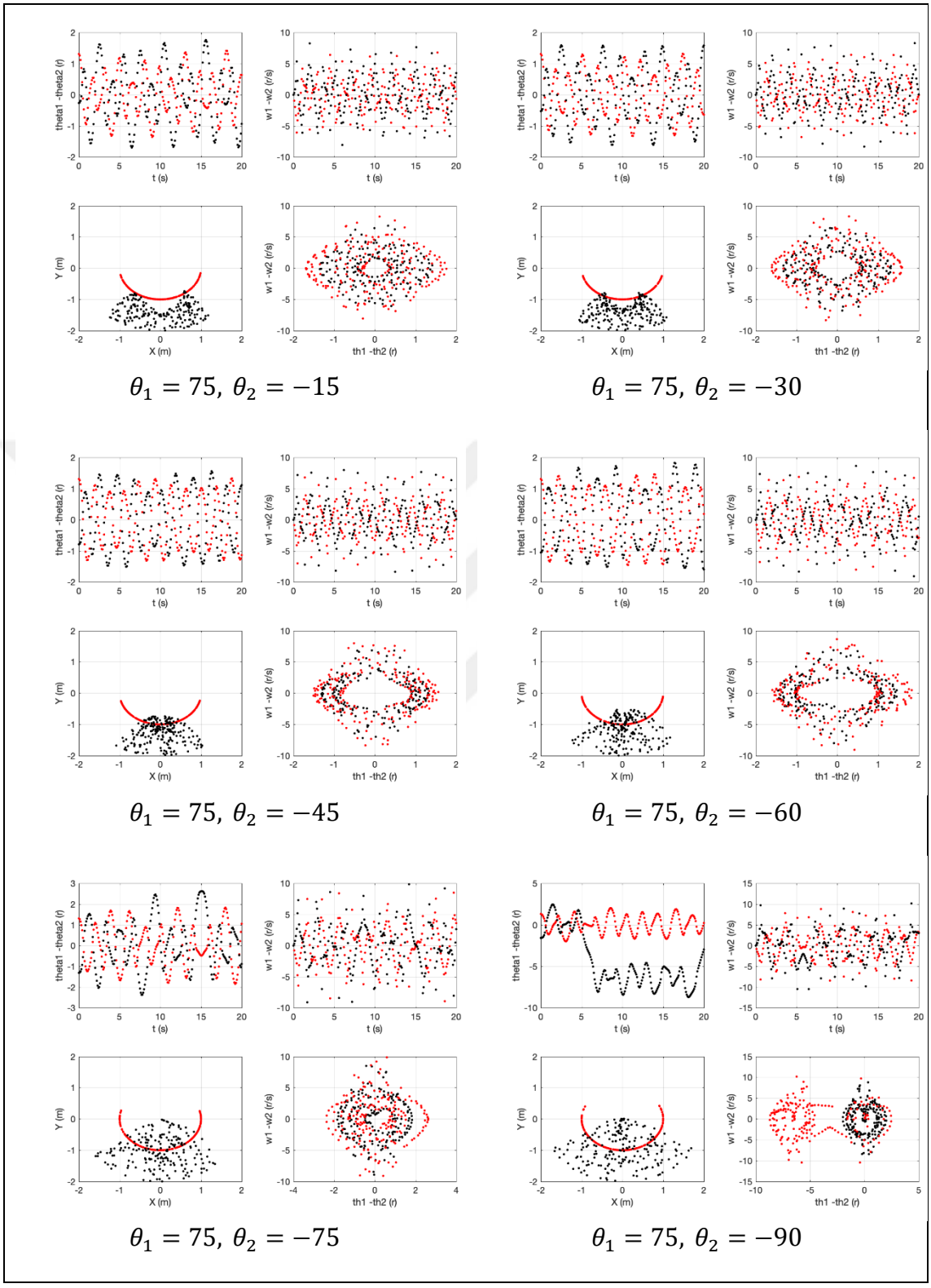


Figure 4.17. The graphical solutions of $\theta_2 = -15, -30, -45, -75, -90$ for small, medium, and large values corresponding to the large angle value of $\theta_1 = 75$. The other parameters are $b_1 = 1, b_2 = 1, m_1 = 1, m_2 = 2, a = 0, \omega = 0$.

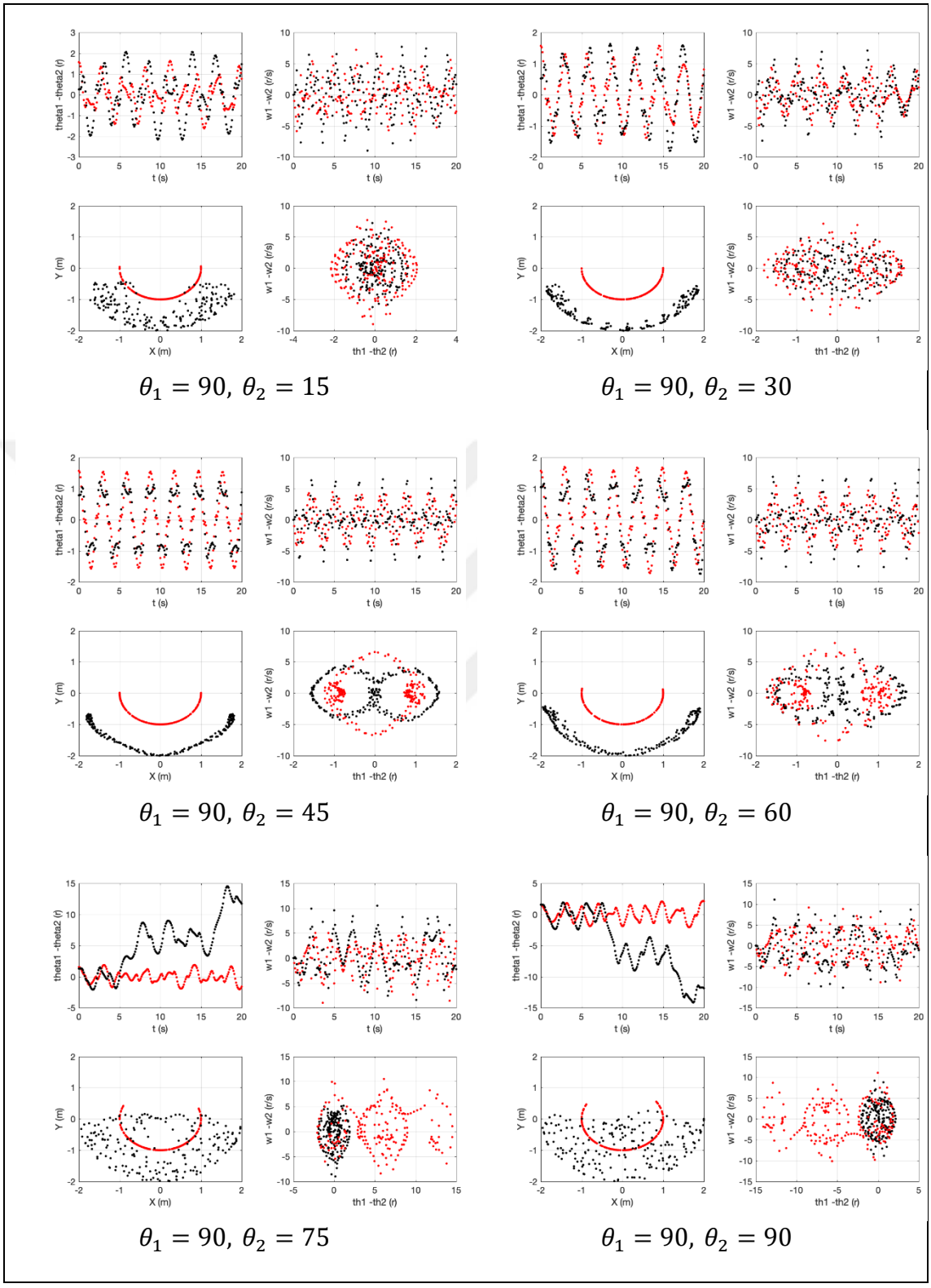
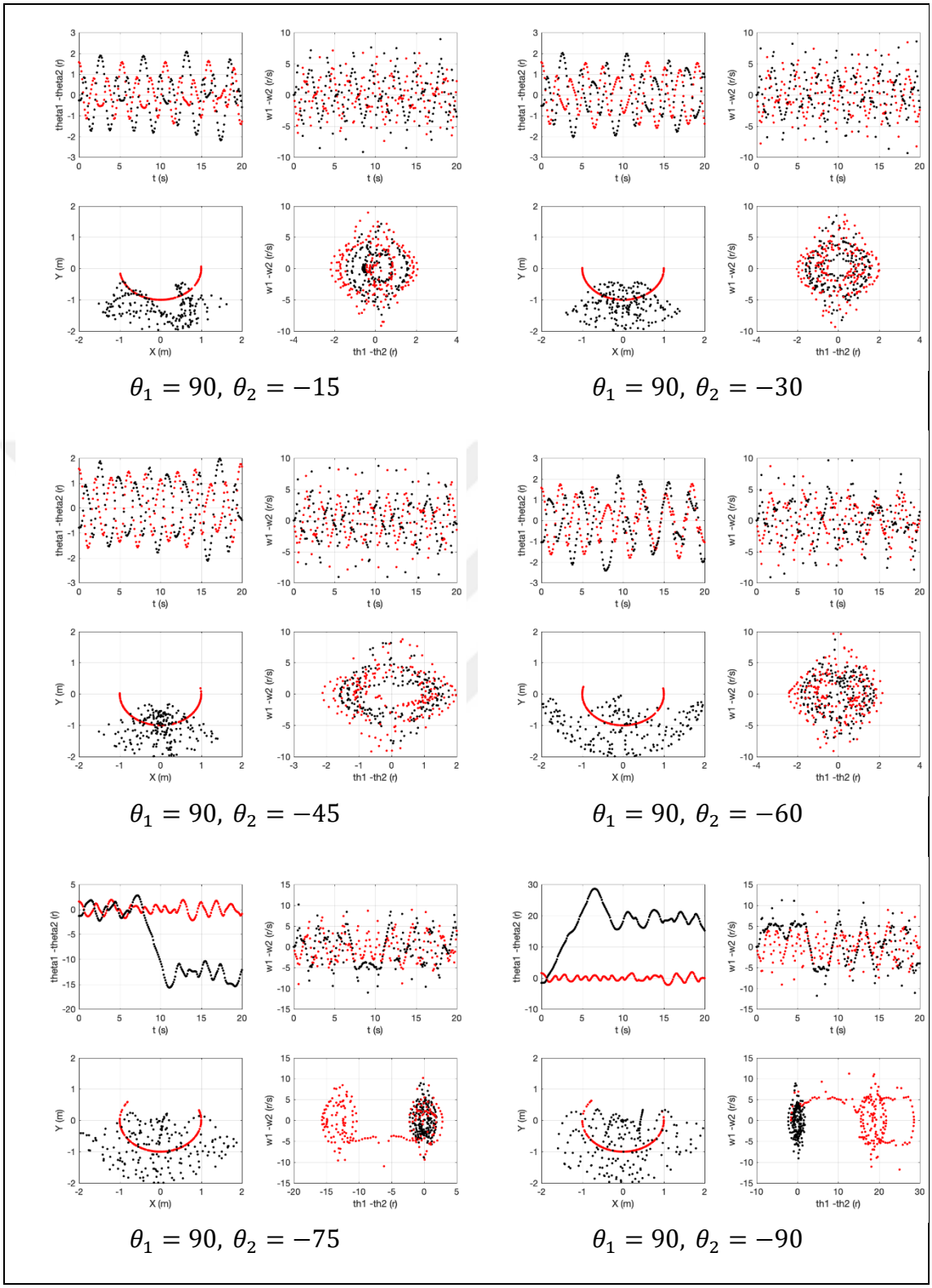


Figure 4.18. The graphical solutions of $\theta_2 = 15, 30, 45, 75, 90$ for small, medium, and large values corresponding to the large angle value of $\theta_1 = 90$. The other parameters are $b_1 = 1, b_2 = 1, m_1 = 1, m_2 = 2, a = 0, \omega = 0$.



$\theta_1 = 90,\ \theta_2 = -15$ $\theta_1 = 90,\ \theta_2 = -30$

$\theta_1 = 90,\ \theta_2 = -45$ $\theta_1 = 90,\ \theta_2 = -60$

$\theta_1 = 90,\ \theta_2 = -75$ $\theta_1 = 90,\ \theta_2 = -90$

Figure 4.19. The graphical solutions of $\theta_2 = -15, -30, -45, -75, -90$ for small, medium, and large values corresponding to the large angle value of $\theta_1 = 90$. The other parameters are $b_1 = 1, b_2 = 1, m_1 = 1, m_2 = 2, a = 0, \omega = 0$.

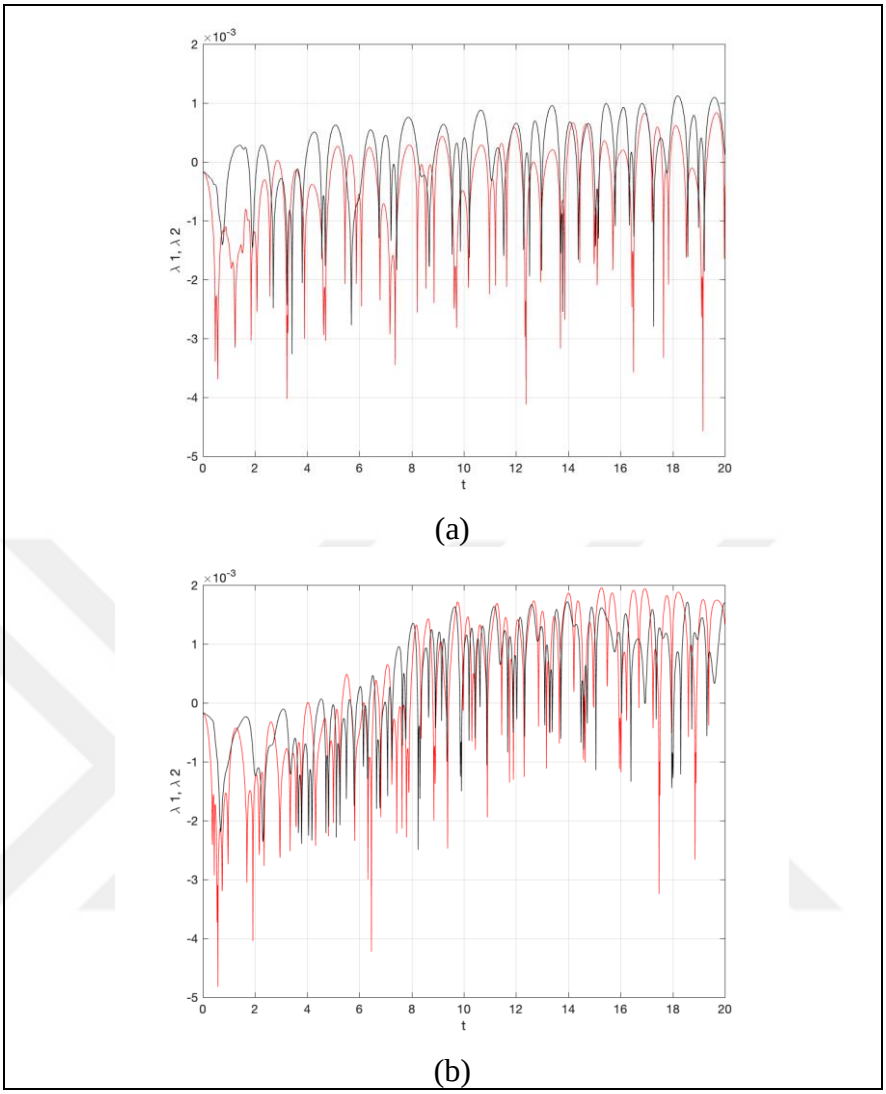


Figure 4.20. The graphic of the lyapunov exponents of double pendulum, (a) $\theta_1 = 45$ and $\theta_1 = 45, b_1 = 1, b_2 = 1, m_1 = 1, m_2 = 0.5, a = 0, \omega = 0$. (b) $\theta_1 = 45$ and $\theta_1 = 45, b_1 = 1, b_2 = 1, m_1 = 1, m_2 = 2, a = 0, \omega = 0$.

4.3. REPRESENTATIONS OF STATIONARY STATES FOR DIFFERENT LENGTH RATIOS

In this part of the thesis the masses of the rods are still the same but the masses of the bobs are not equal, $b_2 = \frac{b_1}{2}$ and $b_2 = 2\,b_1$ in the following analysis. Again this causes a change both in the position of the centre of mass and the moment of inertia of the system. As we stated above the rotational inertia when $m_1 = m_2$ and $b_1 = b_2$ was

$$I_0 = 2\left[m\left(\frac{b}{2}\right)^2\right] = \frac{m\,b^2}{2} \rightarrow I_0 = \frac{m\,b^2}{2}$$

But now $b_2 = \frac{b_1}{2}$ and rotational inertia becomes

$$I_1 = 2\,m\left(\frac{b}{4}\right)^2 \rightarrow I_1 = \frac{m\,b^2}{8}$$

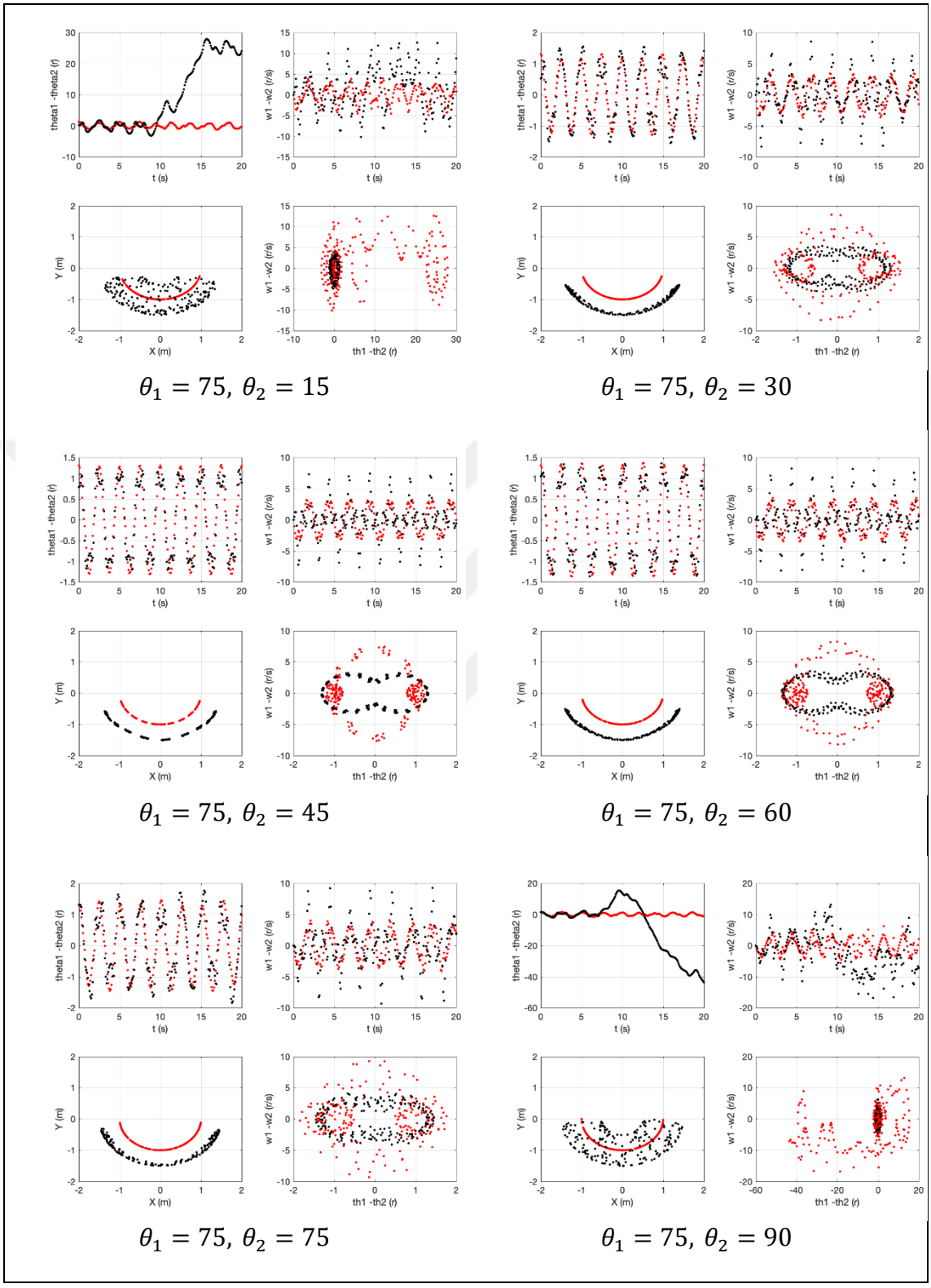
The new rotational inertia is one-quarter of the previous one. This may cause an increase in the angular velocities because the angular momentum is

$$L = I\,\omega$$

As I decreases ω increases. So we expect more full turns now compared with the previous part under the same initial conditions. When we compare the two sets

i- $b_1 = b_2$ and ii- $b_2 = \frac{b_1}{2}$

considering the microstates where the lower rod completes some full turns, we observe totally 7 cases in the first, while a total number of 16 cases in the latter.



$\theta_1 = 75,\ \theta_2 = 15$ $\theta_1 = 75,\ \theta_2 = 30$

$\theta_1 = 75,\ \theta_2 = 45$ $\theta_1 = 75,\ \theta_2 = 60$

$\theta_1 = 75,\ \theta_2 = 75$ $\theta_1 = 75,\ \theta_2 = 90$

Figure 4.21. The graphical solutions of $\theta_2 = 15, 30, 45, 75, 90$ for small, medium, and large values corresponding to the large angle value of $\theta_1 = 75$. The other parameters are $b_1 = 1, b_2 = 0.5, m_1 = 1, m_2 = 1, a = 0, \omega = 0$.

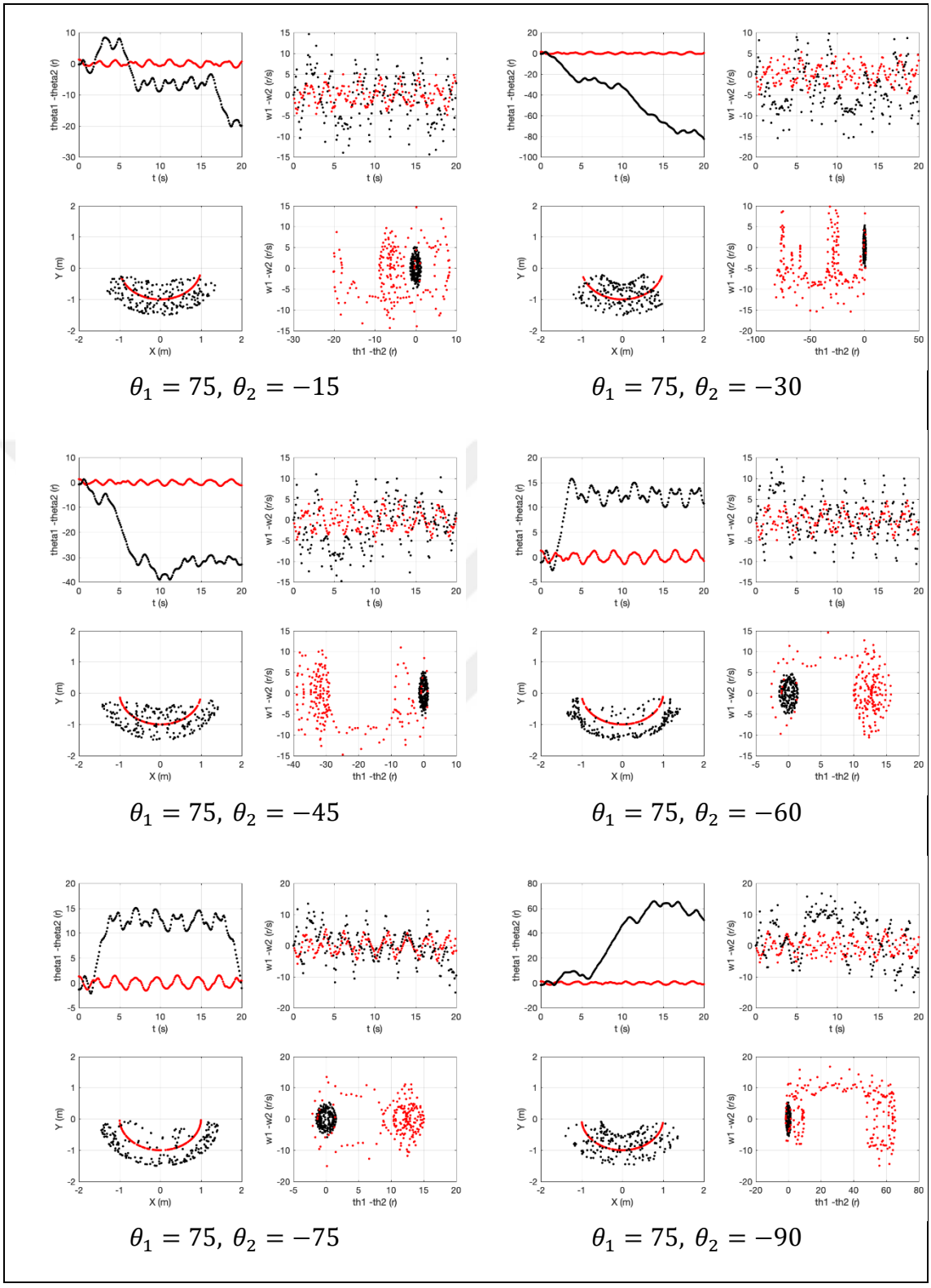


Figure 4.22. The graphical solutions of $\theta_2 = -15, -30, -45, -75, -90$ for small, medium, and large values corresponding to the large angle value of $\theta_1 = 75$. The other parameters are $b_1 = 1, b_2 = 0.5, m_1 = 1, m_2 = 1, a = 0, \omega = 0$.

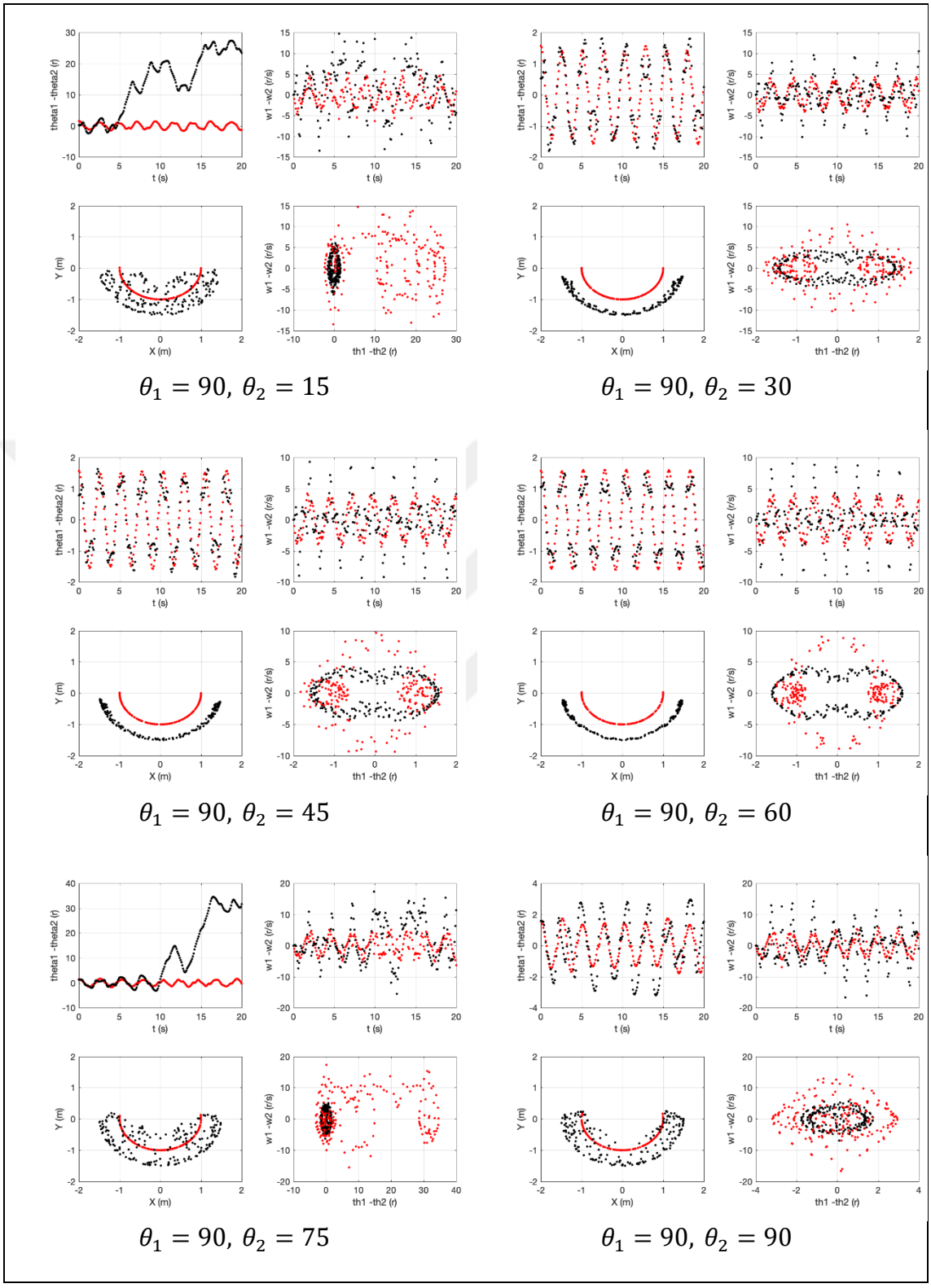


Figure 4.23. The graphical solutions of $\theta_2 = 15, 30, 45, 75, 90$ for small, medium, and large values corresponding to the large angle value of $\theta_1 = 90$. The other parameters are $b_1 = 1, b_2 = 0.5, m_1 = 1, m_2 = 1, a = 0, \omega = 0$.

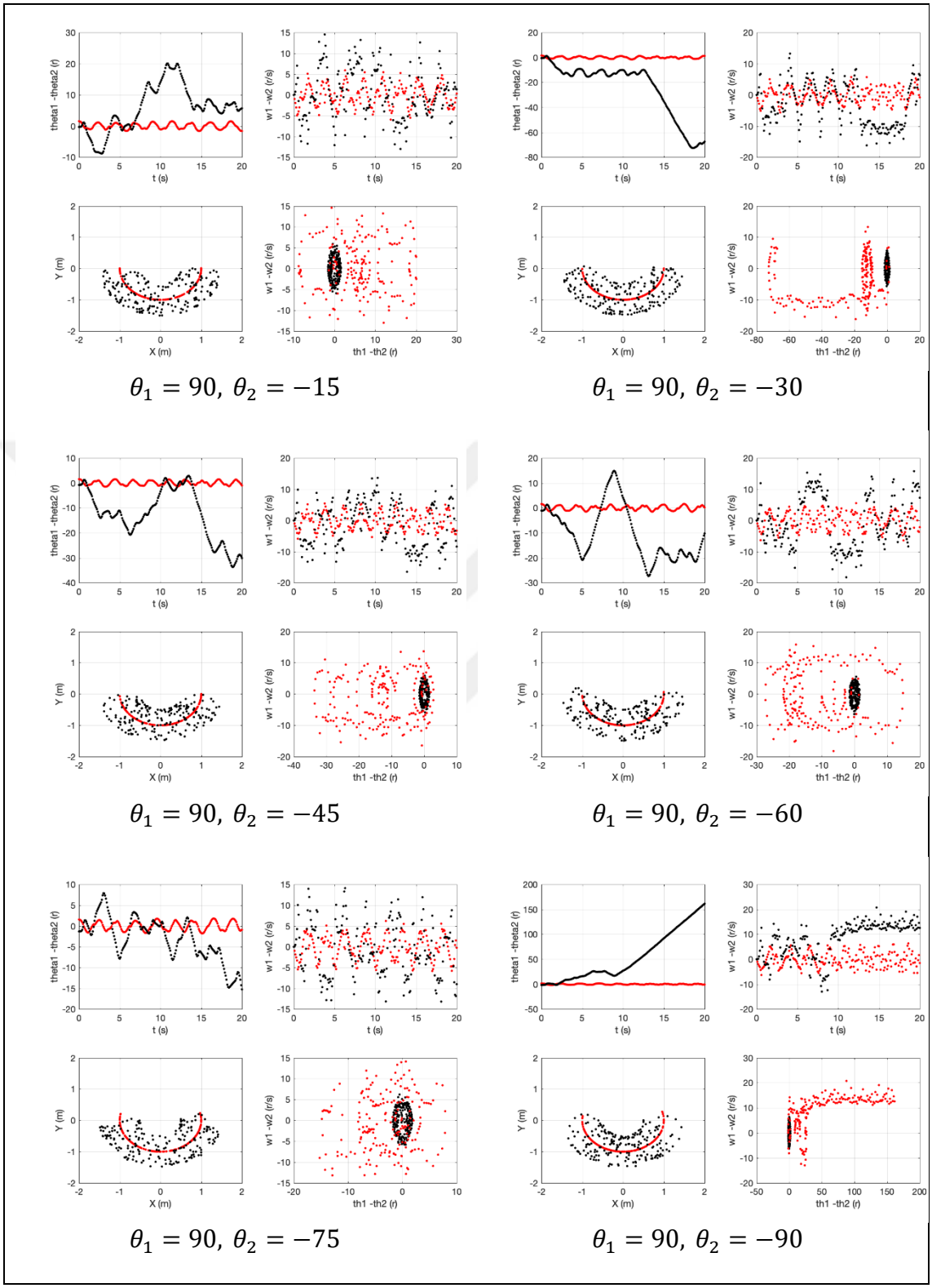


Figure 4.24. The graphical solutions of $\theta_2 = -15, -30, -45, -75, -90$ for small, medium, and large values corresponding to the large angle value of $\theta_1 = 90$. The other parameters are $b_1 = 1, b_2 = 0.5, m_1 = 1, m_2 = 1, a = 0, \omega = 0$.

A mathematical model was developed where the mass and rod lengths are equal and the mass is taken as a variable. As a third system, a mathematical model was created where the rod lengths vary. If the rod length of the mass above is assumed to be $b_1 = l$, the first model was studied with the length of the rod of the mass below reduced by half. Figures 4.21. and 4.23. show the graphs with increasing differences of 15 degrees in θ_2 from 15 to 90 degrees for large initial values of θ_1, where theta1 takes the values of 75 and 90 degrees. In Figure 4.23, in the graphs obtained for $\theta_2$values of 15 and 90, we observed that at the 10th second of the oscillations of the lower mass, it bifurcates and deviates from the oscillation as a full turn, performing somersaults both clockwise and counter clockwise. For other initial values, the upper and lower mass oscillated in phase, producing a periodic motion profile. Figures 4.22 and 4.24 were created with the symmetric values of θ_2. In both large angle values of θ_1, which are 75 and 90 degrees, bifurcations and somersaults were observed for all θ_2 values. The lower mass has irregular behaviour, making clockwise or counter clockwise rotations. In the large-angle motion starting from θ_1 =75 degrees, the system fully transitions to chaotic behaviour due to the effect of reducing the length of the rod of the lower mass by half.

Another mathematical model was created for a sub system, which was designed by doubling the length of the lower mass relative to the upper mass, as a second sub system after the system where the bar length was reduced to half. This lower system with the formulated mathematical model caused the opposite scenario in the motion profile compared to the system where the bar length was halved. Nearly all initial conditions of theta1 or theta2 exhibited small-amplitude, periodic, and quasiperiodic phase portraits. As seen in Figures 4.25 and 4.27, the lower and upper masses oscillated in the same phase and at the same frequency. The results obtained for the symmetric values of θ_2 in Figures 4.26 and 4.28, unlike periodic oscillation, had irregular oscillations with smaller angles that dampened each other due to the initial conditions of θ_1 and θ_2.

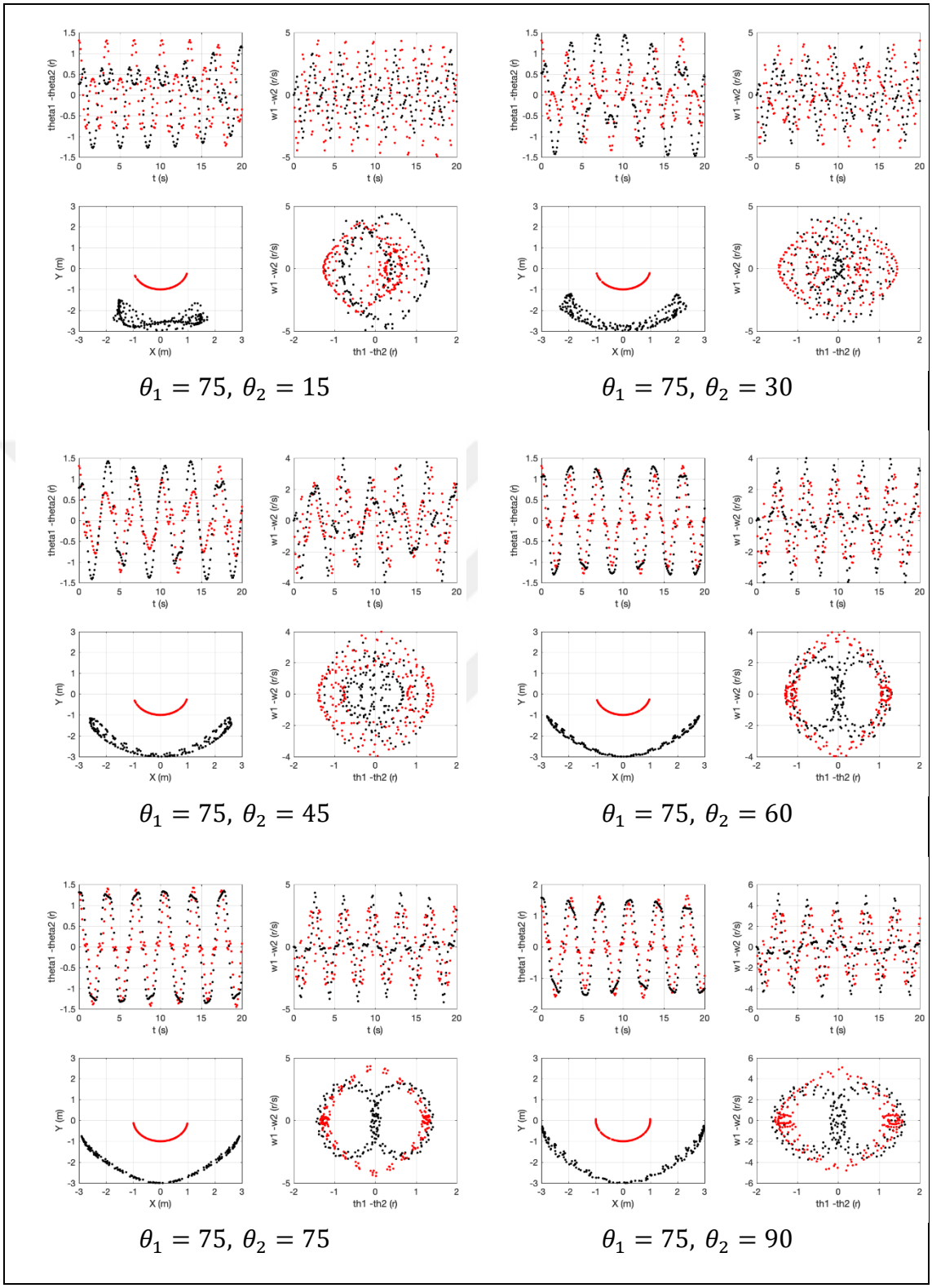


Figure 4.25. The graphical solutions of $\theta_2 = 15, 30, 45, 75, 90$ for small, medium, and large values corresponding to the large angle value of $\theta_1 = 75$. The other parameters are $b_1 = 1, b_2 = 2, m_1 = 1, m_2 = 1, a = 0, \omega = 0$.

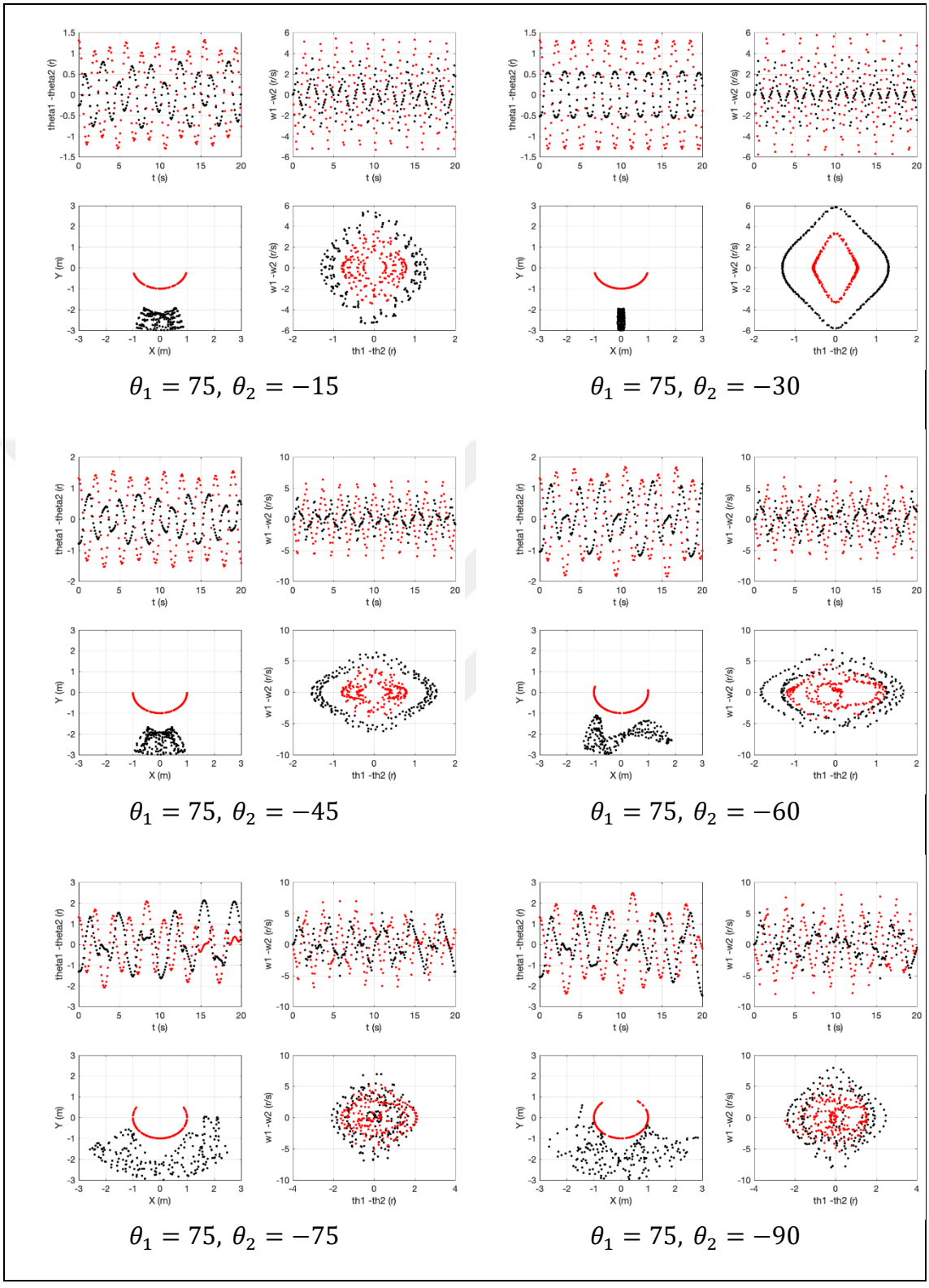


Figure 4.26. The graphical solutions of $\theta_2 = -15, -30, -45, -75, -90$ for small, medium, and large values corresponding to the large angle value of $\theta_1 = 75$. The other parameters are $b_1 = 1, b_2 = 2, m_1 = 1, m_2 = 1, a = 0, \omega = 0$.

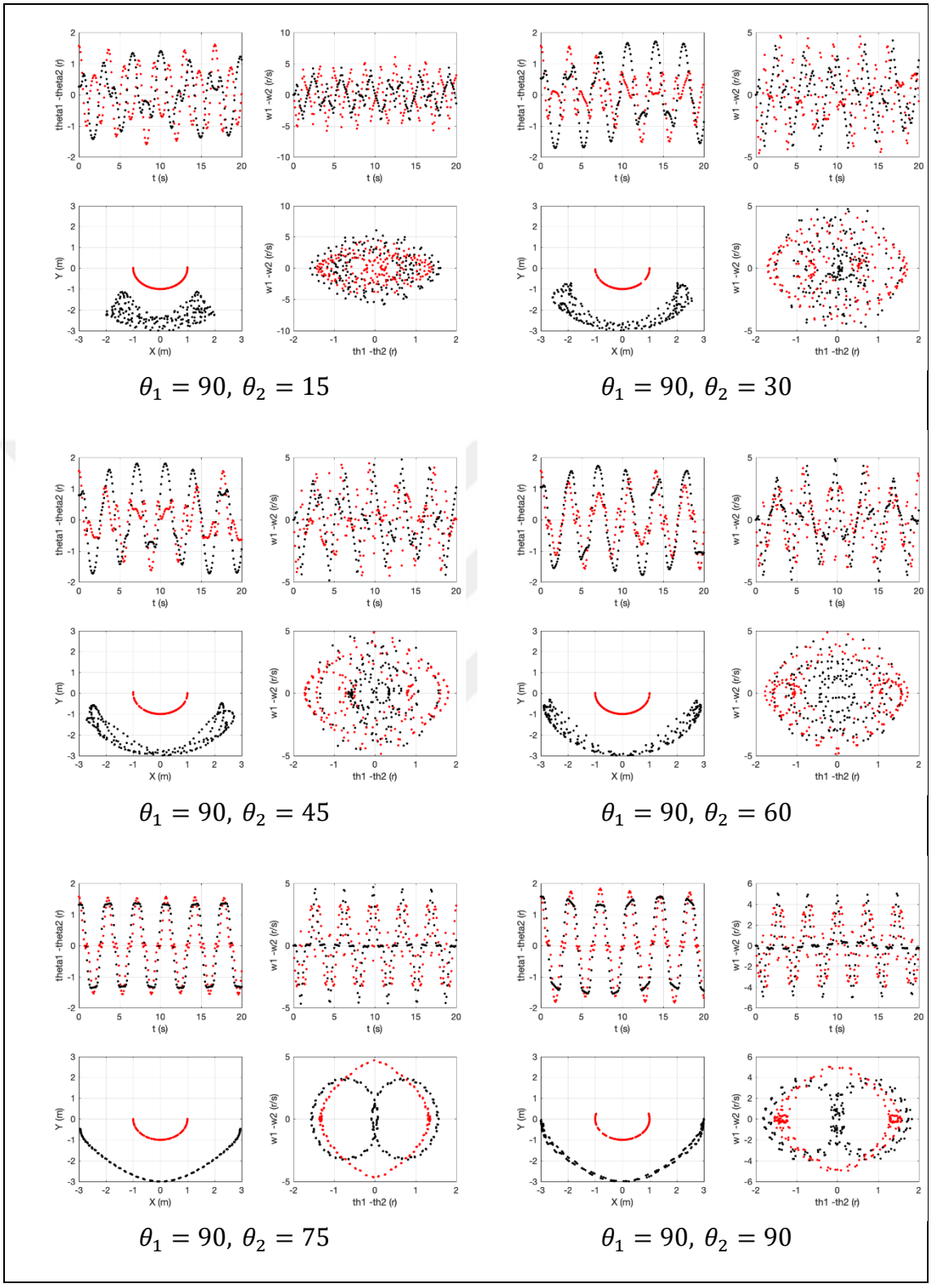


Figure 4.27. The graphical solutions of $\theta_2 = 15, 30, 45, 75, 90$ for small, medium, and large values corresponding to the large angle value of $\theta_1 = 90$. The other parameters are $b_1 = 1, b_2 = 2, m_1 = 1, m_2 = 1, a = 0, \omega = 0$.

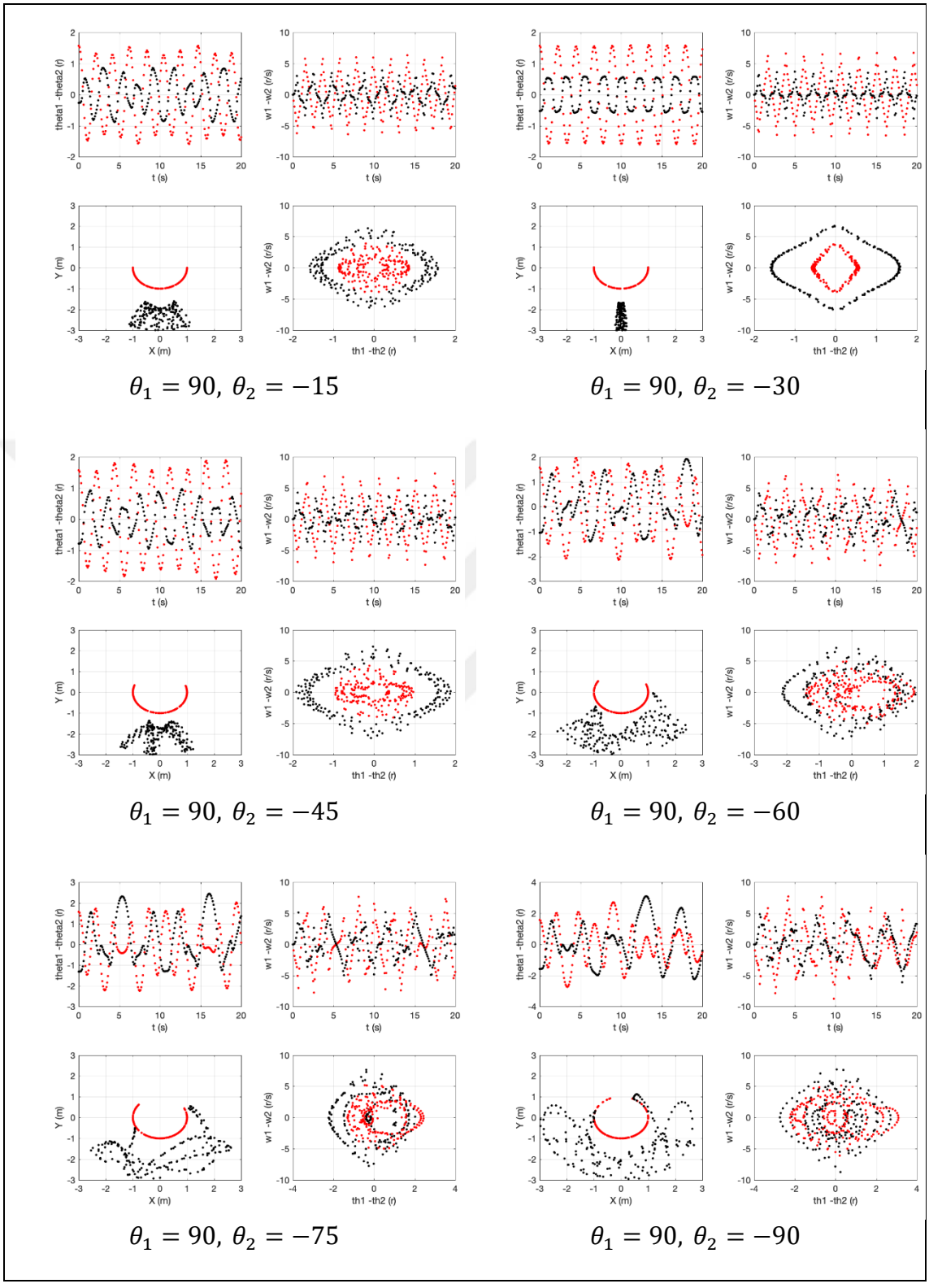
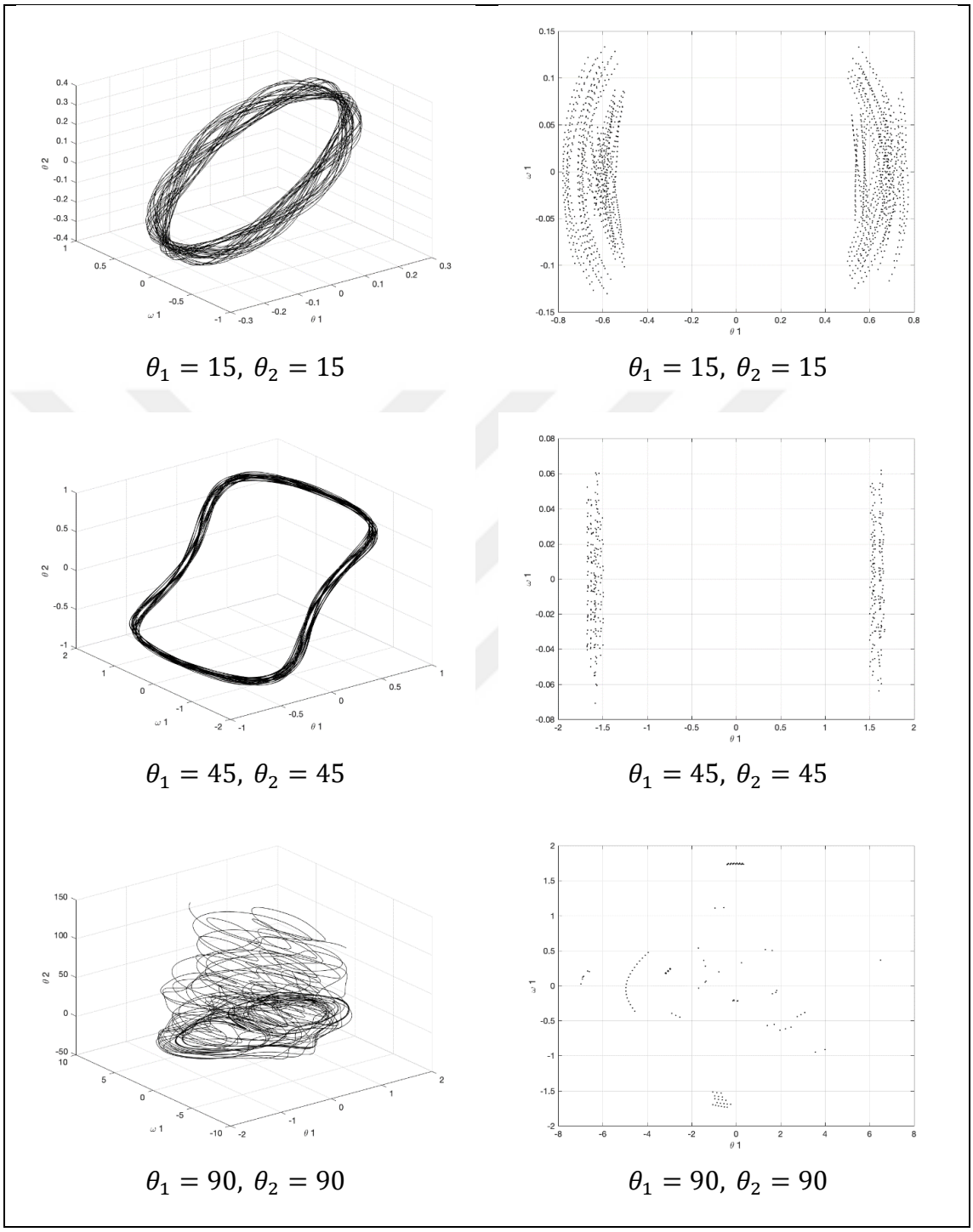


Figure 4.28. The graphical solutions of $\theta_2 = -15, -30, -45, -75, -90$ for small, medium, and large values corresponding to the large angle value of $\theta_1 = 90$. The other parameters are $b_1 = 1, b_2 = 2, m_1 = 1, m_2 = 1, a = 0, \omega = 0$.



$\theta_1 = 15,\ \theta_2 = 15$ $\theta_1 = 15,\ \theta_2 = 15$

$\theta_1 = 45,\ \theta_2 = 45$ $\theta_1 = 45,\ \theta_2 = 45$

$\theta_1 = 90,\ \theta_2 = 90$ $\theta_1 = 90,\ \theta_2 = 90$

Figure 4.29. The representation of phase portraits and Poincaré sections for system of double pendulum, $(\theta_1; \theta_2)$ = (15,15),(45,45),(90,90), The other parameters are $b_1 = 1, b_2 = 0.5, m_1 = 1, m_2 = 1, a = 0, \omega = 0.$

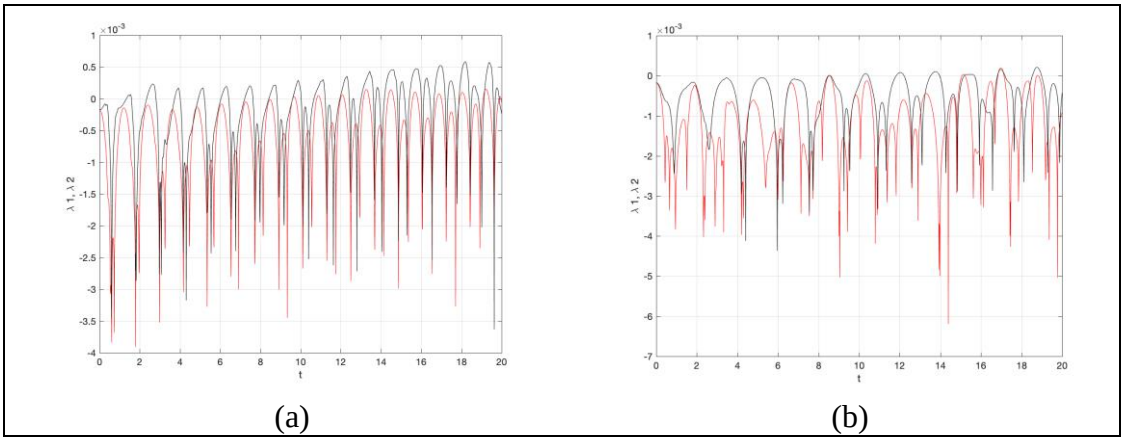


Figure 4.30. The graphic of the lyapunov exponents of double pendulum, (a) $\theta_1 = 45$ and $\theta_2 = 45$, $b_1 = 1, b_2 = 0.5, m_1 = 1, m_2 = 1, a = 0, \omega = 0$. (b) θ_1=45 and θ_2=45, $b_1 = 1, b_2 = 2, m_1 = 1, m_2 = 1, a = 0, \omega = 0$.

In Figure 4.29. we look phase diagrams at the 3D graph consisting of $\theta_1, \omega_1, \theta_2$, for small, medium, and large angle values of θ_1 and θ_2. We can see that oscillations starting with the same initial values for θ_1 and θ_2 exhibit oscillations in phase for small and medium angles, but for large angles, where the system actually has high energy, The system goes to chaotic region. When the Poincare sections are also examined, we observed that the sections are periodic and in order for small and medium angles, but for large angles, they become irregular, completely deviating from order and transitioning to chaos.

We calculated the Lyapunov exponents for this system and were unable to obtain positive exponents for the sub-system where we doubled the length of the lower mass. With the negative or zero exponents we calculated, the system exhibited regular behavior, while keeping the λ is negative. However, when we halved the length of the lower mass, we obtained positive Lyapunov exponents as shown in Figure 4.30. Positive Lyapunov exponents indicate a transition to chaotic behaviour of the system.

5. VIBRATING STATES OF DOUBLE PENDULUM

5.1. HORIZONTAL VIBRATIONS

In this part of the study, as shown in the figure the joint will be subject to external horizontal vibrations in the form of a harmonic function $x = a\cos\omega t$ where a is the amplitude and ω is the frequency that may be chosen at will. Therefore, the new coordinates of the bobs will respectively be

$$x_1 = a\cos\omega t + b_1\sin\theta_1 \tag{5.1}$$

$$y_1 = -b_1\cos\theta_1 \tag{5.2}$$

$$x_2 = a\cos\omega t + b_1\sin\theta_1 + b_2\sin\theta_2 \tag{5.3}$$

$$y_2 = -b_1\cos\theta_1 - b_2\cos\theta_2 \tag{5.4}$$

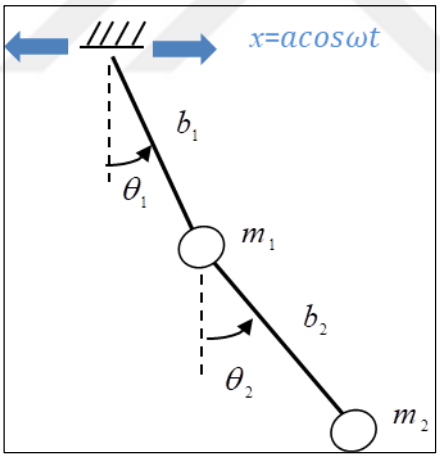


Figure 5.1. External horizontal vibrations of the joint according to a sinusoidal function.

Now the equations for the kinetic and potential energy for the horizontal oscillations are respectively

$$T = \frac{m_1}{2}\left(\dot{x}_1{}^2 + \dot{y}_1{}^2\right) + \frac{m_2}{2}\left(\dot{x}_2{}^2 + \dot{y}_2{}^2\right) \tag{5.5}$$

$$V = m_1 g y_1 + m_2 g y_2 \tag{5.6}$$

$$V = -m_1 g b_1\cos\theta_1 - m_2 g\left(b_1\cos\theta_1 + b_2\cos\theta_2\right) \tag{5.7}$$

Since in this analysis we apply Lagrange formalism

$L = T - V$ and $\frac{d}{dt}\frac{\partial L}{\partial \dot{\theta}_1} - \frac{\partial L}{\partial \theta_1} = 0$ where L is the Lagrangian, T is the kinetic energy and V is the potential energy.

$$\dot{x}_1 = -a\omega \sin \omega t + b_1 \dot{\theta}_1 \cos \theta_1 \tag{5.8}$$

$$\dot{y}_1 = b_1 \dot{\theta}_1 \sin \theta_1 \tag{5.9}$$

$$\dot{x}_2 = -a\omega \sin \omega t + b_1 \dot{\theta}_1 \cos \theta_1 + b_2 \dot{\theta}_2 \cos \theta_2 \tag{5.10}$$

$$\dot{y}_2 = b_1 \dot{\theta}_1 \sin \theta_1 + b_2 \dot{\theta}_2 \sin \theta_2 \tag{5.11}$$

So the kinetic energy of the system is

$$\begin{aligned} T &= \frac{m_1}{2}\left[a^2\omega^2 \sin^2 \omega t + b_1^2 \dot{\theta}_1^2 \cos^2 \theta_1 - 2ab_1\omega\dot{\theta}_1 \sin \omega t \cos\theta_1 + b_1^2\dot{\theta}_1^2 \sin^2 \theta_1\right] \\ &+ \frac{m_2}{2}\begin{bmatrix} a^2\omega^2 \sin^2 \omega t + b_1^2\dot{\theta}_1^2 \cos^2 \theta_1 + b_2^2\dot{\theta}_2^2 \cos^2 \theta_2 \\ +2\left(-ab_1\omega\dot{\theta}_1 \sin \omega t \cos\theta_1 - ab_2\omega\dot{\theta}_2 \sin \omega t \cos\theta_2 + b_1b_2\dot{\theta}_1\dot{\theta}_2 \cos\theta_1 \cos\theta_2\right) \\ + b_1^2\dot{\theta}_1^2 \sin^2 \theta_1 + b_2^2\dot{\theta}_2^2 \sin^2 \theta_2 + 2b_1b_2\dot{\theta}_1\dot{\theta}_2 \sin\theta_1 \sin\theta_2 \end{bmatrix} \end{aligned} \tag{5.12}$$

$$V = -m_1 g b_1 \cos\theta_1 - m_2 g\left(b_1 \cos\theta_1 + b_2 \cos\theta_2\right) \tag{5.13}$$

The new Lagrangian can therefore be written as

$$\begin{aligned} L &= \frac{m_1}{2}\left[a^2\omega^2 \sin^2 \omega t + b_1^2\dot{\theta}_1^2 - 2ab_1\omega\dot{\theta}_1 \sin \omega t \cos\theta_1\right] \\ &+ \frac{m_2}{2}\begin{bmatrix} a^2\omega^2 \sin^2 \omega t + b_1^2\dot{\theta}_1^2 + b_2^2\dot{\theta}_2^2 \\ +2\left(-ab_1\omega\dot{\theta}_1 \sin \omega t \cos\theta_1 - ab_2\omega\dot{\theta}_2 \sin \omega t \cos\theta_2 + b_1b_2\dot{\theta}_1\dot{\theta}_2 \cos\theta_1 \cos\theta_2\right) \\ + 2b_1b_2\dot{\theta}_1\dot{\theta}_2 \sin\theta_1 \sin\theta_2 \end{bmatrix} \\ &+ m_1 g b_1 \cos\theta_1 + m_2 g\left(b_1 \cos\theta_1 + b_2 \cos\theta_2\right) \end{aligned} \tag{5.14}$$

$$\begin{aligned} \frac{\partial L}{\partial \theta_1} &= m_1\left[ab_1\omega\dot{\theta}_1 \sin \omega t \sin\theta_1\right] + m_2\left[ab_1\omega\dot{\theta}_1 \sin \omega t \sin\theta_1 - b_1b_2\dot{\theta}_1\dot{\theta}_2 \cos\theta_1 \sin\theta_2\right] \\ &- \left(m_1 + m_2\right)gb_1 \sin\theta_1 \end{aligned} \tag{5.15}$$

$$\frac{\partial L}{\partial \dot{\theta}_1} = m_1 b_1\left[b_1\dot{\theta}_1 - a\omega \sin \omega t \cos\theta_1\right] + m_2 b_1\left[b_1\dot{\theta}_1 - a\omega \sin \omega t \cos\theta_1 + b_2\dot{\theta}_2 \cos\left(\theta_1 - \theta_2\right)\right] \tag{5.16}$$

$$\frac{d}{dt}\frac{\partial L}{\partial \dot{\theta}_1} = m_1 b_1\left[b_1\ddot{\theta}_1 - a\omega\left(\omega\cos\omega t\cos\theta_1 - \dot{\theta}_1\sin\omega t\sin\theta_1\right)\right]$$
$$+ m_2 b_1\left[b_1\ddot{\theta}_1 - a\omega\left(\omega\cos\omega t\cos\theta_1 - \dot{\theta}_1\sin\omega t\sin\theta_1\right) - b_2\ddot{\theta}_2\left(\ddot{\theta}_1 - \ddot{\theta}_2\right)\sin(\theta_1 - \theta_2)\right] = 0 \quad (5.17)$$

$$\frac{d}{dt}\frac{\partial L}{\partial \dot{\theta}_1} - \frac{\partial L}{\partial \theta_1} = m_1 b_1\left[b_1\ddot{\theta}_1 - a\omega^2\cos\omega t\cos\theta_1 + a\omega\dot{\theta}_1\sin\omega t\sin\theta_1\right]$$
$$+ m_2 b_1\left[b_1\ddot{\theta}_1 - a\omega^2\cos\omega t\cos\theta_1 + a\omega\dot{\theta}_1\sin\omega t\sin\theta_1 - b_2\ddot{\theta}_2\left(\ddot{\theta}_1 - \ddot{\theta}_2\right)\sin(\theta_1 - \theta_2)\right] \quad (5.18)$$
$$- m_1 a b_1\omega\dot{\theta}_1\sin\omega t\sin\theta_1 - m_2 b_1\left[a\omega\dot{\theta}_1\sin\omega t\sin\theta_1 - b_2\dot{\theta}_1\dot{\theta}_2\cos\theta_1\sin\theta_2\right] = 0$$

$$(m_1 + m_2)b_1\left[\ddot{\theta}_1 - a\omega^2\cos\omega t\cos\theta_1\right] + m_2 b_2\left[\dot{\theta}_1\dot{\theta}_2\cos\theta_1\sin\theta_2 - \ddot{\theta}_2\left(\ddot{\theta}_1 - \ddot{\theta}_2\right)\sin(\theta_1 - \theta_2)\right] = 0 \quad (5.19)$$

$$\frac{\partial L}{\partial \theta_2} = \frac{m_2}{2}\left[2\left(ab_2\omega\dot{\theta}_2\sin\omega t\sin\theta_2 - b_1 b_2\dot{\theta}_1\dot{\theta}_2\cos\theta_1\sin\theta_2\right) + 2b_1 b_2\dot{\theta}_1\dot{\theta}_2\sin\theta_1\cos\theta_2\right] - m_2 g b_2\sin\theta_2 \quad (5.20)$$

$$\frac{\partial L}{\partial \theta_2} = m_2 b_2\left[a\omega\dot{\theta}_2\sin\omega t\sin\theta_2 - b_1\dot{\theta}_1\dot{\theta}_2\cos\theta_1\sin\theta_2 + b_1\dot{\theta}_1\dot{\theta}_2\sin\theta_1\cos\theta_2 - g\sin\theta_2\right] \quad (5.21)$$

$$\frac{\partial L}{\partial \dot{\theta}_2} = m_2\left[b_2\dot{\theta}_2 - ab_2\omega\sin\omega t\cos\theta_2 + \frac{1}{2}b_1 b_2\dot{\theta}_1\cos\theta_1\cos\theta_2 + b_1 b_2\dot{\theta}_1\sin\theta_1\sin\theta_2\right] \quad (5.22)$$

$$\frac{\partial L}{\partial \dot{\theta}_2} = m_2 b_2\left[\dot{\theta}_2 - a\omega\sin\omega t\cos\theta_2 + \frac{1}{2}b_1\dot{\theta}_1\cos\theta_1\cos\theta_2 + b_1\dot{\theta}_1\sin\theta_1\sin\theta_2\right] \quad (5.23)$$

5.2. HORIZONTAL VIBRATING STATES

Now the joint is vibrated horizontally (in *x* direction) at an amplitude equal to the length *b* of the rods ($a = b$) and at two frequencies $\omega_1 = 2\pi$ rad/s and $\omega_2 = 4\pi$ rad/s. $\omega_1 = 2\pi$ rad/s is the velocity at which the linear frequency of the external vibrations is $\vartheta = 1$ Hz ($1\ s^{-1}$). For instance a ket like $\left|\theta_1 = 45, \theta_2 = 15; V_{x/a=1/\omega=1}\right\rangle$ denotes that at time $t = 0$ the upper and lower rods make angles of 45 and 15 degrees with the vertical respectively and the joint is *V*ibrated in the *x* direction with an amplitude of *a* ($= b$) and with a frequency $\omega = \omega_1 = 2\pi$ rad/s while a ket like $\left|\theta_1 = 30, \theta_2 = -60; V_{x/a=1/\omega=2}\right\rangle$ denotes that at time $t = 0$ the upper and lower rods make angles of 30 and –60 degrees with the vertical respectively and the joint is Vibrated in the *x* direction with an amplitude of *a* ($= b$) and with a frequency $\omega = \omega_2 = 4\pi$ rad/s. The amplitude *a* was assigned different values around *b*, the length of the rod, but it was observed that the variations of the amplitude *a* have a little effect on the subsequent motion of the pendulum. Instead, the variation of the frequency ω of the external vibrations

can have a much larger effect on the motion. So a is set equal to the length b for both horizontal and vertical vibrations.

Let us again group the macrostates as in the stationary cases. In this part of the analysis we will try to see the effects of the external vibrations of the joint on the subsequent motion of the double pendulum.

The graphs of the analysis of a system subjected to horizontal vibration from the vibrating states systems were presented in Figure 5.2. In relation to the horizontal movement, the first system examined had an amplitude of 0.5 meters and a frequency of $\omega = 1$. Regardless of whether the amplitude is small or large, the frequency primarily leads the motion profile of the system. A frequency value of 1 resulted in a profile that was almost equivalent to a stationary state. Upon examining Figures 5.2 and 5.4, it can be observed that for all cases, only 3 complete revolutions were obtained in 3 regions for 3 initial values of θ_1 and θ_2.

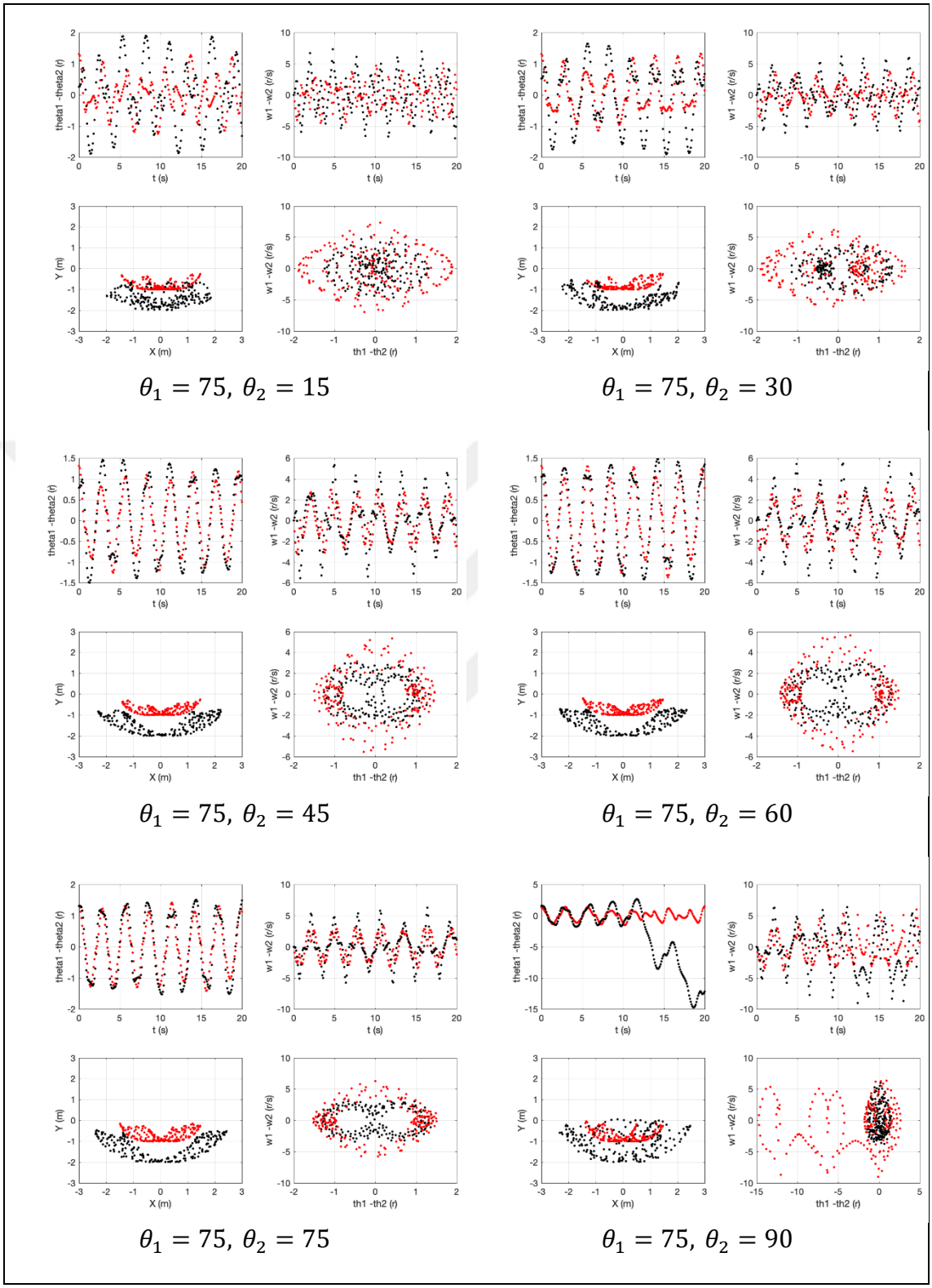


Figure 5.2. The graphical solutions of $\theta_2 = 15, 30, 45, 60, 75, 90$ for small, medium, and large values corresponding to the large angle value of $\theta_1 = 75$. The other parameters are $b_1 = 1, b_2 = 1, m_1 = 1, m_2 = 1, a = 0.5, \omega = 1$, horizontal vibrating.

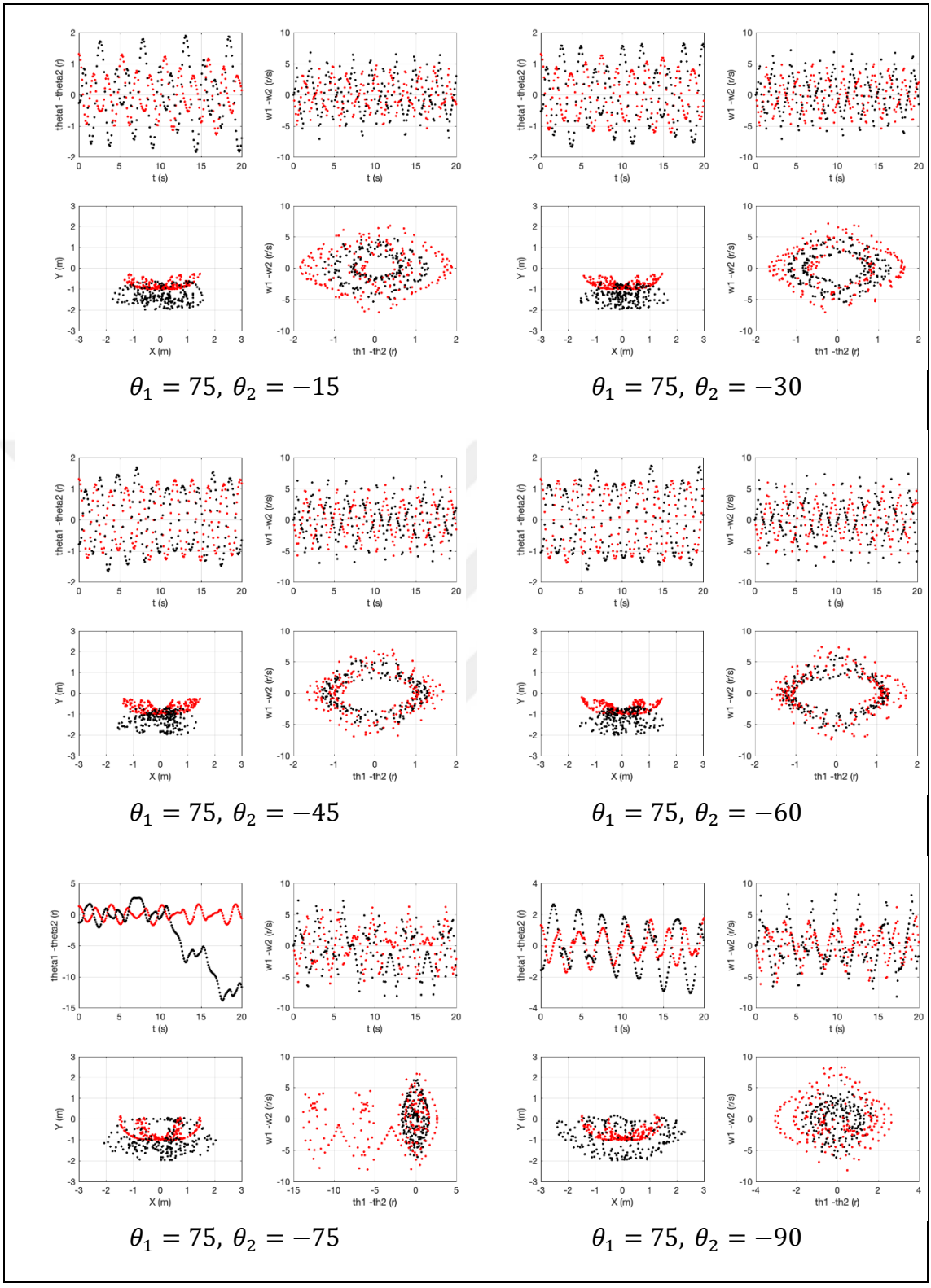


Figure 5.3. The graphical solutions of $\theta_2 = -15, -30, -45, -60, -75, -90$ for small, medium, and large values corresponding to the large angle value of $\theta_1 = 75$. The other parameters are $b_1 = 1, b_2 = 1, m_1 = 1, m_2 = 1, a = 0.5, \omega = 1$, horizontal vibrating.

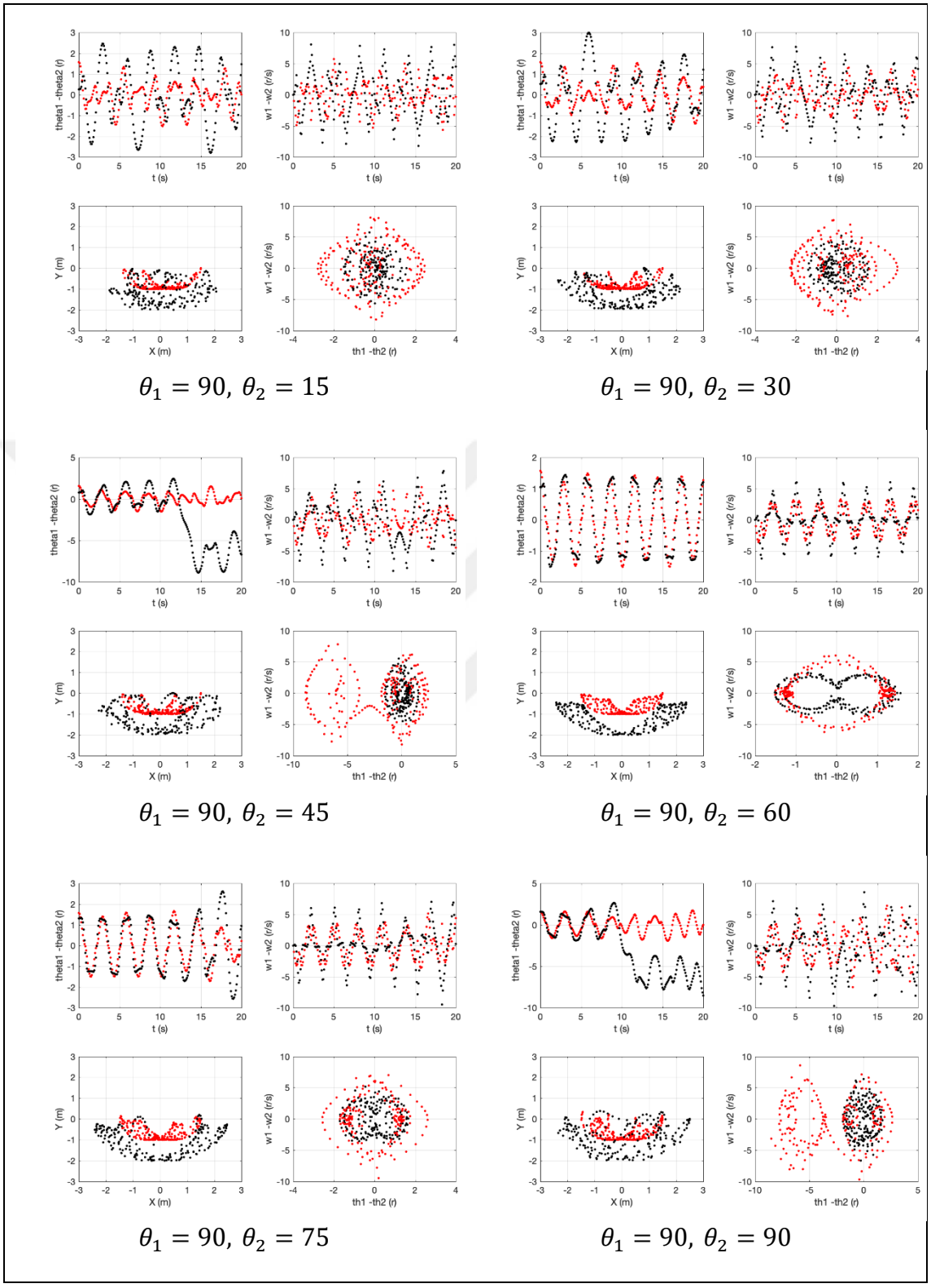


Figure 5.4. The graphical solutions of $\theta_2 = 15, 30, 45, 60, 75, 90$ for small, medium, and large values corresponding to the large angle value of $\theta_1 = 90$. The other parameters are $b_1 = 1, b_2 = 1, m_1 = 1, m_2 = 1, a = 0.5, \omega = 1$, horizontal vibrating.

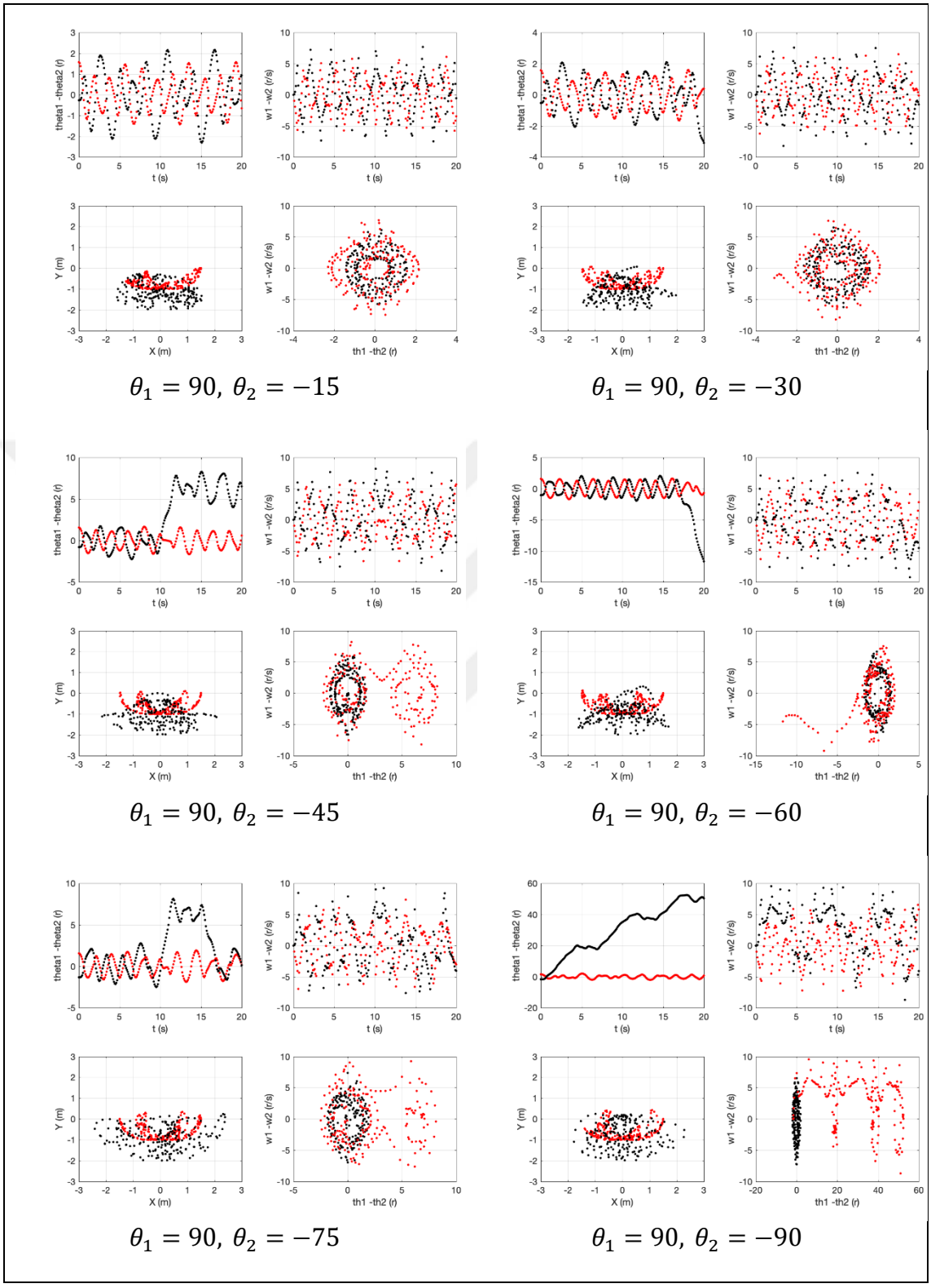


Figure 5.5. The graphical solutions of $\theta_2 = -15, -30, -45, -60, -75, -90$ for small, medium, and large values corresponding to the large angle value of $\theta_1 = 90$. The other parameters are $b_1 = 1, b_2 = 1, m_1 = 1, m_2 = 1, a = 0.5, \omega = 1$, horizontal vibrating.

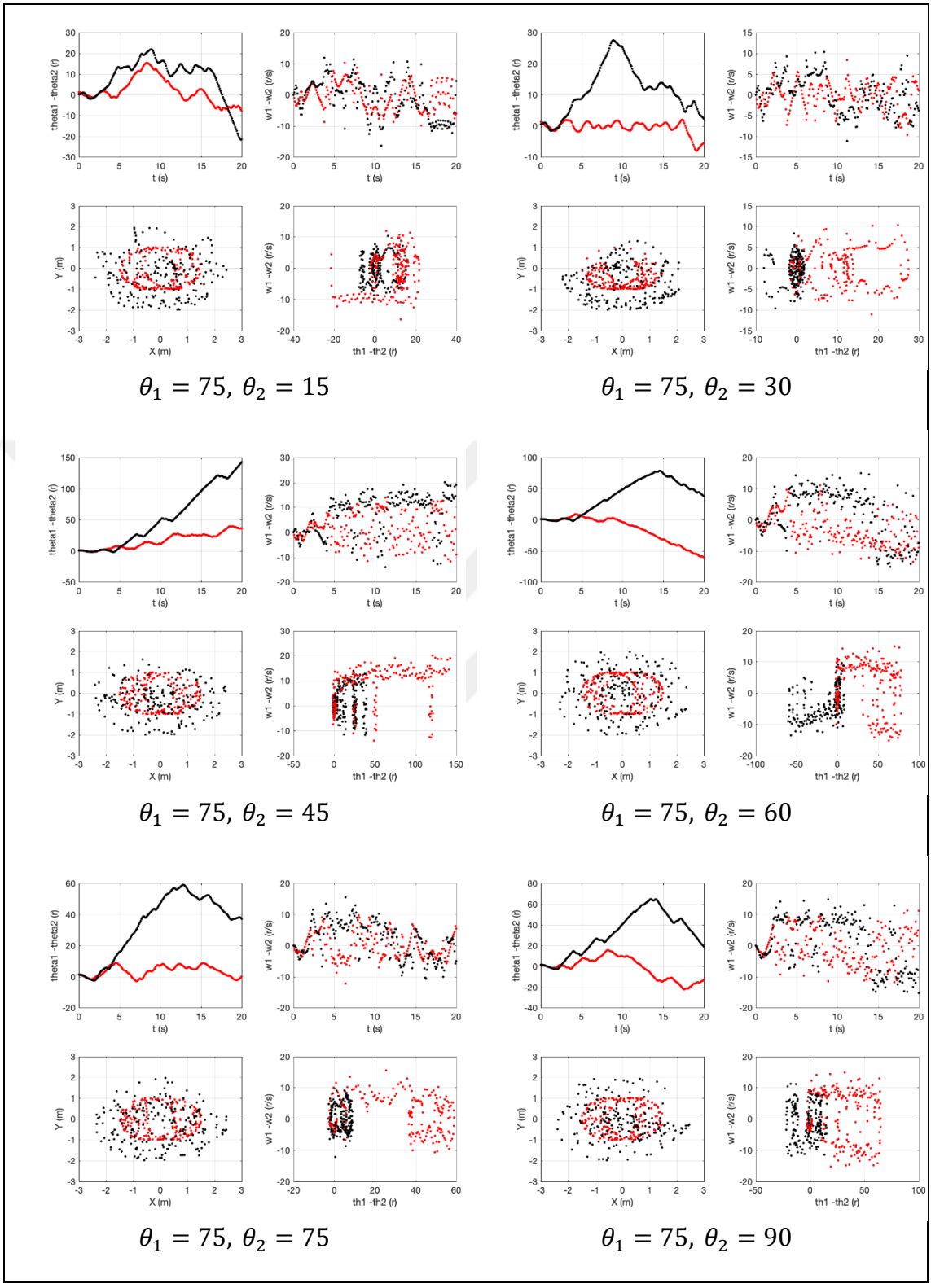


Figure 5.6. The graphical solutions of $\theta_2 = 15, 30, 45, 60, 75, 90$ for small, medium, and large values corresponding to the large angle value of $\theta_1 = 75$. The other parameters are $b_1 = 1, b_2 = 1, m_1 = 1, m_2 = 1, a = 0.5, \omega = 3$, horizontal vibrating.

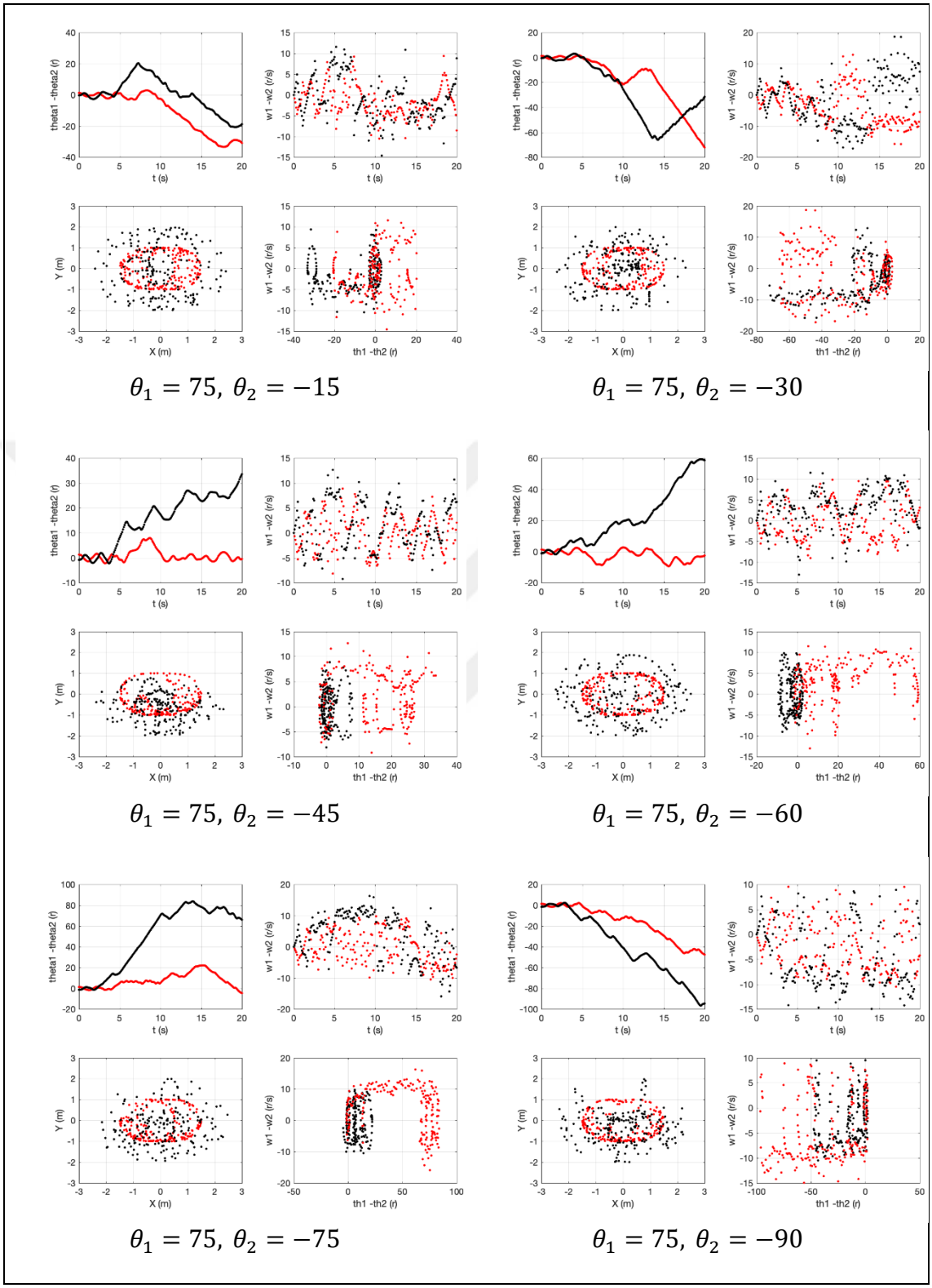


Figure 5.7. The graphical solutions of $\theta_2 = -15, -30, -45, -60, -75, -90$ for small, medium, and large values corresponding to the large angle value of $\theta_1 = 75$. The other parameters are $b_1 = 1, b_2 = 1, m_1 = 1, m_2 = 1, a = 0.5, \omega = 3$, horizontal vibrating.

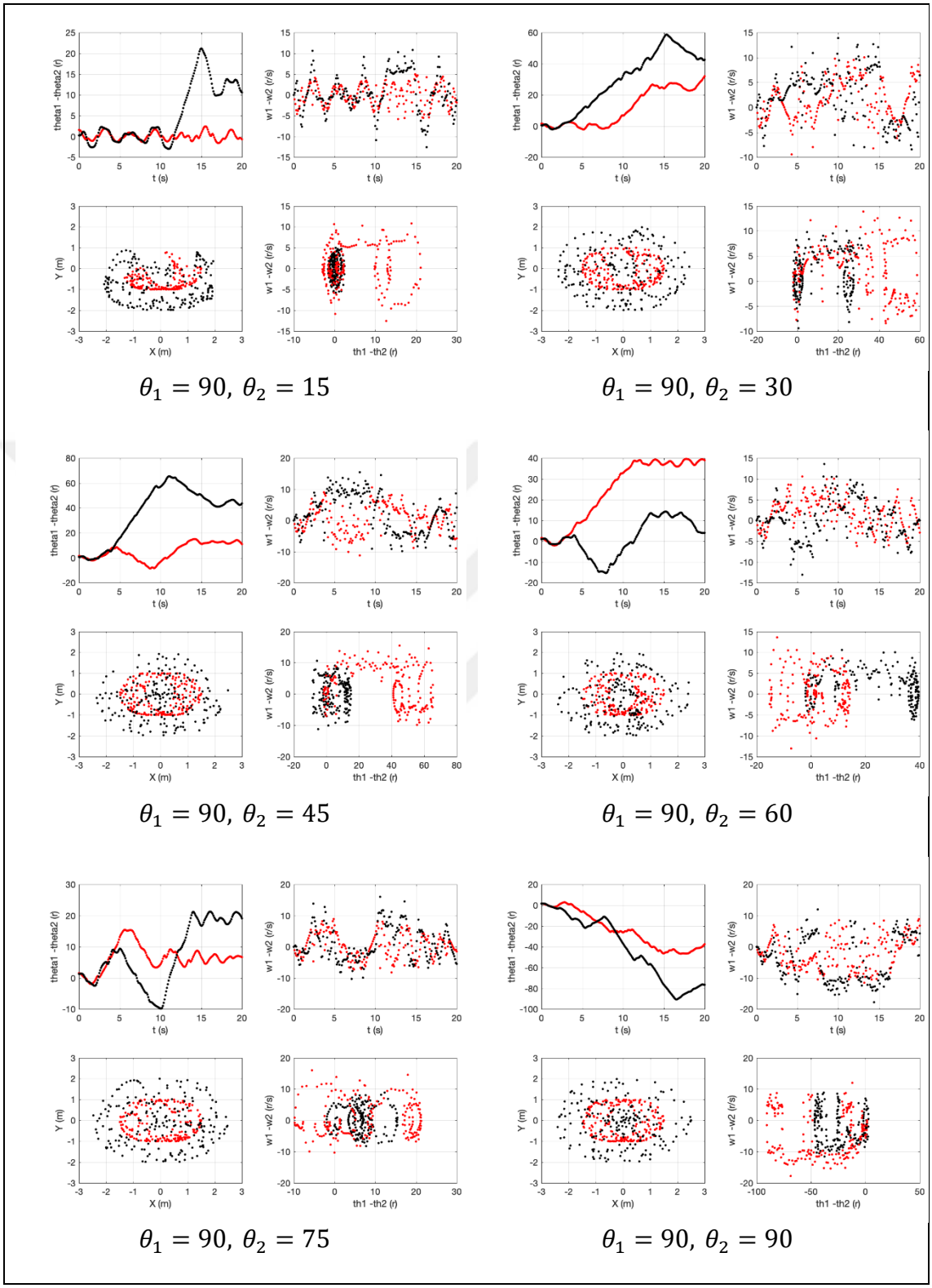


Figure 5.8. The graphical solutions of $\theta_2 = 15, 30, 45, 60, 75, 90$ for small, medium, and large values corresponding to the large angle value of $\theta_1 = 90$. The other parameters are $b_1 = 1, b_2 = 1, m_1 = 1, m_2 = 1, a = 0.5, \omega = 3$, horizontal vibrating.

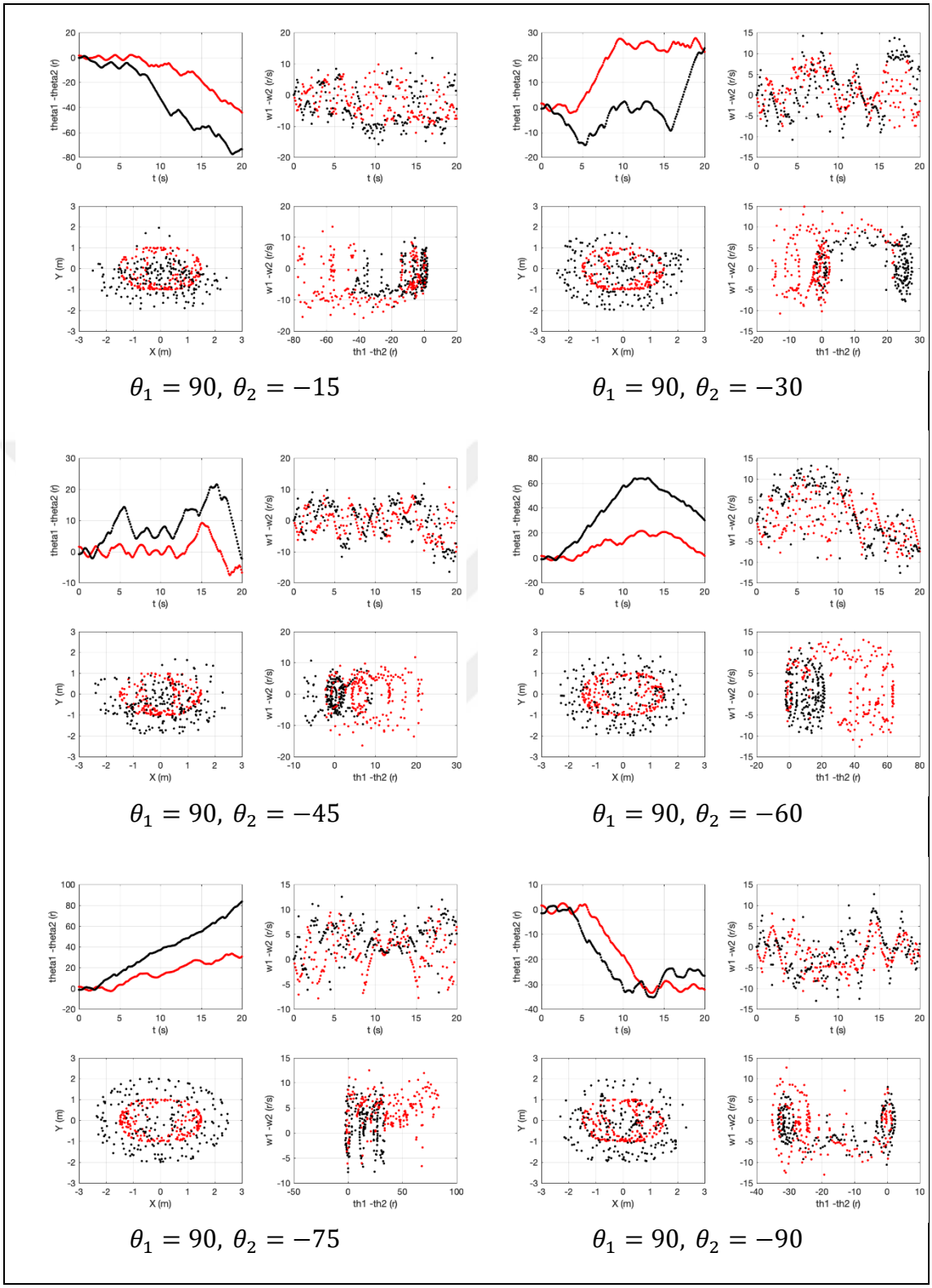


Figure 5.9. The graphical solutions of $\theta_2 = -15, -30, -45, -60, -75, -90$ for small, medium, and large values corresponding to the large angle value of $\theta_1 = 90$. The other parameters are $b_1 = 1, b_2 = 1, m_1 = 1, m_2 = 1, a = 0.5, \omega = 3$, horizontal vibrating.



Figure 5.10. The graphic of the lyapunov exponents of double pendulum, (a) $\theta_1 = 90$ and $\theta_2 = 90$, $b_1 = 1, b_2 = 1, m_1 = 1, m_2 = 1, a = 0.5, \omega = 1$. (b) $\theta_1 = 90$ and $\theta_2 = 90$, $b_1 = 1, b_2 = 1, m_1 = 1, m_2 = 1, a = 0.5, \omega = 3$.

By keeping the amplitude value at 0.5 meters and increasing the frequency value from 1 to 3, we obtained another sub-system within the horizontal vibrating system and examined the system that was exposed to horizontal vibration with equal values of mass and rod length. Figures 5.6 and 5.8 illustrate the results for θ_2 at small, medium, and large angles corresponding to θ_1 at 75 and 90-degree values. Compared to our previous model, we achieved a model with significant changes in the motion profile, with an increased number of chaotic regimes and irregular motions. The increase in frequency value indicates that it is more effective compared to the used vibration amplitude. Figures 5.7 and 5.9 were obtained by using the symmetric values of θ_2 angles, and they show the continuation of the same motion behavior, where the high frequency dominates the entire motion profile.

5.3. VERTICAL VIBRATIONS

In the second section of this part of the study, as shown in the figure the joint will be subject to external vertical vibrations in the form of a harmonic function $y = a\cos\omega t$ where a is the amplitude equal to the length b of the rods ($a = b$) and at two frequencies ω_1 and ω_2.

Therefore, the new coordinates of the bobs will respectively take the forms

$$x_1 = b_1 \sin\theta_1 \tag{5.24}$$

$$y_1 = a\cos\omega t - b_1\cos\theta_1 \tag{5.25}$$

$$x_2 = b_1\sin\theta_1 + b_2\sin\theta_2 \tag{5.26}$$

$$y_2 = a\cos\omega t - b_1\cos\theta_1 - b_2\cos\theta_2 \tag{5.27}$$

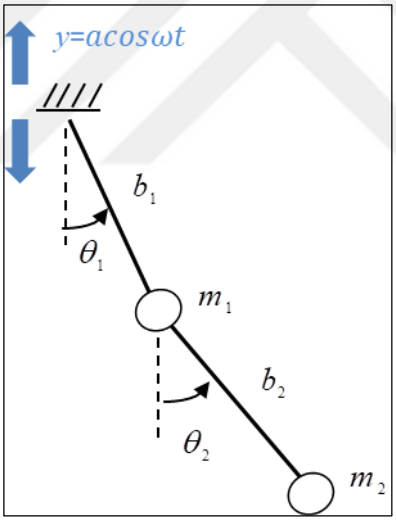


Figure 5.11. External vertical vibrations of the joint according to a sinusoidal function.

Now the equations for the kinetic and potential energy for the vertical oscillations (case **ii**) are respectively

$$T = \frac{m_1}{2}\left(\dot{x}_1{}^2 + \dot{y}_1{}^2\right) + \frac{m_2}{2}\left(\dot{x}_2{}^2 + \dot{y}_2{}^2\right) \tag{5.28}$$

$$V = m_1 g y_1 + m_2 g y_2 \tag{5.29}$$

$$\dot{x}_1 = b_1\dot{\theta}_1 \cos\theta_1 \tag{5.30}$$

$$\dot{y}_1 = -a\omega \sin\omega t + b_1\dot{\theta}_1 \sin\theta_1 \tag{5.31}$$

$$\dot{x}_2 = b_1\dot{\theta}_1 \cos\theta_1 + b_2\dot{\theta}_2 \cos\theta_2 \tag{5.32}$$

$$\dot{y}_2 = -a\omega \sin\omega t + b_1\dot{\theta}_1 \sin\theta_1 + b_2\dot{\theta}_2 \sin\theta_2 \tag{5.33}$$

So the kinetic energy of the system is

$$\begin{aligned} K = {} & \frac{m_1}{2}\left[a^2\omega^2 \sin^2\omega t + b_1^2\dot{\theta}_1^2 - 2ab_1\omega\dot{\theta}_1 \sin\omega t \sin\theta_1\right] \\ & + \frac{m_2}{2}\begin{bmatrix} a^2\omega^2 \sin^2\omega t + b_1^2\dot{\theta}_1^2 + b_2^2\dot{\theta}_2^2 \\ + 2\left(-ab_1\omega\dot{\theta}_1 \sin\omega t \sin\theta_1 - ab_2\omega\dot{\theta}_2 \sin\omega t \sin\theta_2 + b_1b_2\dot{\theta}_1\dot{\theta}_2 \sin\theta_1 \sin\theta_2\right) \\ + 2b_1b_2\dot{\theta}_1\dot{\theta}_2 \sin\theta_1 \sin\theta_2 \end{bmatrix} \end{aligned} \tag{5.34}$$

$$V = m_1 g\left(-b_1 \cos\theta_1\right) + m_2 g\left(a\cos\omega t - b_1\cos\theta_1 - b_2\cos\theta_2\right) \tag{5.35}$$

The new Lagrangian can therefore be written as

$$\begin{aligned} L = {} & \frac{m_1}{2}\left[a^2\omega^2 \sin^2\omega t + b_1^2\dot{\theta}_1^2 - 2ab_1\omega\dot{\theta}_1 \sin\omega t \cos\theta_1\right] \\ & + \frac{m_2}{2}\begin{bmatrix} a^2\omega^2 \sin^2\omega t + b_1^2\dot{\theta}_1^2 + b_2^2\dot{\theta}_2^2 \\ + 2\left(-ab_1\omega\dot{\theta}_1 \sin\omega t \cos\theta_1 - ab_2\omega\dot{\theta}_2 \sin\omega t \cos\theta_2 + b_1b_2\dot{\theta}_1\dot{\theta}_2 \cos\theta_1 \cos\theta_2\right) \\ + 2b_1b_2\dot{\theta}_1\dot{\theta}_2 \sin\theta_1 \sin\theta_2 \end{bmatrix} \\ & + m_1 g b_1 \cos\theta_1 + m_2 g\left(b_1\cos\theta_1 + b_2\cos\theta_2\right) \end{aligned} \tag{5.36}$$

5.4. VERTICAL VIBRATING STATES

In the second section of this part of the study, as shown in the figure the joint will be subject to external vertical vibrations in the form of a harmonic function $y = a\cos\omega t$ where a is the amplitude equal to the length b of the rods ($a = b$) and at two frequencies $\omega_1 = 2\pi$ rad/s and $\omega_2 = 4\pi$ rad/s. For instance a ket like $\left|\theta_1 = 45, \theta_2 = 15; V_{y/a=1/\omega=2}\right\rangle$ denotes that at time $t = 0$ the upper and lower rods make angles of 45 and 15 degrees with the vertical respectively and the joint is *V*ibrated in the *y* direction with an amplitude of a ($= b$) and with a frequency $\omega_2 = 4\pi$ rad/s.

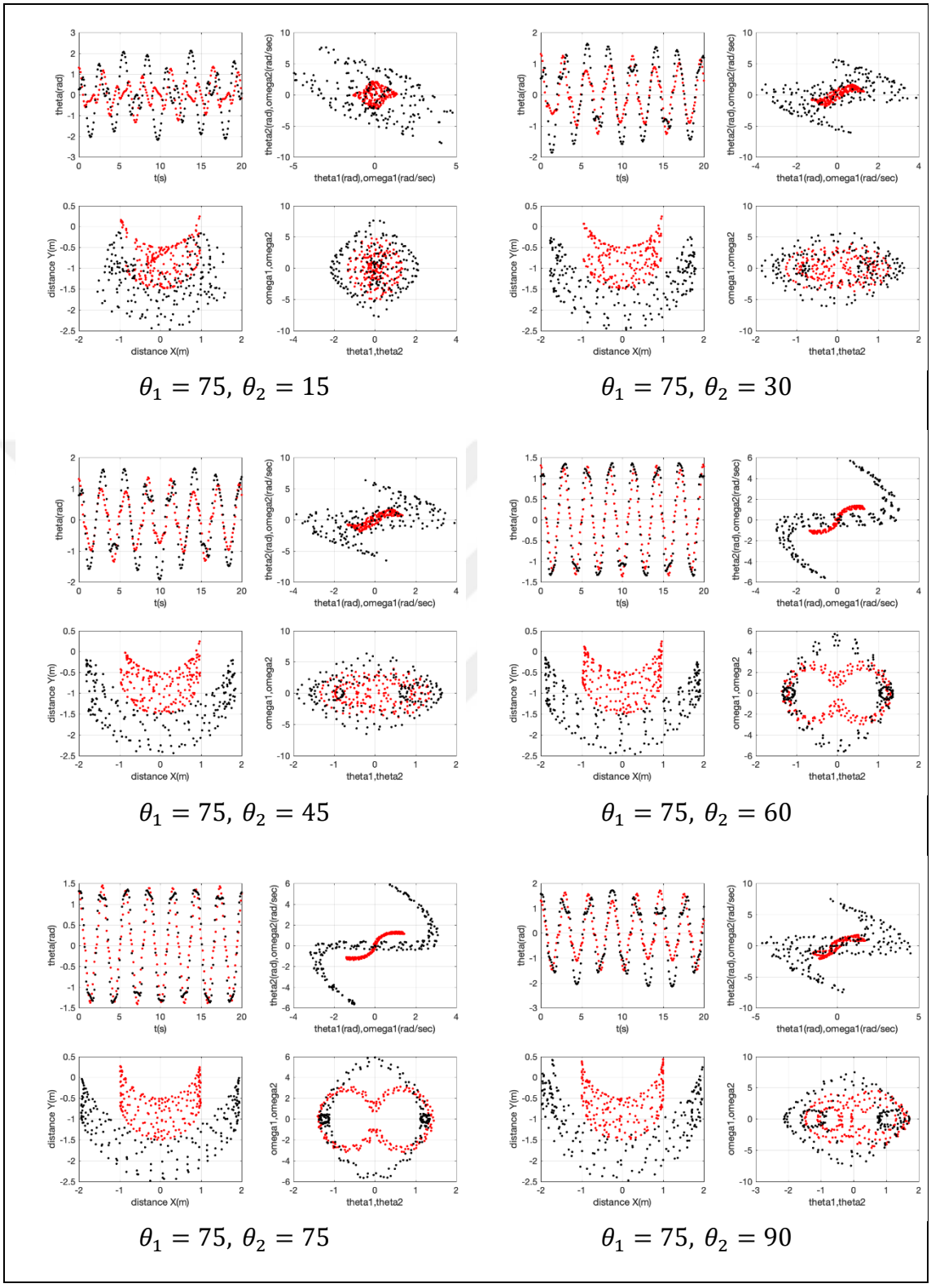


Figure 5.12. The graphical solutions of θ_2 =15, 30, 45, 75, 90 for small, medium, and large values corresponding to the large angle value of $\theta_1 = 75$. The other parameters are $b_1 = 1, b_2 = 1, m_1 = 1, m_2 = 1, a = 0.5, \omega = 1$, vertical vibrating.

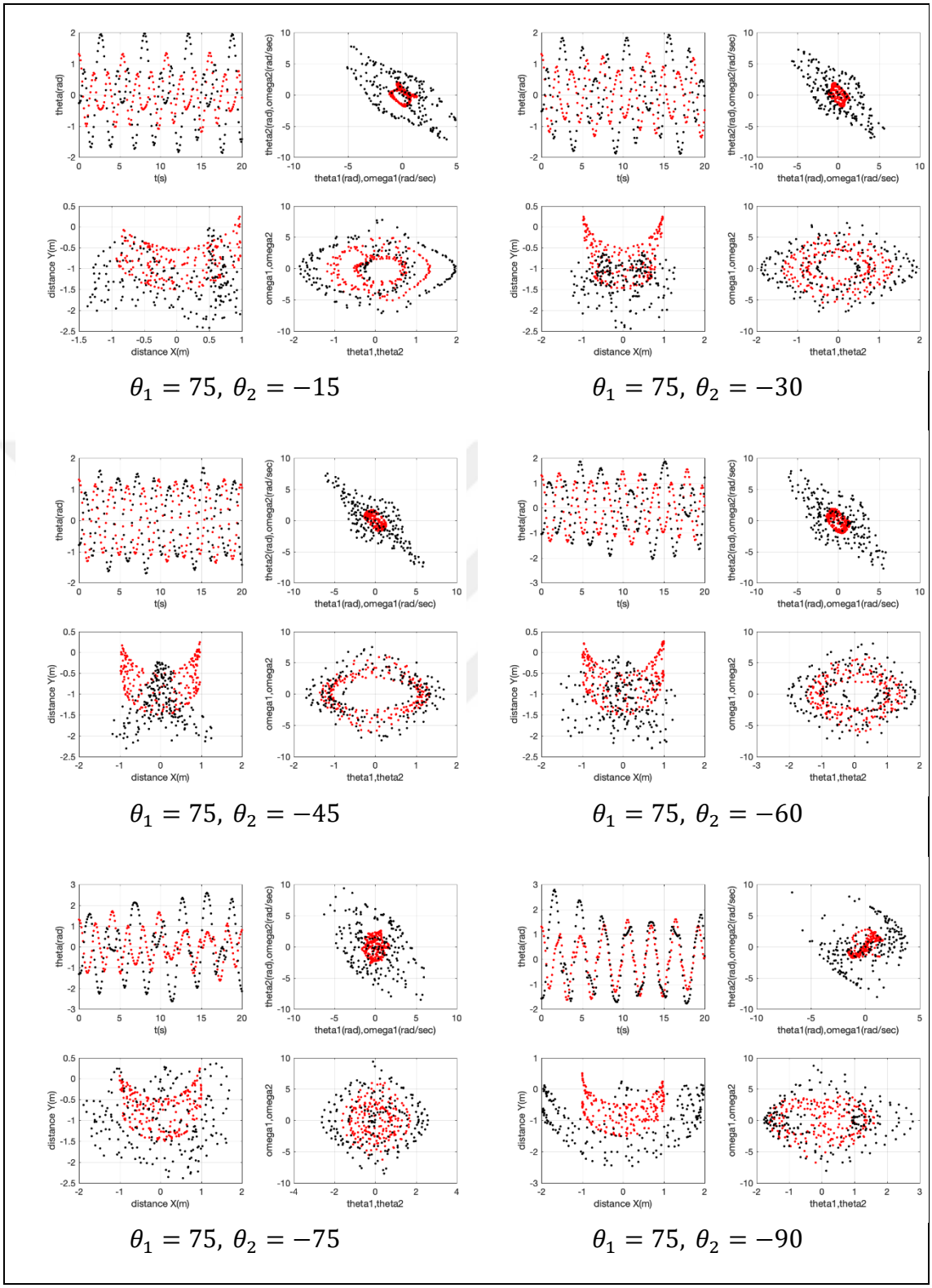


Figure 5.13. The graphical solutions of $\theta_2 = -15, -30, -45, -75, -90$ for small, medium, and large values corresponding to the large angle value of $\theta_1 = 75$. The other parameters are $b_1 = 1, b_2 = 1, m_1 = 1, m_2 = 1, a = 0.5, \omega = 1$, vertical vibrating.

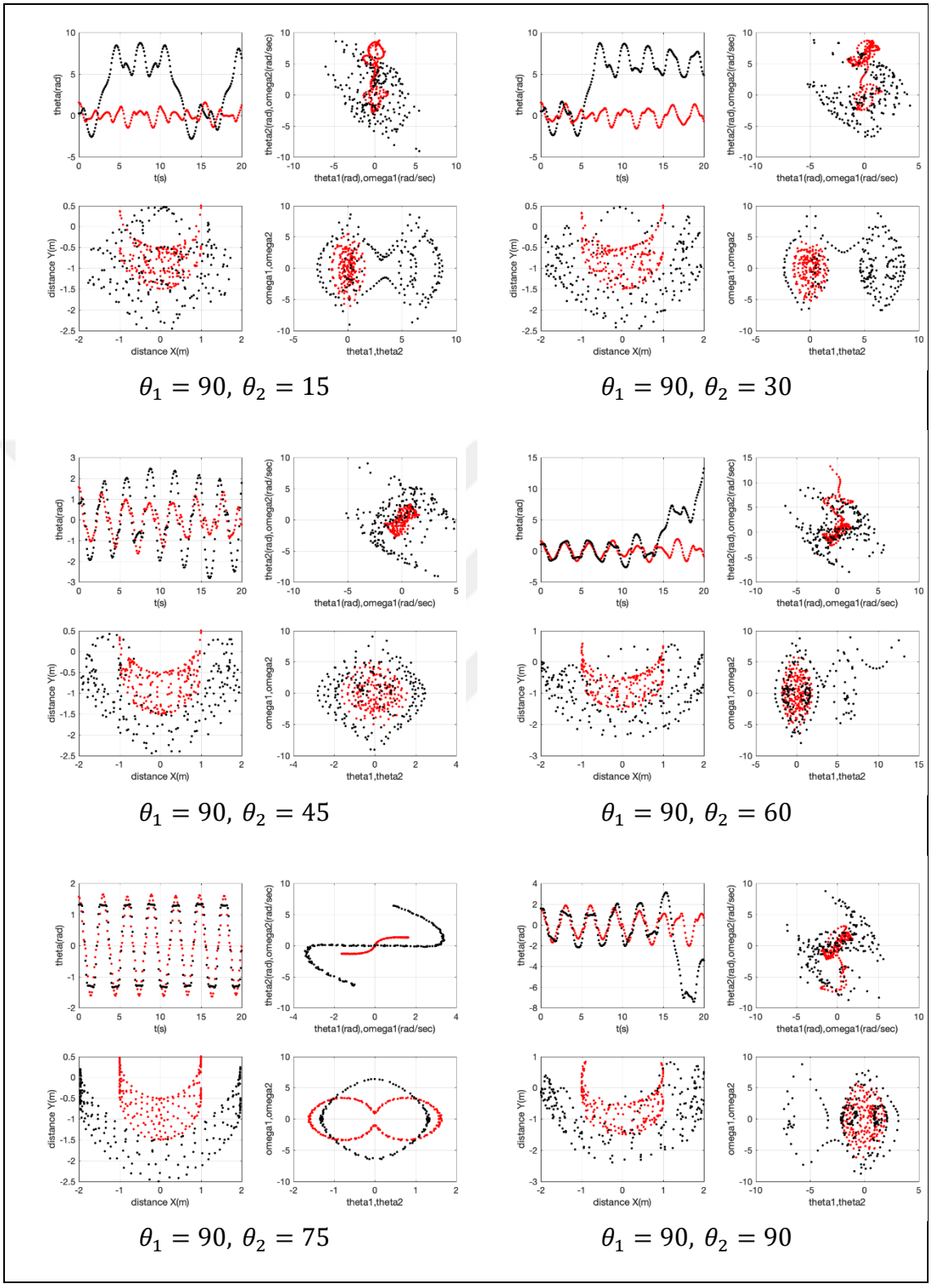
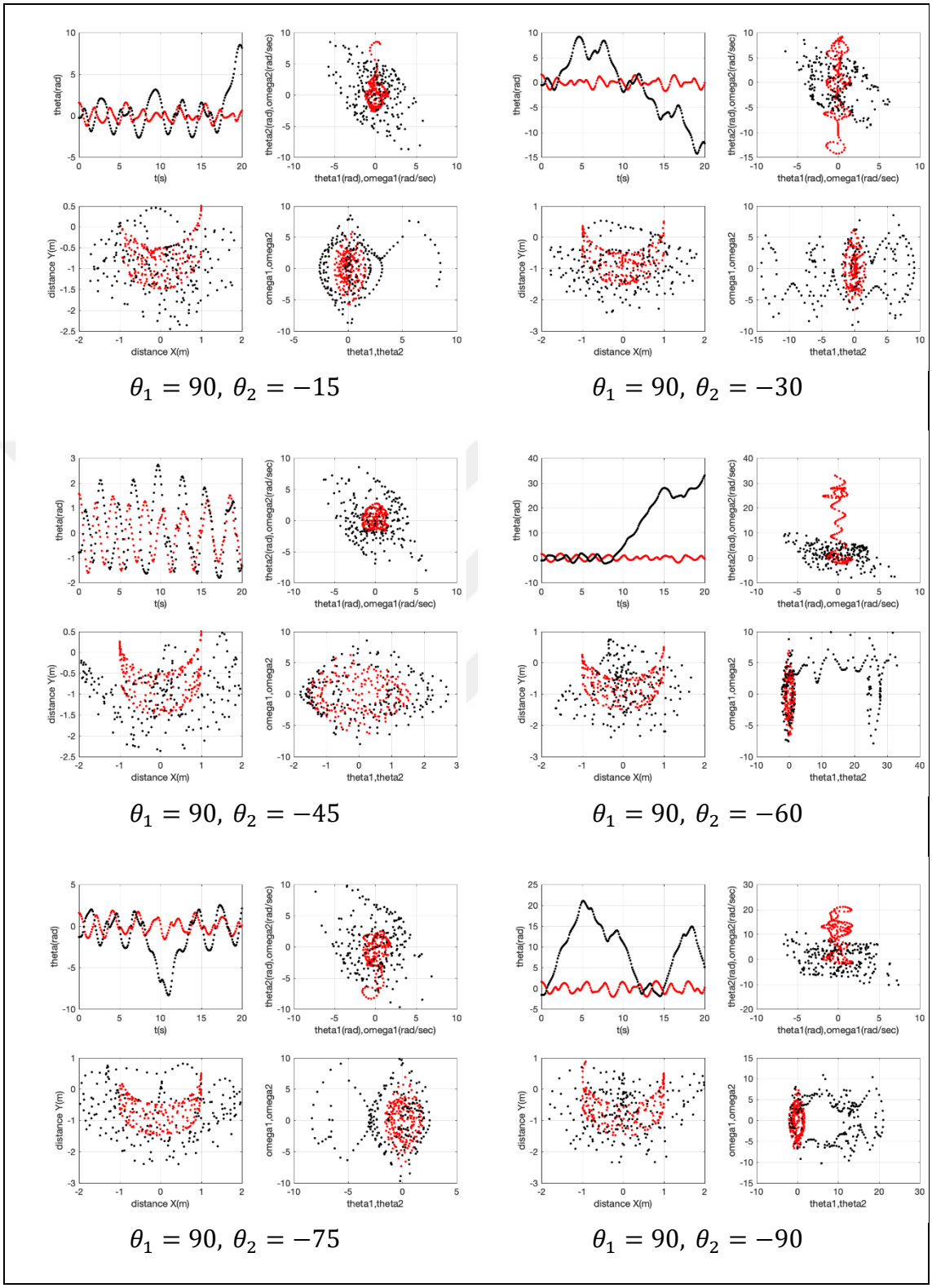


Figure 5.14. The graphical solutions of $\theta_2 = 15, 30, 45, 75, 90$ for small, medium, and large values corresponding to the large angle value of $\theta_1 = 90$. The other parameters are $b_1 = 1, b_2 = 1, m_1 = 1, m_2 = 1, a = 0.5, \omega = 1$, vertical vibrating.



$\theta_1 = 90,\ \theta_2 = -15$ $\theta_1 = 90,\ \theta_2 = -30$

$\theta_1 = 90,\ \theta_2 = -45$ $\theta_1 = 90,\ \theta_2 = -60$

$\theta_1 = 90,\ \theta_2 = -75$ $\theta_1 = 90,\ \theta_2 = -90$

Figure 5.15. The graphical solutions of $\theta_2 = -15, -30, -45, -75, -90$ for small, medium, and large values corresponding to the large angle value of $\theta_1 = 90$. The other parameters are $b_1 = 1, b_2 = 1, m_1 = 1, m_2 = 1, a = 0.5, \omega = 1$, vertical vibrating.

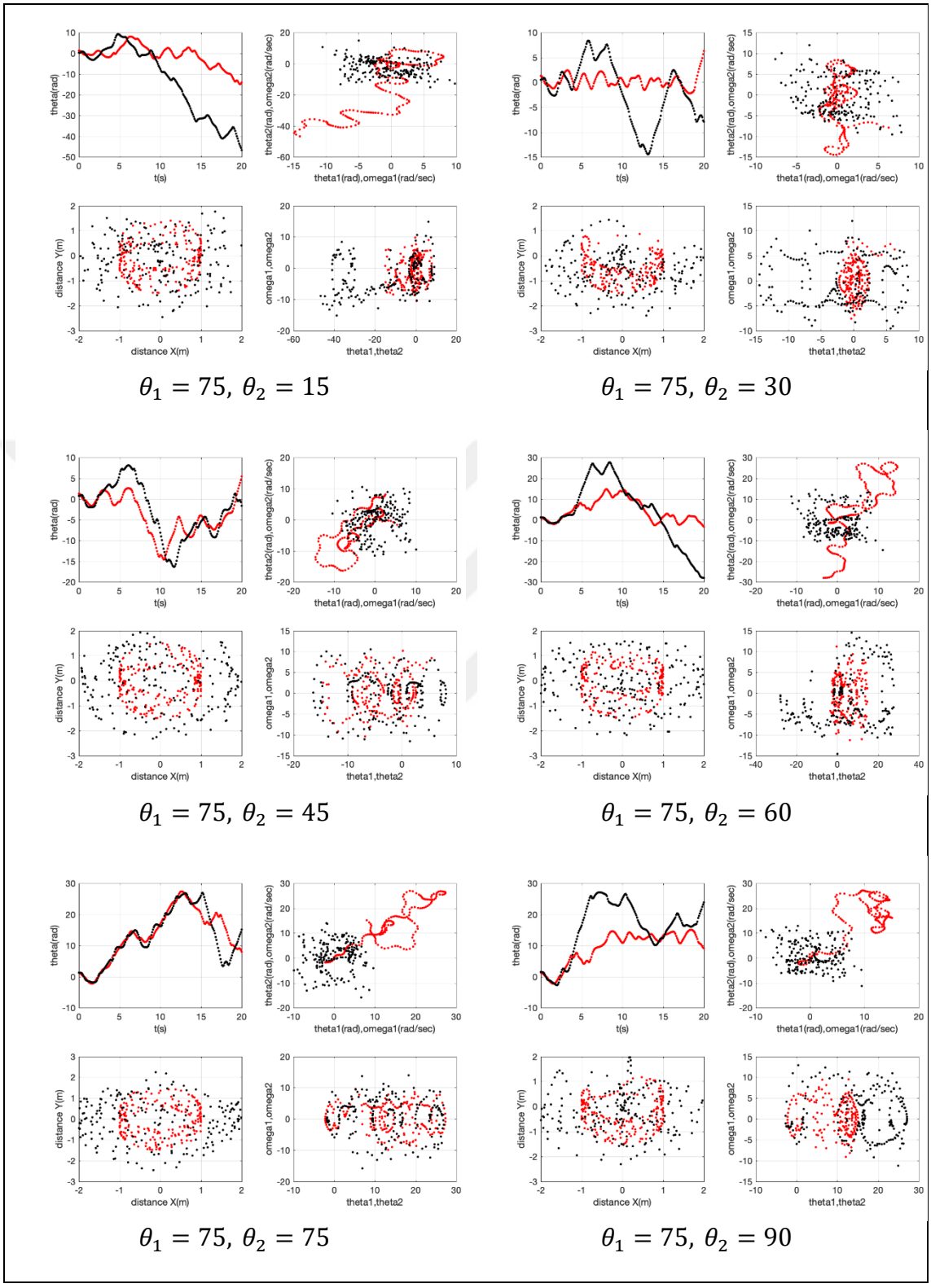


Figure 5.16. The graphical solutions of $\theta_2 = 15, 30, 45, 75, 90$ for small, medium, and large values corresponding to the large angle value of $\theta_1 = 75$. The other parameters are $b_1 = 1, b_2 = 1, m_1 = 1, m_2 = 1, a = 0.5, \omega = 3$, vertical vibrating.

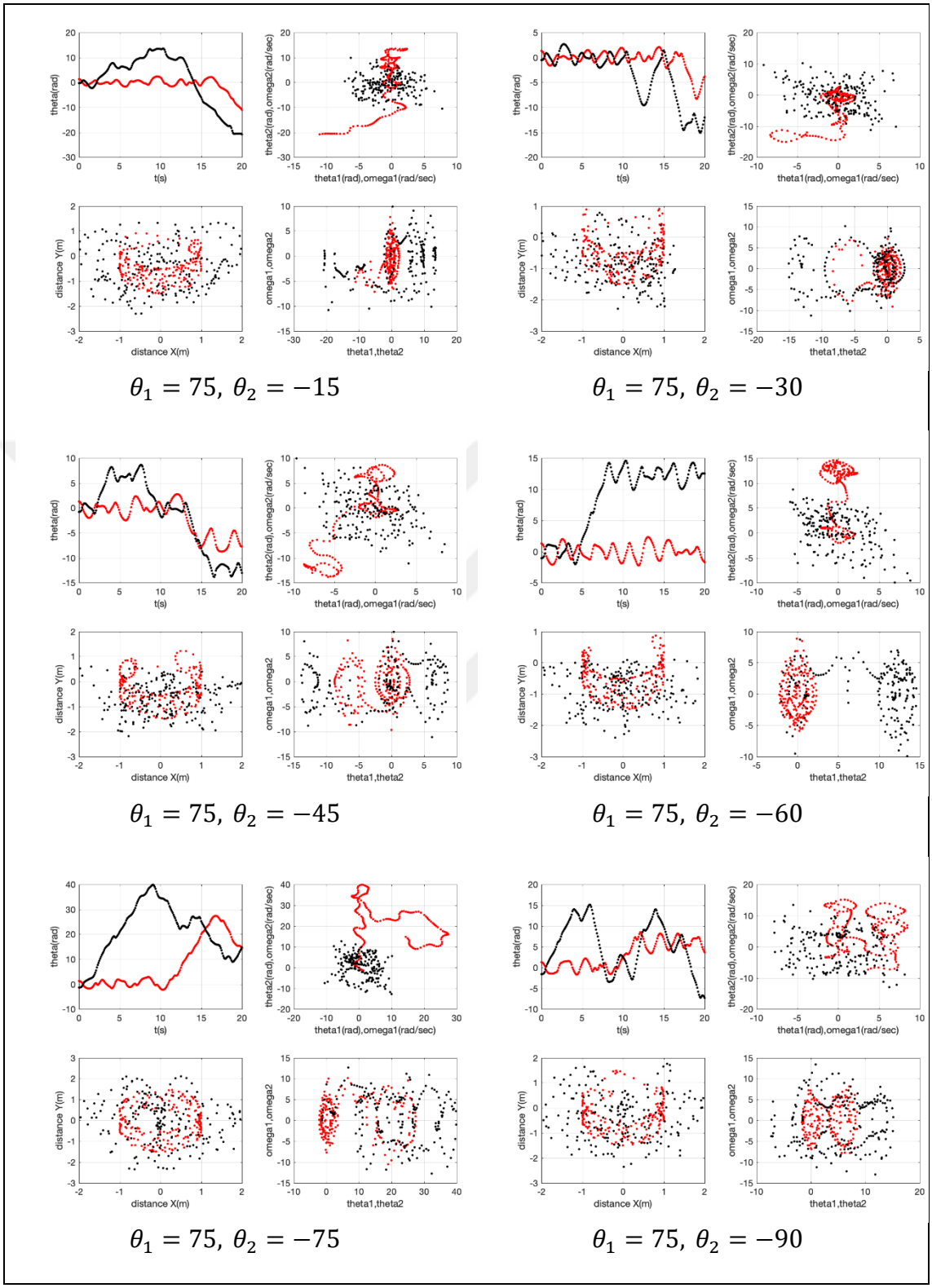


Figure 5.17. The graphical solutions of $\theta_2 = -15, -30, -45, -75, -90$ for small, medium, and large values corresponding to the large angle value of $\theta_1 = 75$. The other parameters are $b_1 = 1, b_2 = 1, m_1 = 1, m_2 = 1, a = 0.5, \omega = 3$, vertical vibrating.

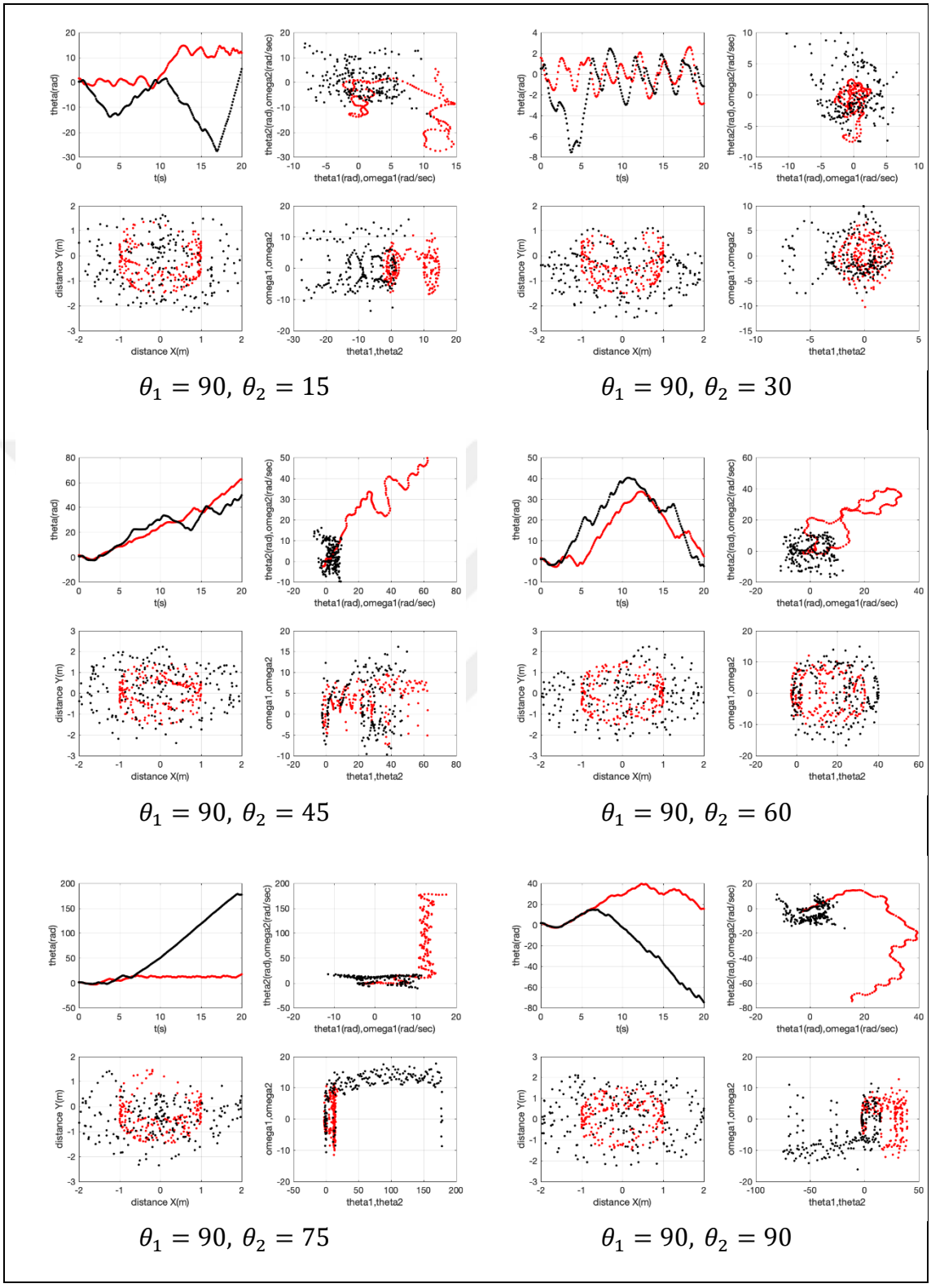
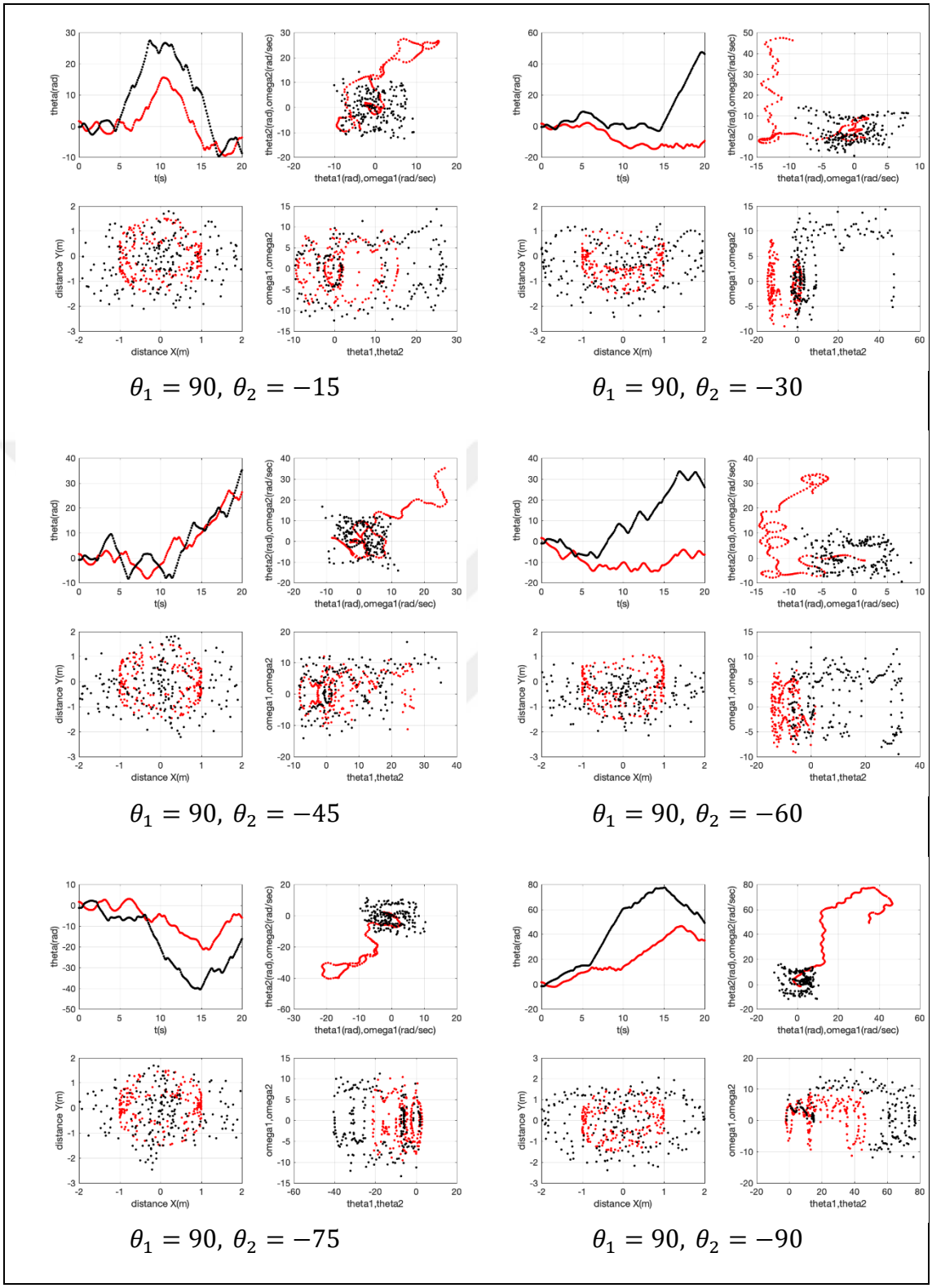


Figure 5.18. The graphical solutions of $\theta_2 = 15, 30, 45, 75, 90$ for small, medium, and large values corresponding to the large angle value of $\theta_1 = 90$. The other parameters are $b_1 = 1, b_2 = 1, m_1 = 1, m_2 = 1, a = 0.5, \omega = 3$, vertical vibrating.



$\theta_1 = 90,\ \theta_2 = -15$ $\theta_1 = 90,\ \theta_2 = -30$

$\theta_1 = 90,\ \theta_2 = -45$ $\theta_1 = 90,\ \theta_2 = -60$

$\theta_1 = 90,\ \theta_2 = -75$ $\theta_1 = 90,\ \theta_2 = -90$

Figure 5.19. The graphical solutions of $\theta_2 = -15, -30, -45, -75, -90$ for small, medium, and large values corresponding to the large angle value of $\theta_1 = 90$. The other parameters are $b_1 = 1, b_2 = 1, m_1 = 1, m_2 = 1, a = 0.5, \omega = 3$, vertical vibrating.



Figure 5.20. The graphic of the lyapunov exponents of double pendulum, (a) $\theta_1 = 90$ and $\theta_2 = 90$, $b_1 = 1, b_2 = 1, m_1 = 1, m_2 = 1, a = 0.5, \omega = 1$.(b) $\theta_1 = 90$ and $\theta_2 = 90$, $b_1 = 1, b_2 = 1, m_1 = 1, m_2 = 1, a = 0.5, \omega = 3$.

6. STATIONARY STATES OF THE TRIPLE PENDULUM

Again the initial states are represented in a way similar to the quantum mechanical states by kets (vectors) like in triple pendulum. For example a ket like $|\theta_1 = 15, \theta_2 = 0, \theta_3 = 30; S\rangle$ represents that at time $t = 0$ the upper angle is $\theta_1 = 15$ degrees, the lower angles are $\theta_2 = 0, \theta_3 = 30$ degrees and the *S* means that the joint where the triple pendulum is attached to the wall is *S*tationary.

In the following analysis the stationary (*S*) states using different combinations of the three angles are compared. In the study all of the three angles are incremented in various steps.

In each of the figures the red dots represent the position or velocity of the upper bob (ball) and the black dots do the same for the second bob and blue dots for the third bob.

We have obtained solutions at a basic type for a triple pendulum consisting of equal masses, $m_1 = m_2 = m_3 = m$ and equal massless rods, $b_1 = b_2 = b_3 = b$. Figure 6.1 illustrates the motion of θ_3 within the small, medium, and large angle ranges from 15 to 90 degrees, corresponding to the example of a 15-degree angle in the small angle range of θ_2 and a 75-degree angle in the large angle range of θ_1. Figure 6.2 presents the resulting graphs of θ_3 with symmetric angles in Figure 6.1 for the same large small angle value of θ_1 and θ_2. Similarly, Figures 6.3. and 6.4 depict the graphs corresponding to the largest angle range of θ_1.

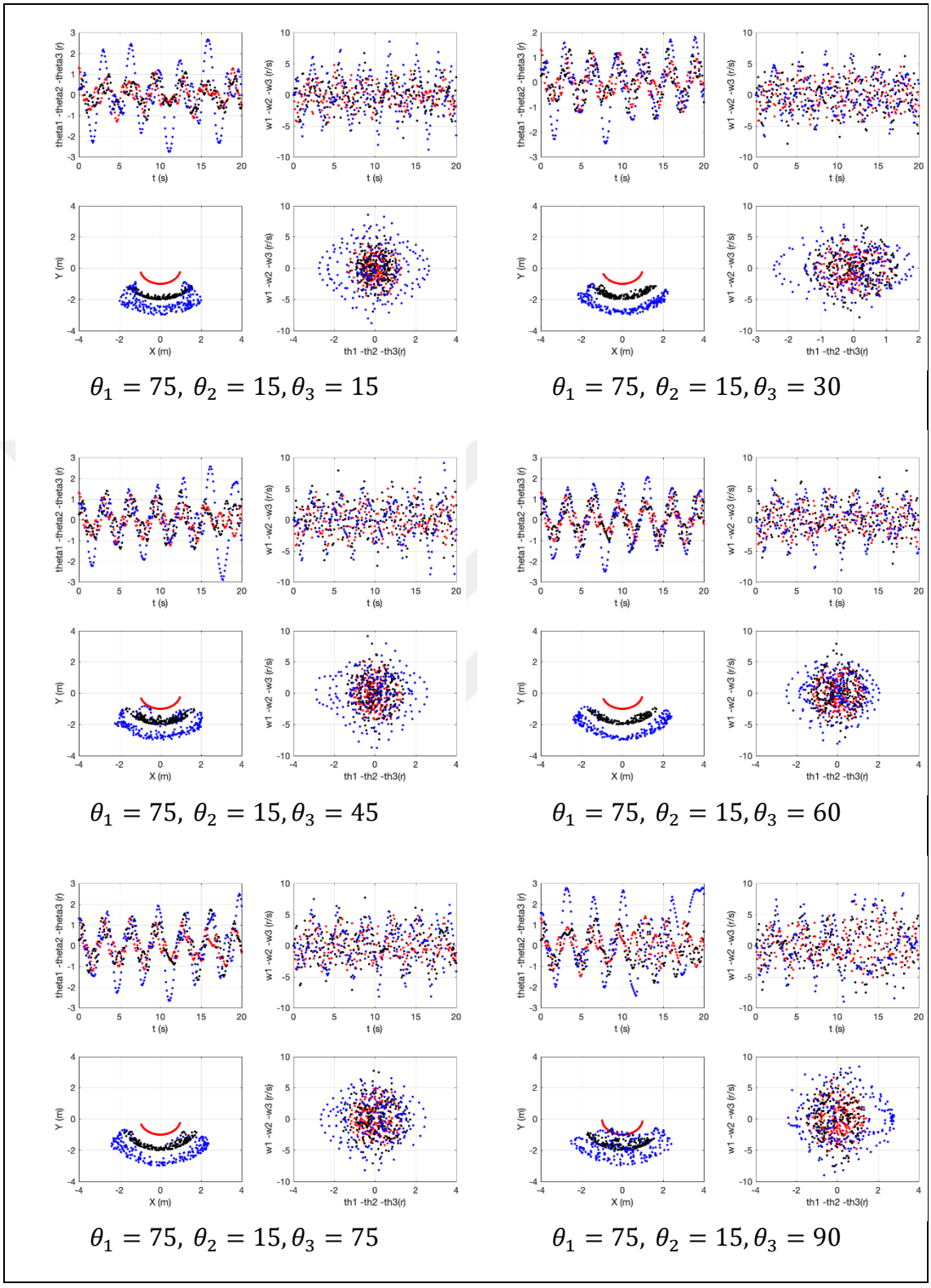


Figure 6.1. The graphical solutions of $\theta_3 = 15, 30, 45, 75, 90$ for small, medium, and large values corresponding to the large and small angle values of $\theta_1 = 75$, $\theta_2 = 15$. The other parameters are $b_1 = 1, b_2 = 1, b_3 = 1, m_1 = 1, m_2 = 1, m_3 = 1, a = 0, \omega = 0$.

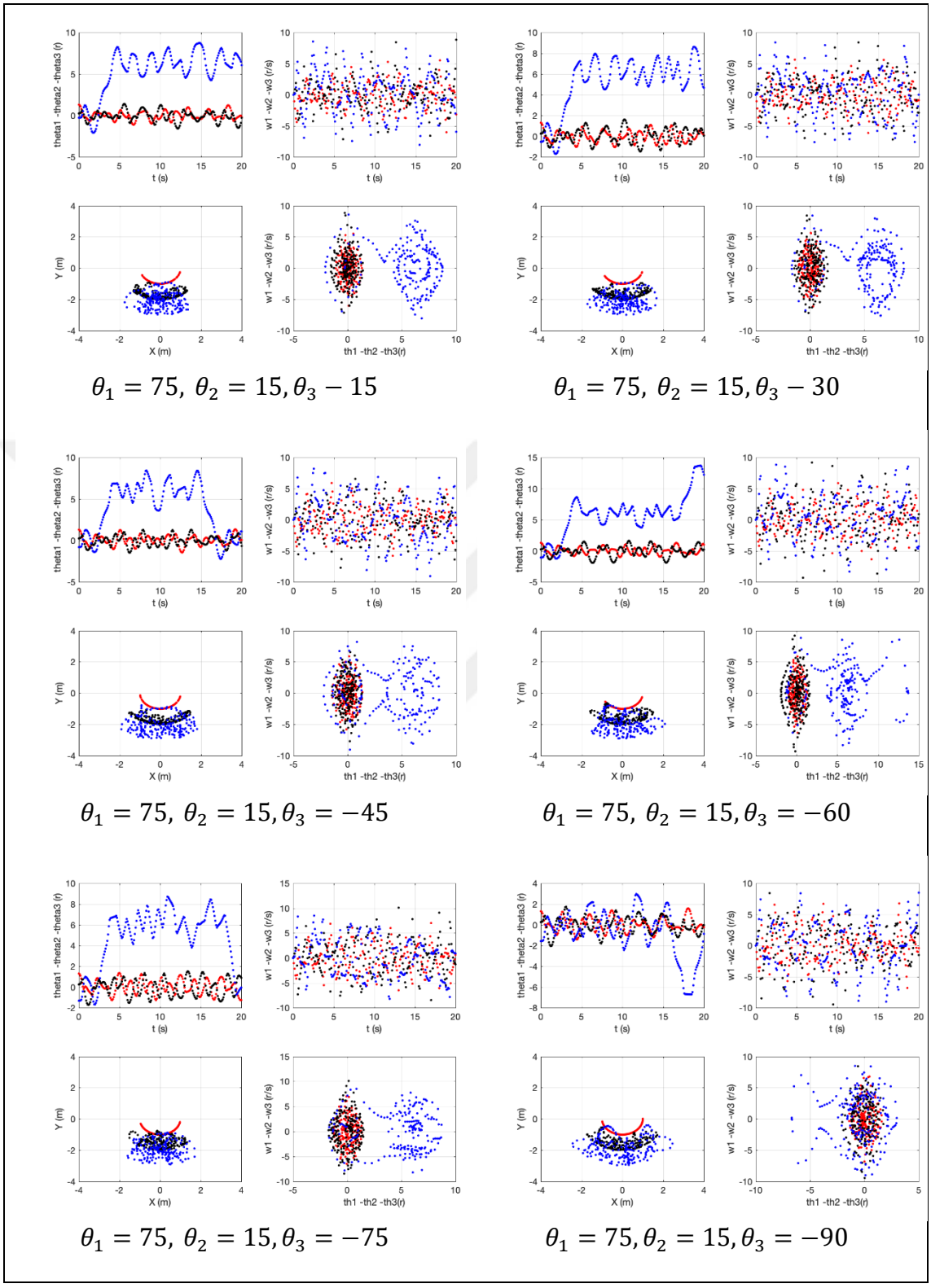


Figure 6.2. The graphical solutions of $\theta_3 = -15, -30, -45, -75, -90$ for small, medium, and large values corresponding to the large and small angle values of $\theta_1 = 75$, $\theta_2 = 15$. The other parameters are $b_1 = 1, b_2 = 1, b_3 = 1, m_1 = 1, m_2 = 1, m_3 = 1, a = 0, \omega = 0$.

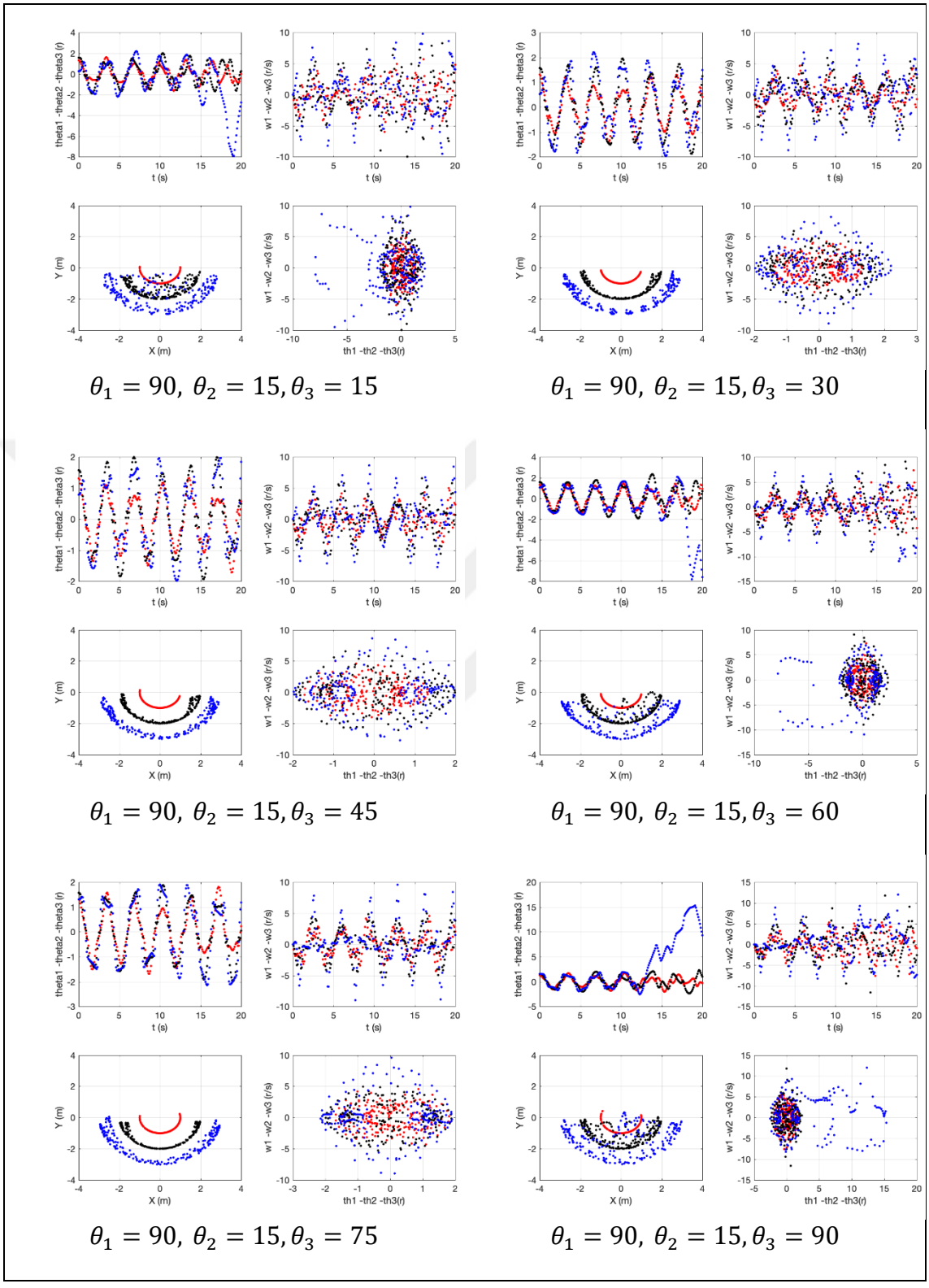


Figure 6.3. The graphical solutions of $\theta_3 = 15, 30, 45, 75, 90$ for small, medium, and large values corresponding to the large and small angle values of $\theta_1 = 90$, $\theta_2 = 15$. The other parameters are $b_1 = 1, b_2 = 1, b_3 = 1, m_1 = 1, m_2 = 1, m_3 = 1, a = 0, \omega = 0$.

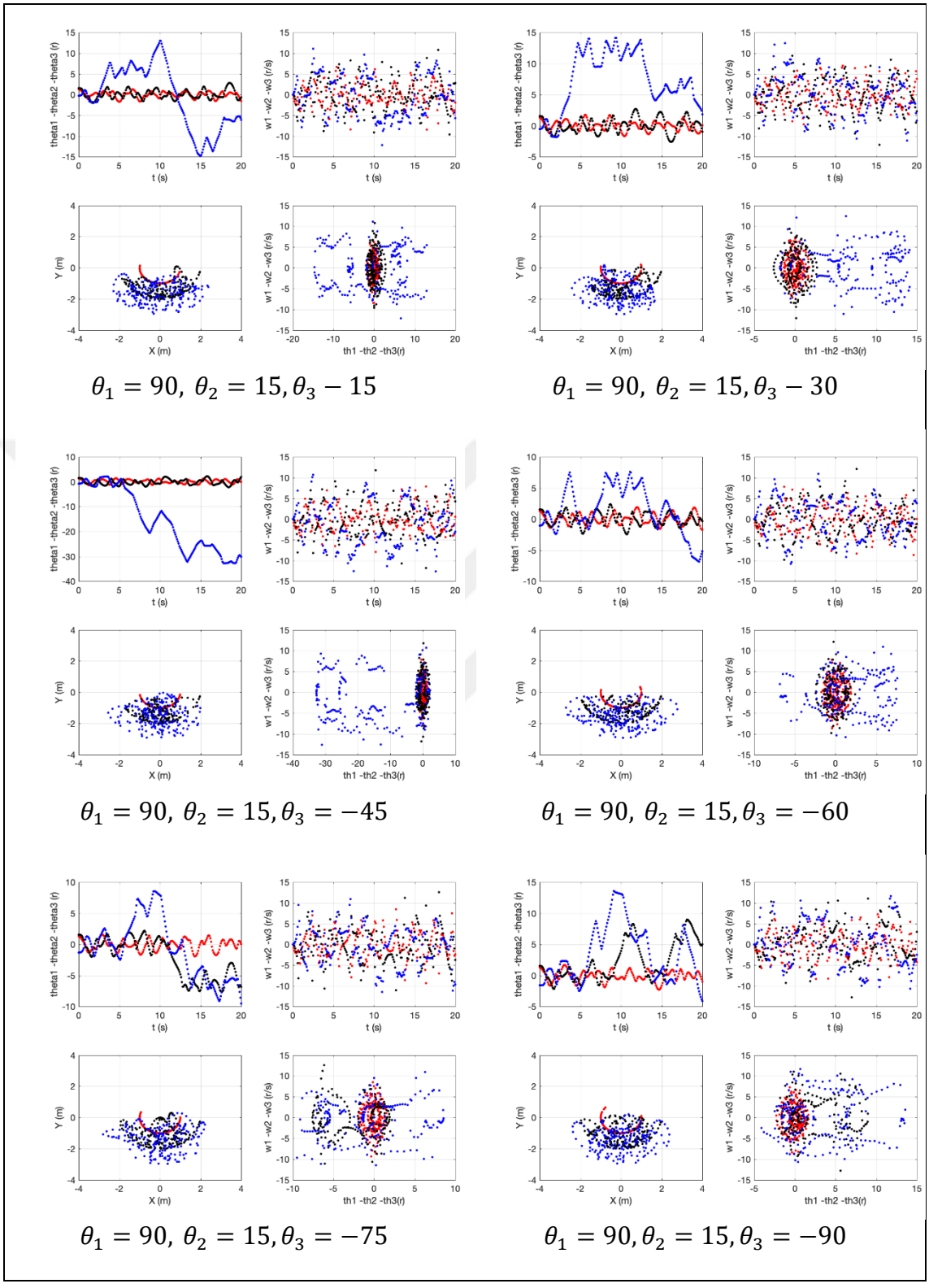


Figure 6.4. The graphical solutions of $\theta_3 = -15, -30, -45, -75, -90$ for small, medium, and large values corresponding to the large and small angle values of $\theta_1 = 90$, $\theta_2 = 15$. The other parameters are $b_1 = 1, b_2 = 1, b_3 = 1, m_1 = 1, m_2 = 1, m_3 = 1, a = 0, \omega = 0$.

7. RESULTS AND DISCUSSIONS

In the stationary states, for small values for both angles such as the case $|\theta_1 = 15, \theta_2 = 15; S\rangle$, angles are observed, only some limited widening in the graphs and curling up in the arcs followed by the bobs. For medium values of the angles, single sinusoids are again observed. Parts d in the figures first split into a few loops then into wider regions meaning that there is not a one-to-one relationship between the angular velocities and angles. For larger initial values for the angles, some unexpected cases are observed. Since the initial potential energy of the system is relatively larger compared with low and medium initial angles there are several more ways of converting this potential energy into rotational kinetic energy, so that the lower rod and lower bob exhibit even some full turns under certain initial circumstances.

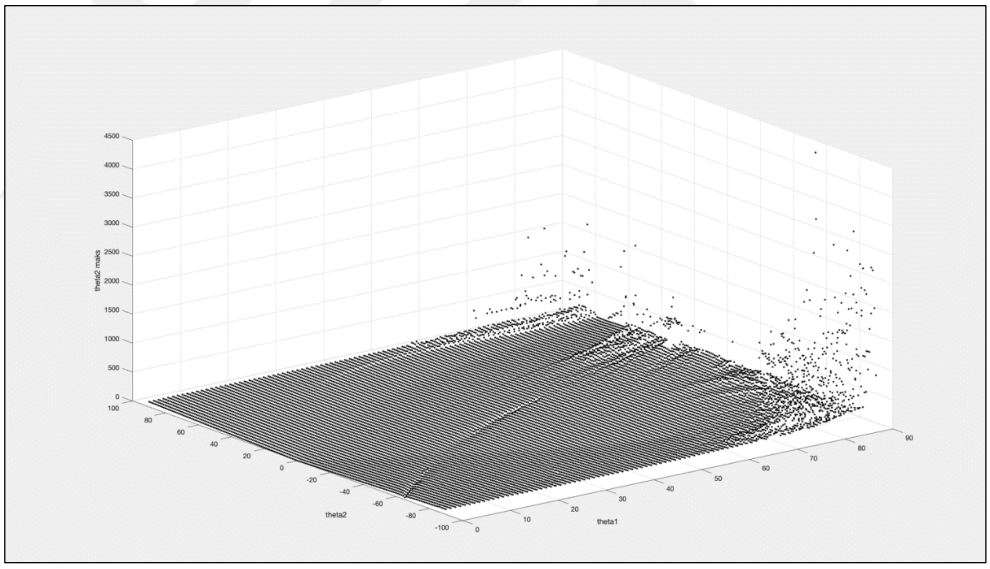


Figure 7.1. Maximum θ_2 angle values occurring versus θ_1, θ_2 values for all initial conditions. (Angle values are in degrees)

When we completely examine and graph the movement of θ_2 in the 20 seconds range of motion according to all θ_1 and θ_2 initial values, we get the graph in Figure 7.1. Accordingly, we observe that θ_1 is the main factor that enables θ_1 to move more, especially θ_2 , on the pendulum. When θ_1 goes above 70 degrees, the change in θ_2 becomes less important, and at more initial values, we act at larger angles, even getting more than a full

turn to somersault. We can see that θ_1 and θ_2 values above 75^o, θ_2 values with too many rounds are obtained.

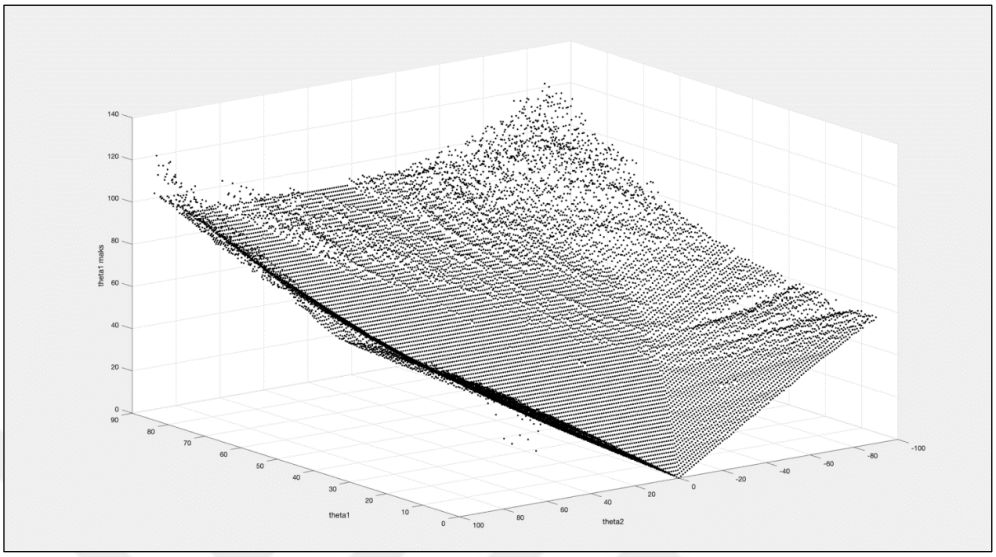


Figure 7.2. Maximum θ_1 angle values occurring versus θ_1, θ_2 values for all initial conditions. (Angle values are in degrees)

When we solved the initial values for the double pendulum in all ranges in the 1st region, that is, θ_1 changes from 0^o to 90^o and θ_2 changes in values from -90^o to 90^o at intervals of 90^o, we have shown the collective graph of θ_1 and θ_2 according to the energy levels formed in Figure 7.2. We see that θ_1 rises in parallel with the energy levels in the form of a band, in a relatively range depending on the energy levels. However, for θ_2 maximum values, we see that the maximum rotation values increase even before the energy levels reach the highest values. Although θ_1 does not have any somersault movement, we see that θ_1 values increase less, but the effect on θ_2 is more and it increases θ_2 movements.

We created Tables 7.1 and 7.2 to examine the detailed numerical values obtained from the graphs above. These tables were generated by running simulations of different pendulum structures with various operating conditions. For each pendulum structure, the solution was computed using all initial values of θ_1 ranging from 0° to 90° and θ_2 ranging from $-90°$ to 90° degrees with a step size of 1°. Table 7.1 consists of the values of θ_1 generated by the upper mass. It can be observed that θ_1 exceeds a full rotation, i.e., 2π, for certain initial values, resulting in a change in the motion profile and the occurrence of flips. Similarly, Table 7.2 provides information on θ_2, the angle produced by the lower mass, indicating at

which initial conditions the oscillatory motion starts to exceed a full rotation and the corresponding values at which the oscillation changes phase.

Table 7.1. Number of full turns of upper bob for all solutions.

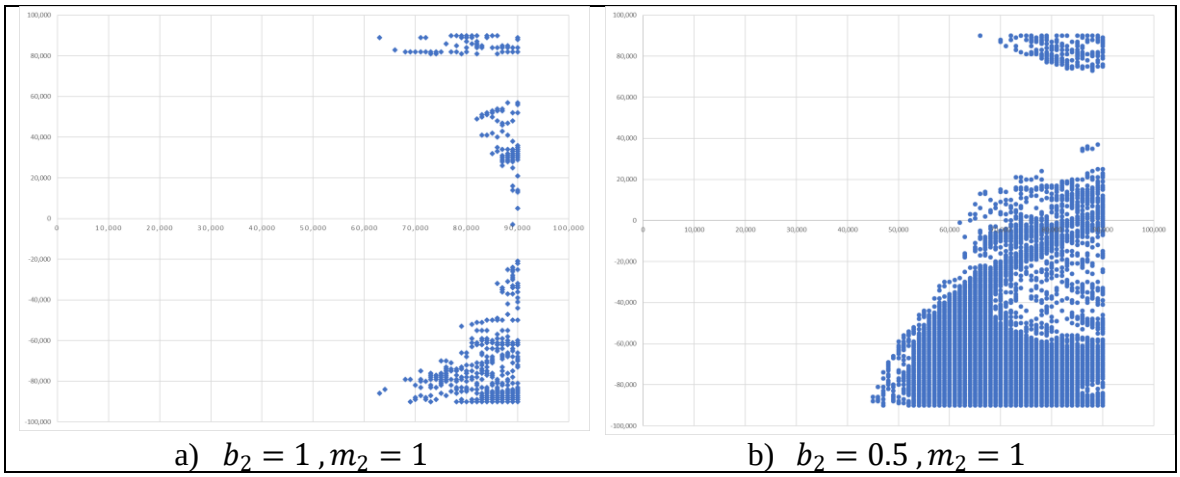
Solution Sets		*Number of full-turn of* θ_1	*Starting Angles of full turn*
a=0, w=0	b2=1 m2=1	0	
a=0, w=0	b2=2 m2=1	2	θ_1 =89, θ_2 =-90
a=0, w=0	b2=0.5 m2=1	0	
a=0, w=0	b2=1 m2=0.5	0	
a=0, w=0	b2=1 m2=2	0	
a=0.25, w=1	b2=1 m2=1	0	
a=0.5, w=1	b2=1 m2=1	0	
a=0.25, w=3	b2=1 m2=1	1974	θ_1 =0, θ_2 =74
a=0.5, w=3	b2=1 m2=1	8077	θ_1 =0, θ_2 =59

Table 7.2. Number of full furns of lower bob for all solutions.

Solution Sets		*Number of full-turn of theta2*	*Number of Negative values of initial angles*	*Number of Positive values of initial angles*	*Starting Angles of full turn*
a = 0 ω = 0	b_2 = 1, m_2 = 1	415	291	124	θ_1=63, θ_2=89
a = 0 ω = 0	b_2 = 2 m_2 = 1	0	0	0	
a = 0 ω = 0	b_2 = 0.5, m_2 = 1	2774	2384	390	θ_1=45 θ_2=-88
a = 0 ω = 0	b_2 = 1, m_2 = 0.5	1660	722	938	θ_1=67 θ_2=-89
a = 0 ω = 0	b_2 = 1, m_2 = 2	269	140	129	θ_1=65 θ_2=-88
a = 0.25 ω = 1	b_2 = 1, m_2 = 1	350	268	82	θ_1=63, θ_2=90
a = 0.5 ω = 1	b_2 = 1, m_2 = 11	309	263	46	θ_1=68 θ_2=-89
a = 0.25 ω = 3	b_2 = 1, m_2 = 1	5154	2751	2403	θ_1=0 θ_2=59
a = 0.5 ω = 3	b_2 = 1, m_2 = 11	12099	5681	6418	θ_1=0 θ_2= 4

We examined the motion structure of double pendulum according to all interval values in the solution sets which we applied for the double pendulum, we observed the pendulum "goes over the top" state of the movement. We have achieved 3 effect patterns that will make the upper bob of θ_1 angle do somersaults. The first was to increase the variable m_2 mass, which changed only very few motion patterns. Apart from that, the indicator that magnifies the movement and enables it to roll over with high values is the generation of horizontal or vertical vibration. While the increase in amplitude does not primarily change the movement, the increasing frequency of the game has affected the motion structure. While the magnitude of the frequency up to 1 does not affect the movement much, the increase of the frequency to 3 levels has changed the entire movement profile. The pendulum goes over the top.

Figure 7.3 illustrates the graphic patterns generated by the values in the preceding tables. The comparison of the graphs from the six sets reveals the influence of length and mass variations on the pendulum motion profile. In the baseline version where both lower and upper lengths and masses are equal, the visual representation consists of a small number of points. However, with a decrease in the lower mass and a decrease in the lower length of the pendulum, the number of points significantly increases, resulting in a substantial increase in the motion profile and the occurrence of flips. Conversely, an increase in the lower mass and an increase in the length of the pendulum lead to a significantly higher number of smaller oscillations in the graphic representations, resulting in a different pattern of motion.



a) $b_2 = 1\,, m_2 = 1$ b) $b_2 = 0.5\,, m_2 = 1$

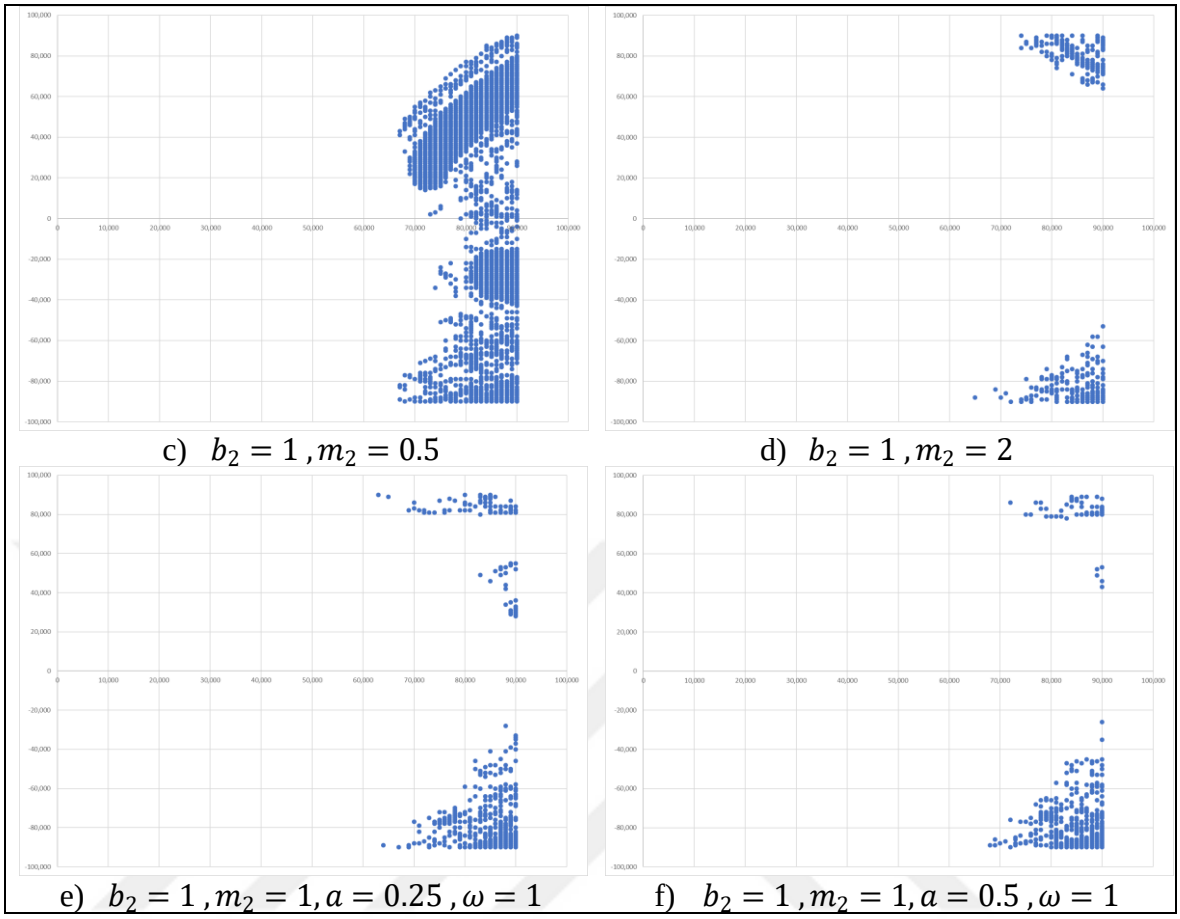
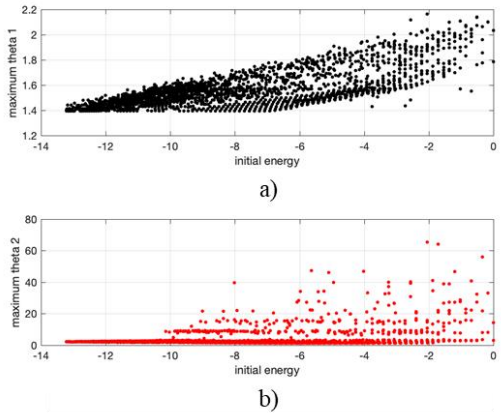
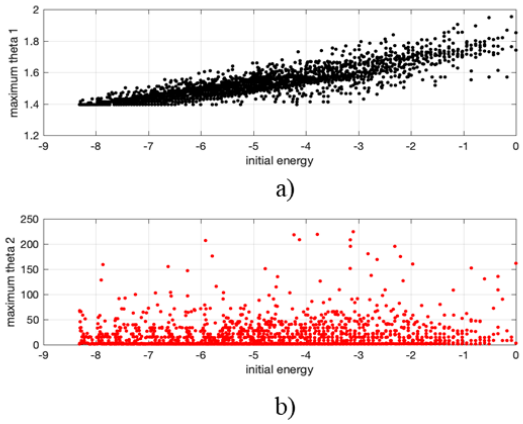


Figure 7.3. The representation of θ_1, θ_2 generating the maximum angle values for all initial conditions under different parameters. (Angle values are in degrees)

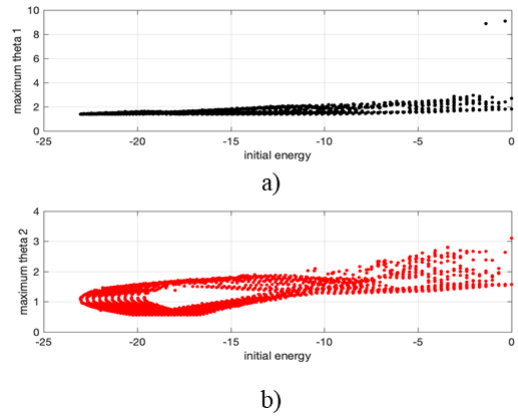
Figure 7.4 presents a comprehensive graph displaying the maximum values of θ_1 and θ_2 angles generated by different pendulum types based on their energy levels. It can be observed that θ_1 exhibits relatively stable variations, and the motion profile is not significantly affected by changes in the pendulum structure, unless it experiences external perturbation, particularly in the form of horizontal oscillations, which leads to a deviation from the regular motion pattern. On the other hand, as previously indicated in the tables above, θ_2 demonstrates higher sensitivity to variations in fundamental parameters such as mass and length of the pendulum.



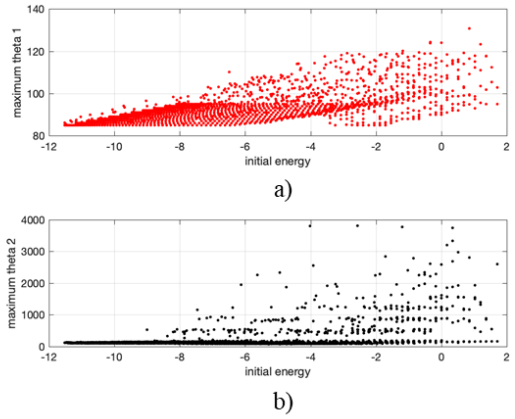
i. $m_1 = m_2, b_1 = b_2$



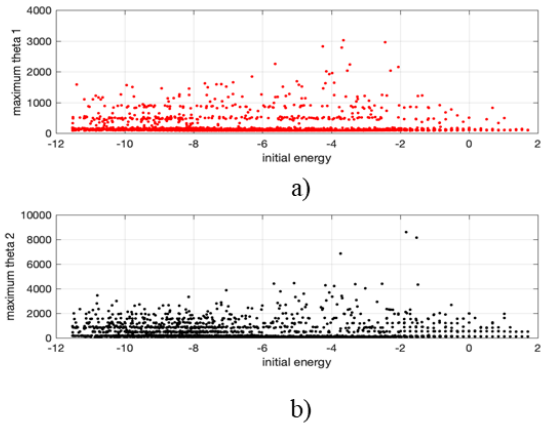
ii. b2 = 1, m2 = 2



iii. b2 = 1, m2 = 1, a =0.25, w =1



iv. b2 = 1, m2 = 1, a =0.5, w =1



v. b2 = 1, m2 = 1, a =0.25, w =3

Figure 7.4. a) maximum θ_1, b) maximum θ_2 angle values occurring versus initial energy levels under different parameters.

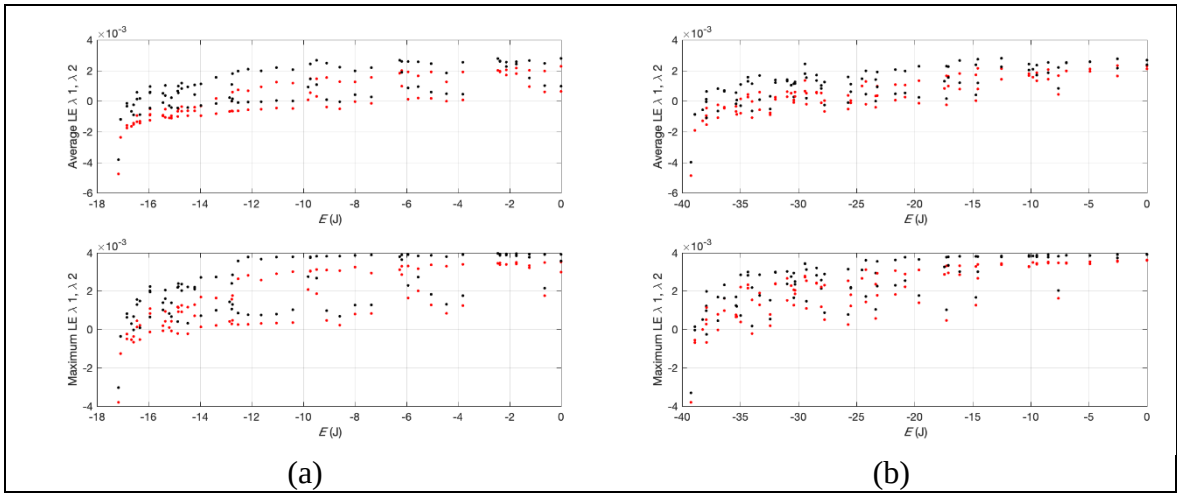


Figure 7.5. The representation of the values of lyapunov expoents for the system of double pendulum (a) $\theta_1 = 0$ to 90, $\theta_2 = -90$ to 90, $b_1 = 1, b_2 = 0.5, m_1 = 1, m_2 = 0.5, a = 0, \omega = 0$. (b) $\theta_1 = 0$ to 90, $\theta_2 = -90$ to 90, $b_1 = 1, b_2 = 0.5, m_1 = 1, m_2 = 2, a = 0, \omega = 0$.

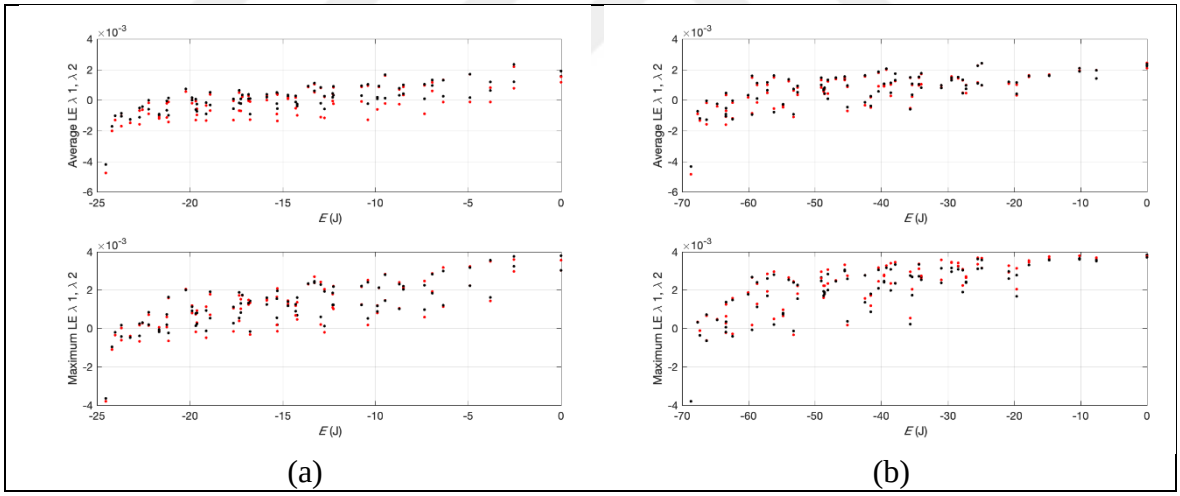


Figure 7.6. The representation of the maximum values of lyapunov exponents for the system of double pendulum (a) $\theta_1 = 0$ to 90, $\theta_2 = -90$ to 90, $b_1 = 1, b_2 = 2, m_1 = 1, m_2 = 0.5, a = 0, \omega = 0$. (b) $\theta_1 = 0$ to 90, $\theta_2 = -90$ to 90, $b_1 = 1, b_2 = 2, m_1 = 1, m_2 = 2, a = 0, \omega = 0$.

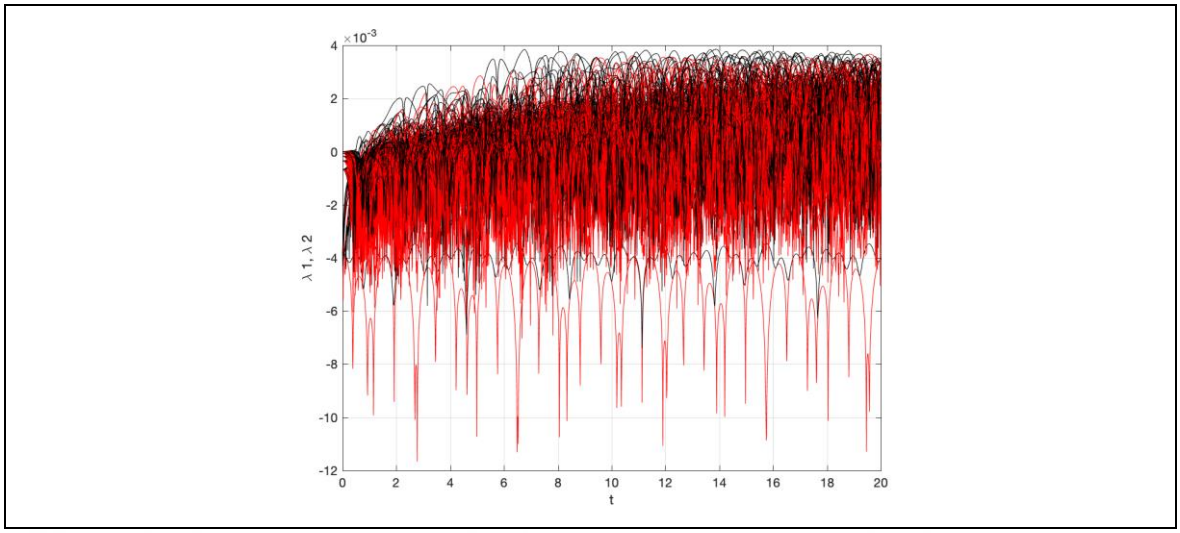


Figure 7.7. The representation of the spectrum of lyapunov exponents for system of double pendulum. $\theta_1 = 0$ to 90, $\theta_2 = -90$ to 90, $b_1 = 1, b_2 = 1, m_1 = 1, m_2 = 1, a = 0, \omega = 0$.

Figures 7.5 and 7.6 depict the average and maximum Lyapunov exponents for all pendulum models used. These graphs present both the average values and the maximum Lyapunov exponents from each series corresponding to different initial conditions, representing different energy levels. The Lyapunov exponents were calculated for each series within the generated data, and the positive Lyapunov exponents from these series were aggregated in the graphs. It is worth noting that the value of the Lyapunov exponent serves as a primary indicator in predicting the nature of the motion. Negative values indicate fixed point dynamics, zero value corresponds to regular dynamics, while positive values indicate unstable dynamics, signifying chaotic behavior. The graphs presented in this study include only the positive values of the Lyapunov exponents for all selected pendulum models across various initial conditions. The time-dependent graphs of all Lyapunov exponents for the pendulum with the properties of $b_1 = 1, b_2 = 1, m_1 = 1, m_2 = 1, a = 0, \omega = 0$ are plotted in Figure 7.7.

8. CONCLUSIONS

It is observed that the frequency has a larger effect than the amplitude *a* of the external vibrations. The frequency ω takes two values in the analysis: $\omega = 1$ and $\omega = 2$. Further, the effect of the horizontal oscillations (in *x*-dir.) have a larger impact on the angular values of especially the lower rod. Because in some cases when the frequency is increased to $\omega = 2$ then the lower rod is observed to sweep larger angles which means it makes several rotations around an axis perpendicular to the page

However, the increase in the frequency of oscillations in *y*-dir. does not have such large effects. As a result of the higher frequency the upper rod is limited to a shorter band of angles, while the lower rod can make a few rotations in both senses.

In our study, different mathematical models with distinct physical quantities for binary and triple pendulums were created and investigated. The basic binary pendulum with equal masses and rod lengths was followed by a second system with different hanging masses, a third system with different rod lengths, a fourth system with horizontal vibrations, a fifth system with vertical oscillations, and a sixth system consisting of a triple pendulum with an additional mass. For each mathematical model system, sub-systems were obtained with the values taken as samples, and calculations were performed together with all sub-models. Lagrange formulation was used to obtain the motion equations for all systems, and motion profiles were derived. Physical properties such as initial angles, energy levels, angular momentum and symmetry were followed in the motion profile and their effects were observed. Behaviour of system, motion trajectories, phase portraits, Poincare maps, and Lyapunov exponents were calculated for all modelled dynamic systems to predict their behaviour. Periodic and chaotic regime regions were found in all scenarios. The regions where the mass exhibiting bifurcation behavior completes a full turn were analyzed. Lyapunov exponents, which facilitate our prediction of chaos regime, were calculated, and for negative results, periodic and in-phase oscillations were confirmed, while chaotic behaviour of system were confirmed for positive values. The obtained motion profiles and simulations for the systems can easily be used to develop sub-systems, and the obtained data will support new design and system analysis.

REFERENCES

1. Bevivino J., The path from the simple pendulum to chaos. Dynamics. 2009.

2. Burra L:, Zanolin F., Chaotic dynamics in a vertically driven planar pendulum. *Nonlinear Analysis*. 2010; 72:1462-1476.

3. Ge Z. M., Yang H., Chen H., Lee C., Nonlinear dynamics and chaos control of a physical pendulum with vibrating and rotating support. *Journal of Sound and Vibration*. 2001; 242(2):247-264.

4. Sofromiov A., Bishop S., Dynamics of a parametrically excited system with two forcing terms. *Mathematics*. 2014; 2:172-195.

5. Sprott J.C., A simple chaotic delay differential equation. *Physics Letters A*. 2007;366:397-402.

6. Feng Z., Sun H., A High speed motion control method of pendulum driven spherical robot, *IEEE International Conference on Artificial Intelligence and Computer Algortihms*, 2021.

7. Li Q., Meng F., Yu Z., Huang Q., Dynamic torso compliance control for standing and walking balance of position-controlled humanoid robots. *IEEE/ASME Transactions on Mechatronics*. 2021; 26(2);679-688.

8. Zhang Z., Zhang L., Xin S., Xiao N., Wen X., Robust walking for humanoid robot based on divergent component of motion. *Micromachines*. 2022; 2072-666x.

9. Petro B., Kiss R., Validation of the estimated torques of on open-chain kinematic model of the human body. *Periodica Polytechnica Mechanical Engineering.* 2022; 10.3311 /PPrime.19920.

10. Chen Y., Li Y., Huang Y., Li M., Liv Y., An efficient algorithm based on braydons and generalized method for large scale flexible multibody systems. *Applied Mathematical Modelling*. 2022; 0307904x.

11. Pappalardo C., Guida D., Dynamic analysis and control design of kinematically driven multibody mechanial systems. *Engineering Letters*. 2020; 1816-093x:EL28-4-19.

12. Petro B., Kiss B., Kiss R., Analyzing human balance recovery action using calculated torques of a double pendulum model. *Materials Today: Proceedings*. 2019;12:431-439.

13. Wang J., Liu K., Wang S., Chen H., Niu A., Li H., Dynamic analysis and experiment of underactuated double pendulum anti-swing device for ship mounted cranes. *Polish Maritime Research*. 2022; 29(4):145-154.

14. Zhang W., Chen H., Yao X., Li D., Adoptive tracking of double pendulum crane with payload hoisting/lowering. *Automation in Construction*. 2022;141; 104-368

15. Kang X., Chai L., Liv H., Anti swing and positioning for double pendulum tower cranes using improved active disturbance rejection controller. *International Journal of Control Automation and Systems*. 2023; 1598-6446.

16. Miao X., Zhu H., Li S., Xu X., Adaptive back- stepping based controller design for double pendulum rotary cranes. *ISA Transactions*. 2022; 0019-0578.

17. Li G., Ma X., Li Z., Guo P., Li Y., Kinematic coupling-based trajectory planning for rotary crane system with double pendulum effects and output constraints. *Journal of Field Robotics*. 2023; 40(2): 289-305.

18. Yao X., Chen H., Liu Y., Dong Y., Tracking approach of double pendulum cranes with variable rope lengths using sliding mode technique. *ISA Transactions*. 2022; 0019-0578.

19. Wu Q., Wang X., Hua L., Xia M., Improved time optimal anti swing control system based on low-pass filter for double pendulum crane system with distributed mass beam. *Mechanical Systems and Signal Processing*. 2021; 0888-3270.

20. Qian Z., Zhang D., Jin C., A regularized approach for frictional impact dynamics of flexible multi-link manipulators arms considering the dynamic stiffening effect. *Multibody System Dynamics*. 2018; 43(3):229-255.

21. Zhao Y., Wu X., Li F., Ziang Y., Positioning and swing elimination control of the overhead crane system with double pendulum dynamics. *Journal of Vibration Engineering and Technologies*. 2023; 10.1007/542417.

22. Shi H., Yao F., Yuan Z., Hu X., Fu L., Enhanced-coupling based tracking control of double pendulum gantry cranes. *International Journal of Control Automation and Systems*. 2022; 1598-6446:10.1007.

23. Parker J.P., Goluskin D., Vasil G.M., A study of the double pendulum using polynomial optimization. *Chaos*. 2021; 31(10):103102.

24. Choudhary A., Lindner J., Holliday E.G., Miller S.T., Ditto W.L., Forecasting Hamiltonian dynamics without canonical coordinates. *Nonlinear Dynamics*. 2021; 103(2):1553-1562.

25. Zhang H., Fan H., Wang L:, Wang X., Learning hamiltonian dynamics with reservoir computing. *Physical Review E*. 2021;104(2): 024205.

26. Greenwood T. Donald. *Principles of Dynamics.* Cambridge Prentice-Hall, Inc; 1996

27. Greenwood T. Donald. *Advanced Dynamics.* Cambridge University Press; 2003

28. Greiner W., *Classical Mehanics Systems of Particles and Hamiltonian Dynamics.* Springer -Verlag Berlin Heidelberg; 1992

29. Koruba Z., Awrejcewicz J., *Classical Mechanics Applied Mechanics and Mechatronics*. Spinger; 2012

30. Awrejcewicz J. *Classical Mechanics.* Springer Science + Business Media New York; 2012

31. Awrejcewicz J. *Numerical Analysis - Theory and Application.* Intechweg.org; 2011

32. Strogatz S., *Nonlinear Dynamics and Chaos with Applications to Physics, Biology, Chemistry, and Engineering*, Perseus Books, 1994

33. D. Sado and K. Gajos, Note on Chaos in Three Degree of Freedom Dynamical System with Double Pendulum,*Meccanica*, Vol. 38, No. 6, 2003, pp. 719-729, 2003

34. Stachowiak T., Okada T., A Numerical Analysis of Chaos in the Double Pendulum, *Chaos Solitons and Fractals*, Vol. 29, pp 417-422, 2006

35. Awrejcewicz J., Lamarque C. H., Analysis of Bifurcations and Chaos in Three Coupled Physical Pendulums with Impacts, *Proceedings of DETC'01*, 2001

36. Wolf A., Swift J. B., Swinney H. L., Vastano A., Determining Lyapunov Exponents From a Time Series, *Physica D*, 16 285-317, 1985

37. Meador C-E. E., Numerical Calculation of Lyapunov Exponents for Three-Dimensional Systems of Ordinary Differential Equations, Thesis Master of Arts, *Mathematics*, 2011

38. Awrejcewicz J., Kudra G., Lamarque C-H., Investigation of Triple Pendulum with Impacts Using Fundamental Solution Matrices, *International Journal of Bifurcation and Chaos*, Vol.14, 4191-4213, 2004

39. Leiven R. B., Tan S. M., Double Pendulum: An Experiment in Chaos, *American Journal Physics*, 61(11), 1993

40. Avanço R.H., Balthazar J.M., Tosset A.M., Ribeiro M.A., Short comments on chaotic behaviour of a double pendulum with two sub harmonic frequencies and in the main resonance zone. *ZAMM*. 2021;101(12): e202000197.

41. Chapra S., Canale R., *Numerical Methods for Engineers*. MacGraw-Hill Education; 2006

42. Thornton S., Marion J. B., *Classical Dynamics of Particles and Systems.* Thomson Brooks /Cole;2002

43. Angeles J., *Dynamic Response of Linear Mechanical Systems Modeling, Analysis, Simulation.* Springer Science + Business Media New York; 2011

44. Awrejcewicz J., Kudra G., Nonlinear Dynamics of a Triple Physical Pendulum, *Krajowa Konferencja*; 1999

45. Shinbrot T., Grebogi C., Wisdom J., Yorke J., Chaos in a Double Pendulum, *Journal of Physics*; 1991

46. Furi M., Martelli M., O'neill M., Staples C., Chaotic Orbits of a Pendulum with Variable Length, *Electronic Journal of Differential Equations,* 1072-6691, 2004

47. Calvao C., Penna T.J., The Double Pendulum: a Numerical Study, *European Journal of Physics*, 36-045018, 2015

48. Kwiatkowski R., Dynamic Analysis of Double Pendulum with Variable Mass and Initial Velocities, *Procedia Engineering*, 136 175-180, 2016

49. Rafat M. Z., Wheatland M. S., Bedding T.R., Dynamics of a Double Pendulum with Distributed Mass, *American Association of Physics Teachers*, 2008

50. Awrejcewwicz J., Sendkowski D., Geometric of the Dynamics of a Double Pendulum, *Journal of Mechanics of Materials and Structures*, 2007

51. Smiechowicz W., Loup T., Olejnik P., Lyapunov Exponents of Early Stage Dynamics of Parametric Mutations of a Rigid Pendulum with Harmonic Excitation, *Mathematical and Computational Applications*, 2019

52. Amer T. S., Galal A. A., Abolila A. F., On the Motion of a Triple Pendulum System under the Influence of Excitation Force and Torque, *Kuwait J. Sc*. Vol48, 2021

53. Espindola R., Dle Valle G., Hernandez G., Pineda I., MUcino D., Diaz P., The Double Pendulum of Variable Mass: Numerical Study for Different Cases, *Journal of Physics* 1221 012049, 2019

54. Rosenstein M. T., Collins J. J., De Luca C. J., A Practical Method for Calculating Largest Lyapunov Exponents from Small Data Sets, *Physica D*. 65 117-134, 1993

55. Botha A. E., Qi G., Analysis of the Triple Pendulum as a Hyperchaotic System, *Chaotic Modeling and Simulation*, 2: 297-304, 2013

56. Chiroiu V., Nedelcu N., Munteanu L., Moşnegutu V., On the Double Pendulum Flexible Manipulator, *Romanian Journal of Mechanics*, 2537-5229, 2020

57. Przybylska M., Szuminski W., Non-integrability of Flail Triple Pendulum, *AMS*, 1211.6045, 2012

58. Firmo D. L., Torres L. A. B., Nepomuceno E. G., Simulation and Dynamical Characterization of an Active Mechanical Chaotic Double Pendulum, *Procedings of COBEM*, 2007

59. A. Ohlhoff and P. H. Richter, Forces in the Double Pendulum, *Journal of Applied Mathematics and Mechanics*, Vol. 80, No. 8, 2000, pp. 517-534, 2000

60. A. A. Martynyuk and N. V. Nikitina, The Theory of Motion of a Double Mathematical Pendulum, *International Applied Mechanics*, 2000; 36(9), 1252-1258

61. U. Mackenroth, Robust Stabilization of a Double Pendulum with an Elastic Joint and Uncertain High-Frequency Dynamics, *16th Mediterrenean Conference on Control and Automation*, 2008, 1490-1495

62. Feckan M., Bifurcation and Chaos in Discontinuous and Continuous Systems, *Nonlinear Physical Science*, Springer, 2011

63. Espindola R., Del Valle G., Pineda I., Mucino D., Diaz P:, Gu,josa S., The double pendulum of variable mass: numerical study for different cases. *Journal of Physics*. 2018; 1221:

64. Laudelino J., Cabral H., Parametric stability of a pendulum with variable length in an elliptic orbit. *Regular and Chaotic Dynamics*. 2020;25(4): 323-329.

65. Belyakov A., Seyranian A., Luango A., Dynamics of the pendulum with periodically varying length. *Physica D*. 2009; 238:1589-1597.

66. Burra L:, Zanolin F., Chaotic dynamics in a vertically driven planar pendulum. *Nonlinear Analysis*. 2010; 72:1462-1476.

67. Ge Z. M., Yang H., Chen H., Lee C., Nonlinear dynamics and chaos control of a physical pendulum with vibrating and rotating support. *Journal of Sound and Vibration*. 2001; 242(2):247-264.

68. Bevivino J., The path from the simple pendulum to chaos. *Dynamics*. 2009.

69. Lu C., Chaos of a parametrically excited undamped pendulum. *Communications in Nonlinear Sceince and Numerical Simulation*. 2007;12:45-57.

70. Maiti S., Roy J., Mallik A.K., Nonlinar dynamics of a rotating double pendulum. *Physics Letters A*. 2016; 380:408-412.

71. Cid A., Diaz P:, Granados J., Mina A., Zuita A., Dynamic study of the pendulum-n and the beginning of chaos. *Journal of Physics Conference Series*. 2022; 2307:012059.

72. Awrejcewicz J., Kudra G., Experimental and numerical investigation of chaotic regions in the triple physical pendulum. *Nonlinear Dynamcis*. 2007; 50:755-766.

73. Awrejcewicz J., Kudra G., Lamarque C., Investigation of triple pendulum with impacts using fundamental solution matrices. *International Journal of Bifurcation and Chaos*. 2004; 14(12): 4191-4213.

74. Gupta M., Bansal K., Singh A., Mass and length dependent chaotic behaviour of a double pendulum. *Third International Conference on Advances in Control and Optimization of Dynamical Series*, 2014.

APPENDIX A: EXPERIMENTAL DOUBLE & TRIPLE PENDULUM

Mechanical Structure: It is an experimental setup designed to investigate the motion of a triple pendulum under different initial conditions. (Figure A.1) In order to achieve a massless rod-to-mass ratio of the pendulum, the mass of the rod was kept at 1/20 of the total mass using aluminium material. Three encoders were used to record the rotation angles at each joint and transfer the values to the computer. A signal converter was used to transfer the data to the PC and a program written on the PC was used to accumulate the data. Oscillation observations and data were collected using initial angles within the small angle region up to 30 degrees. However, for oscillations beyond small angles, mathematical models and simulations were used instead of the experimental setup.

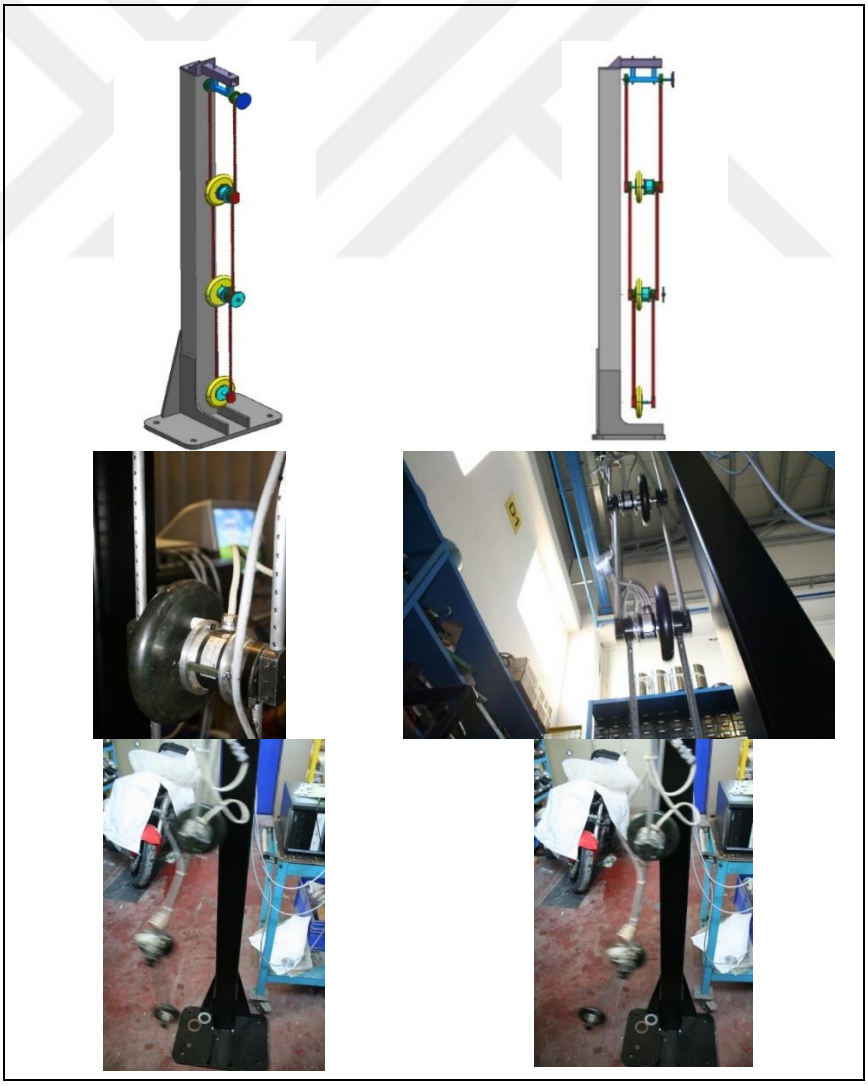


Figure A.1. The model of experimental pendulum

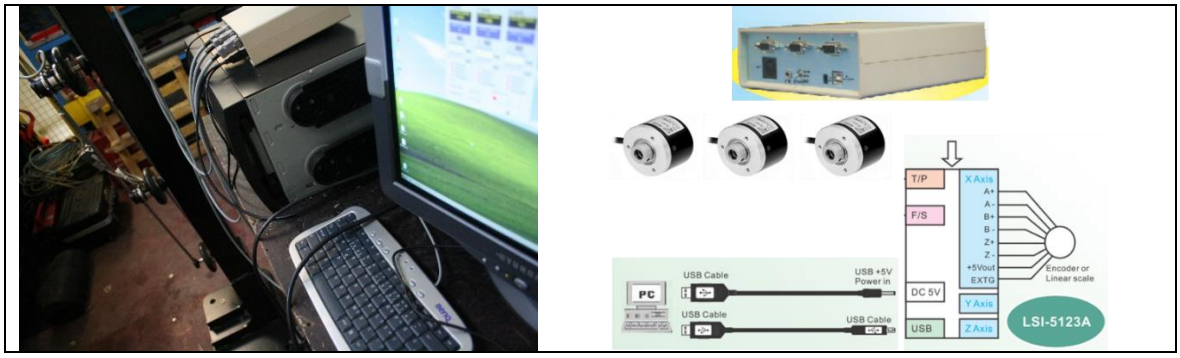


Figure A.2. The encoder and electric structure of experimental pendulum. (hardware, software application.)

The encoder and electrical connection used in the experimental setup are schematically shown in Figure A.2. We utilized the LSI-5123A (3-Axis Quadrature Encoder Counter Interface) as an interface to transfer data to the PC, and a PCI card was used for the PC-based control applications. The LSI-5123A integrates 3 axes counters in one USB interface, and the developer software used was C++ Builder. The PCI card and program enabled the acquisition of 10 values per second. Figure A.3 shows the PC user interface screen used for the experiments, where real-time values of the 3 axes can be monitored and recorded as a dataset using the start, stop, and reset commands. The system was operated with a 100-millisecond data acquisition interval using the encoder, and the data collection time was set to 20 seconds.

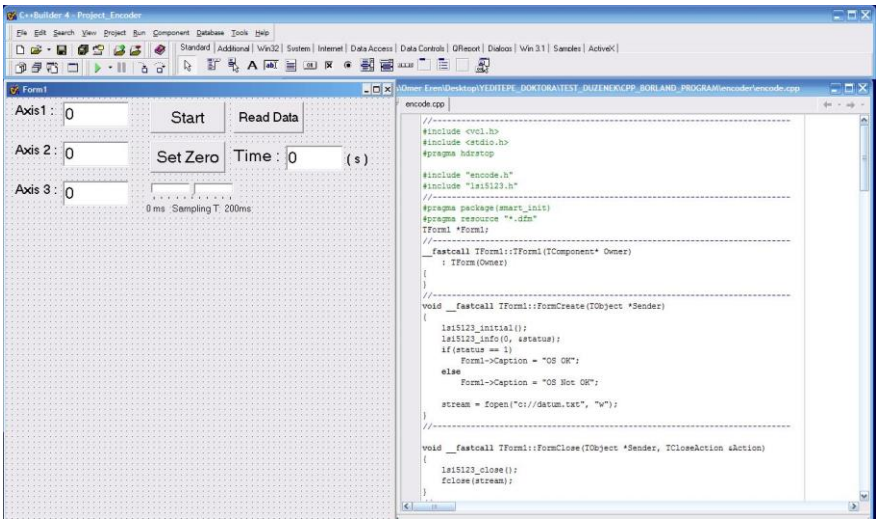


Figure A.3. The user interface of encoder data on PC of experimental pendulum.

APPENDIX B: ALGORITHM OF PENDULA SOLUTION IN MATLAB

```
clear all; close all; clc;
syms t b1 b2 b m1 m2 m g a w
t0 = 0;  tf = 20; time = [t0:.1:tf];
th1_i_d = input ('theta1 initial(derece) = ');
th1_f_d = input ('theta1 final(derece) = ');
th2_i_d = input ('theta2 initial(derece) = ');
th2_f_d = input ('theta2 final(derece) = ');
diffang_d = input ('Arttirim (derece) = ');
th1_i = th1_i_d*pi/180
th2_i = th2_i_d*pi/180
th1_f = th1_f_d*pi/180
th2_f = th2_f_d*pi/180
diffang = diffang_d*pi/180
theta1 = [th1_i:diffang:th1_f];
theta2 = [th2_i:diffang:th2_f];
th1_l = length(theta1)
th2_l = length(theta2)
time_l = length(time)
s=0;
b2=[1];%1 0.5 2
m2=[1];%1 0.5 2
a=[0];%0 0.25 0.5 0.75 1
w=[0]; %0 1 2

for ii = 1:length(b2);

   for jj = 1:length(m2);

      for mm = 1:length(a);

         for nn = 1:length(w);

for i=1:th1_l;

         for j=1:th2_l;
s = s + 1;
[t,x] = ode45(@(t,x)DP_lagrange_ho(t,x,b2(ii),m2(jj),a(mm),w(nn)), time, [theta1(i),
0, theta2(j), 0]);
x1 = x(:,1); % theta1
x2 = x(:,2); % omega1
x3 = x(:,3); % theta2
x4 = x(:,4); % omega2
th1int = theta1(i)*180/pi; th2int = theta2(j)*180/pi;
th1fin = theta1(th1_l)*180/pi; th2fin = theta2(th2_l)*180/pi;
mrot = m2(jj); brot = b2(ii); arot = a(mm); wrot = w(nn);
g=9.81;b1=1;m1=1;
```

```
xC = arot.*cos(wrot*t);
yC = zeros(201,1);
xA = arot.*cos(wrot*t) + b1.*sin(x1);
yA = -b1.*cos(x1);
xB = arot.*cos(wrot*t) + b1.*sin(x1) + brot.*sin(x3);
yB = -b1.*cos(x1) - brot.*cos(x3);
yAint = -b1*cos(theta1(i));
yBint = -b1*cos(theta1(i)) - brot*cos(theta2(j));

figure(1);
set(gcf,'visible','on');
subplot(2,2,1);
plot(t,x1,'r',t,x3,'k');
grid on; hold on;
xlabel('t (s)'),ylabel('theta1 -theta2 (r)');
subplot(2,2,2);
plot(t,x2,'r',t,x4,'k');
grid on; hold on;
xlabel('t (s)'),ylabel('w1 -w2 (r/s)');
subplot(2,2,3);
plot(xA,yA,'r',xB,yB,'k');
grid on; hold on;
xlabel('X (m)'),ylabel('Y (m)');
axis([-2 2 -2 2]);
subplot(2,2,4);
plot(x1,x2,'k',x3,x4,'r');
grid on; hold on;
xlabel('th1 -th2 (r)'),ylabel('w1 -w2 (r/s)');
% energy max theta1 & theta2 values
figure(2);
set(gcf,'visible','on');
subplot(2,1,1);
plot(InitialE,makstheta1,'.k', 'MarkerSize',8);
grid on; hold on;
xlabel('initial energy'),ylabel('maximum theta 1');
subplot(2,1,2);
plot(InitialE,makstheta2,'.r', 'MarkerSize',8);
grid on; hold on;
xlabel('initial energy'),ylabel('maximum theta 2');
   end
end
          end
       end
   end
end
```

APPENDIX C: ADDITIONAL REPRESENTATIONS OF DOUBLE PENDULUM SOLUTIONS

Different pendulum types were examined in the thesis and solutions were applied to θ_1 and θ_2 for small, medium, and large angles with corresponding graphs plotted. More emphasis was given to the graphs that illustrate significant changes in the motion profile. In this section, we have completed the solutions with graphs depicting motion profiles and orientations for other angle values as well.

Graphs for θ_1 with small and medium angles of $15°$ and $45°$, respectively, are presented for the case where the m_2/m_1ratio is 0.5 from Figure C.1. to Figure C.4. Additionally, pendulum type solutions under vertical vibration are available from Figure C.5. to Figure C.12. Graphs were plotted for θ_1 starting at $15°$ and $45°$, with an amplitude of 0.5 meters, and solutions corresponding to frequencies of $1s^{-1}$ and $3s^{-1}$. The pendulum subjected to vertical vibration is implemented with equal masses and rod lengths for the upper and lower masses. Particularly, when the frequency reaches 3, different motion patterns emerge.

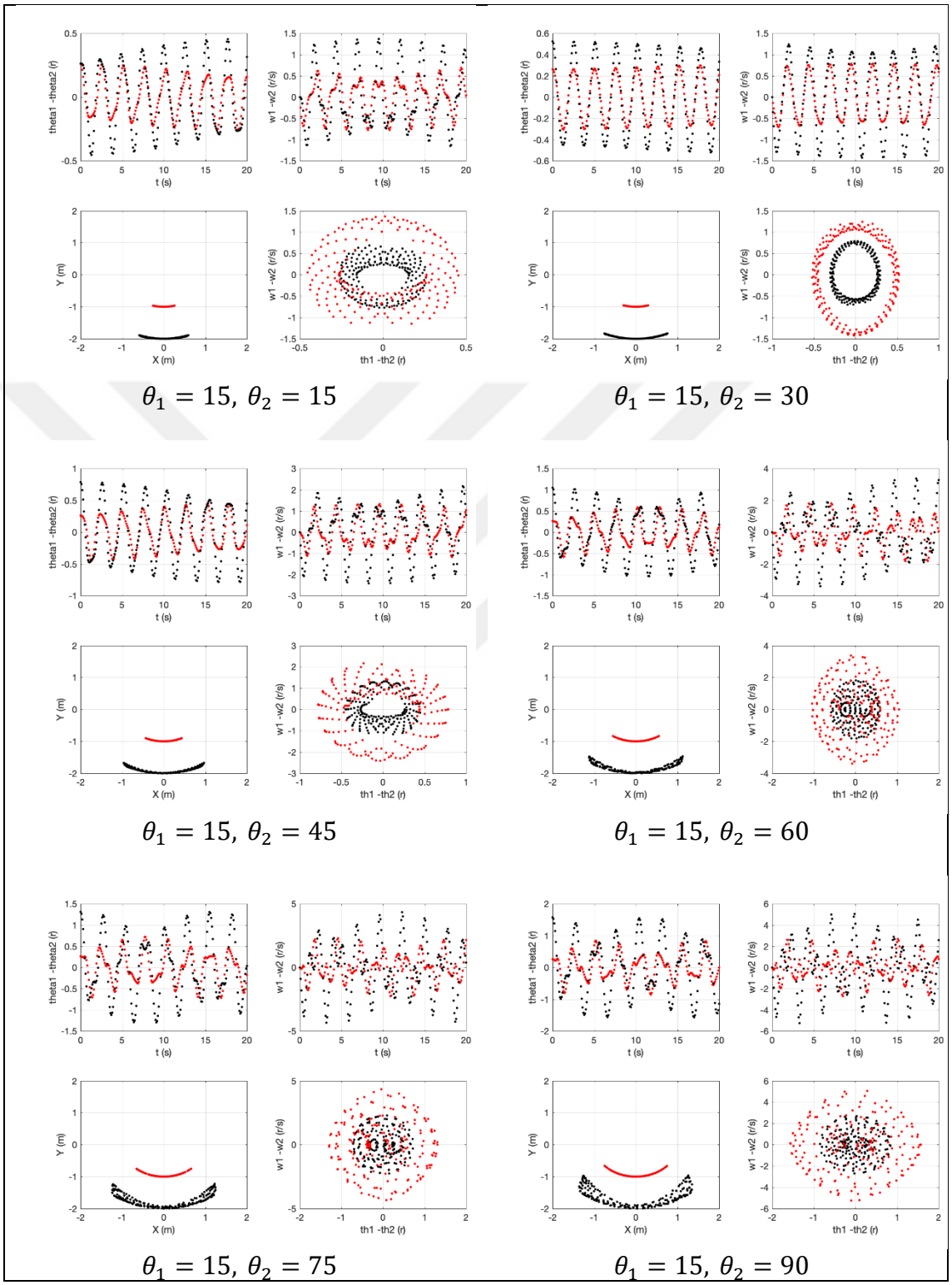


Figure C.1. The graphical solutions of $\theta_2 = 15, 30, 45, 60, 75, 90$ for small, medium, and large values corresponding to the small angle value of $\theta_1 = 15$. The other parameters are $b_1 = 1, b_2 = 1, m_1 = 1, m_2 = 0.5, a = 0, \omega = 0$.

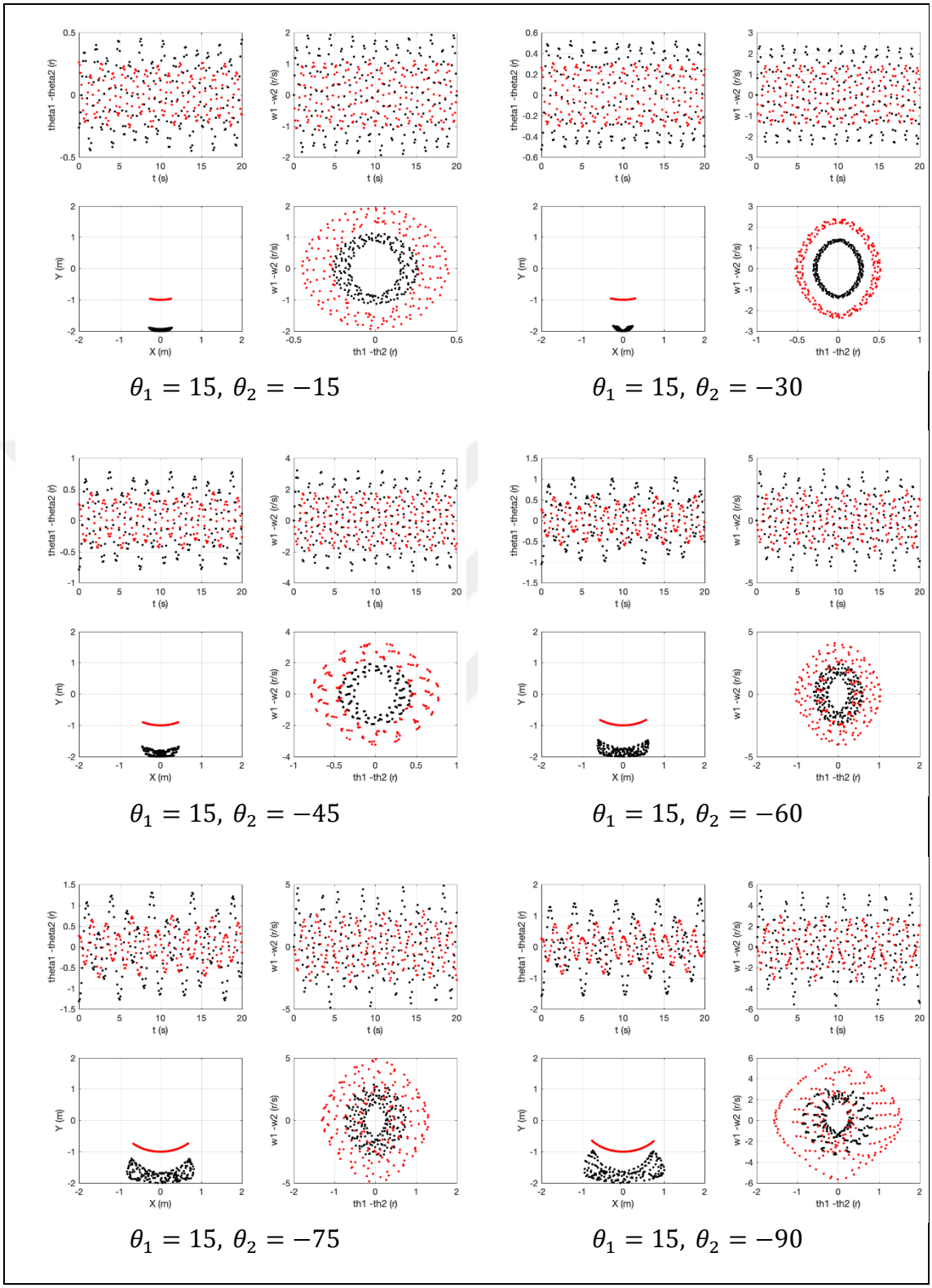


Figure C.2. The graphical solutions of $\theta_2 = -15, -30, -45, -60, -75, -90$ for small, medium, and large values corresponding to the small angle value of $\theta_1 = 15$. The other parameters are $b_1 = 1, b_2 = 1, m_1 = 1, m_2 = 0.5, a = 0, \omega = 0$.

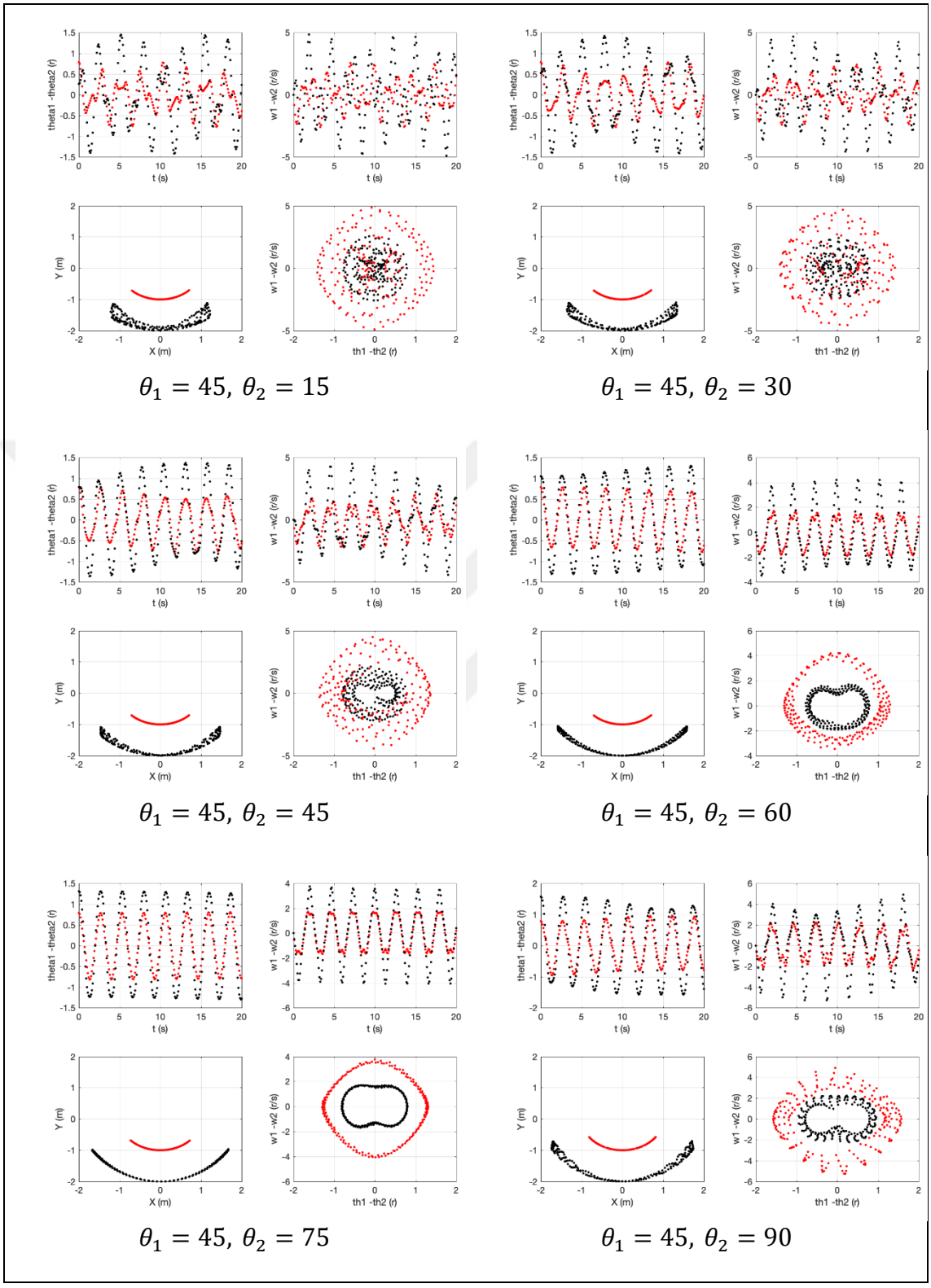


Figure C.3. The graphical solutions of $\theta_2 = 15, 30, 45, 60, 75, 90$ for small, medium, and large values corresponding to the small angle value of $\theta_1 = 45$. The other parameters are $b_1 = 1, b_2 = 1, m_1 = 1, m_2 = 0.5, a = 0, \omega = 0$.

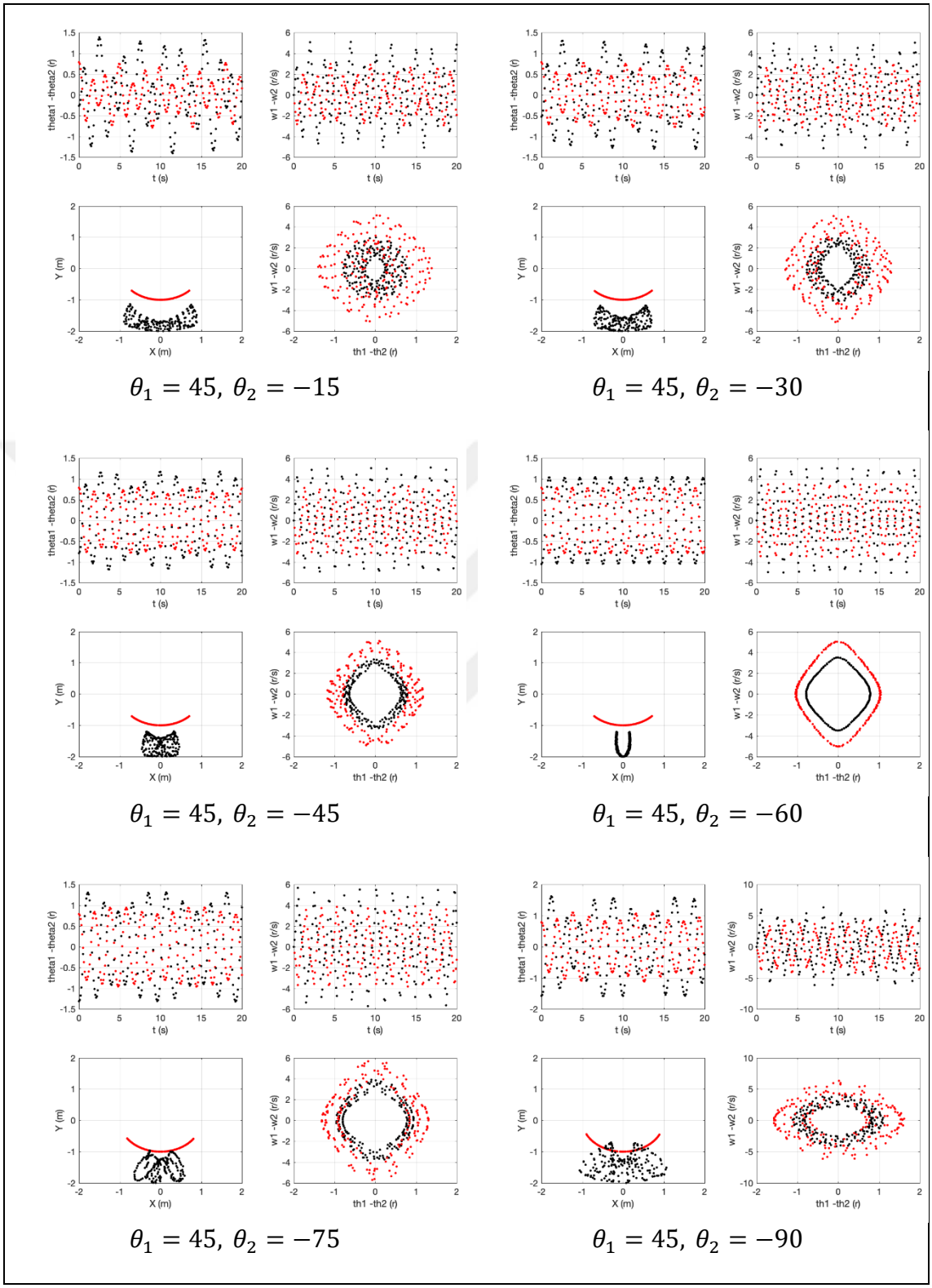


Figure C.4. The graphical solutions of $\theta_2 = -15, -30, -45, -60, -75, -90$ for small, medium, and large values corresponding to the small angle value of $\theta_1 = 45$. The other parameters are $b_1 = 1, b_2 = 1, m_1 = 1, m_2 = 0.5, a = 0, \omega = 0$.

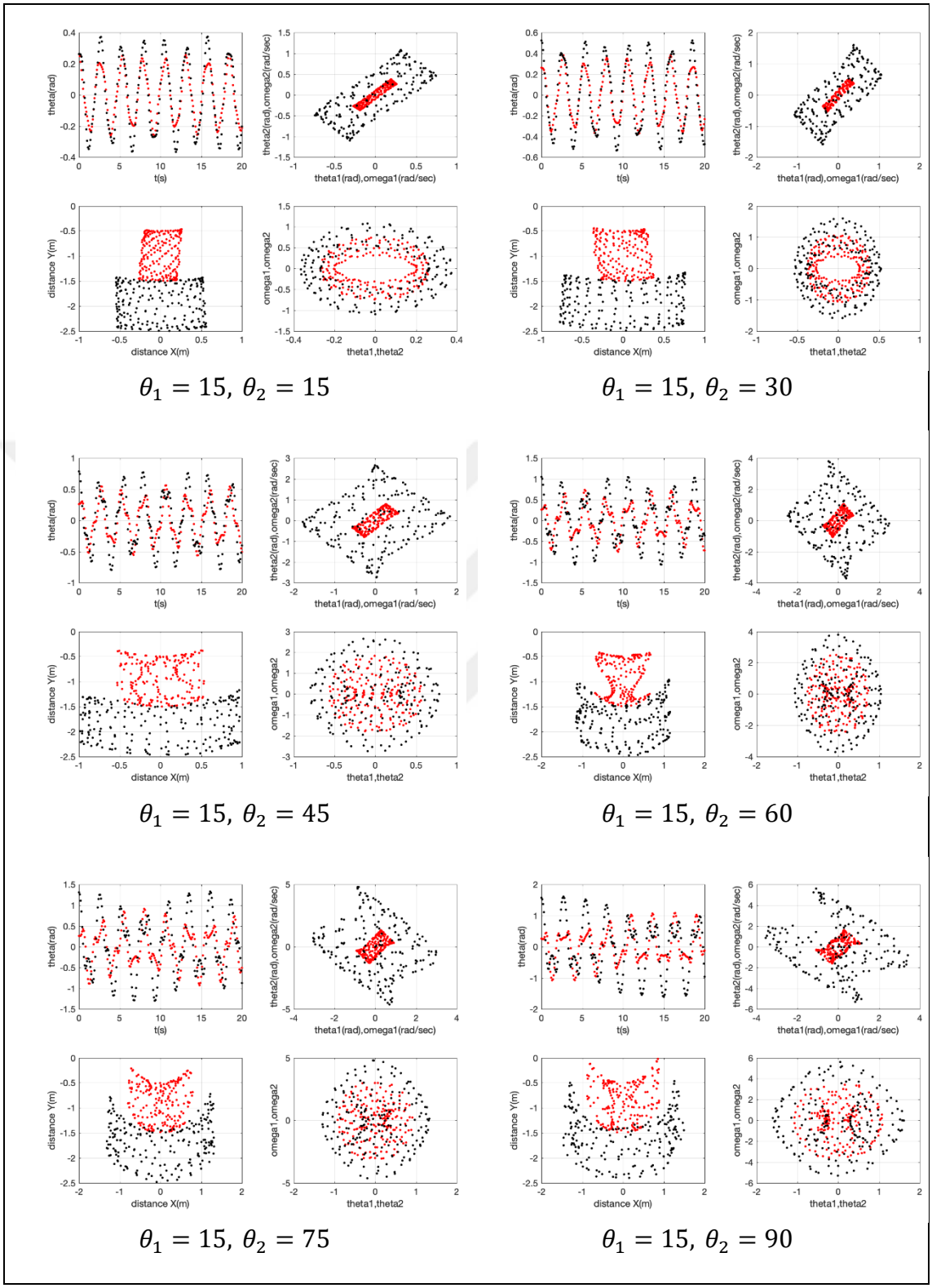


Figure C.5. The graphical solutions of $\theta_2 = 15, 30, 45, 60, 75, 90$ for small, medium, and large values corresponding to the large angle value of $\theta_1 = 15$. The other parameters are $b_1 = 1, b_2 = 1, m_1 = 1, m_2 = 1, a = 0.5, \omega = 1$, vertical vibrating.

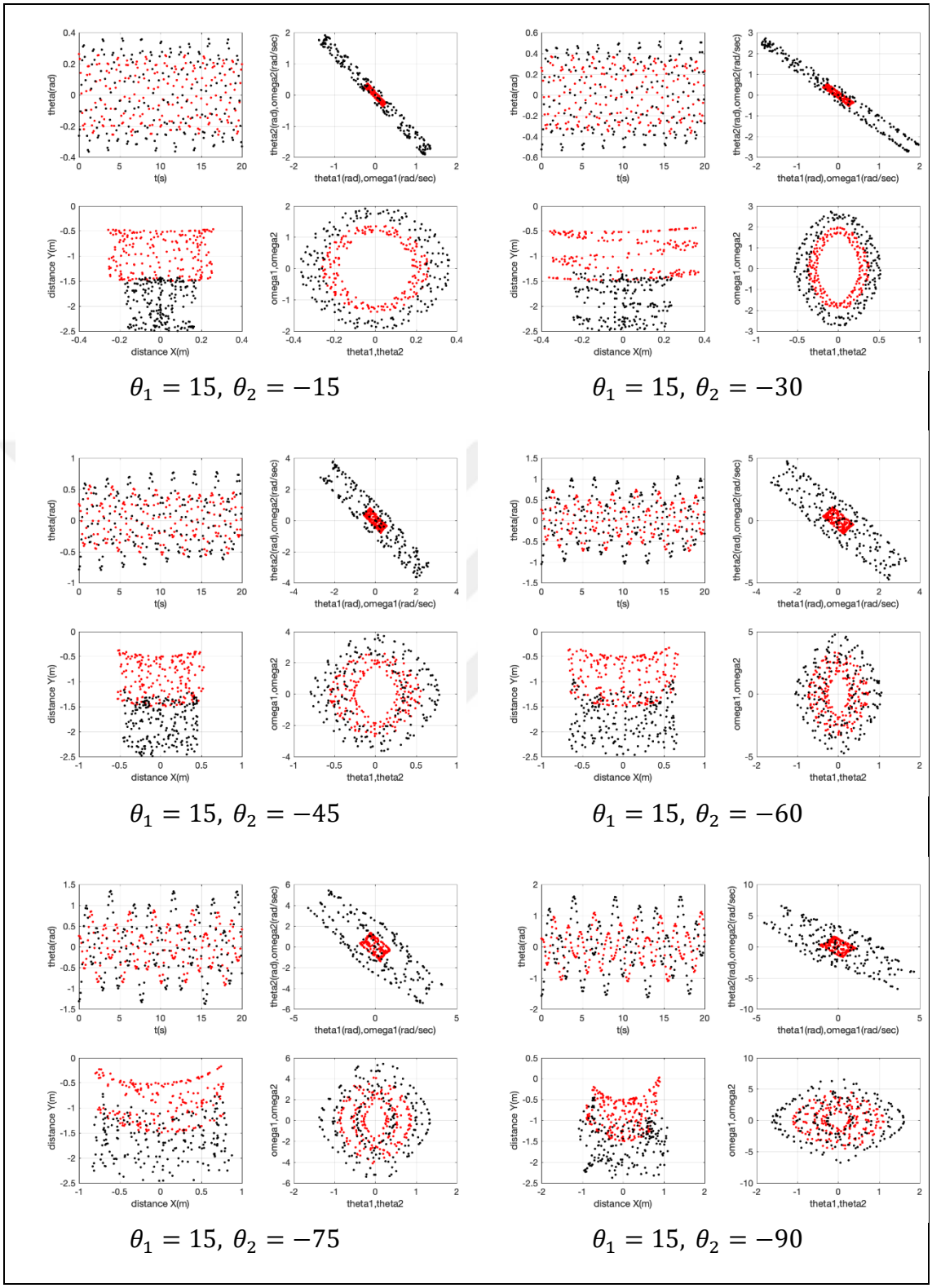


Figure C.6. The graphical solutions of $\theta_2 = -15, -30, -45, -60, -75, -90$ for small, medium, and large values corresponding to the large angle value of $\theta_1 = 15$. The other parameters are $b_1 = 1, b_2 = 1, m_1 = 1, m_2 = 1, a = 0.5, \omega = 1$, vertical vibrating.

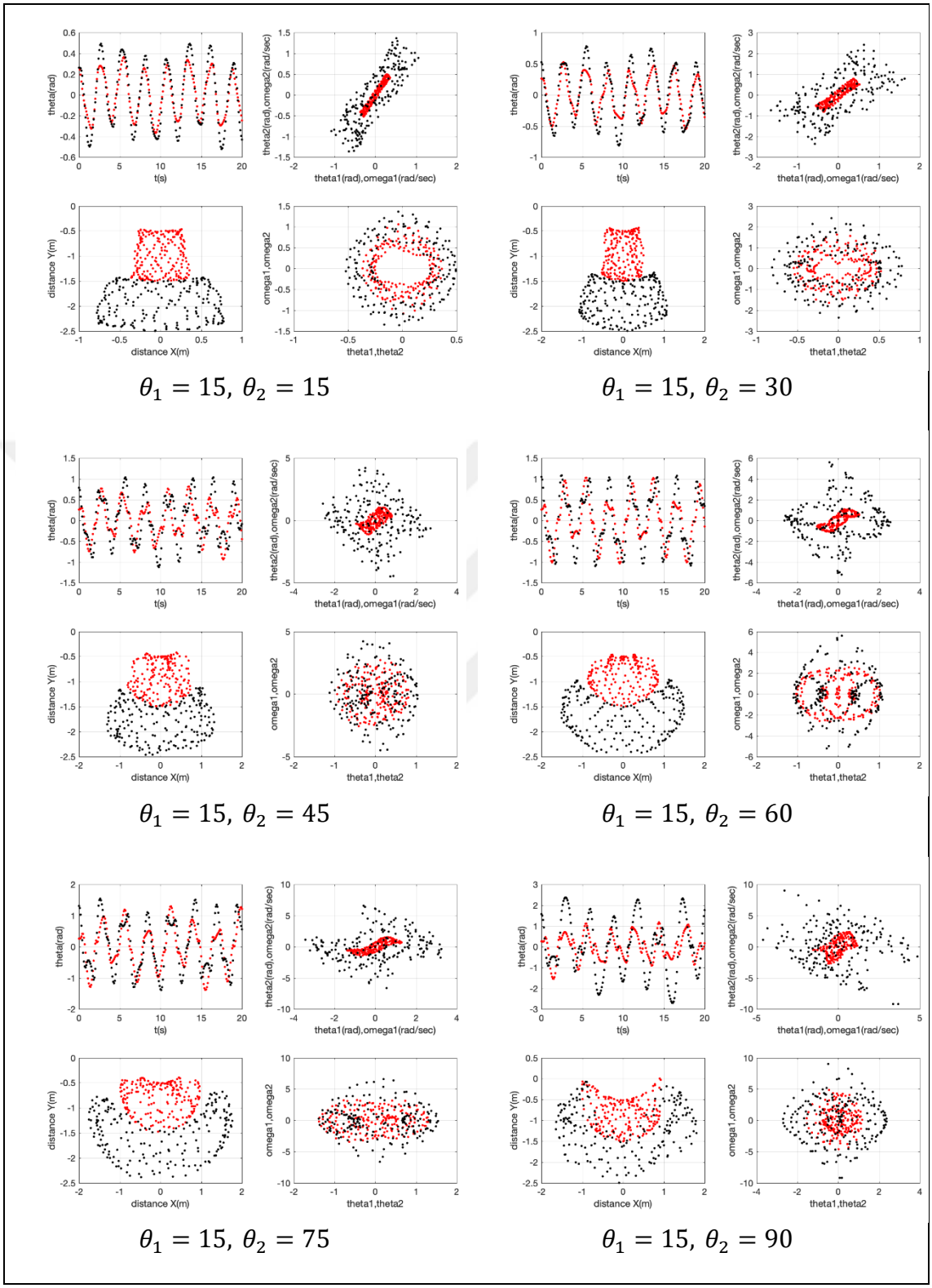


Figure C.7. The graphical solutions of $\theta_2 = 15, 30, 45, 60, 75, 90$ for small, medium, and large values corresponding to the large angle value of $\theta_1 = 15$. The other parameters are $b_1 = 1, b_2 = 1, m_1 = 1, m_2 = 1, a = 0.5, \omega = 3,$ vertical vibrating.

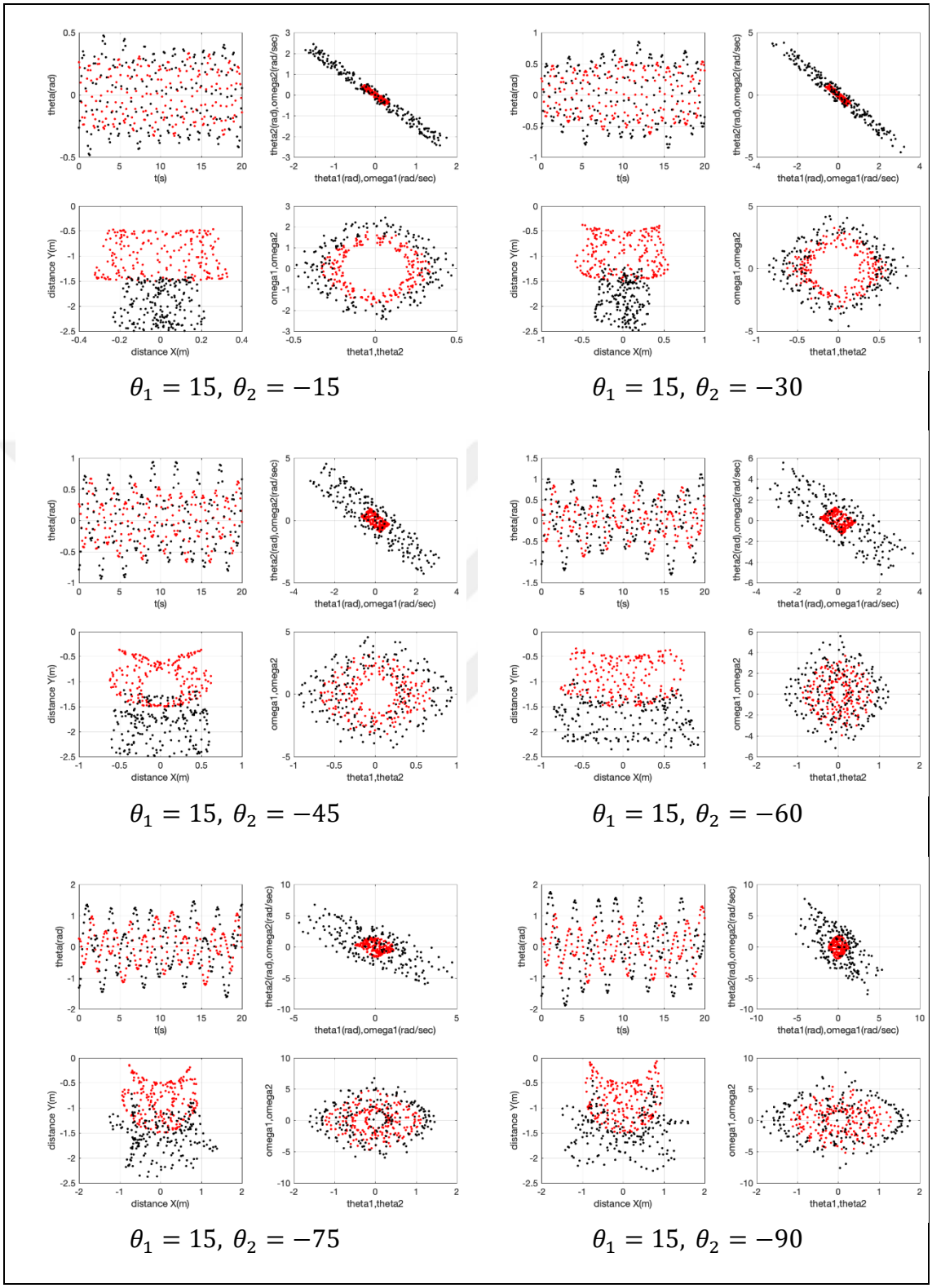


Figure C.8. The graphical solutions of $\theta_2 = -15, -30, -45, -60, -75, -90$ for small, medium, and large values corresponding to the large angle value of $\theta_1 = 15$. The other parameters are $b_1 = 1, b_2 = 1, m_1 = 1, m_2 = 1, a = 0.5, \omega = 3$, vertical vibrating.

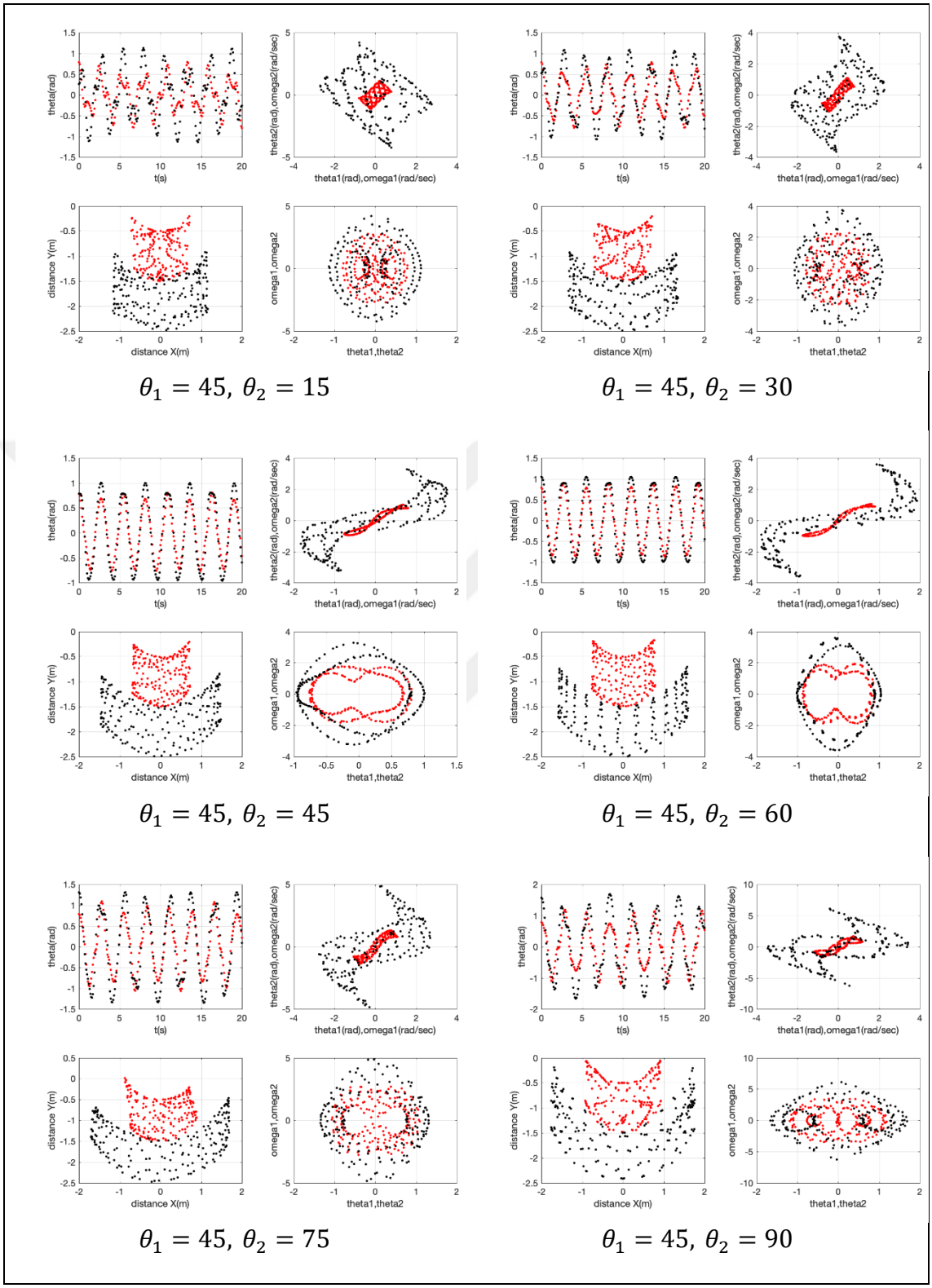


Figure C.9. The graphical solutions of $\theta_2 = 15, 30, 45, 60, 75, 90$ for small, medium, and large values corresponding to the large angle value of $\theta_1 = 45$. The other parameters are $b_1 = 1, b_2 = 1, m_1 = 1, m_2 = 1, a = 0.5, \omega = 1$, vertical vibrating.

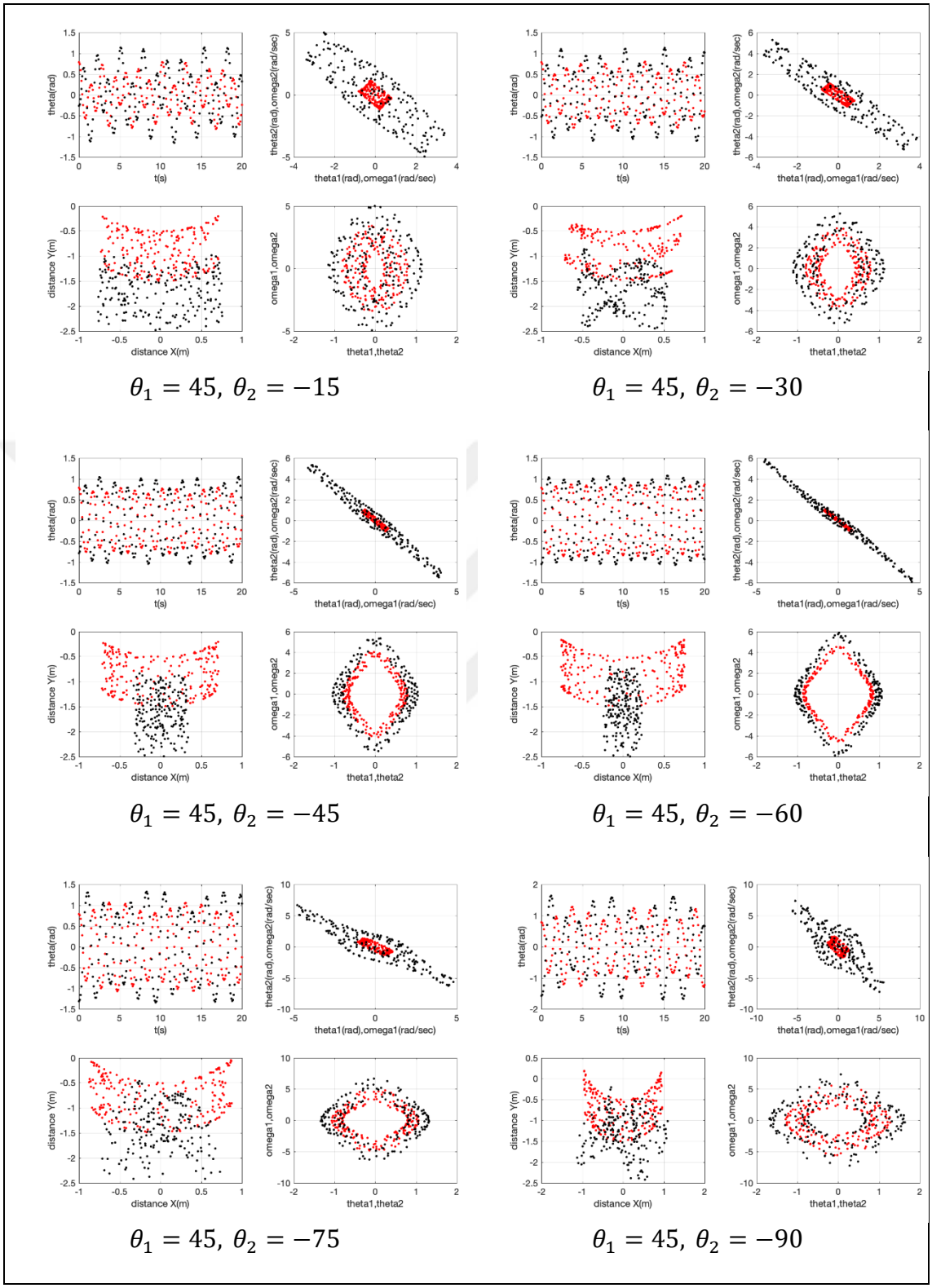


Figure C.10. The graphical solutions of $\theta_2 = -15, -30, -45, -60, -75, -90$ for small, medium, and large values corresponding to the large angle value of $\theta_1 = 45$. The other parameters are $b_1 = 1, b_2 = 1, m_1 = 1, m_2 = 1, a = 0.5, \omega = 1$, vertical vibrating.

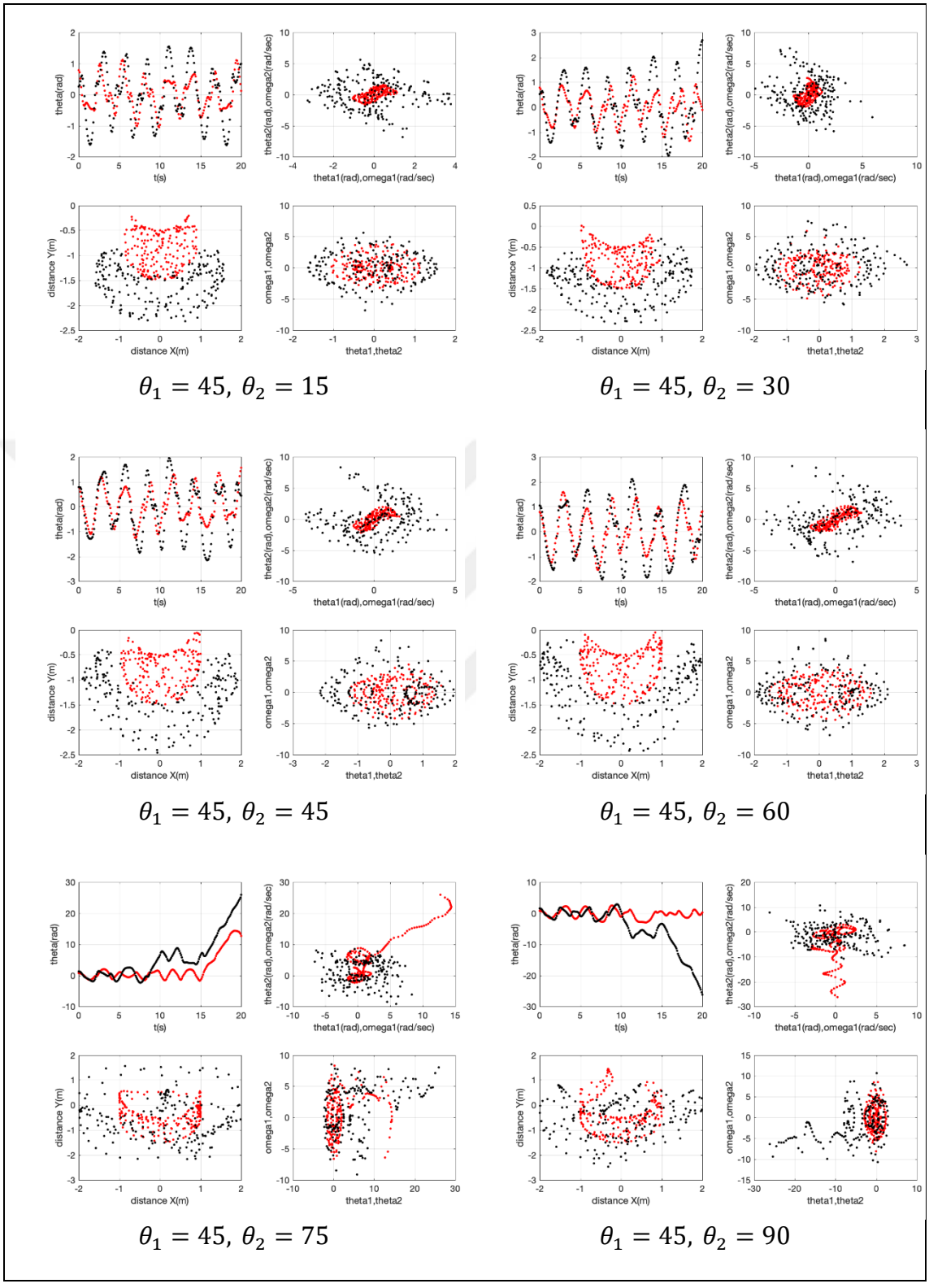


Figure C.11. The graphical solutions of $\theta_2 = 15, 30, 45, 60, 75, 90$ for small, medium, and large values corresponding to the large angle value of $\theta_1 = 45$. The other parameters are $b_1 = 1, b_2 = 1, m_1 = 1, m_2 = 1, a = 0.5, \omega = 3$, vertical vibrating.

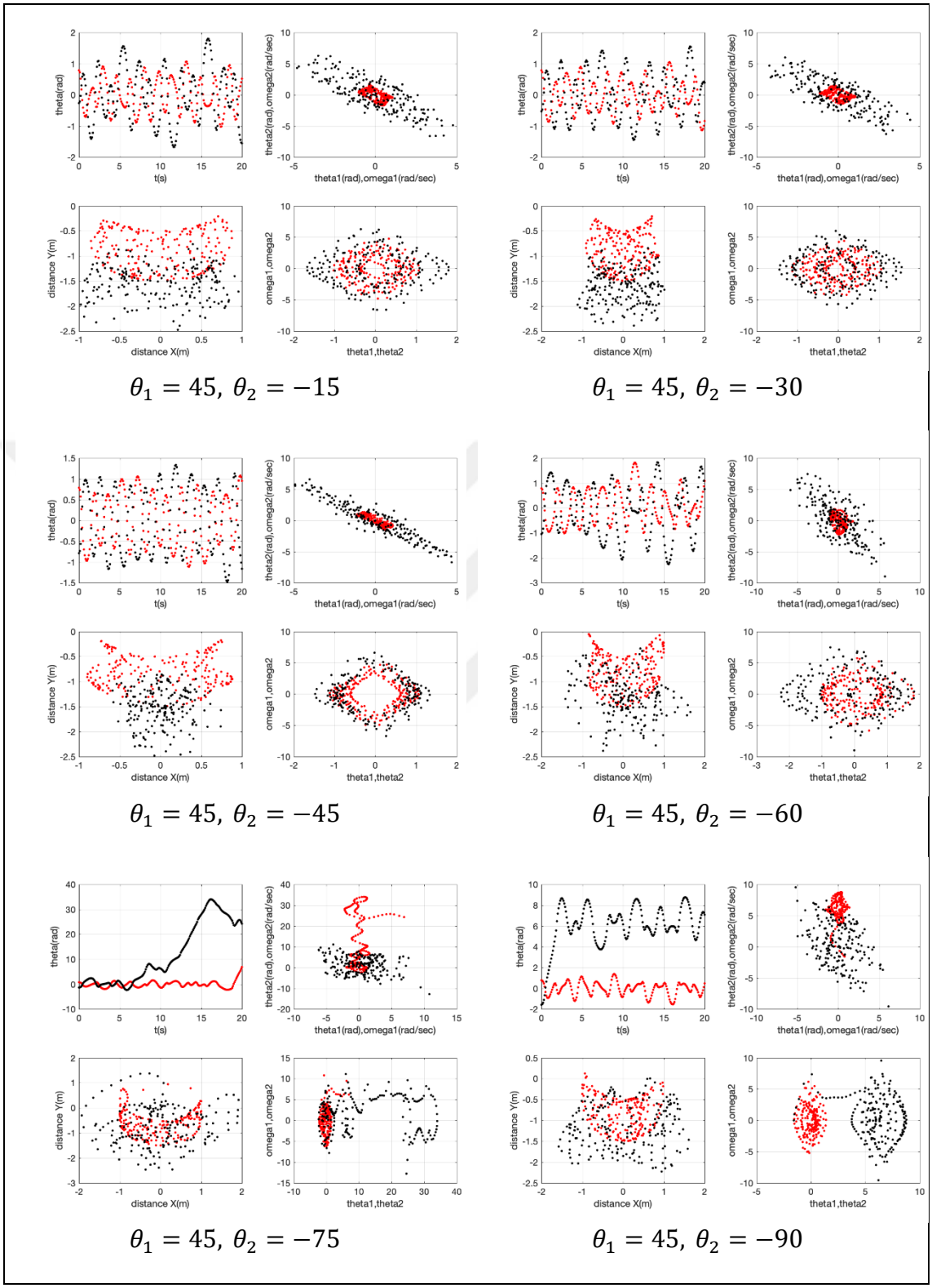


Figure C.12. The graphical solutions of $\theta_2 = -15, -30, -45, -60, -75, -90$ for small, medium, and large values corresponding to the large angle value of $\theta_1 = 45$. The other parameters are $b_1 = 1, b_2 = 1, m_1 = 1, m_2 = 1, a = 0.5, \omega = 3$, vertical vibrating.